# POLITECNICO DI TORINO

Corso di Laurea Magistrale in Ingegneria Energetica e Nucleare
Innovazione nella produzione di energia
A.Y. 2020/2021

## Master of Science Thesis

## *Modelling and analysis of CO2 reuse in a PtX system based on reversible Solid Oxide Cell*

**Advisors:**
Prof. Massimo Santarelli
Prof. Domenico Ferrero

**Candidate:**
Vincenzo Cascio

# Abstract in Italian

La diminuzione del contenuto di anidride carbonica in atmosfera è la sfida che deve essere superata nei prossimi decenni. Uno dei metodi da implementare agisce sui sistemi di produzione dell'energia elettrica e termica, i quali contribuiscono per una elevata percentuale alle emissioni di gas ad effetto serra, i principali responsabili del surriscaldamento globale.

A tale scopo, il seguente lavoro di tesi mira a modellizzare ed analizzare un prototipo di centrale poligenerativa, in grado di soddisfare il fabbisogno elettrico di un centro urbano di 30 mila persone, producendo al tempo stesso una serie di vettori energetici (idrogeno e gas naturale sintetico) col compito di immagazzinare l'energia in eccesso prodotta da un campo fotovoltaico. La taglia di quest'ultima tecnologia è 9 MW, ed è in grado di soddisfare per un terzo il fabbisogno elettrico del centro urbano. La rimanente porzione scoperta viene integrata con l'utilizzo di una cella reversibile ad ossidi solidi (rSOC) operante sia come cella combustibile (SOFC), con taglia di 6 MW per la produzione dell'energia elettrica mancante, sia come elettrolizzatore (SOEC) per l'immagazzinamento dell'energia in eccesso, con taglia di 30 MW, determinando un rapporto di potenza tra le due modalità pari a 5, scelto per garantire l'ottimizzazione termica del dispositivo.

La SOFC sfrutta il gas naturale prelevato dalla rete di distribuzione nazionale, caratterizzato da una elevata percentuale di $CH_4$. Con l'utilizzo di un pre-reformer esterno al dispositivo elettrochimico, questo elemento viene convertito in $H_2$ e CO, elementi che subiranno le effettive reazioni elettrochimiche, evitando ogni problema di deposito di sostanze carbonacee. La SOEC invece, produce sia idrogeno utilizzando $H_2O$ demineralizzata in ingresso e, inviandolo in seguito ad una sezione di stoccaggio per rifornire con cadenza settimanale una refilling station, sia syngas ($H_2$&CO), sfruttando $H_2O$ e $CO_2$. Proprio quest'ultimo stream acido viene inviato dalla sezione di rimozione dell'anidride carbonica (CCS), in grado di depurare tramite processi di absorbimento uno stream "sporco" di biogas, rendendolo biometano ed immettendolo in rete con il rispetto degli standard previsti. Il syngas prodotto è a sua volta stoccato in uno storage apposito, per essere rilasciato a portata costante all'interno di un impianto di metanazione. Quest'ultimo impianto, caratterizzato da una serie di reattori di metanazione con interposti degli scambiatori di calore in grado di raffreddare lo stream trattato, permette la conversione del syngas in gas naturale sintetico e la sua immissione in rete.

Il terzo capitolo della tesi prevede la modellizzazione degli impianti, mentre il quarto descrive le simulazioni effettuate su Aspen Plus®, le analizza e riporta i risultati finali. Infine, l'ultimo capitolo riporta un'analisi economica centrata sulla metodologia del costo netto presente, calcolando delle importanti variabili economiche: Levelized Cost Of Products. Queste permettono di valutare il costo del vettore energetico in uscita dalla centrale, rapportandolo al costo totale dell'impianto produttivo.

# Contents

# List of figures

# List of tables

# Nomenclature

## Symbols

| | | |
|---|---|---|
| LHV | MJ/kg or MJ/m$^3$ | Low Heating Value |
| $\rho$ | kg / m$^3$ | Density |
| $n$ | mol | Mole |
| MM | g/mol | Molecular Mass |
| $V$ | V | Voltage |
| $I$ | A | Current |
| Wel | W | Electrical power |
| Gfe | kJ/mol | Gibbs Free Energy |
| $H$ | J | Enthalpy |
| $S$ | J/K | Entropy |
| ASR | $\Omega$m$^2$ | Area Specific Resistant |
| PR | / | Performance Ratio |
| OCV | V | Open Circuit Voltage |
| $F$ | C/mol | Faraday constant |
| Ø \| D | m | Diameter |
| $v$ | / | Stoichiometric coefficient |
| $\mu$ | kJ/mol | Chemical Potential |
| $T$ | °C or K | Temperature |
| $p$ | bar | pressure |
| $G$ | W/m$^2$ | Solar Radiation |
| $\phi$ | W | Heat Flux |
| $\dot{n}$ | mol/s | Molar Flow Rate |
| $\dot{m}$ | kg/s | Mass Flow Rate |
| $V$ | m$^3$/s | Volume Flow Rate |
| Na | particle/mol | Number Of Avogadro |
| qe- | C | Charge of an electron |
| Zr | / | Charge Number |
| $i$ | A/cm$^2$ | Density Current |
| $\eta$ | % | Efficiency |
| $R$ | J/molK | Universal Molar Constant of Gas |
| $K$ | / | Equilibrium costant of chemical reaction |
| GG | / | Gas Gravity |
| HHV | kJ/kg or kJ/m$^3$ | High Heating Value |
| WI | kJ/kg or kJ/m$^3$ | Wobbe Index |
| FU | / | Fuel Utilization |
| AU | / | Air Utilization |
| $Q_{rel}$ | W | Heat Exchange by the Cell |
| $h$ | h | Hours |
| $y$ | y | Years |
| $V_{TN}$ | V | Thermoneutral Voltage |
| $\lambda$ | W/mK | Thermal Conductivity |
| $A$ | m$^2$ | Area |

## Abbreviations

| | |
|---|---|
| GHG | GreenHouse Gasses |
| GWP | Global Warming Potential |
| WMO | World Meteorological Organization |
| UNFCC | United Nations Framework Convention on Climate Change |
| COP | Conference Of the Parties |
| EIT | Economy In Transition |
| CDM | Clean Development Mechanism |
| CER | Certified Emissions Reduction |
| JI | Joint Implementation |
| ERU | Emissions Reduction Units |
| INDC | Intended Nationally Determined Contribution |
| IEA | International Energy Agency |
| SNG | Synthetic Natural Gas |
| RES | Renewable Energy Source |
| rSOC | Reversible Solid Oxide Cell |
| TFEC | Total Final Energy Consumption |
| CCS | Carbon Capture and Sequestration |
| TPES | Total Primary Energy Supply |
| SMR | Steam Methane Reforming |
| PSA | Pressure Swing Adsorption |
| DMR | Dry Methane Reforming |
| WGS | Water Gas Shift reaction |
| SOEC | Solid Oxide Electrolytic Cell |
| YSZ | Yttria Stabilized Zirconia |
| tps | Three phase boundaries |
| MIEC | Mixed Ionic Electronic Conductor |
| LSM | Lanthanum Strontium Manganite |
| ITM | Ion Transfer Membrane |
| MEA | MonoEthanolAmmine |
| BOP | Balance Of Plant |
| PtX | Power-to-X |
| DS | Design Specification |
| CB | Calculator Block |
| ELECNRTL | Electrolyte Non-Random Two Liquid model |
| GFDL | GNU Free Documentation License |
| NPC | Net Present Cost |
| LCOP | Levelized Cost Of Product |
| CAPEX | CAPital EXpenditure |
| OPEX | OPerating Expenditure |
| REPL | REPLacement cost |
| FOC | Fixed Operating Cost |
| VOC | Variable Operating Cost |
| EPRI | Electric Power Research Institute |
| ARERA | Autorità di Regolazione per Energia Reti e Ambiente |
| CEPCI | Chemical Engineering Plant Cost Index |
| MSECI | Marshall and Swift Equipment Cost Index |

| | |
|---|---|
| AIT | Air Ignition Temperature |
| PEM | Proton Exchange Membrane |
| SOFC | Solid Oxide Fuel Cell |
| SOEC | Solid Oxide Electrolityc Cell |
| TSO | Transmission System Operator |
| SI | International measurement System |

# 1 Introduction

The history of the Earth, in the last 10 thousand years, has been characterized by a period of climatic stability, with temperatures that varied every ten years by plus and minus one degree. This period of well-being allowed the humankind to increasingly evolve, until the advent of the industrial revolution in the Eighteenth Century. This event marked the fate of humanity due to the beginning of the (over)exploitation of fossil sources, causing the effects we experience today: the Earth is in danger and it needs an immediate intervention in order to guarantee climatic stability, favoring human well-being and development.

The energy sector is one of the most influential concerning environmental pollution, as its residues and waste are highly polluting substances, with a worrying greenhouse gases content. Until a few decades ago, no one had ever questioned the consequences of the release of these substances into the atmosphere. But nowadays, an intervention that could have a significant impact would be the use of technologies that work by exploiting renewable sources.

Among them, the carbon capture and sequestration systems allow to remove pollutants from the harmful fumes of industrial processes. The benefit of this plant lies in the fact that it can be implemented in support of other new technologies, but above all for those already existing by a retrofitting action. In fact, in the last decades the knowledge related to the capture of acid substances and the sciences connected to it (new materials, types of plants) are becoming increasingly advanced, aiming at their diffusion as soon as possible. Another technology worthy of interest is that of electrochemical devices: electrolysers and fuel cells. Also in this case, the technology of these plants is becoming increasingly sophisticated, thanks to its coupling capacity with renewable energies such as photovoltaic and wind power, which promotes the storage of excess energy and the production of clean electricity.

In the present thesis work, a polygeneration power plant with an rSOC as its heart will be designed, i.e. an electrochemical device able of acting both as a fuel cell and as an electrolyser. This latest mode will be coupled with a carbon dioxide capture system, capable of providing it with a pure stream of $CO_2$ and of processing it to create syngas that will be stored in a specially sized storage. Furthermore, to obtain an increase in the quality of this substance, the syngas produced will be transformed into synthetic natural gas thanks to the coupling with a methanation plant, capable of carrying out this upgrade by exploiting the chemical reactions called methanation. The electrolyser, in addition to producing syngas, by receiving carbon dioxide and liquid water as input, will be able to produce a pure stream of hydrogen and to choose for a certain number of days of the week to operate only with the use of water. The hydrogen thus produced will also be stored in a special storage, with the aim of supplying at a later time a refilling station used for refuelling vehicles with hydrogen. The fuel cell mode of the rSOC, on the other hand, will operate in combination with a photovoltaic field, in such a way as to guarantee an electrical production required by an urban center of 30 thousand people. This photovoltaic field will also provide the electricity needed for electrolysis processes in times of energy surplus.

Initially, a description of these technologies will be carried out in order to establish their current level of the state of the art. Subsequently, each section will be modelled and reproduced on the Aspen Plus® software, allowing a simulation of the processes involved. Downstream of the simulations, the data obtained will be collected, processed in Matlab® and analysed, drawing at the end a series of descriptive performance parameters for each plant section used.

Once the technical analysis of the plant is concluded, a short economic study will also be carried out, according to the net present cost methodology, with the determination of important economic parameters, the levelized costs of product that will allow to quantify the costs at which various energy carriers will be sold.

## 1.1 Environmental problem: Global Warming

Since the formation of the Earth, around 4.6 billions years ago, life on the planet has always been regulated by natural processes. It is scientifically proven, by the paleoclimatology science, that the historical climate changes of the Earth are continuously evolving during time, considering different time scales: era (millions of years), period (thousands of years) or decades. Many natural occurrences have perturbed the equilibriums of the planet, causing changes, often even extreme effects with the risk of the Earth's life extinction. In the past, the causes were only attributed to internal variabilities, which happen naturally random, as the plate tectonics movement, volcanism activities, solar and space activities, orbital variations and greenhouse gasses.

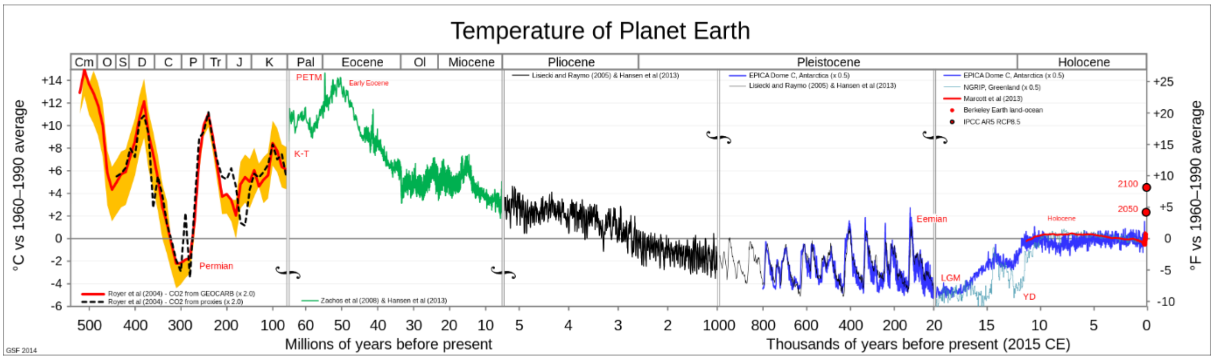

*Figure 1 [1]- Global average temperature estimated for the last 540 million years.*

The study of these phenomena throughout the existence of our planet has caused an important and equally alarming effect, which is shown in fig. 1 above: the trend of the average global temperature. As can be seen from the final red line, which describes only the few last years characterized by the human presence, an impressive increase of the thermal gradient $(\frac{dT}{dt})$ emerges within a very short period of time. This problem should not be underestimated, and to better understand a comparison with what has happened in the past could be useful. For instance, in the ancient Ice Ages, when the average global temperature was slightly low, a large surface of ice covered the Earth (due to the action of the Earth's orbital perturbation). The ice increased the reflection of solar radiations by the ground, thanks to the high reflection of solid water. This phenomenon, combined with volcanic eruptions caused by continental rifts and the consequent emission in the atmosphere of great amounts of greenhouse gasses as carbon dioxide, entrapped the heat coming by the sun radiations and contributed at the same time to the rising of the average planet temperature. It took thousands of years to produce this variation in the average temperature, and that is why the situation today is to be considered alarming. Despite nowadays the Earth seems to be invulnerable, and the perfect place where life can naturally thrive by good geoclimatic conditions, as shown in the red line from fig.1, in the past few decades the presence of a hostile entity has been disturbing the global equilibrium, as an external negative force: the human. The modern human has walked

---

[1] Glen Fergus: https://commons.wikimedia.org/wiki/File:All_palaeotemps.svg

this Earth for two hundred thousand years, a time completely insignificant compared to the Earth's life. Despite this, his actions have produced almost irreversible changes on the Earth conditions which, as said before, should rather happen naturally in a longer period of time. Global warming is the main problem, humans are causing it with their lifestyle and habits, exploiting and impoverishing the natural resources of the planet, enhancing the global temperature. Although technological innovations improve the well-being of the people, their destructive effects on the natural balance are badly managed. The most harmful anthropic activities, the ones with the higher impact on the environment are the energy produced by power plants, civil heating and vehicular traffic.

Until a few years ago, climate change and pollution were not considered as global issues, due to a still widespread lack of knowledge on these topics and to the expanding global capitalism. In recent years, however, the level of awareness has been growing among the population, as climate anomalies such as summer snow, hot temperatures in winter, premature blossoming of fruits, the increment of hurricanes and dangerous storms etc., are becoming more and more common. As a consequence, the number of studies and researches within the scientific community has increased tremendously in the past decades. Generally, the Earth thermodynamic interacts with everything that covers it, exchanging energy by conduction from the ground, convection with the atmosphere and irradiation. Irradiation is the most important phenomenon, because most of the energy that allows life to proliferate is the energy coming from the sun.

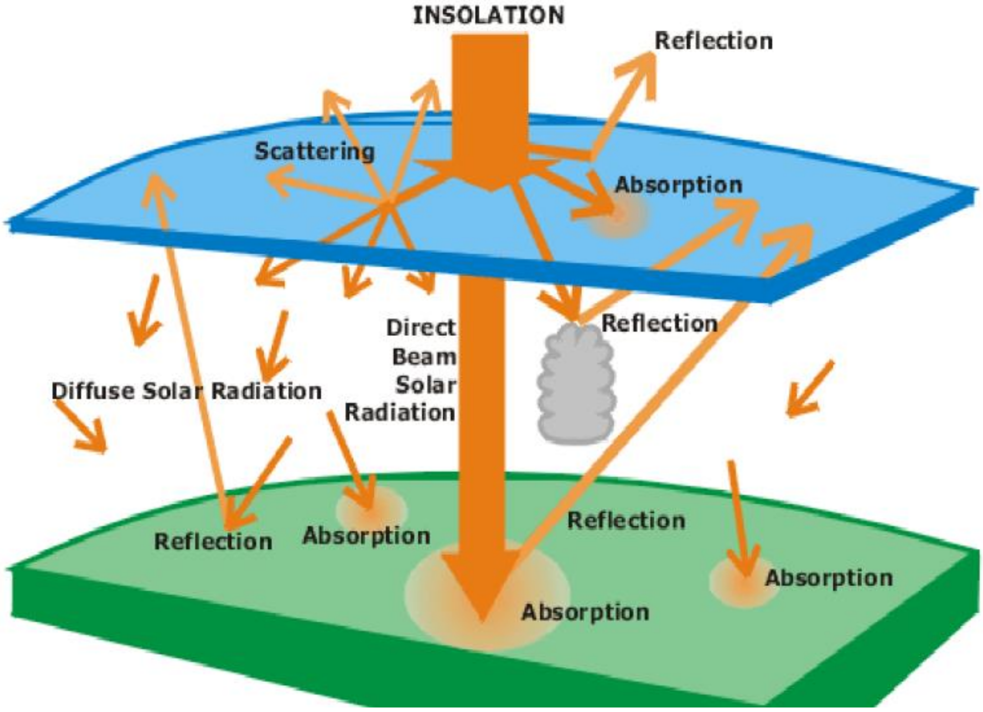

*Figure 2- Energetic balance of the Earth, image by Karen A.Lemke.*

As shown in fig. 2, the solar radiation reaches the Earth travelling in the space. It is interesting to examine this natural mechanism a little better: the first shielding is the magnetic field of the Earth which avoids that gamma rays (produced by the radioactive decays in the Sun's chemical molecule nuclei) and x rays (produced by variation of the kinetic of electrons around the nuclei always in the Sun) manage to reach the ground. In general, these radiations are extremely dangerous because of their high energy content which could penetrate the matter and damage the cells' molecules, developing genetic mutations or death in the human beings. The second protective layer is the atmosphere, which blocks the ultraviolet radiations, again highly energetic, characterized by low wavelength and high frequency. The remaining part of the solar radiation gets absorbed by the atmosphere and then re-emitted with an altered wavelength (toward the Earth or the space) or can be directly reflected avoiding any possible interaction or it can be directly pass through, reaching the Earth's surface. When the solar radiation reaches the ground of the Earth it happens through the same mechanisms, it can be absorbed and re-emitted or reflected.

It is evident that the atmosphere plays a fundamental role for the regulation of the thermodynamic Earth's balance, indeed its composition varies the physical interaction with the radiations, because depending on its chemical composition (the amount and kind of chemicals which compose the atmosphere) several wavelength can be absorbed whereas others are not. Researchers have continued to investigate and study these chemical interactions in order to find more precise information about what kind of substances improve these phenomena. Nowadays it's known that: Water vapour ($H_2O$) helps the absorption of the wavelengths lower than 8 [µm] and higher than 18 [µm]; Carbon Dioxide ($CO_2$) instead, favours 2,7 [µm], 4,3 [µm] and the band between 13 and 18 [µm]; Ozone ($O_3$) 10 [µm]; Methane ($CH_4$) 8 [µm]; chlorofluorocarbons (CFC) the band between 7 and 13 [µm]. More details are reported in the next fig.3, representing the absorption plot with the corresponding chemicals that interact.

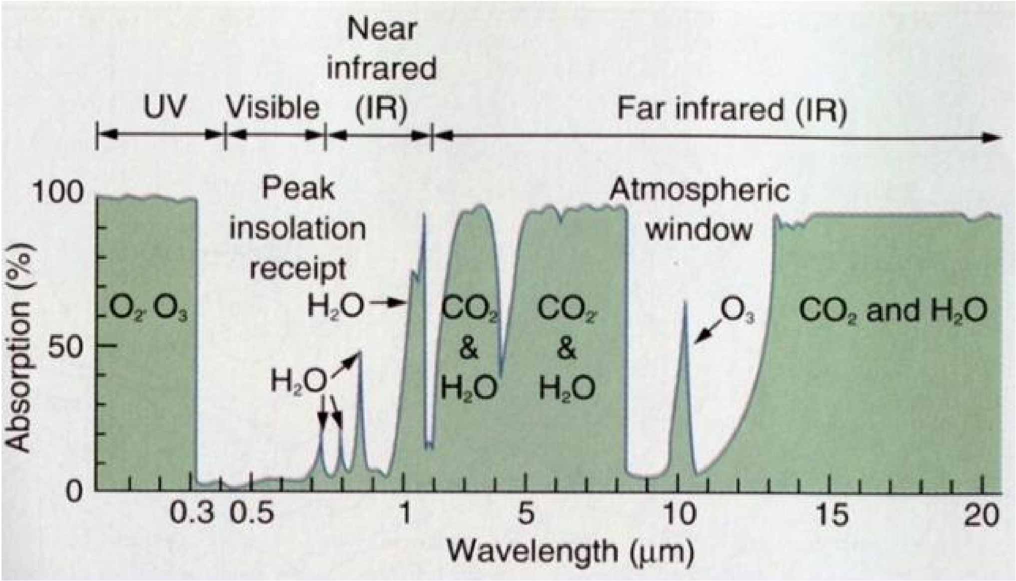

*Figure 3 - Absorption of solar radiation by gasses. Source: Chegg®Study.*

Considering what has just been mentioned, the importance of human pollution can be better understood: the anthropic activities set out before are becoming a greater and greater danger as they release in the atmosphere huge amounts of dangerous gasses, some of them already emphasized before, known as GreenHouse Gasses (GHG). Their peculiarity is the high absorption of the Sun and Earth wavelength bands and especially they remain suspended in the atmosphere for a long time continuing their negative action, entrapping heat and producing the fast increase of global temperature. Moreover, the damages do not depend on the location of the emission, because the gasses move throughout the atmosphere. These substances have been classified according to a criterion named “Global Warming Potential (GWP)”, which provides for a fixed time interval, a quantitative effect related to the carbon dioxide upshot. Indeed, this chemical is defined as a parameter to set and make comparisons with other substances, because it is the element that is commonly produced in each anthropic sector, and its presence in the atmosphere is high with an own resident time not negligible. The comparison between chemicals is displayed in tab.1, which reports the most important GHG with their GWP.

| **GHG** | **20 years** | **100 years** | **500 years** | **Time to reduce 1/3 concentration** |
|---|---|---|---|---|
| $CO_2$ | 1 | 1 | 1 | Century |
| $CH_4$ | 56 | 21 | 6,5 | Decade |
| $N_2O$ | 280 | 310 | 170 | Century |
| HFC-23 | 9100 | 11700 | 9800 | Years to centuries |
| HFC-32 | 2100 | 650 | 200 | Years to centuries |
| $SF_6$ | 16300 | 23900 | 34900 | Years to centuries |

*Table 1 - GWP - source: Uso Ottimale dei Sistemi Energetici Polito*

This paragraph therefore had the purpose of introducing one of the most serious contemporary problems, global warming, and placing it at the centre of this thesis. With the aim of considering new alternatives for those anthropogenic sectors that are contributing to this problem, and in particular to the energy production sector, through a renewable-based polygenerative plant, in such a way as to be a starting point and perhaps the subject of further studies, for an eco-sustainable future, guaranteeing the protection of the earth and its inhabitants. The following paragraph will aim to present the various world organizations that have already started this path and what goals they intend to achieve.

## 1.2 International treaties

In order to safeguard the wellness of the Earth and of its habitants, several global agencies have been founded, with the purpose of investigating, monitoring and studying these pollutant phenomena in more detail, finding all the future sceneries and consequently, trying to prevent future hostile scenarios. The fundamental goal is to mitigate damages produced currently by greenhouse gasses, finding alternative solutions as alternative fuel, different and new chemical/physical processes, in order to keep, without repercussions, the same lifestyle, but in a more environmentally cautious manner, thinking to the next generation. Nowadays the most important associations are:

- World Meteorological Organization (WMO), established in 1950 is a specialized agency of the United Nations which involves 193 Member States and Territories. It is based on an international cooperation at global scale for the development of meteorology and operational hydrology. WMO is dedicated to international cooperation and coordination providing general framework of monitoring, intervention and especially contribution to the safety, security and sustainable development of society as well as to the economic welfare, considering firstly the protection of the environment. Moreover, the WMO with Hydrological Services and National Meteorological provide weather, climate and water-related data useful for technology applications, and for monitoring the environment [5].
- United Nations Environment Programme (UNEP), founded in 1972, is endorsed by 193 Member States and it has the purpose to inform, enable and inspire nations and people to improve their quality of life, identifying and addressing the most relevant environmental issues, working in partnership with governments, the scientific community, the private sector, civil society and other United Nations entities and international organizations. The goals for the United Nations 2030 Agenda for Sustainable Development vary from the solution for the poverty and hunger in the world, to gender equality and eco-friendly economic growth [6].
- The Intergovernmental Panel on Climate Change (IPCC) was founded in 1988 by the WMO, and now it has 195 Member countries. It studies the science related to climate change, determining the state of knowledge, identifying agreement in the scientific community, finding where further research is needed, providing future impacts and risks but also options for adaptation and mitigation. The main topics are the physical science basis of climate change, the climate change impacts, adaptation and vulnerability and the mitigation actions of climate changes. The task groups produce reports where they summarize their development and the further study of topics/problems, providing innovative solutions and raising the knowledge [7].

These are only some of the many associations which take care of the safeguard and wellness of the planet, investigate and find the best solutions for an eco-friendly lifestyle. Moreover, as well as global entities exist, there are also associations at national level, imposed by the governments on their own territory. For instance, in the United States there is the Environmental Protection Agency (EPA) while for European countries there is the European Environmental Agency (EEA).

Among the most important and significant organization to protect the planet, the United Nations Framework Convention on Climate Change (UNFCCC or FCCC) also known as UNFCCC secretariat (UN Climate Change) is the most famous. UNFCCC is the United Nations entity which supports the global response to the threat of climate change. It was established in 1992 as Earth Summit in Rio de Janeiro and entered into force on 21 March 1994 after being ratified by enough countries. The State Members gather in negotiating sessions called Conference of the Parties (COP), several times each year, discussing, analysing and reviewing climate change reported data and information by Parties. During each COP, the Bureau is elected: it's the political and technical body of the Conference composed by eleven members chosen among the Parties, including the President, Vice-Presidents, the Chairs of the subsidiary bodies and the "Rapporteur". Each of the five regional groups (African States, Asian States, Eastern European States, Latin American and Caribbean States, and the Western Europeans) is represented by two Bureau members that are elected for an initial term of one year and may serve for no more than two consecutive terms. The purpose of the Bureau is to provide advice and help the President in the management: for instance, they help implementing the Convention's goals by establishing working programs for COP's activities, advise countries on issues concerning prevention, and solve environmental and technological problems, forming working groups on implementation and development to address matters. Moreover, it submits reports which take into consideration all the progresses performed. Until today, 25 global meetings have been organized. Among them those that have gone down in history for having been the most impactful for member states, urging a change for a better future, are COP3, also known as Kyoto Protocol, and COP21 best remembered as the Paris Agreement.

### 1.2.1 Kyoto protocol, COP3

The real first attempt to reduce GHG emissions was made on 11 December 1997 with the ratification of the Kyoto Protocol in Japan, as a result of the third UNFCCC negotiations. To be approved, the Protocol had to be accepted by at least 55 of the countries which contributed to the production of at least 55% of global $CO_2$. This requirement was reached only in 2004 with the ratification of the treaty by Russia and Canada, allowing its entry into force in 2005. The members of the Protocol have been divided into three main categories:

1. The Annex B non-EIT (Economy In Transition) countries, which are Germany, Japan, Spain, Italy, UK, France, Netherlands, New Zealand, Austria, Belgium, Norway, Denmark, Finland, Greece, Portugal, Ireland, Luxembourg, Switzerland, Sweden. Considering as industrialized countries, with heavy industry-based economies, they apply high consumes of fossil fuel for energy generation, which provide services and essential and non-essential goods for the human lifestyle, but at the same time generate high levels of GHG. These countries have emission caps.

2. Annex B EIT countries which are divided into small EITs, with less than 1 billion tonnes of $CO_2$ production, as Czech Republic, Bulgaria, Slovakia, Romania, Lithuania, Hungary, Slovenia, Latvia and large EITs with more than 1 billion tonnes of $CO_2$ as Russian Federation, Poland and Ukraine. They also have emission caps.
3. Finally, the non-Annex B countries characterized by a middle-low income. Their technological progress has improved in the last decades, as well as their economy, indeed some of them will become highly industrialized countries in the foreseeable future considering their rapid development. These countries don't have any emission caps because of the lower level of emissions, compared to the other Annex Countries.

The U.S.A, despite being responsible of the 36.2% of global $CO_2$ emissions, has never subscribed the Protocol. Canada removed its subscription before the end of the first period, while Russia, Japan and New Zealand have never taken part in the second one. Nowadays the Protocol is applied to only 14% of the global emissions.

Each State Member must respect a threshold for the reduction of GHG emissions, which depends on their individual economic development. The level of responsibility of each country varies therefore, depending on the amount of GHG emitted in the atmosphere. Even if the limits are different among countries, the most industrialized, the Annex B, were expected to reach the minimum target of $CO_2$ emission reduction (5.2%), within the protocol's first commitment period (2008 – 2012). Then, there was also a second period known as the Doha Amendment (2012 – 2020), where the minimum threshold was fixed at 18%. Therefore, the Kyoto Protocol introduced specific tools able to fulfil the commitments in a cheap-efficient manner: the flexible mechanisms (the "Kyoto Mechanisms"). They enabled international cooperation between Annex B countries and others which were not bound by any obligation to respect their reductive targets. The Protocol defined two main flexibility mechanisms that can be used by Annex B Parties in meeting their emission limitation commitments:

- Clean Development Mechanisms (CDMs) allow the reduction of the GHG emissions, realizing projects in non-Annex B countries by the industrialized annex B, producing at the same time both the right environmental development of the country, enriching it, and achieving the Protocol's objectives. The difference between the real amount of GHG emitted and the one which should be emitted without the realization of the projects is called "avoiding emission" and it is quantified as coal credit by Certified Emission Reductions (CERs). Indeed the positive aspect of the CDMs are lower costs for the reduction of emissions (because it is more convenient to operate in non-Annex B countries due to the lower cost of average life), the increment of the investment's revenue because it is also possible to sell the CERs produced (1 CER is equal to 1 ton of $CO_2$), finally it is an industrial and economic opportunity for Annex B countries to enter new financial markets in the field of clean energy, technological innovation, industrial requalification and energy efficiency. Thus, CDMs are designed to encourage production of emission reductions in non-Annex B Parties aiming to low carbon development.

- Joint Implementations (JI) allow the reduction of the GHG emissions, realizing projects in Annex B countries by countries of the same group. In this case the “avoiding emissions” are named Emissions Reduction Units (ERU), where 1 ERU is the equivalent of 1 ton of $CO_2$. The main difference between CDM and JI is that the ERU produced only in the Annex B countries cannot be sold but can only be used to actualize the Kyoto Protocol’s targets only in the country which produces the project or in the host country. Thus, JI encourage emission reductions in Annex B Parties.

Each Annex B country must submit an annual report of inventories of all anthropogenic greenhouse gas emissions and nominate a person in charge ("designated national authority"). Instead, non-Annex B countries have to establish a designated national authority to manage their Kyoto obligations, specifically the "CDM process".

### 1.2.2 Paris Agreement, COP21

Despite the huge effort conducted in the years after the COP3, many countries did not respect the environmental targets that were further analysed and studied for the safeguard of the Earth. The efforts performed were insufficient. For this reason, during the twenty-first Conference of Parties in 2015 in Paris, another important framework for the future was created, marking a milestone in the course of international efforts on global climate action. As for the Kyoto Protocol, the Paris Agreement would become binding only if at least 55 of the countries which contributed to the production of at least 55% of global $CO_2$ would ratify the Agreement. There were doubts whether some countries, especially the United States, would agree, but in 2016, with a joint presidential statement with China, they joined the Agreement making it valid for all the members.

The past experience with the Kyoto Protocol made clear the necessity to avoid enforcement mechanisms, the application of penalties or fiscal pressure (for example the carbon tax), because such measures didn't produce any positive effect. On the contrary, they encouraged bad behaviours. In order to further lower carbon pollution, each Party that ratifies the Agreement has to perform its personal target of emission reductions, called Intended Nationally Determined Contributions (INDCs) outlining its post-2020 climate actions, in a voluntarily manner to hold global warming below 2.0 °C or, at best, to limit it at 1.5 °C in the next century, because only the last warming scenario permits ecosystems to remain within the Holocene status (the current geological epoch). Instead, 2 °C or more of warming, produce irreversible perturbations of ecosystems. Scientists at NASA’s Goddard Institute for Space Studies (GISS) affirm that the worldwide temperatures are about 0.85 °C higher than during 1880–1920, increasing at a rate of roughly 0.15 – 0.20 °C per decade. Thus, the Paris Agreement should have the role of informant, as soon as possible, and help Parties making the best decision possible. The key component is to recognize the best adaptation at local, regional, national and international level, to create the conditions for long term positive effects on climate change, taking into account the needs of more vulnerable countries. The actual regime is not appropriate for the future sustainable development, but Parties acknowledge that actions should follow modern concepts to obtain the maximum results. Country-driven mechanisms must be performed in order to obtain the best results, because not the same technology is suitable for all the parties, it depends on the economy and morphology of the country. The intervention choice must be transparent, and should involve the participation of the population, taking into consideration vulnerable groups and communities, following the best available scientific approaches, integrating socioeconomic and environmental policies. In spite of the dissimilarity and variety of policies, the Paris Agreement aims to the collaborations between its components by sharing information, experiences and lessons learned, including planning and implementations. Moreover, the Paris Agreement supports the assistance of Annex-B countries with technical support and guidance, the identification of priorities and encouragement of future correct behaviours. Furthermore, exchanging information produces the strengthening of scientific knowledge on climate, including aids for research, finding gaps in the knowledge and future challenges for further improvements.

Periodically, each party should submit and update an adaptation communication, including its priorities, implementations and support needs, plans and action by describing the national goals achieved, in order to make the results public also for the other Parties.

The Paris Agreement brought attention to the important role of providing incentives for emission reduction activities, including tools such as domestic policies and carbon pricing: capital flows need to be increasingly directed to low-carbon solutions, then scaled-up and optimized. Carbon markets are necessary for the development of a future climate regime, which means that for policy strategies carbon pricing mechanisms should be established. Governments should take into consideration low carbon investments, and place a realistic, foreseeable regulatory and institutional framework. The benefits of carbon markets are maximizing efforts to reduce GHG emissions using most cost-effective strategies, stimulating investments in innovative low carbon technologies. Moreover, carbon markets increase fair competitiveness between participants, by incentivizing private sector solutions through existing and new technology in many fields.

A study [12] has shown that the mitigation of GHG emissions and the limitation of 2 °C warming can be provided imposing a cumulative $CO_2$ emissions budget constraint of 1300 [$Gt_{CO2}$] in the period between 2011 and 2100. Another study conducted by IEA (International Energy Agency) established that in order to maintain the temperature increment below 2 °C, the governments should spend USD 48 trillions on energy supply and efficiency investments between 2014 and 2035. Despite all these guidelines produced with a better knowledge and awareness of what is going on, the efforts are not enough. The next paragraph is going to focus firstly on a global vision and then on Italy, in order to better understand what measures have been chosen and what the actual conditions are.

## 1.3 Global energy scenario

Civilization goes hand in hand with evolution and development of energy technologies, from the prehistoric fire to fossil fuels and renewables. Energy evolution went through several transactions in terms of energy sources, technologies and ways of exploitation by societies. In ancient times the knowledge was underdeveloped, so the main sources of energy were animal and physic human power that were employed principally in the agriculture sector. During the mid-age also water and wind power were exploited, for instance in water/wind-mills, for the development of the average lifestyle. Everything changed in the 18th century: the industrial revolution started the transition toward the "fossil fuel economy", characterized by the introduction of steam engines and coal as key energy commodities. This important historical moment led to a rapid and relevant technological development: the knowledge of basic physics assumptions increased allowing the construction of even better machineries, which helped in each aspect of life. The following century, instead, was characterized by the penetration of electricity as energy commodity which continued to increase inexorably, in terms of consumption and production, until the 20th and 21st centuries, with the overfishing of fossil fuel (oil, coals and natural gas mainly), resulted in a dramatic climate scenario due to the emission of huge amounts of GHG as mentioned in the sections before. Even if the scenario seems to be irreversible, there is still hope considering renewable energy.

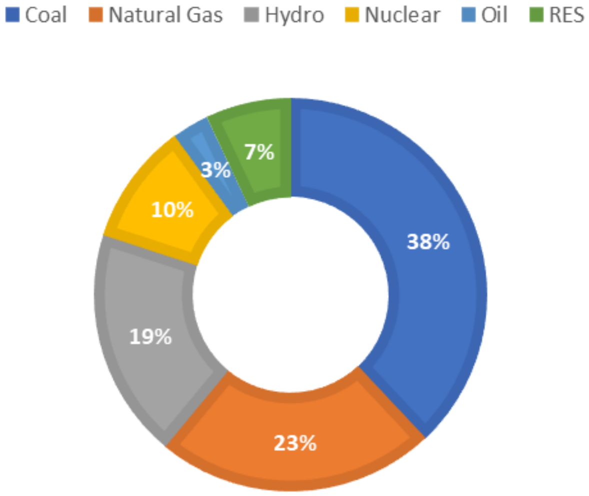

*Figure 4 – Global electricity production in 2018[2] – IEA 2019*

Given that the present thesis envisages the design and analysis of a polygenerative plant, with the aim of producing electricity and fuel such as SNG (Synthetic Natural Gas) and hydrogen in an eco-sustainable manner, it is of interest to report fig.4, which shows the latest data available on world electricity production, collected in 2018 by the IEA. RES (Renewable Energy Source) taken into consideration are only solar and wind production as well as geothermal at high enthalpy, whereas the nuclear commodity is not taken into consideration (10 %). Thus,

---

[2] 26730065 GWh, data source IEA: https://www.iea.org/data-and-statistics/data-tables?country=WORLD&energy=Electricity&year=2018

renewables only account for around 26 % of global electricity production while 64 % is still dominated by and dependent on fossil fuels. It is not a great result if compared with data of more than 30 years ago: again, according to IEA, electricity production in 1990 was 11’897’196[3] TWh, when globally renewables made up around 19.72 %. This shows that the share of electricity produced by renewable has actually slightly improved, despite all the literal and moral efforts that have been made. Fortunately, for sustainable development we are not only bound to the production of electricity, but also to the improvement of the efficiency of production systems.

Related to the low utilization of RES and the GHG emissions involved, in recent years another urgency has come up: the availability of resources. As displayed by the diagram for the production of electricity, it is possible to state that most of the primary energy consumed is produced through the use of fossil fuels, which are concentrated in few problematic countries because many of these suffer from high political instability and low overall development. Moreover, in addition to the supply problem, several world areas show a significant level of energy dependency, which means that if net energy imports divided by gross available energy are under 100 %, the country needs to import energy from other countries. Eurostat Statistics Explained [19] says that in 2018, in the European Union, the average on primary energy imports was 58.2 %. The total energy imported by the European Union in 2018 was 886 Mtoe (where one ton of oil equivalent is 11’630 kWh). Italy imports 146.56 Mtoe of energy, which correspond to 78.6 % of the total primary energy consumed in the country.

Unfortunately, there is another problem directly related to fossil fuels, in fact as discussed before the last and current centuries are characterized by uncontrolled high fossil fuel exploitation, which has led to the shortage of natural resources. The Earth Overshoot Day marks illustratively the calendar day in which humanity consumes the natural resources which the planet is able to produce for that year. The date is calculated each year by the Global footprint network (Gfn), a global organization which deals with environmental accounting, and calculates the ecological footprint. In 2019 the Overshoot day was on the 29th July; these terrible data tell us that humanity is consuming the planet resources faster and faster, 1.75 times faster than the natural ecosystem is able to regenerate them, overexploiting the planet. Following the current trend the resource depletion will increase year after year, due to the socioeconomic growth, causing further increase of energy consumption. Even if during recent years technological improvements in energy efficiency were done following the framework suggested by the Paris Agreement, the efforts turned out to be insufficient from the ecological and environmental perspective. More decarbonization goals are needed.

Data provided by REN21 [20], establish that in 2017 the average global Total Final Energy Consumption (TFEC) per capita was 53.6 GJ per person. In the same year, at a national level, the same indicator showed large differences ranging from 1.8 GJ per person in South Sudan

---

[3] Data by IEA: https://www.iea.org/data-and-statistics/data-tables?country=WORLD&energy=Electricity&year=1990

to 430 GJ per person in Qatar. In general, African countries were characterized by very low levels of energy consumption, on average 19.8 GJ per person. In China TFEC was equal to 60.1 GJ per person, in India to 18.3 GJ/person, in European Countries, still on average 94.2 GJ/person. Italy showed a slightly lower value compared to the European average, with a per capita TFEC of 82.4 GJ/person.

Therefore, taking into consideration all these assumptions is clear that the actual energy model is unsuitable, and there is an urgent need for a transition toward a new system paradigm. As discussed before, the increase in energy production worldwide, mainly from fossil fuels over the last century, had environmental negative effects. Moreover, the economic improvement of new developing countries could lead to even more severe effects if a radical energy transition is not undertaken in time: alternatives to fossil fuel have to be utilized in order to produce decarbonization. It is therefore necessary to produce electricity, but more in general energy, using renewable sources as solar photovoltaic power, collectors of solar or wind power, in conjunction with clean fuels such as hydrogen or synthetic natural gas. Moreover, taking advantage of new technologies as CCS (Carbon Capture and Sequestration) or rSOC (reversible Solid Oxide Cell), could be the right solution. Indeed, the present thesis takes as a model of analysis an UVAM (Unità Virtuale Abitativa Mista), and, taking into consideration all the innovative technologies above mentioned, aims to suggest how to produce commodities in an alternative green way, avoiding any pollutant emission.

In conclusion it is clear that a better sustainable development needs more renewable power contribution. IEA estimates that in 2015, the global energy consumption by all human activities is around 18 TW per year [26], a small amount compared to the energy coming from other RESs. For instance, it is estimated that only from the sun could be extracted each year 86000 TW, instead of wind-extractions (870 TW each year) and geothermal energy (44 TW per year). This huge potential could solve all energetic problems even if, nowadays, any appropriate technology is still not able to exploit all the energetic potential of the renewable sources. Nevertheless, the opportunity for sustainable development could represent a real future possibility.

## 1.4 Italy energy scenario

Focusing on Italy, the energy scenario is still dominated by fossil fuel. In the previous section it is already mentioned that, in 2018, 146.56 Mtoe of primary energy was supplied from other countries (principally natural gas and oil) on a total of 158.51 Mtoe of Total Primary Energy Supply (TPES) [25]. Historical data provided by IEA tell us that TPES trend has been decreasing in the last fifteen years, because of both the negative impact of the 2008/2009 global economic crisis, which reduced Italy's final consumptions and the industrial production, but also the improvement of overall efficiency of energy systems. Always considering data from IEA, in 2018 Italy's electricity final consumption amounts to 303.4 TWh [25], in this case the global crisis cited above was more impacted in this key energy statistic, because the wealth of the country collapsed and only in recent years the trend seems raise toward previously levels prior to the crisis.

| 2018 | Solids | Gas | Oil | RES | Eletricity | Total |
|---|---|---|---|---|---|---|
| **1 Production** | 0,25 | 4,46 | 4,68 | 34,00 | 0,00 | 43,40 |
| **2 Import** | 9,48 | 55,59 | 81,49 | 1,57 | 10,38 | 158,41 |
| **3 Esport** | 0,25 | 0,32 | 29,53 | 0,27 | 0,72 | 31,09 |
| **4 Changes in inventories** | 0,24 | 0,22 | -1,92 | 0,00 | 0,00 | -1,47 |
| **5 Availability of internal consumption (1+2+3+4)** | 9,24 | 59,51 | 58,57 | 35,30 | 9,66 | 172,28 |
| **6 Consumptions and losses of energetic sector** | -0,18 | -1,91 | -3,72 | 0,00 | -39,16 | -44,97 |
| **7 Electricity conversion** | -6,90 | -19,81 | -1,68 | -26,37 | 54,75 | - |
| **8 Final consumption (5+6+7)** | 2,16 | 37,80 | 53,18 | 8,93 | 25,25 | 127,32 |
| **Industry** | 2,11 | 12,64 | 2,88 | 0,13 | 9,48 | 27,23 |
| **Transport** | - | 0,83 | 37,06 | 1,24 | 0,99 | 40,12 |
| **Civil use** | 0,00 | 23,58 | 2,78 | 7,52 | 14,25 | 48,14 |
| **Agriculture** | 0,00 | 0,13 | 2,29 | 0,04 | 0,52 | 2,99 |
| **Not energetic purpose** | 0,05 | 0,62 | 5,02 | 0,00 | - | 5,69 |
| **Bunker** | - | - | 3,15 | - | - | 3,15 |

*Table 2- National Energy Balance, Italy, 2018, [25]*

Tab.2 shows Italy energetic balance. It reports data in Mtoe, showing each contribution required. Considering these data, natural gas (NG) with 59.51 Mtoe has a decrease of 3.3 % compared to 2017, but it is still the most used commodity for internal consumption. Immediately after NG comes oil, with 58.57 Mtoe, that on the contrary has a positive variation by 1.4 %. Last but not least: coal, with 9.2 Mtoe. The fossil fuel, as mentioned before, still has an important role covering the 74 % of internal consumption for Italy, while renewables increase their contribution covering 11.4 % with 3.3 Mtoe.

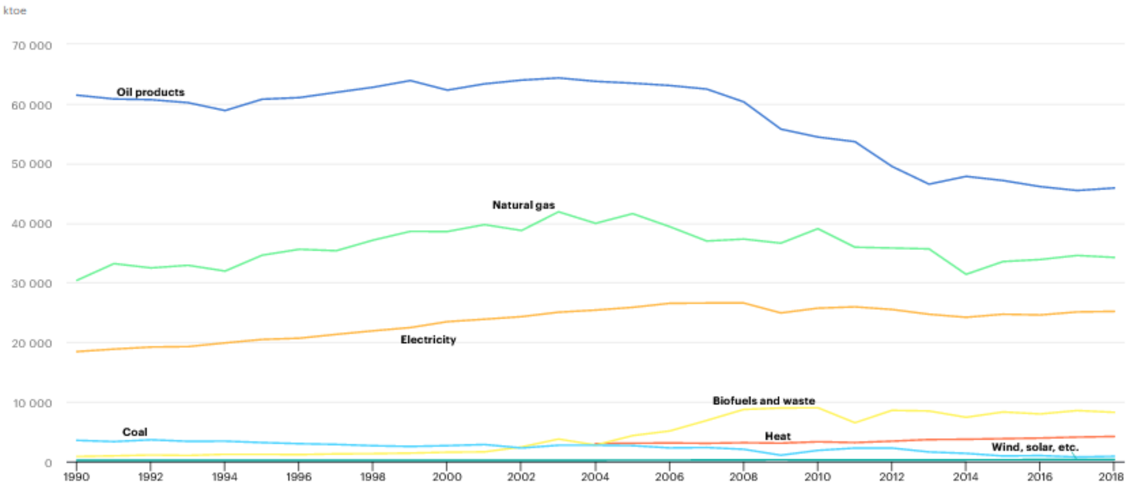

*Figure 5 - Total final consumption by source, Italy 1990-2018 [24]*

Fig.5 shows the Italian configuration of commodities used to provide energy for total final consumption since 1990. It represents the aggregate of all energy that is used to provide various energy services.  Oil and NG' trends tend to be flattered in recent years, continuing to assume too high values compared to RES (wind, solar, etc.), which is almost non-existent: 45'886 and 347 ktoe respectively.

From the point of view of energy, the 2018 report of the Italian Regulatory Authority for Electricity, Gas and Water informs that the total number of electricity producers in Italy are 13'311: 398 of them produce thermoelectric energy and are mainly characterized by a large plant, whereas 12'671 producers concentrate on renewable energy - quite a large number, considering that most of them are represented by private citizens. Indeed, these results were possible thanks to the liberalization process started in 1999, with a regulatory instrument: the Legislative Decree of 16 March, 1999 n.79. From this historic moment the electricity market developed in each of its supply chains, from production to end consumers. Production and sales became completely liberalized, while distribution was converted into locally licensed businesses. Terna s.p.a manages almost the whole electricity transmission grid. Therefore, as already highlighted, the majority of the renewable systems are exploited by the economy (small grid of the villages, and industries). This allows consumers to make different choices regarding supply sources but nevertheless fossil fuels still have a dominant role.

Another interesting topic for the thesis work is the electrification status in Italy. It is almost aligned with the European average, in turn higher compared  to the global one. Considering end-users, the transportation sector is characterized by the lowest penetration, while half of the final uses in commerce and services sectors are already totally electrified due to the higher density of electrical appliances and the wider use of air conditioning systems. In Italy, the residential sector shows the lowest electrification rate compared to the EU and world standard, making it a sector with wide potential for further electrification, considering especially both space and water heating. In the industrial sector, a wider electrification of the productive processes, both direct (including the use of electricity for heat generation used for industrial processes) and indirect (i.e. by using electricity for producing hydrogen or synthetic gases to be used in industrial processes), could be technically feasible over the next decades. In the transport sector, three main drivers will render electrification crucial: firstly, the reduction of air pollutant emissions and greenhouse gases, secondly the reduction of total transport costs and finally, the increase of reliability and system availability. Indeed, the substitution of internal combustion engines (ICE) with electric motors can deal with all these elements. Moreover, the actual possibility of increasing the electrification of transport systems is also related with technological advances in the batteries field and in energy storage in general. To perform all these goals, sectoral policies are needed in order to support the penetration of appropriated technologies coupled with a decrease of the electricity costs for final users. Currently the EU is overseeing the "Piano Nazionale Integrato per l'Energia ed il Clima" (PNIEC), promulgated in Italy in 2018, which aims to 43 % reduction of primary energy consumption and a 33 % reduction of greenhouse gas emissions (from energy sectors) by 2030, compared to the values of 1990 in order to respect and follow the general framework of the Paris agreement. This should be coupled with a share of 30 % of renewables in the total energy consumption by 2030, which should be covered by 55.4 % in the power generation, by 33 % in the thermal sector and by 21.6 % in the transport one. Moreover, over the years and supported by scientific progress, this national strategy will undergo changes in order to go head by head with it, and periodical consultation must be realized to obtain the best results. The constant update will be supported by monitoring and will allow a better planning of the energetic mix and its supply, the reduction of the risks connected with climate changes, health prevention for the population and the preservation of the natural heritage.

This last paragraph concludes the brief introduction on the current global and Italian condition regarding the complex political and administrative field of energy. The following chapter will illustrate the state of the art of the technologies of interest for the thesis, as well as a brief but complete description of hydrogen, a key element for this study and assurance for future technological developments.

# 2 Technologies: State of the art

The state of the art is a step of primary importance, especially in the scientific field, as it intends to make the reader aware of the current state of the debated technologies. Using it as a start, it is possible to distinguish the innovations that the study purposes attempt to develop. Initially, hydrogen will be introduced, the element which is the basis of the technologies that will later be treated: Power-To-X, rSOC and CCS systems.

## 2.1 Hydrogen

Digging into the history of hydrogen, we find first traces of its recognition by the scientific community in 1766, when the British chemist Henry Cavendish used pig bladders to collect a mysterious gas resulting from the action of vitriol (sulfuric acid) on metals. He noted that this gas burned in the air and produced water. He named it the “flammable air.” Later, in 1781, the French chemist Antoine-Laurent de Lavoisier, assisted by Jean-Baptiste Miller of Laplace, carried out the first chemical synthesis of water. He understood that it was a composite material, formed by flammable air (hydrogen) and “vital air” (oxygen). Lavoisier later named this strange flammable air hydrogen, which means “forming water” [27], [28]. Successively, this innovative element was always analysed better and better, until all properties that characterized it were discovered. Nowadays hydrogen can be used in many fields of application, using innovative technologies based on the principles of highly efficiency and sustainability, following the general framework of the Paris agreement, to realize the best possible future for the next generation. One negative aspect is that hydrogen is not a primary energy source because, although it is the most abundant element on Earth, it cannot be found in nature. However, rather than a barrier, this represents a large range of possibilities, since hydrogen can be obtained from a great variety of sources, but it requires energy to be separated from molecules containing those atoms. It can be considered as a secondary source of energy that requires a primary energy source like electricity, in order to be produced [29]. Moreover, hydrogen contained in natural gas, biomass (cellulose) and hydrocarbons can be extracted in a totally green way, if combined with different arrays of primary renewable energy sources, such as wind, solar, geothermal, nuclear and hydropower. Hence, hydrogen can be produced from a variety of resources (water, fossil fuels, or biomass) and is a by-product of other chemical processes. Among the candidates of alternative energy resources for replacing fossil fuels, hydrogen holds a preeminent position because of its environmental compatibility: among all the energy carriers, hydrogen has emerged as a friendly solution for climate change in global terms and air pollution in local terms. It has a high energy content comparable with hydrocarbon, a large amount of energy is released through its combustion.

Thus, considering hydrogen from the environmental point of view, it is clear that it could be a possible solution to Global Warming. As mentioned above, one of the amazing properties of hydrogen is that its combustion produces water and heat (exothermic reaction):

$$2\,H_2 + \;O_2 \rightarrow 2\,H_2O \qquad\qquad \Delta h^0 = -286\frac{kJ}{mol} \tag{1}$$

In the following sections hydrogen will be analysed in more detail, with the intention of describing its characteristic properties and what are, today, the main production methods related to this interesting gas.

The first formula, (1), shows the combustion of hydrogen. From a thermodynamic point of view $\Delta h^0$ is the variation of enthalpy, which represents the amount of heat released or absorbed depending on its value: for a negative enthalpy the heat is released (exothermic), on the contrary for a positive value it is absorbed (endothermic). The apex 0 means that the calculation of the thermodynamic variable is conducted considering normal conditions: 20 °C and 1 bar. The only product is water, considering this first property it is obvious the huge range of application, because the use of hydrogen avoids any problem related to the production of GHG and other pollutant chemicals. Using it as a fuel, for instance in the field of urban mobility, it can reduce smog and therefore allow the population to breath clean air, reducing at the same time the number of deaths related to local pollution, especially in the most industrialized areas. Always considering it as a fuel, in a hypothetical way where it can replace oil and natural gas in the power plant, it can mitigate or better solve all the GHG emission issues caused by the exhaust gasses. As will be demonstrated in the next section “2.2.1.1” another interesting application is the combination of hydrogen and carbon monoxide, which produces a chemical called syngas. For a century this gas has been analysed, studied and treated in various processes, and nowadays it is considered as one of the most valid alternatives for the future in the field of energy and chemicals production (as it is a precursor for other chemicals as SNG, methanol and other synthetic hydrocarbon). Another positive aspect of hydrogen exploitation is that it can be used to store energy, also to improve the transportation of energy from the place of production to the place of consumption, like electricity. Thus, considering its huge potential, the hydrogen economy will emerge in the near future.

### 2.1.1 Proprieties

The hydrogen atom, H, is the first element of the periodic table, it is the smallest and lightest of the atoms because it is characterized always by only one proton in the nucleus and only one electron which orbits around. Based on the number of neutrons present in its nucleus, hydrogen can exist in the form of three different isotopes. Its most stable form is the one with no neutron, it is also the most common (99% of all hydrogen in the entire universe). The second form is the deuterium, characterized by only one neutron in the nucleon and the last, the tritium, with two neutrons in the nucleus, known to humanity as it is present in nature only in traces caused by interaction between cosmic rays and the atmospheric gasses. Regarding the molecule of hydrogen, $H_2$, has two different configurations: ORTO and PARA form. The difference between them is the spin of the single electron outside the nucleon. The molecule configuration strictly depends on temperature: if it decreases, an exothermic conversion happens, from orto to para, producing heat. In case of chilling operations this process doesn’t help because it opposes naturally to it, increasing the total amount of removed energy required to decrease the temperature. As stated in the introduction to this paragraph (section 2.1), the first discovery of hydrogen dates back to 1766, since then there have been many studies on this element, and almost all of its nature has been discovered. The next table 3 reports the main interesting properties.

| **Properties** | **Values** | |
|---|---:|---|
| Gas density (273.15K) | 0,08988 | kg/Nm3 |
| Liquid density (20,3K) | 70,79 | kg/m3 |
| Boiling point (1bar) | 20,3 | K |
| Freezing/Melting point | 13,95 | K |
| Lower Heating Value (LHV) | 120 | MJ/kg |
| Higher Heating Value (HHV) | 141,7 | MJ/kg |
| Specific heat at constant pressure | 14,33 | kJ/kg K |
| Specific heat at constant volume | 10,296 | kJ/kg K |
| Specific volume | 11,99 | m3/kg |
| Low Flammable Limit | 4 | % |
| High Flammable Limit | 74 | % |
| Liquefation latent heat | 3,92 | kWh/kg |
| Coefficient of diffusity | 0,61 | cm2/s |

*Table 3 - Hydrogen properties*

Analysing the contents of the table, one of the most important and interesting properties for the energy field is the huge energy content of $H_2$ in term of mass, described by the variable $LHV_{H2(g)}$ (Low Heating Value) equals to 120 MJ/kg. It is one of the highest if compared to all the other fuels, gasses as well as solid and liquid. As can be seen from the LHV unit of measurement, it represents an energy content as a function of the mass of hydrogen considered, and has a very high value, but if we consider it from a volumetric point of view, the energy content is incredibly low and insufficient $LHV_{H2(g)} \cong 9.72\ MJ/m^3$. In economic terms, a low volumetric energy content is much more serious than a massive one, as this is generates a number of relevant issues because, the more space hydrogen needs to store, the more expensive the system will be where $H_2$ is stored. Fortunately, this problem can be overcome spending an amount of energy to alter the $H_2$ conditions in order to obtain a different, more suitable state. Usually, the variable on which we intend to act is the density "ρ", as the higher this parameter, the less volume it will occupy with the same space, because it will have a greater weight. This concept can be easily explained by considering the law of natural gases, explaining the moles (n) as mass (M) per molecular weight (MM) and making shifts from one member to another, in order to obtain the following equation:

$$\rho = \frac{p}{R^* T} \qquad (2)$$

It is easy to see how, by increasing the pressure, the density increases. The same variation occurs in the case of a decrease in temperature.

Therefore, as mentioned before hydrogen is the lightest gas because at room temperature (usually 20 °C and 1 bar) its ρ is around 0.0089 kg/m$^3$. However, increasing the pressure of the gas to 200 bar, its "ρ" increases, becoming 16.42 kg/m$^3$, while bringing it to 700 bar, the improvement becomes still more evident, reaching the value of 57.47 kg/m$^3$. Compared to the basic value for room temperature, this property is hugely upgraded, but from a technological point of view it is not enough as it would still be inconvenient at an economic level. Furthermore, the higher the gas pressure becomes, the more complex and expensive the operations to reach it, which means that the pressure in the gas state cannot increase beyond a certain value. In order to further increase the hydrogen "ρ ", it is necessary to operate on another parameter, its temperature. Liquefying $H_2$ at 77 K and 1 bar of pressure, the "ρ" increases at 71 kg/m$^3$. The liquid state provides better performance than the compressed gas, but, even if the density assumes a proper value suitable for technological purposes, the passage of state requires cryogenic processes, very expensive in terms of energy also due to the exothermic energy released by the passage of configuration from orto to para. There is still a third technology that allows to overcome these issues, a new technique discovered in recent years: the chemical absorption of the gas in a solid matrix, where the most performants are the metal hydrides. This method is less expensive than the previous ones, and it allows to achieve a higher density level, with an average of $\rho_{metal_H_2}$between 100 ÷ 200 kg/m$^3$, confirming itself as an important method of hydrogen storage for the future.

In addition to its peculiarity relating to low weight, hydrogen has another important characteristic, a thermodynamic feature. Hydrogen is characterized by its high specific heat, the ability to vary its temperature by exchanging energy with the surrounding environment. To highlight its energy potential, a comparison is therefore made with other natural elements, at standard condition: 0 °C and 1 bar. Hydrogen specific heat is 14.33 kJ/kgK, while air value is 1.055 kJ/kgK, and water is 4.186 kJ/kgK. The comparison shows an order of magnitude more for hydrogen, compared to the other two reference elements, demonstrating how useful its exploitation can be in terms of energy. For instance its exploitation in a thermal cycle, considering the same amount and the same variation of temperature, produces a bigger amount of thermal energy (heat = m*cp*ΔT) compared to the referent elements. Unfortunately, there are still many technological problems that prevent the use of hydrogen for thermal applications, as a power plant. It is not recommended because the temperature reached during the combustion is too high for some of the construction materials in the combustion chamber or turbine, like the joining materials. The heat can break construction elements and make them useless. Directly connected with the thermal potential of the gas, it has been mentioned its similar auto-ignition temperature (AIT) comparable with the one of the standard hydrocarbon fuels:

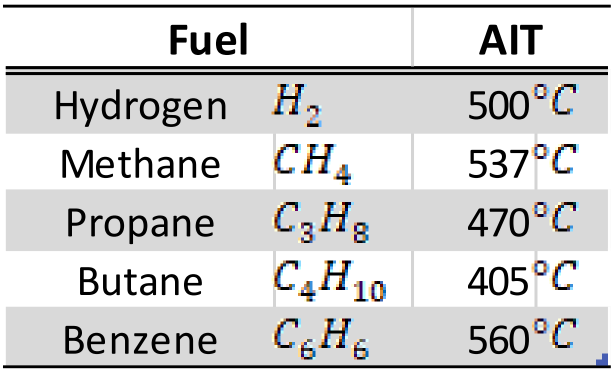

| Fuel | | AIT |
|---|---|---|
| Hydrogen | $H_2$ | $500°C$ |
| Methane | $CH_4$ | $537°C$ |
| Propane | $C_3H_8$ | $470°C$ |
| Butane | $C_4H_{10}$ | $405°C$ |
| Benzene | $C_6H_6$ | $560°C$ |

*Table 4 - Comparison of AIT between hydrogen and hydrocarbon fuels*

As already stated, despite these characteristics it is unusual to find hydrogen in thermal cycles because a great number of issues is still to be solved, but recently several studies have been conducted to allow its use in other innovative technologies as rSOC (electrochemistry application). This cell, which will be described more in depth in the next sections, will be the key element of the Polygeneration plant in this thesis work. It allows to connect different systems, which operate with different material flows, in a single plant. As for the hydrogen stream, it will be present in the rSOC presented in this thesis at 33.1 bar. Unfortunately, the negative aspect of this altered fluid for thermochemical applications is that the high specific heat makes the process truly expensive in terms of energy consumption required by the compressor of the gas to increase the pressure ($L_{compr} = cp*\Delta T/\eta_{compr}$).

Finally, the last element of note to be examined better in tab. 3 is the high coefficient of diffusivity of this gas. The importance of this parameter relates to considerations on plant safety. The parameter represents the tendency to escape from the storage system which contains the gas, so it is extremely important to take into consideration all the possible leaks and the environments that would be in direct contact with the escape of this gas, as if it moves outside, it could react with the oxygen present in the air, and possibly cause dangerous explosions.

Although it appears to be extremely complicated to work with this element, current research studying its applications, interactions and performance shows that if the system is well designed, the benefits of using it outweigh the negative aspects, in every area. Therefore, after discussing its main characteristics, it is of interest to understand what are, nowadays, the methods for producing this element that is not directly present in nature.

### 2.1.2 Production

Regarding hydrogen production processes, the upcoming years are mainly focused on technological challenges. The system efficiency is one of the most important elements in terms of conversion and purification: there is a need of improvements in order to further reduce operation costs. Moreover, the capital cost can benefit from it because if the technologies become more reliable the production would start generating at the same time the decrement of the initial cost for all the applications that exploit hydrogen. There are many other benefits such as the reduction of emissions which can be further realized by employing renewable resources in processes. Besides, all these new technologies have to be economically supported in order to provide the best development, by a framework that includes policies and the integration of the whole project stakeholders, along with the implementation of safety codes, standards, certifications and education programs that enhance the community acceptability and comfort with hydrogen technologies. At present the total world production of hydrogen is approximately 50 million tons per year. In energy terms, this corresponds to the equivalent of million tons of oil (130 Mtoe), which is barely 1.5 % of the world production of primary energy, which makes the gap between the use of these two energy sources evident. As already mentioned above, hydrogen is not available in the form of raw material in nature, but is obtained as a secondary product, for the most part by working and purifying fossil fuels, as hydrocarbons and coal. The following tab. 5 shows the most used applications to produce hydrogen, and briefly summarizes the strengths of these technologies, their weaknesses and the main future prospects that will allow us to achieve even more useful objectives.

| Technology | Strengths | Weaknesses | Prospectives/Challenges |
|---|---|---|---|
| 1) Steam reforming | Established and mature technology | High energy consumption and operating costs | improve product purification |
|  | High thermal efficiency | CO2 emissions | Renewable feedstocks (biofuels, biogas) |
|  | Cheapest production method (currently) | Catalyst deactivation | Process intensification (membranes, on-site units) |
| 2) Electrolysis | No pollution - decarbonized pathway | High electricity consumption | Improve efficiency |
|  | Hydrogen purity | Low system efficiency | Renewable sources integration |
|  | Link between electrical and chemical energy | High capital cost | Durable and cheap materals |
| 3) Gasification | Abundant and cheap feedstock (biomass) | High reactor costs | Product purification |
|  | Environment-friendly | System efficiency | Handle with feedstock variability |
|  | Favorable for large scale production | Greenhouse gas emissions | Process cost and efficiency |
| 4) Renewable and Biochemical production | No pollution - decarbonized pathway | Young technologies, high costs | Investiment costs |

*Table 5 - production technologies of $H_2$ [31]*

Of all the methods in the table, there is a common denominator that binds them all together: the plants in which they are used are currently still very immature technologically. Being contemporary technologies, some of them are not yet 100 % optimized, and therefore only operated in niche fields. This results in a high cost. By shifting attention to the future, despite this ever-present problem for young technologies, they promise to become low-cost and of primary importance. In the next paragraphs, these production methods will be illustrated in more detail.

#### 2.1.2.1 Reforming reactions

The most common and performant ways for hydrogen production are the reforming reactions, which consist mainly in using hydrocarbons in electrochemical reactions. The most important of the reforming reactions is the one that uses water, named the steam reforming of natural gas (Steam Methane Reforming, SMR). It is the most mature technology and common process to produce hydrogen around the world. It usually also uses a metal catalyst to favour the reactions between methane and steam, producing syngas which, as we already know, is a mixture of $H_2$ and CO. The process begins with the purification of raw methane containing pollutants, such as sulphur, halogens and siloxane compounds in order to avoid the poisoning of the catalyst in the next phase, in which reforming reactions take place. They are carried out using a nickel-based catalyst and under temperature and pressure ranging between 700 and 900 °C and 3-30 bar respectively. In eq. (3), reported below, are represented the chemical reaction that takes place and its energy content value under standard conditions ($\Delta h^0$). As can be seen, the main feature and directly related to the production of hydrogen is that it performs the higher ratio hydrogen/carbon, because through the reaction of one molecule both of methane and water, three molecules of hydrogen and only one of carbon monoxide can be obtained.

$$CH_4 + H_2O \leftrightarrow 3\, H_2 + CO \qquad \Delta\hat{\mathrm{h}} = +206 \frac{kJ}{mol} \tag{3}$$

From the thermodynamic point of view, a positive variation of specific enthalpy means that the reaction is endothermic, thus it requires heat to sustain the reaction. In general, in a plant that involves endothermic reactions, such as in the polygenerative plant presented in the thesis work, the endothermic reactions should have positive impact. They can be exploited as thermal sinks, in order to reduce the amount of heat that must be dissipated, avoiding an excessive increment of the system temperature. Despite this, the SMR turns out to be an advantage if high temperatures are reached, because it would mean that the equilibrium is shifted toward the products and specifically at 800 °C SMR is considered complete. For the plant studied in the thesis work, this is a positive aspect because the temperature involved is about 850 °C in the rSOC component, and right here the amount of hydrogen is fundamental.

Usually, in order to further increase the amount of hydrogen and, at the same time, reduce the amount of free carbon in the syngas produced, another reaction is coupled with SMR: the water-gas shift reaction (WGS), expressed in the next eq. (4).

$$CO + H_2O \rightarrow H_2 + CO_2 \qquad \Delta\hat{h} = -41\frac{kJ}{mol} \tag{4}$$

The reaction is thermodynamic characterized by a low exothermic behaviour; hence a low amount of heat is produced during the process. As for this chemical reaction itself, at high temperature the reaction is shifted toward the product, even if it is also shifted at lower temperature, between 200 and 350 °C. This range of temperature is suggested to be the best in terms of performance. This reaction will be resumed and analysed in more detail, as it is fundamental for the determination, during the modelling phase, of the key parameters in the rSOC.

Continuing the production process, the resulting gas stream (rich in $H_2$) is subjected to separation/purification from carbon monoxide and dioxide, by means of a final expensive clean-up section. Pressure Swing Adsorption (PSA) process is one of the common, nevertheless there are numerous others, such as the use of selective permeability membranes or the chemical absorption processes [30]. All of them enable the removal of carbon phases from the mixture, allowing to obtain a high purity hydrogen flow. These technologies would require extensive discussion and are therefore only named in this thesis work. After the detailed analysis of SMR, the second type of reforming reaction will be discussed, the DMR (Dry Methane Reforming), expressed in eq. (5). Unlike the steam, the reaction requires carbon dioxide in order to produce hydrogen.

$$CH_4 + CO_2 \leftrightarrow 2\,H_2 + 2\,CO \qquad \Delta\hat{h} = +247\frac{kJ}{mol} \tag{5}$$

This process is quite interesting because from the chemical point of view it directly involves carbon dioxide, useful to reach the environmental goal of GHG emission reductions, and from the thermal point of view it is more endothermic than the SMR, so it is considered as a better thermal sink. The worst aspect which makes the reaction unprofitable is that, in order to perform such a process, both one molecule of methane and one of carbon dioxide are consumed, producing two molecules of hydrogen and carbon monoxide. It means that the ratio between hydrogen and carbon is equal to one, too low to perform a hydrogen enrichment in the syngas stream. Furthermore, considering the kinetics of the reaction, in a process involving SMR and DMR, the former is favoured over the latter as its reaction rate is much higher. This will be an important consideration during the modelling phase of the methanation reactors involved in the polygeneration plant.

#### 2.1.2.2 Electrolysis

Electrolysis is an electrochemical phenomenon that allows the production of $H_2$ using water as a primary source. The device that exploits this innovative natural phenomenon is the rSOC, and specifically the SOEC (Solid Oxide Electrolytic Cell). A very detailed discussion will be carried out in the following chapter "3.2".

#### 2.1.2.3 Gasification

Gasification is another important process presented in tab.5. In general, its aim is to improve the fossil fuel quality, increasing the efficiency by transforming it into a material with higher thermochemical potential. This purpose is achieved by increasing or introducing through chemical reactions hydrogen into the composition of the initial fuel. Thus, the gasification process converts any carbonaceous (carbon-based) raw material such as coal into fuel gas, also known as syngas. Then syngas can be treated in order to produce hydrogen or another alternative chemical compound, more convenient and suitable for the target process.

The main advantage of gasification is the environmental solution to global warming related to fossil fuel consumptions. Combined with technologies that filter the pollutants produced during industrial processes, it would be possible to exploit in an eco-sustainable manner these resources, which until now have caused an uncontrolled increase in pollution. Furthermore, all raw materials such as coal, industrial residues, asphaltenes, heavy oils, gas or biomass, which are very harmful from an environmental point of view, and not very profitable from an energy point of view, would be exploited in a safe and profitable way through their conversion into syngas. Thus, this would make a low-value product or waste monetizable and harmless. In the future this process could become an increasingly important part of the world's energy and industrial markets. In particular, of all resources, coal, with its stable price and abundant availability throughout the world makes it the main material option for gasification technologies going forward.

The chemistry of gasification is quite complex. It is accomplished through several physical transformations and chemical reactions, but in general the most important are the "gasification" and "pyrolysis" ones. The first one consists in a partial oxidation of fossil fuels, which means that less oxygen is present compared to a stochiometric reaction. This allows only a partial combustion producing carbon monoxide and hydrogen, and in a minor amount also carbon dioxide and water. Going into more detail, as a first step the fuel is heated up to around 600 °C in total absence of oxidant agent. This makes the vaporization of the volatile parts as light gasses and tar, remaining with only the solid part (char and ashes). Successively, char is gasified by endothermic reactions with oxygen, steam and hydrogen. The heat required is auto generated by the exothermicity of the partial oxidation. At the end, syngas is produced, depending on the temperature, pressure and time of residence, its composition can vary. On the other hand, pyrolysis is a thermal decomposition of fuel carried out in total absence of oxidant agent. In this case the volatile part is not vaporized but transformed into gasses and/or liquids such as oils, while the fixed carbon is transformed into char. Usually both pyrolysis and gasification phenomena occur in reactors. However, based on the substance being processed, the process times vary substantially and usually one tends to prevail over the other. For example, for coal, the pyrolysis process is negligible as it is really fast, while for biomass, composed of stronger molecular structures, pyrolysis is slower than gasification. Considering the objective of the paragraph, for the production of hydrogen it is more convenient to discuss the phenomenon of gasification. So, the fig. 6 [31] below shows even more in detail the most important reactions involved inside a gasification reactor. Considering for example coal as initial material, the starting carbon content is quite high. During the process the initial composition varies and eventually, the main elements which can be distinguished and found after reactions are carbon monoxide, carbon dioxide, hydrogen, water and methane, making the final composition of the syngas vary, as can be seen in the column on the far right.

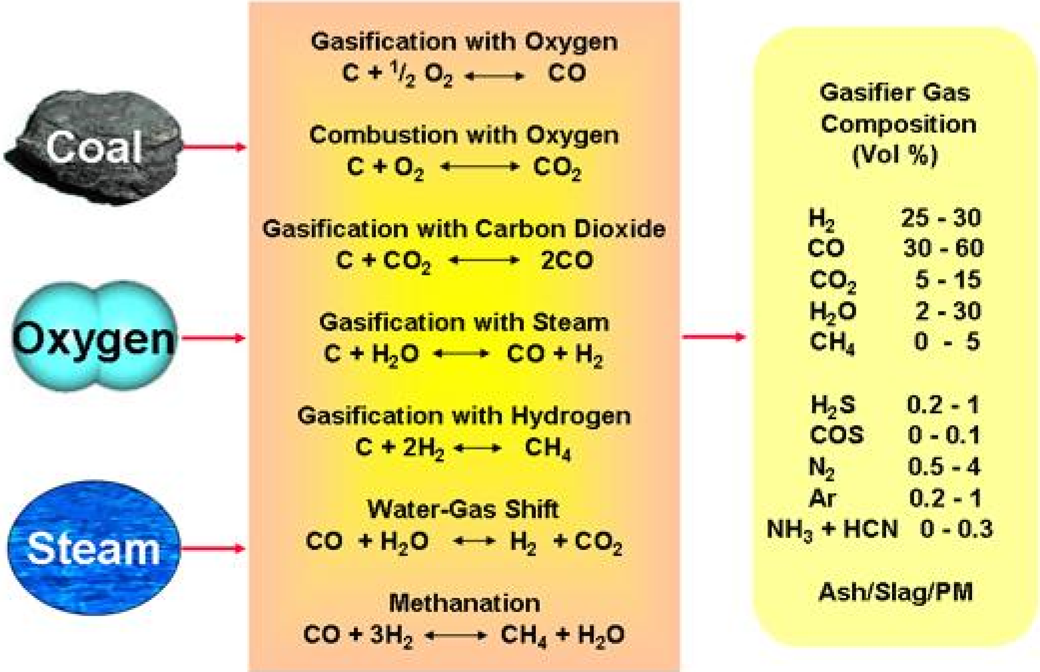

*Figure 6 - main reactions involve in gasification [31]*

In general, gasifier reactors can be classified according to a wide variety of characteristics such as bed temperature and type, pressure, oxidant flow through the equipment and ash formations. The oxygen agent is fundamental for the temperature control of the reactor because the reactions between fuel and oxygen are exothermic and can be used to enhance the temperature level, while reactions between fuel and steam or carbon dioxide are endothermic, so they have the opposite behaviour of requiring/subtracting heat. This means that the control of the amount of oxygen is important for the best efficient operations, in order to obtain the most suitable temperature which directly influences both the efficiency and the cost of operations. While the presence of ash influences the choice of temperature because if the temperature is below their softening point, they remain solid and are easy to be removed, but if the temperature is above the ash melts down and they become slag, a material characterized by really high viscosity. In this case its remotion can be performed only increasing the temperature, reaching a proper suitable level for the cleaning purposes.

From the point of view of the technologies in which this process is applied, the most conventional group of reactors considered are entrained-flow, fluidized-bed and moving-bed gasification technologies. Currently entrained-flow gasifiers are the most efficient alternative and have the smallest environmental impact and the largest production capacity, thus they represent the major part of the commercial market for centralized syngas plants. This technology is characterized by operating at high temperatures (1100-1500 °C), which allows good conversions in short reaction times, and avoids technical limitations in the feedstock type. At the second place there are fluidized-bed reactors, which offer a homogeneous temperature environment promoting the heat and mass transfer between the reactants. The main advantages of these gasifiers are their easy scale-up and adaptation to changes in the feedstock, as well as the better temperature control, whereas their drawbacks are related to the need of specific particle sizes and lower conversion compared to other gasification options. Lastly the moving-bed reactors, are commonly used for biomass gasification and are divided into co-current (downdraft), and counter-current (updraft) gasifiers. Among these, downdraft gasifiers are the preferred option for small scale application, and on-site applications due to their relatively easy design, fabrication and operation, as well as their low tar content in the product.

#### *2.1.2.4 Renewable and Biochemical $H_2$ production*

Lastly the production of hydrogen from renewable sources will be described. Technological progress across the years created valid alternatives to fossil fuel for the production of hydrogen, even if many of them are still in development stages. Both renewable and biochemical methods of production are clean and eco-friendly, as well as quite interesting in terms of environmental safeguard as it is established by the general framework of green policies. From the renewable point of view, the main aim is to transform the energy, thermal or electricity, produced by RES, in a stack form of energy through hydrogen production. This could overcome many problems related to the fluctuation of energy produced using RES and respects all the necessity of the load requests. The first and most interesting technology is the one of the photo-electrochemical cells. Its physical principles of operation allow it to directly produce hydrogen from sunshine and water, as a sort of photovoltaic cell devoted to the storage of sun energy in $H_2$. Another production method consists not of a specific technology, but of a series of processes that take the name of chemical loop. These thermochemical processes are driven by heat, which can be collected through RES, as solar irradiance concentration for instance. In general, the chemical loops are a series of chemical reactions in the form of a closed loop which generate useful effect in one or more intermediate steps. These are processes that have not been studied for a long time, and knowledge in this area will certainly grow in the future, resulting in more and more benefits. Today, in fact, the theory reveals that the benefits of these chemical loops do not concern only the area of $H_2$ production, but also other innovative and prominent processes such as fuel decarbonization, CCS and so on.

Further production methods of $H_2$ are, moreover, the biochemical methods. In general, they exploit microorganisms, vegetation such as micro-algae cultures and wastes (wood, agricultural crops, human and animal residues). Through the use of low value materials, hydrogen is produced without any ecological perturbations. Moreover, these natural processes are highly controlled inside a reactor, in order to avoid any possible pollutant products. They are named bio-reactors, and they must be thermal controlled, because the organisms used in the processes can survive only under specific conditions.

The combination and/or integration of other mature technologies, such as conventional gas cycles, with these biological processes, allow to obtain enormous advantages. Both from an energetic and exergetic point of view, and from an environmental one. For example, a benefit would be that of being able to clean the exhaust fumes of the highly polluting thermodynamic cycles, storing them inside the bio-reactors. Inside them, the microorganisms present operate through biochemical reactions, "feeding" on the gases. The exhaust gases are completely purified, avoiding an emission that is harmful to the environment, while the products of this process are many and vary according to the type of gas and the type of organism. In general, algae growth can be obtained, from which biofuels, cosmetics, foods, medicines etc. can be obtained. Other gases can be produced, to be used as a precursor of chemicals in other processes.

The next section will analyse in detail the technologies adopted in this thesis work project, which are directly connected with hydrogen or gas compounds that contain it, both from a production and a consumption point of view. In particular, the rSOC, which in SOEC mode will be able to exploit water to produce hydrogen, or water and carbon dioxide to produce syngas. Or in SOFC mode, in order to produce electricity to support a total urban load of 30’000 people, using SNG (Synthetic Natural Gas) which will be transformed, through appropriate reactions and components, into hydrogen and carbon monoxide.

## 2.2 Reversible Solid Oxide Cell – rSOC

Nowadays, one of the most promising technologies in the energy field is the rSOC [32], [37]. Its use allows to exploit highly efficient innovative processes, with benefits also from the environmental point of view, because, as already seen in paragraph 2.1, working with certain elements such as hydrogen/water, waste products are not the classics GHG but rather water/hydrogen, or syngas, if there is also the presence of CO/$CO_2$ chemical elements.

The most important feature of such technology, which distinguishes it from other electrochemical devices is the flexible possibility to operate efficiently in electrolysis mode, named SOEC [34], or in fuel cell mode, named SOFC [33]. The choice of mode, as will be seen in chapter "3", will depend both on the request of the power grid and on the availability of RES. In fact, the project presented in this thesis work aims to satisfy the electricity needs of a small town of 30 thousand people, and to do so in an eco-sustainable way, a dedicated photovoltaic system coupled to an rSOC is used, a key element within the entire polygenerative plant. The combination of these two technologies results in an improvement and stability of the electrical grid, flattening the transient curve of electricity fluctuation produced by the intermittent RES, which is strictly dependent on the meteorological conditions: in fact the sunshine is not available at night, meaning zero electric production by PV plant.

In general, in order to respect the decarbonization objectives set, a higher penetration of intermittent renewable energy sources in the energy mix poses certain critical challenges that rSOC can solve: the bidirectional operability enabled, as regards the SOEC mode, an efficient energy conversion from RES to chemical storage in form of $H_2$ or SNG, depending on starting fuel. Avoiding the waste of the electricity surplus that results sometime during the day. On the other hand, in the reverse mode as SOFC, where $H_2$ taken from storage section (for instance) or SNG taken from the natural gas grid can be exploited in order to produce electricity, fulfilling the electric needs for possible loads.

### 2.2.1 Introduction and field of application

Until today the hypothetical autonomy of small grid is unthinkable, because the conventional power plants would be too expensive if they were designed in small size, and also the most problematic issues of GHG deriving from the conventional fossil fuel have taken to the current problems. Another negative aspect is the low efficiency of these technologies, because they require many energy conversions: starting from the primary energy stored as chemical energy inside the fuel, in order to produce electricity the fuel has to be burn (combustion), converting chemical energy into thermal one, then the hot exhaust gasses are sent in a turbine which transforms the thermal energy (proportional to the kinetic of the gasses) into mechanical energy and finally, using an alternator, the conversion into electric unit takes place. During each passage, losses occur (such as thermal losses, efficiencies of devices, irreversibility, etc.), decreasing the performance of the whole system. Despite all of this, in the last decades new emergent technologies as rSOC have been discovered and studied in order to overcome these issues. One of the many rSOC's benefits, in specific when it operates as SOFC, is that it could directly convert chemical energy into electricity, ensuring higher efficiency than other conventional methods of production. Moreover, the contemporary researchers are studying systems which combine this innovative device with other technologies, in order to further increase the efficiency and to produce a green development for the future applications. Thus, the global interest is driven to the use of RES, because its free energy supply can be used to exploit the process that characterized rSOC operations, at the same time producing little, if any, GHG emissions.

Basically, rSOC is an electrochemical cell where a global transformation is performed, but without any physical contact between the reagents. Such transformation is possible due to the design of the cell: it is always structured in anode electrode, cathode electrode and electrolyte layer between the two. The first, the negative electrode, is where the reaction of oxidation occurs in which there is a delivery of free electrons to an external circuit. The second part of the rSOC, cathode, the positive electrode, is the side where the reaction of reduction happens in which there is a gain of free electrons from an external circuit. Finally the electrolyte layer, which physically separates anode and cathode, where only ions can easily pass through, unlike electrons that pass inside an external circuit and molecules, both reagents and products, which respectively are coming or are sent from/to the outside environment. They can continuously supply the system until the stream flows (rSOC is an open system). Regarding the external circuit, it is an electric conductor which links anode with the cathode to promote an easy passage for the electrons produced by the partial oxidation reaction. Therefore, the charges separation gives rise to generation of electrical fields on both electrodes, creating a potential difference (ΔV). Moreover, if the external circuit is close to a load, it allows the circulation of electrons inside it, producing a current (I). The presence of a current I, and a potential ΔV, generates electrical power ($W_{el}$).

$$R_1 + R_2 \rightarrow P \tag{6}$$

$$R_1 \rightarrow O_x + e^- \tag{7}$$

$$R_2 + O_x + e^- \rightarrow P \tag{8}$$

The equations above describe the chemical process that happens inside the rSOC environment. Eq. (6) is the general global reaction that involves all the electrochemical devices, where R are the reactants, and P the product, while eqs. (7) and (8) are respectively the partial reaction of oxidation and reduction that occur separately in the electrodes.

In general, electrochemical cells are classified by the material of the electrolyte layer, which in turn determines the range of temperature operation. In the next paragraphs "2.2.2", the rSOC's materials will be analysed more in details. The rSOCs are characterized by several materials of composition, which are strictly related to the technological issues due to the assembly of different layers. Regarding the costs, as some materials are rare or are produced in small quantities globally, the price of the whole device can be really expensive. Obviously, this increases the capital cost of the initial investment, making it an economically incompatible technology and therefore not taken into consideration, despite its multiple advantages from the point of view of both energy efficiency and eco-sustainability. Last but not least, the temperature. It is a key parameter because depending on it, the electrochemical devices vary their performance, both in terms of power consumed from the electrolysis, and in terms of power generation if it works as a fuel cell. Temperature is important to choose the chemicals which are utilized as reagents influencing the products that can be obtained, which is a truly important factor, as the field of application of the electrochemical cell depends on it. In fact, starting from the temperature, it is possible to study the thermochemistry of the reactions that take place inside the rSOC, optimizing the quantities produced, reducing consumption, and above all, from the point of view of the materials used, it allows to design the rSOC with the most suitable material, i.e. the one that undergoes the least marked degradation phenomena at the chosen temperatures.

| Technology | Operational Temperature | |
|---|---|---|
| Solid Oxide Cell | 700 ÷ 800 | °C |
| Molten Salt Cell | 600 ÷ 650 | °C |
| Phosforic Acid Cell | 250 | °C |
| Proton Exchange Membrane | 50 ÷ 80 | °C |
| Alkalyne Cell | 50 ÷ 80 | °C |
| Direct Methanol Cell | 50 ÷ 80 | °C |

Table 6 – Electrochemical cell state of the art

Tab. 6 shows the several technologies present nowadays, in the research field and already on the market, classifying them according to the temperature value in which they operate [40]. The greater the temperature range, the more stationary the cell operation will be. For instance, at the moment of switching on the device, from cold, therefore to room temperature, the cell must be brought to the operating temperature, and the higher this temperature, the longer it will take. It means that is better longer periods of operation avoiding as stand-by moments as possible due to higher thermal consumptions respect devices with lower levels of temperature. Consequently, electrochemical devices such as PEMs (Proton Exchange Membranes), which operate between 50 and 80 °C, as table 6 shows, will be optimal for more dynamic purposes such as trucking engines. In any case, the one of most interest for this thesis work is the Solid Oxide Cell, the only one which can operate as fuel cell and electrolyzed. The reason is because the polygenerative plant in question must meet the electricity needs of an urban network, which means that it is going to be a small power plant, operating in steady state conditions. As will be explained in the hypotheses of chapter "3.2.1", the transitory between SOEC|SOFC operation and vice versa will be neglected, allowing the hypothesis of always working in steady state, whatever the mode of operation. Secondly, from the point of view of the range of temperatures, it is coherent with the rest of the devices involved in the plant, such as methanation section: in fact, even if it operates at lower temperatures, around 200 ÷ 300 °C, their excess of temperature can be exploited for thermal uses in the rest of the system. Another positive aspect of working with an electrochemical device at a high temperature of operation, is that it improves all the transport phenomena characteristic of the cell, enhancing its efficiency. In confirmation of what has been said, there are many scientific articles that in recent years have focused on the study of the performance of rSOC, such as in [35], [36], [37], which confirm that among electrochemical cells, the SOC has improved electrochemical phenomena, it is more suitable for stationary application and for small scale $H_2$ generation applications.

#### 2.2.1.1 Chemical reactions

As mentioned before, the peculiarity of the rSOC is that it can operate both in SOFC and in SOEC mode. The first one also takes the name of "Galvanic Cell". This is a particular device characterized by the spontaneity of the electrochemical reactions that take place inside it. A reaction is said to be spontaneous if it has a negative Gfe (Gibbs free energy, $\Delta G$). In fact, considering a general chemical reaction that can take place in a galvanic cell, and calculating its enthalpy ($\Delta H$) and entropy ($\Delta S$) variation, expressed as the difference between the values of the thermodynamic variable between products and reactants, the result is always: $\Delta G = (\Delta H - T * \Delta S) <0$. This thermodynamic imbalance is precisely the physical explanation of the spontaneity of the reaction, in the sense that the chemical reactants interact without any need for external inputs, producing the products of the reaction. Therefore, SOFC exploits the spontaneity deriving from these thermal phenomena in electrochemical reactions, with the aim of producing electrical energy thanks to the free electrons circulating in the external circuit, just as can be seen in general eq. (7), allowing to directly transform the chemical potential of the reactants into electrical power. On the other hand, the other modality of the rSOC, the SOEC, is called "Electrolytic Cell", and its behaviour is the reverse of SOFC. The electrochemical reactions that take place inside it are not spontaneous, as their Gfe is positive. This means that in order for the reactions to take place, as the general eq. (7) shows, the cell needs an external input, consuming electrical energy. This phenomenon is extraordinary. In fact, just as it is applied for this thesis work project, it allows to store electrical energy in the form of chemical elements, such as $H_2$ or syngas, in order to use them in a later time of greater need. This is a valid alternative to common batteries, and precisely from the point of view of the fluctuation of renewables, its intelligent integration would allow in the not-too-distant future to stabilize its oscillatory trend [38].

The following fig. 7 shows the two operation modes of rSOC, considering the most common fuels and products that are involved in this technology. In the fuel channel, $CH_4$ | CO | $H_2$ perform the function of fuel in SOFC and that of product in SOEC. $H_2O$ | $CO_2$ instead, perform the function of product in SOFC and of fuel in SOEC. Instead, in the oxygen channel, the oxygen

$O_2$ that interacts in electrochemical reactions does not derive from a pure stream of oxygen but from atmospheric air, which contains 21%$_{mol}$ of it.

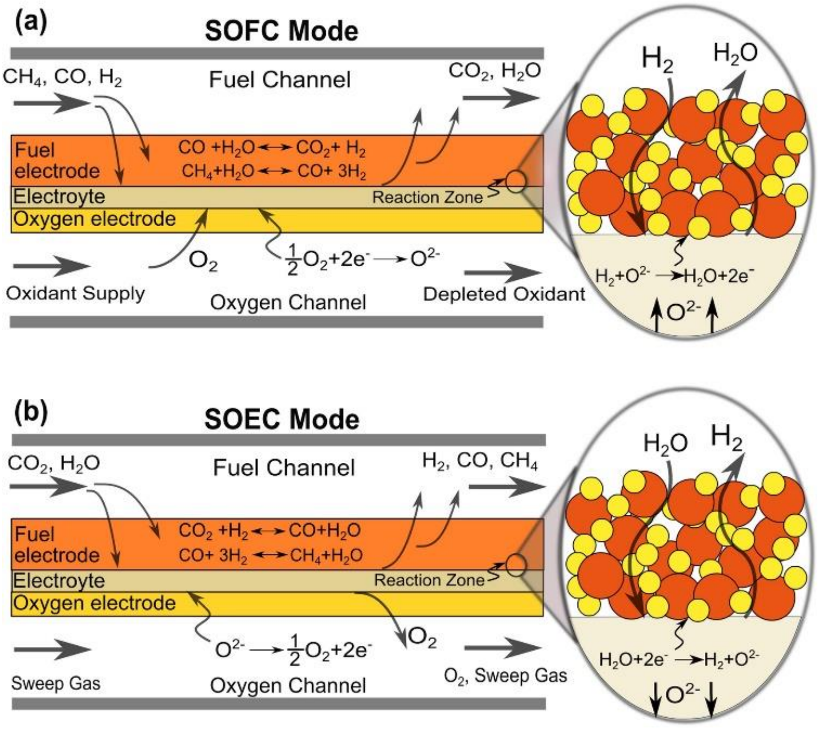

*Figure 7 - (a) fuel cell operation; (b) electrolyser operation*

Focusing on the chemical reactions, the SOFC operation will be analysed first. In this mode, the fuel electrode is the anode, while the oxygen electrode is the cathode. As it is known from electro-chemistry knowledge, the cathode is always characterized by reduction reactions, while the anode by oxidation ones. Reduction reactions decrease the oxidation number of the reactant and are characterized by the capture of free electrons. While those of oxidation tend to increase the oxidation number of the reactant, releasing electrons in the system.

Therefore, considering the study of the present thesis work, when operating in SOFC the incoming fuel is SNG taken from the gas distribution network. Furthermore, as a hypothesis, a composition of the SNG equal to that of the stream produced in the methanation section is used, corresponding to 97%$_{mol}$ of $CH_4$. Furthermore, as indicated in chapter "4.3", the presence of certain chemical reactions in the anode, such as WGS, eq. (4), SMR, eq. (3), and DMR, eq. (5) of paragraph “2.1.2.1”, by reforming the reaction, will also allow to hypothesize $H_2$ and CO as fuel for SOFC. Therefore, the electro-oxidation reactions that occur in the anode are made explicit:

$$CH_4 + 4O_2^{2-} \rightarrow H_2O + CO_2 + 8e^- \tag{9}$$

$$H_2 + O^{2-} \rightarrow H_2O + 2e^- \tag{10}$$

$$CO \ + O^{2-} \rightarrow CO_2 + 2e^- \tag{11}$$

While the electro-reduction reactions in cathode side are:

$$2O_2 + 8e^- \rightarrow 4O^{2-} \tag{12}$$

$$\frac{1}{2}O_2 \ + 2e^- \rightarrow O^{2-} \tag{13}$$

For the SOEC, similarly as for the Gfe of the reactions, the role of the electrodes is also reversed. The fuel electrode becomes the cathode, while the oxygen electrode becomes the anode, the opposite behaviour compared to SOFC mode. This feature finds an enormous benefit in the modelling phase, as the thermophysical values such as ΔH or ΔS are equal and opposite between the two modalities of the rSOC. This allows to calculate them only once. This aspect is highlighted if the reactions are made explicit. Therefore, in the anode side, the electro-oxidation reactions turn out to be:

$$O^{2-} \rightarrow \frac{1}{2}O_2 + 2e^- \tag{14}$$

While the electro-reduction reactions in cathode side are:

$$H_2O + 2e^- \rightarrow H_2 + O^{2-} \tag{15}$$

$$CO_2 + 2e^- \rightarrow CO + O^{2-} \tag{16}$$

As it happens in the SOFC mode, even in the SOEC the high condition of operation, in terms of temperature and pressure, and the simultaneous presence of chemical elements as $H_2$ | $H_2O$ | CO | $CO_2$ in the cathode, enhance the occurrence of other reactions. The most important is the WGS, already expressed by eq. (4) in the previous paragraph “2.1.2.1”, which allows the content of $H_2$ and CO molecules to be balanced within the electrode. The other chemical reactions of interest are those of methanation. These reactions will be better discussed in the next paragraph “2.3.1”, as they constitute the pivotal process for the production of $CH_4$ within methanation reactors. Their chemical formulas are expressed by eq. (17) and eq. (18):

$$4H_2 + CO_2 \rightarrow CH_4 + 2H_2O \qquad \Delta h^0 = -165 \text{ kJ/mol} \tag{17}$$

$$3H_2 + CO \rightarrow CH_4 + H_2O \qquad \Delta h^0 = -206 \text{ kJ/mol} \tag{18}$$

From the equations above it can be deducted that eq. (18) has exactly the opposite behaviour of the SMR, eq. (3). The reactants are nothing more than syngas, $H_2$ and CO, mixed in such a way as to have an H/C ratio of 3, and the product is methane precisely. As for the other equation, (17), its behaviour is extremely similar to the reverse reaction of SMR, the substantial difference lies in the fact that the CO reagent is replaced by $CO_2$ and that the proportions between products and reactants are different. Furthermore, since chemical reactions are complete, the enthalpy variation values in normal condition are also reported.

It is noted that eq. (18) is slightly more exothermic than the other. This is explained by the fact that, during the chemical reaction, more energy is needed to break the $CO_2$ bonds than those of CO alone. Consequently, in the inverse SMR there is more energy released, i.e. greater exothermicity.

It is evident from the formulations above, and from fig. 7, that rSOC works with an anionic electrolyte. As stated in 2.2.1, the electrolyte layer is a thin membrane which needs to conduct ions between the two electrodes. In rSOC negatively charged ions are always conducted: the oxygen ions, $O^{2-}$ (anionic electrolyte). This transition is possible due to the polymorphic nature of the electrolyte membrane. Quoting M. Ferraris et al. [41], polymorph means that the material is able to assume different crystallographic structures depending on the temperature. As analysed in the next section 2.2.2.1, the most used material for this application is a special ceramic, the Yttria Stabilized Zirconia (YSZ), a polymorphic ceramic material which, at the range of temperature of the SOC (600 ÷ 800 °C), promotes the oxygen ions conduction.

Finally, the last important consideration regarding the chemical reactions involved in rSOC, especially for the SOEC mode, is that the electrolysis of $H_2O$ and $CO_2$ assumes a specific name: co-electrolysis, which produces both $H_2$ and CO, so syngas, while if there is only the electrolysis of $H_2O$, it is called steam-electrolysis. Considering co-electrolysis, even if the syngas composition seems in disagreement with the green policy described in the previous sections, due to the carbon content, in recent times it has gained the attention of many researchers and industrialists because of its versatility. In fact, it can be exploited for multiple uses such as heat production into conventional combustion chambers, as a precursor for other chemical species, acting as a depot material for the storage of energy. It also gives the possibility to fix carbonic elements of industrial exhaust gasses inside of it, in order to filter and clean the gas, making its environmental impact near zero or total zero.

In this thesis work, the syngas plays a central role because its production by SOEC operation fixes carbon elements, filtered and sent by the CCS section, avoiding release into the atmosphere and the environmental damage. Subsequently, the syngas is treated within the methanation reactors, for the production of SNG. In the literature there are still other examples, which deal with syngas, such as the article by D.J.L. Brett et al. [39], which explains how the converted syngas can be further used in a subsequent step to produce various hydrocarbon fuels via the Fischer-Tropsch conversion.

In the following paragraph the materials that constitute the elements of the rSOC will be described in more detail.

### 2.2.2 Materials and configurations

After the analysis of the basic phenomena involved in the processes that govern the functioning of the rSOC, in the following section the materials that make up the components of the electrochemical device are reported in more detail. The study of rSOC's materials are influenced by both mode of operation for SOFC and SOEC technology, indeed each of them has its own physic characteristics which influence the performance. An optimal design is reached by using materials that can enhance the performance and the mechanical properties for both modalities of operation, a sort of trade-off aiming to reach the best results.

Regarding the structure of rSOC, the electrochemical devices are always constructed in the same way:  the single cell is the union of different layers, interconnectors (start and end of each cell), the functional layer (anode, electrolyte and cathode) and secondary component as protective layers. The asymmetric cell could be represented according to layers' thickness. The best configuration is indisputably the anode-supported cell which guarantees higher degradation resistance, avoiding performance drops. Another benefit is the enhancement of the number of oxidation reactions, due to an increase of the volume of the fuel electrodes which increases the amount of tpb (three phase boundary) sites. Moreover, this configuration involves the thinnest thickness of the electrolyte layer, which guarantees lower ohmic overvoltage losses. These are losses that affect the performance of the rSOC, decreasing the field of operability in which it can act for both modes. In the following modelling chapter "3.2.2.4" they will be explained in more detail.

As for the physical concept of tpb, it appears to be of fundamental importance to better understand the functioning of rSOCs. As mentioned above, the rSOCs are made of materials that have catalysts inside them, in order to improve the kinetics of the reactions. Provided that the electrochemical reaction takes place, three physical conditions need to occur at the same time, in the same spatial region near the electrode catalyst. The first and trivial requirement is the feeding of the reactants molecules in the point of reaction, the so called "porous phase", thus the fuel and oxidant agent have to be able to reach in a proper time and without many losses the grain of the catalyst where the electrochemical reactions occur. The second condition is related to the electrons produced by the oxidation reactions or received in those of reduction. In this region of the space, called "electronic phase", a good electron conductivity must be guaranteed in such a way as to favour the transport of negative charges inside the electrode.  Finally, the "ionic phase", similar to the previous one, with the difference that a proper ionic conductivity must be guaranteed in order to remove or allow to reach easily the point of reaction by the ions produced/necessary in the electrochemical reaction.

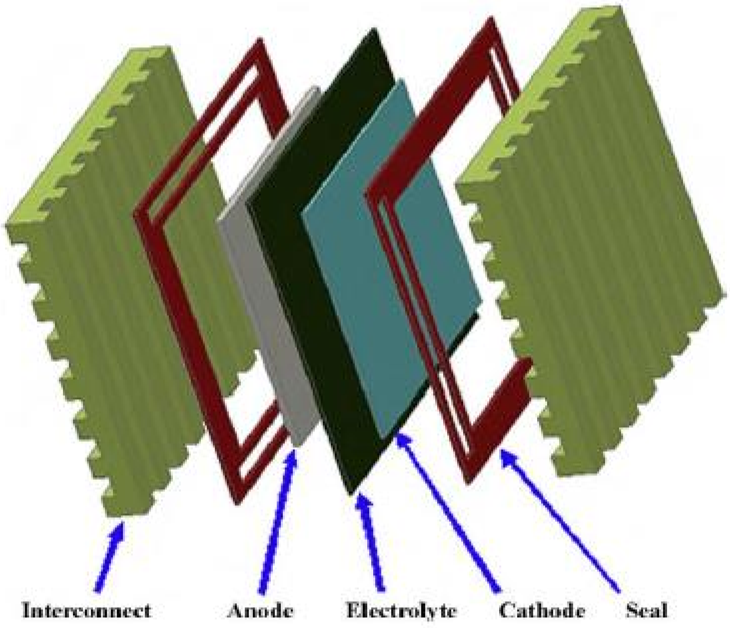

*Figure 8 – Cell configuration*[4]

Fig.8 shows exactly the physical configuration of an assembled cell, and its main components. At the current state of technology, as S.Y. Gomez et al. [37] but not only remark, most of the cell designs are based on a planar configuration, with a classic rectangular shape, such as the one of fig.8. However, in the literature there are also some innovative studies for tubular / cylindrical configurations. For instance, Huang et al. [42] have made a research about the transport phenomena in the electrodes of the tubular cell, Lawlor V. et al. [43] have performed another study based on thermo-fluid dynamics simulations to investigate better the effects of gas cross flows around the perimeter of a high temperature cylindrical electrode.

The rSOC of the thesis work is of the planar typology. Regarding its components, the interconnector is fundamental for its connector function between several single cells into a series configuration, called stack. The purpose of this assembly is to provide a higher voltage value, in order to produce a significant amount of power, because on average, a single cell is able to generate low voltage, between 0.5 and 1.3 V. It means that the stack voltage is the product between the single cell voltage and the number of cells in series, as expressed in the next eq. (19):

$$V_{stack} = V_{cell} * N_{cell} \tag{19}$$

Focusing on the components already mentioned before, the functional layers are the common electrodes (anode and cathode), where the occurrence of electrochemical reactions happens, and the electrolyte membrane, which allows the execution of the reactions without any physical interaction. Instead, the secondary components are interconnectors and sealants. Their function is to protect the configuration, avoiding leakages of fuel and oxygen agents,

---

[4] Mahapatra et al, Journal of Power Sources 195 (2010) 7129–7139

preventing the deterioration of the device, furthermore it guaranteed safety separation between anodic and cathodic streams during neighbouring cells assembly. Hence, the key requirements for the application of rSOC are long-term stability, lifetime and reliability. D.J.L. Brett et al. [39] have performed an experimental research which affirms that rSOC losses performance occurs when operated under constant conditions, with a degradation rates range between 0.3 and 0.8 % per 1000 h operating time, depending on the temperature and pressure chosen during the tests.

Another crucial point directly connected with materials are the capital costs of the technology. Expensive materials adopted in the construction of electrochemical components will produce excessive final energy costs of the technology, making it unfavourable compared with the conventional power plants. Akikur R.K et al [46] claim that the final energy costs may vary in a broad range between 0.149 and 1.104 $/kWh. Moreover, Türkay B.E. et al [47] conduct a study where different renewable systems are compared in order to obtain the differences between the payback time (the time period in which the earnings cover the initial investment) of hybrid wind turbines and hybrid photovoltaic panel systems, which are approximately 3-4 and 6-7 years respectively. On the contrary, the payback time of hydrogen systems as in rSOC takes more time (up to 25 years) because of the high initial investment in the fuel cell, the electrolyser and the hydrogen tank storage. Hence a successful future commercialization will be guaranteed by finding suitable materials with good properties and lower costs.

#### *2.2.2.1 Electrolyte Layer*

The electrolyte for solid oxide cells must be stable in both reducing and oxidizing environments, because it is in contact with both electrodes. According to planar geometry it must be shaped into a thin, dense, strong film [45], and it must guarantee sufficient high ionic conductivity (> 0.1 S/cm [44]), negligible electric and molecular conductivity at the cell operating temperature. In order to meet the last requirement, a very dense material is always used, as a low presence of pores of the internal structure prevents diffusion between one electrode and another through the membrane. If the molecular diffusion is not stopped, there would be a decrease in performance in terms of missing electrochemical reactions, but also in terms of cell temperature increment in the case of exothermic chemical reactions. Regarding the other two requirements, the choice of material is fundamental, as ionic and electrical conductivity are intrinsic phenomena.

Yttria-stabilized zirconia (YSZ) is the most studied electrolyte material for rSOC, although there are many others in the research field and in later stages (commercialization) as ion- conducting materials, zirconia-based, ceria-based, $LaGaO_3$-based, and proton conduction electrolytes. Among all these materials, YSZ stands out as it has the smaller ohmic overvoltage, which, as discussed in chapter "3.2.2.4", represents the loss phenomenon of greatest interest for the electrolyte layer. This phenomenon is responsible for some of the voltage drops that occur inside the rSOC due to the ions and electrons that are able to pass through the membrane. The effect of the phenomenon can be quantified in terms of ASR (Area Specific Resistance), a variable that expresses the passage of charges as a function of the conductivity and thickness of the membrane.

Among the materials mentioned above, YSZ has a smaller ohmic overvoltage, hence lower ASR values, for temperatures higher than 700 °C, and discrete values for lower temperatures, 500 – 700 °C. At these intermediate temperatures, other materials such as protonic electrolytes as $BaCe_{0.5}Zr_{0.3}Y_{0.2}O_{3-\delta}$ (BCZY), or ceria-based electrolytes as samaria-doped ceria (SDC) $20SDC - Li_2CO_3 - Na_2CO_3$ and scandia-ceria-stabilized zirconia (ScCSZ) have lower ASR values, hence better compositions for intermediate temperature operation. The electrolyte layer of rSOC for the present thesis work will be made with YSZ, because of the high temperature of operations involved, 850 °C. Moreover, this material has in general other advantages such as abundance, so it can be easily produced, chemical stability, as already mentioned for temperatures higher than 700 °C, non-toxicity and acceptable costs.

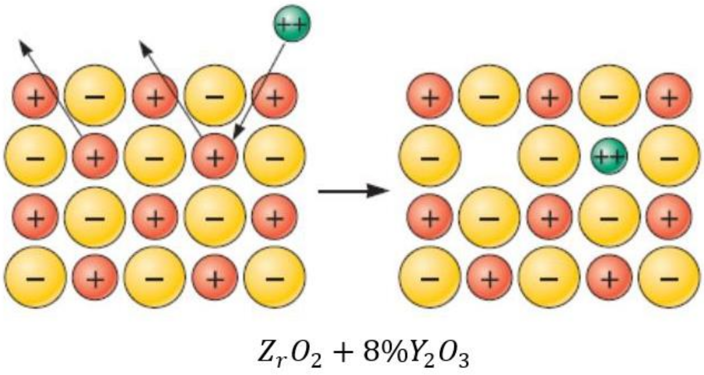

*Figure 9 - YSZ behaviour at microscopic scale – source: [41]*

YSZ is a composite material constituted by mixing a metal (Zirconia - $Z_r$) and rare earth material (Yttria - Y) oxide. Its composition is reported in the previous fig.9, which also shows the stabilized phenomena (S): the 8% of yttria oxide diffuses inside the molecular structure of zirconia oxide, substituting some elements. The yttria ion (green particle with charge ++) is electrically more powerful than the ions of zirconia (red particle with charge +), which means that, in order to guarantee the electrical neutrality of the composite material, for each ion of yttria doped, two ions of zirconia must be ejected from the system. This phenomenon generates a vacancy, a free place where oxygen ions can be exploited during their migration in rSOC operation. This process is hugely enhanced at higher temperatures, making YSZ one of the best oxygen ions conductive materials.

### 2.2.2.2 Fuel Electrode

The next material is the first functional layer in rSOC analyses: the fuel electrode. It must be made by materials able to satisfy all the tpb requirements, enhancing their amount as much as possible. Hence high ionic and electrical conductivity and high molecular diffusion are the goals. As material, in the present thesis work it is going to be used a porous metal-ceramic mixture named “cermet”. The metal part provides the proper electrical conductivity and usually, as Ni does, a remarkable catalyst action able to enhance the kinetic of electrochemical reactions, while the ceramic component provides the ionic conductivity. Instead, an appropriate porosity has to guarantee the suitable molecule migration mechanism for the supply stream of $CH_4$, $H_2$, $H_2O$, $CO_2$, but also for their products, which need to be removed from the physical point of reaction. From literature studies [48] and [49], the target for the overall conductivity of fuel electrode, which take into consideration all three phenomena, is set above around 100 S/cm, even if it depends on the cell design, and particularly on the length of the current path, thus the requirement may relax to as low as 1 S/cm.

A more detailed analysis of this material shows that cermet is a porous matrix composed by Ni (metal) and YSZ (ceramic material). The last is the same material used in the electrolyte section, necessary to guarantee the best compatibility in terms of mechanical and thermal properties. Moreover, as already affirmed in the previous paragraph 2.2.2.1, it is one of the best materials that provides proper value of ionic conductivity. Long-term tests [50], [51], [52] and [53] point out that the electrode degradation is not directly related to the applied current density but rather it is a consequence of adsorbed impurities in the Ni/YSZ. “Carbon deposition” is the most known degradation issue, it is produced when rSOC operates as SOFC, at high operating temperature (around 800 °C), in the presence of fuel with high carbon concentration as $CH_4$. This set configuration produces degradation because of the deposition of solid carbon particles all over the fuel electrode surface, generating the known pore blocking. When carbon deposition becomes significant, a sort of physical barrier made of carbon hinders the usual fuel stream until it cannot reach the tpb in the fuel electrode. In absence of the fuel component, when the oxygen ions pass through the electrolyte reaching the active point in the fuel electrode, they react, and oxidize the Ni component of the electrode obtaining nickel oxide (NiO). These molecules will substitute the Ni atoms in the fuel electrode microstructure, producing the enhancement of mechanical strain because the oxides have much larger volume than the initial atoms. The drawback doesn’t affect the fuel electrode, due to its porous nature which allows to absorb the mechanical stresses, but on the other hand, the electrolyte layer made by only brittle, dense ceramic material (YSZ) will not be able to resist, producing breaks. The rupture of the electrolyte layer will cause the chemical oxidation of the fuel, which in turn generates high temperature due to the exothermicity of the chemical reactions, producing the melting of the cell, an irreversible damage.

From the point of view of degradation in the cell, the phenomenon of carbon deposition is always considered during the design phase, as it occurs every time carbonaceous fuels are used. The next fig.10 shows an important chart which explains how to avoid the phenomenon of carbon deposition, through the control of three important elements, carbon ( C ), hydrogen ( H ) and oxygen ( O ).

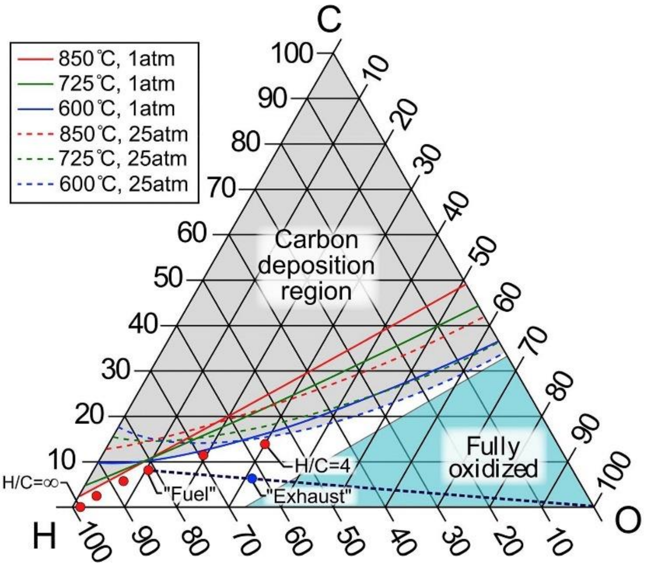

Figure 10 - Triangle diagram of equilibrium – source: [40]

Regarding a fuel exploitation in the electrochemical device, the amount of these elements selects a point in the diagram, and as the chart shows, when they finish in the grey section, the carbon deposition region, the pore blocking starts growing. In order to avoid this, the chemical fuel composition must be modified to move in the safety region. The best method used are the SMR reactions, eq. (3) of paragraph "2.1.2.1". They are defined as reforming reactions, because they produce a mixture characterized by a low carbon content, and expressed by a H/C ratio of 3. Moreover, it is an endothermic reaction, so from a thermal point of view it is also useful because it allows to absorb excess heat from sources at high temperatures.

As further discussed in paragraph "4.4", during the SOFC operation SNG coming from the natural gas grid, will be used as fuel. It is composed by 97% by $CH_4$ due to the assumption to utilize a natural gas with the same composition whose produced by CCS and methanation plant sections. Therefore, to avoid carbon deposition problems a pre-reformer reactor will be inserted in the project plant of this thesis work in order to perform external SMR reactions, without any carbon deposition issues for the SOFC.

Even if carbon deposition is the main degradation issue due to the high carbon content of the common fuel used in rSOC, it is not the only contaminant. There is the presence of low amounts of other elements which influence the cell performance. For instance, many post-mortem studies conducted in recent years, as does [54], have indicated the presence of Zr-oxide nanoparticles on the surface of Ni grains under SOEC operations, with higher degradation intensity as corrosion effect and change of component dimension, comparable to the pore blocking effect. Another issue is promoted by the presence of sulphur elements, especially $H_2S$, halogens as HCl, $C_2Cl_4$ and F or siloxanes, which poison the electrode, compromising its functionality and efficiency. Therefore, future modifications to the traditional Ni/YSZ cermet are necessary in order to prevent this kind of problems, and at the same time, enhance their performances for instance in terms of increment of the tpb areas by reaction sites promoting stability, the promotion of other catalytic activities through other materials and the implement of the corrosion resistance. This paragraph wants to explain the state of the art for fuel electrode, so more detailed descriptions of innovative materials is left to the interest of the reader.

### *2.2.2.3 Oxygen Electrode*

In closing, the oxygen electrode. This functional layer is made by a specific structure, the MIEC ( Mixed Ionic-Electronic Conductor ), also called “perovskites". This material is characterized by a specific structure, which is always based on the following scheme: $ABO_3$. A refers to rare earth element, B to a transit metal and O to the classic oxygen element. The next fig.11 shows the physical representation of the scheme $ABO_3$, the disposition of MIEC’s ions inside the elementary cubic structure.

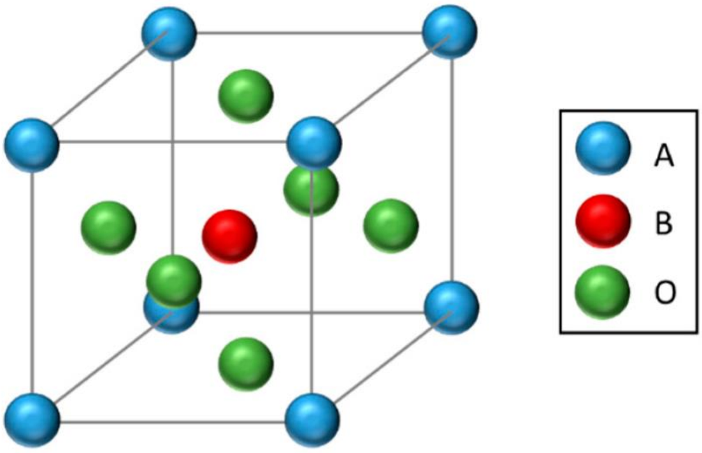

*Figure 11 - MIEC structure* [5]

“A” sites occupy the vertex of the cube, “B” sites occupy the centre of the cube while the oxygen ions occupy the centre of each face of the cube. The most used material for oxygen electrodes in rSOC is LSM (Lanthanum-Strontium-Manganite), expressed in a chemical formula as $La_{1-x}Sr_xMnO_{3-\delta}$. It is highly compatible with other cell materials, especially with the YSZ of the electrolyte, as they both have similar mechanical and thermal properties. Indeed, its thermal expansion coefficient matches with the one of YSZ, avoiding thermomechanical stresses. Moreover, from “the tpb” point of view, it is characterized by numerous paths for electrons and ions, due to high electronic and ionic conductivity, but also to proper porosity which guarantees good oxygen migrations. Actually, there are other different materials with a perovskite structure, but LSM is the most researched because these types of material are subjected to microstructure optimization to fit better in the cell system. Thus, the focus of this study will mainly fall on this type of structure, because of its simple configuration, which allows high three conduction pathways.

---

[5] Source of the img: https://www.mdpi.com/2227-9717/7/3/128

#### *2.2.2.4 Single Repeating Unit components*

The missing elements necessary for the construction of the Single Repeating Unit of a stack of cells are the interconnector and the sealing, that allow safe and leak-free operations towards the environment. The first one, as already mentioned at the beginning of paragraph “2.2.2”, has the important function to link different cells in order to assemble in a stack, enhancing the electrical performance. For this reason, it is in contact with both electrodes, thus it must be made of a material which guarantees specific characteristics. Crofer 22APU is the most appropriate material, it is a very dense structure made of iron with $22\%_{wt}$ of chromium, and small amounts of other elements such as Mn, Ti, P, S and La. The high density prevents molecular transport which could generate unwanted reactions in the wrong electrode, acting as a physical barrier to protect the oxygen electrode from the reducing environment of the fuel on the fuel electrode side. Moreover, it provides electrical connection between the anode of one individual cell to the cathode of neighbouring cell, due to high electron conductivity. Finally, it has adequate stability in terms of microstructure, chemistry and phase at the high operating temperature, with a coefficient of thermal expansion comparable with the adjacent electrodes. The most problematic drawback in the interconnector is the chromium poisoning: during normal cell operations, chromium tends to diffuse in bulk zones of the interconnector, and, on the side of oxygen electrode it can vaporize and react with the air flowing in the air channel, producing chromia ( $CrO_2$ ) which deposits on the cathode surface and reduce the tpb of the oxygen electrode, blocking it and enhancing the polarization losses. The possible solution for this problem is an innovative coating: $(Mn,Co)_3O_4$ spinel. It is a protective layer applied in the interconnector zone where it is in contact with the air channel, avoiding the chromium evaporation. Moreover, it guarantees proper thermomechanical and chemical compatibility with the crofer 22APU material. Nevertheless, the only problem related to this coating is its high cost caused by the presence of cobalt ( Co ).

As for the sealing protecting layer, it has various complementary functions which guarantee a constant functioning of the rSOC operations. Among its most important requirements there is, first of all, the prevention of mixing inside the cell fuel and oxidant streams. At the same time, it prevents also the leaks toward the external environment of the stream, and it is very important especially for $H_2$ fuel because, as reported in paragraph 2.1.1, hydrogen can create an explosive mixture with the ambient air. Recent studies have shown that, when testing single cells without glass sealing layers, small concentrations of impurities in the inlet gasses may cause similar significant degradation of the cells [55]. Furthermore, as the interconnector also does, the glass sealing ensures the mechanical stability of the device, by bonding its components. In order to reach these goals, a glass-ceramic material is the best choice for the rSOC analysed in the thesis work, because it guarantees thermal, mechanical, chemical and electrical properties:

- Acceptable stability at high temperatures in the reducing and oxidizing atmosphere of the stack;
- Capability of withstanding thermal cycling between ambient and operating temperatures;
- Proper coefficient of thermal expansion compared with both electrodes, thus low thermal stresses;
- Generally inexpensive materials;
- Good adhesion and wettability on both sealing surfaces;
- Electrical insulation;
- Resistance to vaporization at high temperatures;
- Flexible design, low processing costs and high reliability.

To conclude the entire section dedicated to the state of the art of the materials used in the rSOC, a summary is provided in tab. (7), of all the components and related materials of which the rSOC of this thesis work is constituted.

| Component of rSOC | Material of the component |
|---|---|
| Fuel electrode | Cermet |
| Oxygen electrode | La0.8Sr0.2MnO3 |
| Electrolyte layer | YSZ |
| Interconnector | Crofer 22APU |
| Sealant | Glass-ceramic |

*Table 7 - rSOC summary materials*

In the next section the concept of Power-to-X plant will be analysed, a fundamental component for this thesis work. This contemporary concept of multifunctional power plant contains important plant sections that are used in the polygenerative plant in question, such as the methanation section, for the production of SNG and the version of the cell in steam electrolysis for the production of pure $H_2$.

## 2.3 Power-to-X

After the second industrial revolution around 1870, the mankind began to exploit a new source of energy to meet his needs: electricity. Over the years, the increase in knowledge in the energy sector has allowed technological evolution, resulting in increasingly productive and efficient systems. From the very beginning, the logistics that governed the internal processes of power plants were always based on the same linear scheme, from the input fuel, which was generally a fossil fuel such as coal or natural gas, only one output was obtained, electricity. Initially, global efficiencies were very low, but they were compensated by the overexploitation of fossil sources, especially coal, because there was an abundance and above all, the environmental consequences of using this resource were not known. Over time, however, because of both the decrease in material reserves and the awareness of the environmental repercussions, an attempt has been made to find alternative ways. We have moved from primitive power plants to plants with higher efficiencies, such as cogeneration plants that allowed the production not only of electricity, but also of heat by exploiting the high temperatures of the outgoing fumes. Combined cycles began to be used, which allowed the coupling of different processes such as gas cycles and Rankine cycles, always with the aim of increasing the performance of the global plant. The evolution of the plants was expanding, trying to improve the starting linear scheme, until the plants named power-to-X became known. The nomenclature indicates that in these plants, starting from a single input, a multitude of outputs (X) are obtained and they are able to make the most of the initial resource, minimizing waste and maximizing efficiencies. Furthermore, in addition to the logistical modification of the process scheme, new forms of renewable resources have been introduced precisely for environmental awareness, in particular $H_2$ and other energy vector, such as syngas. A great number of scientific articles, such as the one of Jochen Lehmann et al. [56], declare that Power-to-X is a very complex connection of procedures based on the conversion of renewable energies into green hydrogen through electrolysis. On the other hand, Francisco Vidal Vázquez et al. [57] claim that Power-to-Gas, Power-to-Liquids, or, more generically, Power-to-X conversion concepts arise as a synergetic solution both for storing energy from intermittent renewable energy sources and producing carbon-neutral fuels from $CO_2$ emissions. Taking into consideration the plant presented in this thesis work, it is designed following the concept of power-to-X, and is called polygeneration plant. It consists of four different sections connected to each other, each with a different purpose, aiming to obtain the maximum result with the least waste, according to an eco-sustainable logic, which avoids the disturbance of the local and global environment. This is fundamental for new plants, and compared to the past years it is also easier to implement thanks to the guidelines set by international treaties and the consultancy obtainable from global and / or national associations.

Going briefly into the details of the polygenerative plant, its previously announced sections are the photovoltaic system, the rSOC, the methanation section and that of CCS. Since the goal of the plant in this thesis work is to meet the electricity needs of an urban network of

30’000 people, the photovoltaic system is designed to meet this need. Considering the fluctuation of the RES in relation to the constant urban load, there will be moments of deficit in which the rSOC, operating in SOFC mode, will produce the missing electricity using SNG taken from the urban network as input, and there will be moments of surplus of electricity produced by the PV, which will be exploited in the SOEC mode according to two different criteria. In certain moments, such as steam-electrolysis, for the production of pure H2 to be sent to a storage to satisfy a constant daily demand for this stream. At other times, such as co-electrolysis, for the production of syngas to be sent to another storage. This latest stream will be processed in the methanation section, with the aim of producing SNGs to be sent to the Italian natural gas network. Finally, the last section, that of CCS, which will allow the production of both a stream of SNG to be fed into the network and a stream of pure $CO_2$ to be used for co-electrolysis. It is evident that the energy and material vectors within the plant are multiple, and that they all together synergize in such a way as to meet the requirements set during the design phase. These processes will be analysed in detail in the next chapters, both from the initial point of view of the modelling of such plants, and from the point of view of the analyses and results.

This chapter continues by discussing and explaining the state of the art of the methanation and CCS process, in order to present a complete introduction of the technologies used in the polygenerative plant in question.

### 2.3.1 From syngas to synthetic natural gas: methanation

For the global plant, the SNG stream plays a very important role. In general, its main component is $CH_4$, a chemical compound with a high energy content that is nowadays used for various fundamental purposes as a fuel for power plants, to produce heat used for civil heating and domestic hot water or also as a fuel for trucking and cars. Compared to other fossil fuels, oil and coal, methane has advantages. Its use releases a small amount of pollutants, GHG, even if this does not reflect the constraints imposed by international treaties. At the same time it also has deficiencies, like other fossil fuels, and in particular the exhaustion of its reserves. Therefore, in order to face all these problems, scientific research has sought a solution in the last century. The responses were methanation reactions. [58], [59] and [60] are some of the scientific publications dealing with this topic. These reactions allow to synthetically produce $CH_4$ starting from other chemical compounds, in particular $H_2$ | $CO_2$ and syngas, naming the process respectively $CO_2$ methanation, eq. (17) and CO methanation, eq. (18).

The logical reasoning behind these processes is power-to-x, which in this case takes the specific name of power-to-gas. The name derives from the fact that, as per the logic of power-to-x, the process starts with a chemical compound, which is treated until the gas, $CH_4$, is obtained. In fact, both production methods must be coupled with other technologies because hydrogen is a secondary product that must be obtained. This means that, most of the time, there is always the presence of SOEC upstream. Also in the present thesis work these two technologies work together, in such a way as to be able to store the excess energy produced by the photovoltaic system, first inside the syngas, and then transforming it into SNG in the methanation section, increasing its exergetic content.

Going into the detail of chemical reactions, $CO_2$ methanation was the first to be discovered in 1902 by Sabatier and Senderens [61], and for this reason it was also named Sabatier reaction. It is expressed by eq. (17), already present in the chapter "2.2.1.1". As can be seen from the reaction, the reactants are $H_2$ and $CO_2$, consequently it can be deduced that the SOEC step operates in steam electrolysis, eq. (20). This is due to the fact that there is no electrolysis process that allows $CO_2$ to be obtained as a product, on the contrary, $CO_2$ is used as a reagent within the electrochemical device. For this reason, steam electrolysis offers the opportunity to produce a stream of pure $H_2$, which is then accompanied by a stream of pure $CO_2$. Coupling eq. (17) and (20), therefore considering a global fictitious plant that includes methanation reactors and SOEC, we obtain eq. (21). As discussed in chapter "4.6.2", it will be of fundamental importance for the determination of an important parameter.

$$4H_2O \rightarrow 4H_2 + 2O_2 \qquad \Delta h^0 = +1143.3\frac{kJ}{mol} \qquad (20)$$

$$2H_2O + CO_2 \rightarrow CH_4 + 2O_2 \qquad \Delta h^0 = +978.7\frac{kJ}{mol} \qquad (21)$$

The change in enthalpy under normal conditions, $\Delta h^0$, of the eq. (21) is obtained simply as the sum of the enthalpies of eq. (17) and (20). It is noted that the endothermic effect of steam electrolysis is significantly higher than the exothermic effect of $CO_2$ methanation, in fact the global equation is endothermic. This means that overall, the plant requires more energy to sustain the reactions than the energy which is produced by some of them. On the other hand, observing the stoichiometry of the reaction (21), it can be stated that the global process sees the formation of one mole of $CH_4$, and two of oxygen, consuming two of $H_2O$ and one of $CO_2$. From the environmental point of view, the advantage is not very high as it allows a $CO_2$ to $CH_4$ conversion with a unit ratio. Despite this, it still represents an advantage, and consequently the process turns out to be very interesting.

As for the other chemical reaction, CO methanation, its discovery took place after the other one, after a number of researches and studies. CO methanation reaction has many strengths, in fact in the literature there are many articles that deal with its applications. For instance [62] reports the first studies, in which CO was removed from syngas to produce ammonia, a process that will be extended with the use of PEMFC (Proton Exchange Membrane Fuel Cell), [63] in order to produce SNG from gasification of coal and many others materials. From the chemical point of view, CO methanation is expressed by eq. (18). Unlike its alternative which reacts with $CO_2$, SOEC operates in co-electrolysis, eq. (22). This allows it to work with incoming $H_2O$ and $CO_2$, generating syngas. It should be noted that in the state of the art of electrochemical devices, only SOCs are able to work with carbon dioxide as an input reagent.

For example, the PEM (Proton Exchange Membrane), which are the electrochemical cells that work at low temperatures, in non-stationary regimes, are composed of platinum, which suffers greatly from the presence of carbonaceous substances. Consequently, nowadays, the only appropriate fuel for these types of cells is $H_2$. That said, as was done for the alternative case of methanation, combining the co-electrolysis, eq. (22) and CO methanation, eq. (18), a global equation is still obtained, eq. (23), representing a fictitious plant consisting of SOEC and methanation reactors.

$$3H_2O + CO_2 \rightarrow 3H_2 + CO + 2O_2 \qquad \Delta h^0 = +1140.5\frac{kJ}{mol} \tag{22}$$

$$2H_2O + CO_2 \rightarrow CH_4 + 2O_2 \qquad \Delta h^0 = +934.5\frac{kJ}{mol} \tag{23}$$

At first glance, eq. (21) and eq. (23) look the same, and from a stoichiometric point of view they are. The substantial difference is instead thermodynamic, because their heat of formation, $\Delta h^0$, is different. In the case involving CO methanation, the total heat required for the global reaction to take place is lower than in the case of $CO_2$ methanation. As already explained in paragraph "2.2.1.1", the exothermic reaction of CO methanation allows to release more heat than that of $CO_2$ methanation, due to the extra energy that is used to break the bond of the second atom of oxygen in the carbon dioxide molecule. As for the electrolysis reactions, besides the chemical compounds involved, there are no other differences. In fact, as can be seen from their $\Delta h^0$ obtained under standard conditions, the values are equivalent. This indicates that from the thermodynamic point of view, the two electrochemical reactions are very similar, a very interesting aspect especially during the modelling phase of the rSOC parameters.

Another fundamental aspect concerns the methanation reactors, in particular the materials with which they are built. Ever since the discovery of methanation reactions, Sabatier and Senderens claimed that there were materials capable of accelerating the chemistry of reactions, acting as catalysts and making the process even more interesting. Furthermore, thanks to the scientific research of the last century, many other materials have been discovered that were able to produce the same results. Fischer et al. [64] was the first to classify these materials, metals, according to their activity, or the degree of interaction that is established between the catalyst and the chemical reaction as a function of the fugacity coefficient, producing this classification: Ru> Ir> Rh> Ni> Co> Os> Pt> Fe> Mo> Pd> Ag. However, Fischer's studies were not exhaustive, as there were variables that were not considered, such as the areas of the catalysts. M.A. Vannice et al. [65] published another study, updated with corrections, and which took into account the missing aspects, producing two different new rankings. The first was still based on the degree of activity, Ru> Fe> Ni> Co> Rh> Pd> Pt> Ir, while the second was based on the selectivity, Pd> Pt> Ir> Ni> Rh> Co> Fe> Ru. Selectivity determines a ratio between the quantity of the final converted reagent and the initial quantity of chemical substance that reacts to become a product. Nowadays, the choice for the catalyst material of the methanation reactions falls on nickel, which is in fact the material chosen for the plant's methanation reactors. This material represents a good compromise between catalyst action and price; therefore it is the best choice.

Catalysts are usually very sensitive to the presence of certain elements in the gas stream that undergoes the methanation process. Chlorine compounds, tars, ammonia and sulphur compounds are the most important ones. In general, both for CO methanation and $CO_2$ methanation, the syngas used as input have a very variable composition, depending on the process that generated them. Usually, they do not have a great abundance of these substances that put the catalyst at risk, but despite this, even small traces can produce undesirable effects, especially the sulphur compounds, which can poison the catalyst by inhibiting all its functions and making it unusable [66]. For this chemical substance, therefore, the reference reaction that is usually taken into consideration in the design phase is the one involving nickel and the hydrogen sulphide, eq. (24), producing nickel sulphide, a material that has no catalysing function for methanation reactions.

$$H_2S_g + NiO_s \rightarrow NiS_s + H_2O \tag{24}$$

In reality, there is still one last chemical reaction of primary importance. However, this reaction has a reduced field of application compared to (24), as it occurs only in CO methanation. The problem is commonly referred to as catalyst fouling. Its effect consists in the physical deposition of pure carbon. In short, it is the same phenomenon that generates pore blocking in SOFC, in fact this aspect has already been explained in paragraph “2.2.2.2”. In the case of CO methanation, carbon monoxide can decompose, generating carbon dioxide and solid carbon which accumulates on the surface of the catalyst, subsequently reacting with the nickel it is formed of. This process reduces its catalyst function due to the decrease in active surface. The chemical reaction that decomposes carbon monoxide is called the Boudouard reaction, and is represented by eq. (25):

$$2CO_g \rightarrow CO_{2(g)} + C_s \tag{25}$$

Regarding the project plant presented in this thesis work, it is hypothesized that equations (24) and (25) do not occur. This is because the percentage of sulphur inside the syngas to be processed in the methanation reactors is considered null. At the same time the kinetics involving eq. (25) can be considered as irrelevant, as it becomes relevant at temperatures ranging between 500 and 600 °C, while the methanation described in this thesis work takes place at the operating temperature of 220 °C.

The last paragraphs of chapter 2 expose the theory on the carbon capture and sequestration section, CCS.

## 2.4 Carbon Capture and Sequestration technology

As pointed out in the first sections of the first chapter, global warming is a problem that needs to be solved. The awareness raised about this issue should dictate a strict conduct for the years to come. Directly responsible for this phenomenon which is becoming increasingly dangerous for life on earth is $CO_2$. According to the WMO, in 2019 the average percentage of $CO_2$ in the atmosphere was 410.5 ppm with a tolerance of 0.2 ppm. Unfortunately, as in recent years and despite the fact that at present no reliable data are available, the WMO states that even in 2020 the trend has been positive. This data is very alarming as it is known from various scientific researches that the maximum limit allowed corresponds to 450 $ppm_{CO2}$. However, thanks to the awareness raised, in recent years new methods have been constantly sought to mitigate this problem, until the trend is reversed. Scientific research has led to the discovery of many technologies that can be used to improve current conditions. Overall, an improved fuel efficiency, mainly in power production and transportation, can be considered as a mid-term goal. In order to achieve long-term goals for the reduction of emissions, the alternation of power sources such as nuclear, solar, and wind power should be considered. The only source which allows short-term results is CCS (Carbon Capture and Sequestration). A very positive aspect of latter technology is its ability to be coupled with other systems, of any industrial or energy type, as it allows to filter and clean process-gases, reducing and / or cancelling their climate altering action. This peculiarity is a direct consequence of the types of CCS currently developed. Nowadays, post-combustion capture, pre-combustion capture and oxy-fuel combustion are the most stable process that are know from the technological point of view. Research in this branch is actually expanding increasingly, and more and more new technologies are being studied, such as cryogenic distillation or the innovative membrane separation. At the same time, also new physical processes - such as hydrate formation, electrocatalysis and ammonium bicarbonate formation - are being discovered. Despite being currently still in the laboratory phase, they allow to achieve the same purpose.

Pre-combustion capture is a well-established logic scheme nowadays, it is always used a posteriori of an already known process, gasification. The latter has been fully explained in paragraph "2.1.2.3", in fact it is known that a gas mix called syngas is obtained from this process. Pre-combustion capture is the process that uses this gas, with the aim of converting the CO contained within it, transforming it into $CO_2$ and then removing it in a kind of separators components. The first step is the conversion into the desired weathering gas, which takes place by exploiting the chemical reaction of WGS, eq. (4) analyzed in detail in paragraph "2.1.2.1", within a shift reactor. The formation of the reaction products, $H_2$ and $CO_2$, is favored by increasing the initial quantity of steam in the reactor. Indeed, from the thermochemical point of view, in order to shift the equilibrium condition of the reaction towards the products, an increment of the quantity of reactants (steam precisely) is needed:

$$Y = \sum_{i=1}^{\#\_reactants} \mathrm{v}_i * \mu_i(T, p_i) - \sum_{i=1}^{\#\_products} \mathrm{v}_i * \mu_i(T, p_i) \tag{26}$$

$$\sum_{i=1}^{\#\_reactants} \mathrm{v}_i * \mu_i(T, p_i) > \sum_{i=1}^{\#\_products} \mathrm{v}_i * \mu_i(T, p_i) \tag{27}$$

$$Y = -\left(\frac{dG}{d\xi}\right) \tag{28}$$

Equations 26, 27 and 28 explain the thermochemical process in detail. Starting from the first, $\mathrm{v}_i$ represents the stoichiometric coefficient of the chemical reaction, $\mu_i$ the chemical potential of that element, defined as the variable which takes into consideration the variation of Gfe caused by the variation in concentration of the chemical species-i, at constant temperature, pressure and concentration of all the other species of the chemical reaction. Y is the affinity, nothing less than the variable that evaluates the difference between reactants and products of the product of $\mathrm{v}_i$ and $\mu_i$. In equilibrium conditions, this variation is zero, or Y = 0. By increasing the amount of reactants, the equilibrium shifts, eq. (27), in other words: Y> 0. Finally, eq. (28) shows that affinity can also be represented as the contrary of the variation of Gfe (dG), by the variation of the degree of advancement of reaction (dξ). From this last equation it follows that (dG / dξ) <0, i.e., that as the degree of advancement increases, the Gibbs free energy decreases, and therefore the equilibrium of the reaction shifts towards greater degrees of advancement, thus towards the formation of more products as equilibrium is the condition in which the Gfe reaches its absolute minimum. The second and last step of the pre-combustion capture process is the separation of the products obtained in the shift reactor, $H_2$ and $CO_2$. Usually, this process occurs with the use of complicated technologies such as Pressure Swing Adsorpion or through innovative membranes that allow one component to be filtered over the other.

The second type of CCS briefly analyzed is that of oxy-fuel combustion. This process is based on the use of an innovative membrane, the ITM (Ion Transfer Membrane), which, as the name implies, allows to filter certain ions, specifically oxygen ions $O^{2-}$. The goal in generating these ions is to make only stoichiometric reactions occur, in order to obtain $H_2O$ and $CO_2$ as products, avoiding any other kind of chemical molecule. In this way, with the use of a simple condenser, it will be extremely easy and low-cost to extract the water, producing a pure alternating climate gas stream. This membrane has been studied and designed to operate inside the combustion chambers, favouring the filtering process at the high temperatures to which it is subjected. Furthermore, pressure plays a main role within the process, because it allows the membrane to pass oxygen ions between the high-pressure part and the one in which it is almost in vacuum conditions. In fact, the real driving force of the phenomena is the oxygen partial gradient across the membrane. The following eq. (29) expresses in detail what has been said:

$$J_{O^{2-}} = \ln\left(\frac{p_{O^{2-}}^{compressed}}{p_{O^{2-}}^{vacuum}}\right) \tag{29}$$

Lastly, the third CCS-type: the post-combustion capture. Focussing on the thesis, this is the method on which the CCS section is based in order to produce the pure stream (99.92 $\%_{mol}$) of $CO_2$ to be sent to the SOEC section operating in co-electrolysis. In general, the function of post-combustion is, as the name suggests, to capture the $CO_2$ as a result of the process that generated it. Usually these processes are industrial ones, such as those used for energy production. An element in favor of this type of CCS derives from the fact that its implementation is not limited only to new plants like most of the uses of the other two types, but can also be used in existing plants (retrofitting). As previously mentioned, the CCS, and in particular the type of post-combustion capture, is able to have an effect in the short term by exploiting the possibility of improving the existing systems. In this way, it is possible not only to guarantee compliance with environmental standards for future plants, but also to correct and improve existing ones.

Nowadays there are many technologies that allow the cleaning of any gaseous stream, from the exhaust fumes of industrial processes to the purification of biogas produced in an anaerobic digester. For example, the work of Abanades J.C et al [70] reports a general review of existing technologies, up to the year 2005, also classifying them according to the level of operational stability. By generalizing them, the post-combustion processes can exploit chemical looping, adsorption phenomena, other absorption phenomena and finally membranes. Of all those available, this thesis will particularly take into consideration and analyze in more detail that of absorption, as it is very important in the structure of this work.

In general, adsorption is a process based on the chemical interaction that exists between a solution, in particular its solvent, and a specific chemical substance within a compound. As chemical substance $CO_2$ will be considered, although the same applies can be done to any other element, when there is compatibility between the substance and the solvent. While considering all the alternatives existing between the various types of solvents (in liquid or solid form) [67] connected to $CO_2$, there are liquid monoethanolamine (MEA), solid calcium/lithium hydroxides, HSC+ solid ceramic, liquid ammonnia ($NH_3$), others liquids amine [69] as diglycolamine (DGA), diethanolamine (DEA), N-methyldiethanolamin (MDEA), and many others kind of solvents, which are at an advanced stage of study and / or already on the market. The wide choice of solvents illustrates both the high number of studies that have been conducted to date, and their importance for future eco-sustainable prospects.

Specifically considering the chemical absorption plant presented in the thesis work, it uses a solution composed of MEA (chemical formula $OHCH_2CH_2NH_2$) and water, in proportion 30 % mol and 70 % mol respectively, to remove $CO_2$ from a biogas stream. Complementary data will be provided during the modeling phase. In general, CCS plants that act through liquid solvents are built with the same plant design and with their main devices: absorption reactor, stripping column and regenerative heat exchanger.

In the absorption reactor are sent as input the gaseous stream of gas to be purified and the liquid mixture composed of MEA and water, called lean. These two streams act in countercurrent in such a way as to increase the effect of the chemical phenomenon, favored at a fairly low temperature ranging on average between 35 and 55 °C. During the process, the liquid solution that runs through the absorption columns from top to bottom is enriched with $CO_2$, capturing it, while the gaseous compound that circulates from the bottom to the top is depleted of the chemical substance in question. Subsequently, the $CO_2$-rich lean exiting from the bottom of the vessel is sent to the stripper, another reactor which instead has the function of regenerating the liquid mixture, through the reverse phenomenon of desorption, in such a way as to purify it and be able to recirculate and reuse it in a new cycle. The rich lean circulates from the top to the bottom of the stripper, resulting in two streams. A gaseous one, composed practically of pure $CO_2$, which comes out near the top of the vessel, and a liquid one, composed mainly of the initial solution of water and MEA, coming out from the bottom. These two streams are further purified, the gaseous one is passed inside a series of coolers and condensers that allow the temperature to be lowered below the boiling point of water. It means that further steam still present and bound to different secondary chemical compounds is condensed. The other stream, the liquid one, passes inside a reboiler, which produces heat with the aim of further promoting desorption phenomena, allowing to obtain a purer solvent at the outlet. In order to increase the performance of the system there is another key device, the regenerative heat exchanger. It allows the passage of heat between the purified lean stream, exiting the stripper at high temperature, in general between 110 ÷ 130 °C, and the $CO_2$-rich lean stream exiting the absorber, which is generally by 50 ÷ 55 °C. This heat exchanger is essential as it recovers the heat that would be lost, respecting and favoring the physics of the system. In other words, the absorption phase is favored at low temperatures, while the desorption phase is favored at higher temperatures.

From the thermodynamic point of view, there is a law which explains the behaviour and the maximization of the chemical absorption process. Henry's law, eq. (30), exposes the variation in the concentration of the chemical element to be removed, in this case $CO_2$, between the stream of rich lean and the initial gaseous mix to be purified, expressing the solubility of the gas in a given solvent as the temperature and pressure vary.

$$\mathrm{X} * H = y * p = p_i \tag{30}$$

The equation above expresses the correlation between the product of the molar fraction of $CO_2$ contained in the solvent of the enriched final solution, X, and the Henry constant, H, and the product between the molar fraction of $CO_2$ contained in the gaseous stream to be purified, y, and the total pressure of the outgoing stream. Furthermore, as known from chemistry, this last product is nothing less than the partial pressure of carbon dioxide in the initial gas. The dependence on pressure is therefore explicitly expressed through this variable, while the dependence on temperature is expressed implicitly since Henry's constant is a function of temperature. In detail, as the temperature increases, the value of the constant increases, until it reaches a point of absolute maximum, after which its value decreases. Taking into consideration what has been said, it is clear that, in order to maximize X, a very high partial pressure of $CO_2$ in the initial gas is necessary, and this can be favored in thermodynamic terms by increasing the total pressure. On the contrary, a low temperature implies a low Henry constant which is compensated by a high value of X. Here comes the MEA, the solvent used for the purification of the gas rich in pollutants. The characteristics of this solvent [71], which vary according to its concentration within the solution, allow to obtain a high degree of purity even at ambient pressures, avoiding high operating costs that would arise due to the pressurization of dirty gas.

Finally, the post-combustion capture process, which exploits absorption through liquid substances, is a methodology that is nowadays consolidated thanks to the extensive studies conducted. However, there are still many shortcomings and problems that accompany it. Meihong Wang et al [68] summarize them effectively, not in order of importance, stating that they are mainly the low $CO_2$ lean and rich loading, i.e. the variable that expresses the ratio between the molar fractions of $CO_2$ and MEA both in the initial solution stream (lean) and in that enriched with $CO_2$ (rich-lean). Further issues are the high equipment corrosion rate promoted by the $O_2$ contained in the flue gas, the amine degradation (MEA) by $SO_2$, $NO_2$, and $O_2$ in the flue gases which induces a high solvent makeup rate, the high energy consumption, named heat duty, during solvent regeneration in the reboiler, and lastly the large equipment size necessary to perform both absorption and desorption stage. By combining these problems, the two main sources of inefficiency are the high initial costs, as the solvents are expensive, being niche products and not globally marketed, and the big size of the components, which make therefore the devices necessary for the process very expansive. Furthermore, the second pivotal problem refers to the operating modes, as the high energy expenditure produced by the heat required for regeneration in the reboiler, produces a drastic decrease in the thermal efficiency of the process. But despite these issues, the scientific community is optimistic about the use of this technology and consider it one of the most valid alternatives for solving climate change problems.

This paragraph concludes the study of the state of art. In the following chapters the system proposed in the thesis will be described in detail. The third chapter aims to specify all the settings that have been imposed during the modeling phase and the various methodologies that have been used.

# 3 Modelling and methodology

The power-to-x scheme of the polygenerative plant studied in this thesis has the main function of producing electricity for an urban network of 30’000 people. One of the production sources is the section of the photovoltaic system, which allows to directly transform solar radiation into electricity. The fluctuation that derives from this technology constitutes for all similar plants a strong disturbance in terms of producibility and reliability, as the solar resource is very unstable due to meteorology to which it is closely connected. Consequently, this technology is flanked by another, of considerable interest in the field of the scientific community, the rSOC. As stated in the previous chapters, the rSOC is an electrochemical device that works both as an electrolyser and as a fuel cell. In fact, the SOFC mode allows the production of electricity, compensating for the moments in which the photovoltaic system is not able to reach the power levels required by the grid, and also allows, with its alternative SOEC mode, to store the exceeding electricity production in form of chemicals, avoiding waste. These compounds for the plant presented in the thesis are both $H_2$ and syngas ($H_2$ and CO). According to the operating mode of the SOEC, it is possible to obtain either the first or the second product, respectively by operating in steam-electrolysis or co-electrolysis. The choice of the electrolysis mode, as well as the overall logic of the entire plant is dealt with in detail in the next chapter "4 Analysis and Results of Polygeneration Plant". Furthermore, in order to store these two streams, there are two storage units, one for the syngas, at a temperature of 20 °C and a pressure of 32.4 bar, i.e. the outlet pressure from the SOEC, and one for the hydrogen, by 20 °C and 250 bar. There is a need for a compressor to further increase the pressure value from the operating conditions of the SOEC to those of the storage, as the hydrogen is produced by operating the SOEC in steam electrolysis (i.e. at 32.4 bar). The first storage tank, that of syngas, is of fundamental importance for the third section of the polygenerative plant of the thesis, the methanation section. This part of the plant allows the production of SNG, which after electricity and hydrogen corresponds to the third outgoing flow, consolidating the congruence with the theory of a Power-To-X plant. The fourth section constituting the global plant is instead of fundamental importance for SOEC, as it allows it to operate in co-electrolysis: it's the CCS section. This part of the plant has the purpose of purifying an initial biogas stream, producing a pure $CO_2$ stream. The purified biogas, as well as the SNG produced in the methanation section, are processed in such a way in order to include them into the Italian national natural gas network. Precisely this gaseous mix, subsequently decoupled with its production phase, is used in the rSOC operating in SOFC for the production of the electricity necessary to compensate for the electrical shortages of the photovoltaic system.

The description above reflects the theoretical representation of the polygenerative plant in question. Subsequently, fig. 12 represents the logic blocks and streams of main interest for the global system.

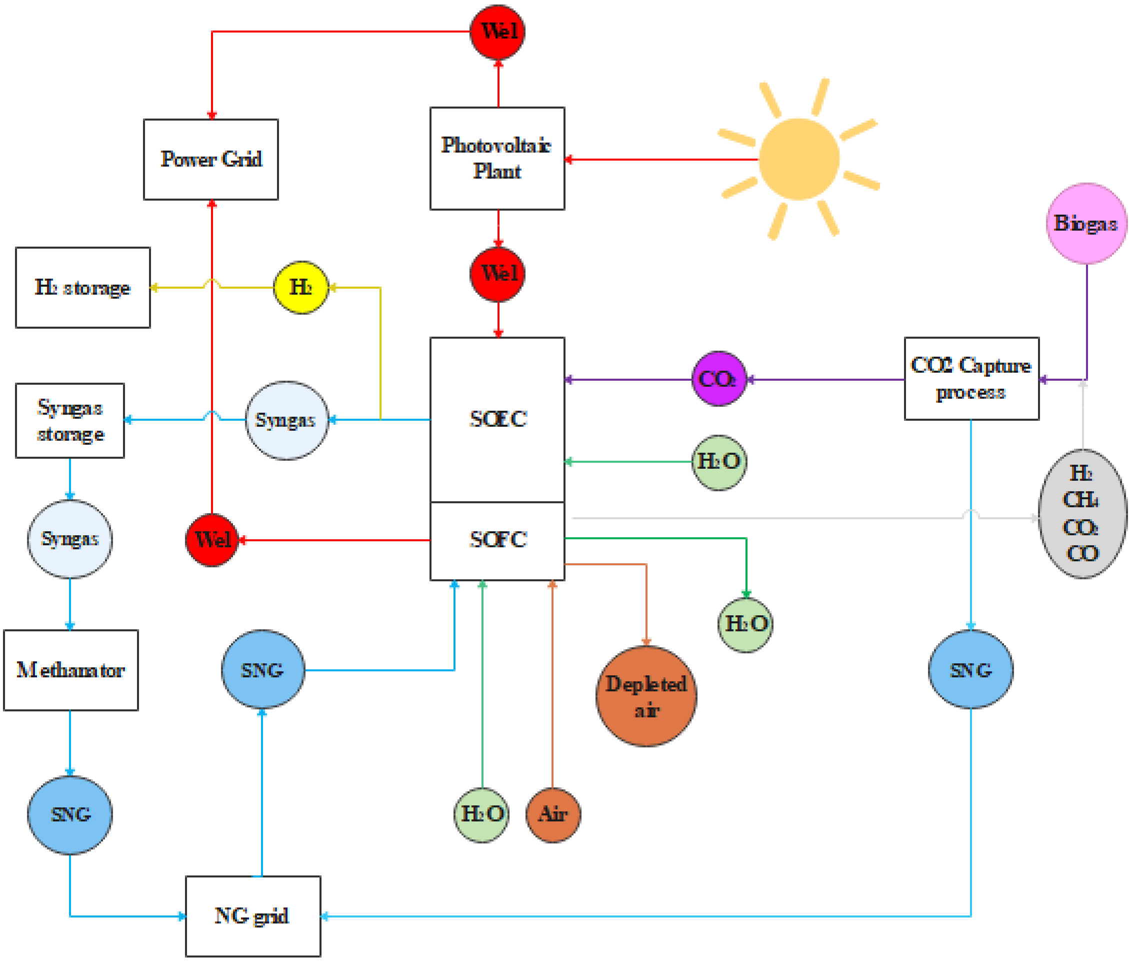

Figure 12 - Polygeneration plant

The aim of the third chapter is to explain the design phase carried out in the framework of the thesis, describing the formulas which determine the fundamental parameters to be exploited in the analysis of the models, which will then be simulated using Aspen Plus software.

## 3.1 Electricity input and output

Electricity production is the primary service performed by the polygeneration plant as a whole. In this regard, it is important to describe the electricity production method, in this case through a now well-known photovoltaic system, whose technology is considered mature and therefore exploited in various fields, from private to public sectors. Moreover, it is also important to consider and describe the urban network that benefits from this eco-sustainable system. At the end of the chapter the output data obtained and the diagrams representing their comparisons will also be reported, however they will consider only the two parts listed above, that are the primary sections that provide the inputs for the rest of the polygeneration plant.

### 3.1.1 Urban load

Before modeling the polygenerative plant, it is of primary importance to establish what energy consumption is to be met during the operational phase of the system. As already mentioned above, the electricity requirement considered is due to an urban network made up of 30 thousand inhabitants, assuming that energy consumption is only those of the civil residential class. It is a crucial criterion, since the different consumption types considered have strong disparities in terms of quantity.

The determination of the data relating to energy consumption has been conducted based on the data available from Terna s.p.a., TSO (Transmission System Operator) in Italy. Through its website it was possible to collect the data necessary for the quantification of a civil urban center of 30 thousand inhabitants. In fact, on the company's website, the data relating to the dispatching of electricity [72] are published almost in real time (with a buffering of a few hours) and are available hour by hour. Furthermore, at the end of each year Terna s.p.a. draws up statistical reports that show the trends in energy consumption and more, with divisions also by energy classes, [73].

The reference year for the thesis work is 2018, during which the Italian population was of 60’359’546 individuals. By proportion considering the number of inhabitants of the hypothetical urban center, 30’000, and the Italian population, an initial percentage was obtained, which makes it possible to relate an Italian national datum to the size of the reference town, with the result of approximately 0.05%. Still using Terna's website, [73], two data were collected regarding the year 2018: the first relating to Italian national energy consumption, equal to 303’433 GWh, and the second relating to the total consumption only in the domestic or civil or residential sector, of 65'137,8 GWh, obtaining a sort of utilization factor or rather a further percentage representing the domestic fraction, equal to 21.47%.

Subsequently, the hourly energy consumption data was selected [72], reported in form of power in GW, for certain reference days. These data referred to the total consumption of the Italian nation, including all categories.

Therefore, using the first fraction it was possible to pass from a national datum to a minor one, which represented the size of the hypothetical town studied in this thesis. Subsequently, by exploiting the previously calculated domestic fraction, it was possible to obtain the civil contribution on the portion of interest through a simple multiplication. As just stated, this process took place only for certain reference days, following a specific logical process. In fact, to avoid collecting 8760 data, one for each hour of the year 2018, only 24 reference days were considered: two days for each month, one weekday and one weekend day, usually chosen in the middle of the month. In this way it was possible to determine a consumption trend for each month, which used the data collected from its weekday reference for all working days, and the same process for non-working days.

The primary data reported in terms of power GW, was easily transformed into MW, and subsequently further converted into energy, represented by the unit of measurement MWh, as this energy value is given by the multiplication between a power and a time interval. Therefore, considering that all the data reported an hourly frequency, it was possible to convert them directly from power to energy by averaging the power data between two adjacent hours, and subsequently multiplied by one, i.e. the unit of time between the data. The following table 8 exemplifies the calculations made for Monday 15 January 2018, corresponding to the working days of the month of January:

| ORA | BILANCIO CONSUNTIVO [GW] | Centro Urbano [GW] | Centro Urbano RESIDENZIALE [GW] | Centro Urbano RESIDENZIALE [MWh] |
|---|---|---|---|---|
| 01:00 | 26,079 | 0,012961827 | 0,002782417 | 2,695089523 |
| 02:00 | 24,442 | 0,012148203 | 0,002607762 | 2,573460812 |
| 03:00 | 23,799 | 0,011828618 | 0,002539159 | 2,529823845 |
| 04:00 | 23,624 | 0,011741639 | 0,002520488 | 2,54598766 |
| 05:00 | 24,102 | 0,011979215 | 0,002571487 | 2,696156442 |
| 06:00 | 26,439 | 0,013140755 | 0,002820826 | 3,201182322 |
| 07:00 | 33,569 | 0,016684519 | 0,003581539 | 4,002811551 |
| 08:00 | 41,466 | 0,020609499 | 0,004424084 | 4,696255242 |
| 09:00 | 46,568 | 0,023145303 | 0,004968426 | 5,074744587 |
| 10:00 | 48,561 | 0,024135867 | 0,005181063 | 5,188531447 |
| 11:00 | 48,701 | 0,02420545 | 0,005196 | 5,181009671 |
| 12:00 | 48,42 | 0,024065787 | 0,005166019 | 5,01014267 |
| 13:00 | 45,498 | 0,02261349 | 0,004854266 | 4,854105837 |
| 14:00 | 45,495 | 0,022611999 | 0,004853946 | 4,90094356 |
| 15:00 | 46,376 | 0,023049875 | 0,004947941 | 4,984910047 |
| 16:00 | 47,069 | 0,023394311 | 0,005021879 | 5,062741753 |
| 17:00 | 47,835 | 0,02377503 | 0,005103605 | 5,205388759 |
| 18:00 | 49,743 | 0,024723347 | 0,005307173 | 5,268283606 |
| 19:00 | 49,014 | 0,024361018 | 0,005229394 | 5,14697497 |
| 20:00 | 47,469 | 0,02359312 | 0,005064556 | 4,92516261 |
| 21:00 | 44,856 | 0,022294402 | 0,00478577 | 4,60305991 |
| 22:00 | 41,431 | 0,020592103 | 0,00442035 | 4,17671927 |
| 23:00 | 36,864 | 0,018322205 | 0,003933088 | 3,739709445 |
| 24:00 | 33,239 | 0,016520502 | 0,00354633 | 3,164373634 |
| **Total** | 950,659 | 0,472498087 | 0,101427569 | 101,4275692 |

*Table 8 - Reference daily consumption of energy required by the urban load during 15 January 2018*

For each hour it was possible to obtain the final balance from the Terna site, i.e. the quantity of electrical power dispatched during the reference day.

This process took place for all 24 reference days, and at the end of the collection and processing of such data, the annual trend of the residential urban load was obtained. This trend is therefore the energy demand that must be satisfied by our multi-energy plant.

The following two figures show the trends obtained on the reference days, fig. 13 for weekdays, while fig. 14 for non-working days:

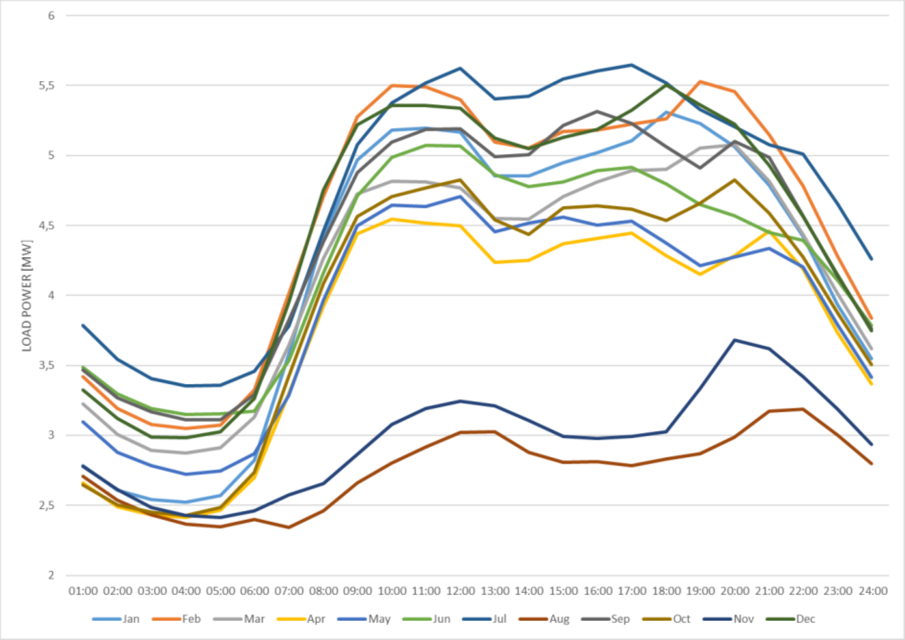

*Figure 13 - weekday energy consumption behaviour*

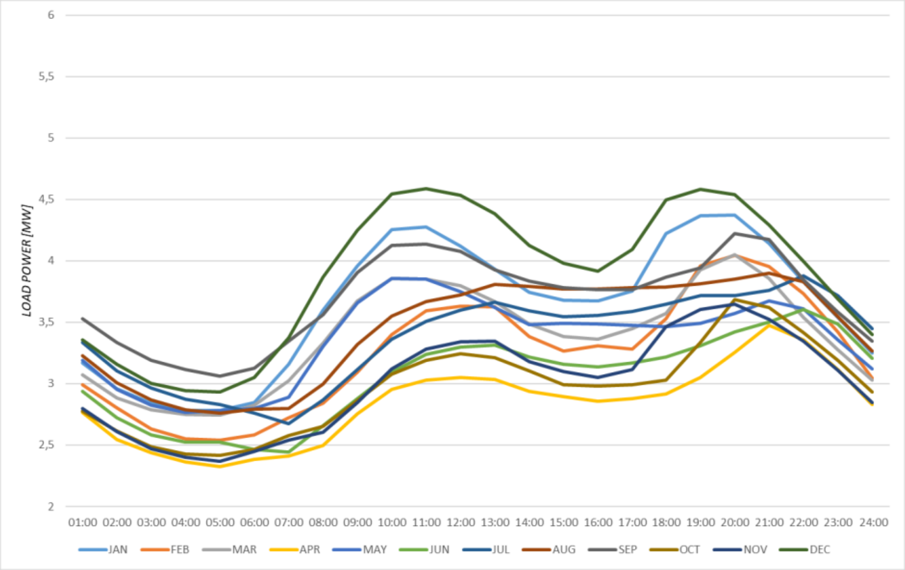

*Figure 14 - weekend energy consumption behaviour*

The trend illustrated in the two figures is in line with city habits. During the night, both on weekdays and on non-working days, energy consumption reaches its minimum, as most of the population is sleeping and not using any sort of appliances. While there are two maximum peaks during the day, generally at the beginning / mid-morning and at the end of the working day.

Instead, considering the annual trend, but also analyzing the graphical outputs expressed by the figures above, the maximum power required by the urban load was easily identified, equal to about 5.6446 MW, on Wednesday 18 July 2018, at 17:00. This datum is of fundamental importance for the thesis work because, as shown successively, it will set the size of the SOFC, which must guarantee a power able to satisfy this maximum value. In addition, it will also be useful for the photovoltaic part, as it will be used as a term of comparison on which to establish the size of this section of the polygenerative system. Finally, as last piece of data collected, it is of primary importance the total amount of energy required by the urban center. The numerical determination of the hourly trend of Italian energy consumption in the residential sector, in terms of energy, made it possible, using the Excel software, to easily calculate this data by making a cumulation of this trend. The final result, in 2018, was approximately 33.975 GWh consumed.

The procedure performed made it possible to identify the initial variables. The design of the photovoltaic field will be explained in the next paragraph.

### 3.1.2 Photovoltaic field, the solar power system

The production of electricity from photovoltaics was modelled using an online software, PVGIS [74]. This software was developed in collaboration between the Joint Research Center, the Institute for Energy and Transport and the European Commission. It provides an online simulator that calculates the solar radiation (amongst others solar quantities), in a specific geographical position, requesting a series of basic elements as initial data.

Through the direct analysis of the data chosen for the thesis work, the municipality of Menfi (AG) was chosen as the geographical location of the photovoltaic field, specifically the countryside on the outskirts of the city, with latitude coordinates equal to 37.612, longitude of 12.935 and 103 m asl as altitude. Subsequently, the program allows to choose between different solar radiation databases, which differ according to the method of data collection, satellite or climatic processing, but also based on the uncertainty of the data provided. In this thesis work, the PVGIS-SARAH, of the satellite type, recommended as the most reliable and with the lowest measurement error, was used as a database. Subsequently, the simulator requires to enter specific data relating to the panels used: the technology used was that of crystalline silicon, now consolidated and which guarantees a good electrical conversion performance, about 21%, and low system, about 14%. Subsequently, the system size was entered. Considering the data obtained in the previous paragraph “3.1.1”, and considering that the energy production would also have been carried out through SOFC, the size of 9 MW was chosen, a compromise between cost / size and producibility. The last data necessary for the program were the position of the panel, chosen through the ground mounting method, its slope and its azimuth, which were not chosen directly but through the simulator: it was possible to opt for a suggested optimization by checking the slope and azimuth optimization options, which resulted in final values of 32° and 3° respectively.

Once the analysis was carried out, it was possible to download the hourly data related to the entire year of 2018 and report them on an Excel sheet to be able, later, to carry out further processing. As stated at the beginning of the paragraph, the main data is that of global irradiance on the inclined plane, G [W/m$^2$]. In addition to this piece of data, the direct irradiance on inclined plane, $G_{b,n}$ [W/m$^2$] was obtained, the diffuse irradiance on inclined plane, $G_{d,h}$ [W/m$^2$], the reflected irradiance on the inclined plane, $G_{t,h}$ [W/m$^2$], the Sun height, $h_{sun}$ degree, the 2 m air temperature, $T_{2,m}$ [°C] and 10 m total wind speed, $WS_{10,\ m}$ [m/s]. By using this data it was possible to perform two types of modeling, which vary according to their degree of accuracy. The first, the simplest, has the effect of producing a less accurate analysis. It is based on standard parameters, specifically the global irradiance at standard test condition, $G_{stc}$, with a value of 1000 W/m$^2$ and the standard cell temperature, $T_{cell}$, STC equal to 20 °C. Known the nominal size of the photovoltaic system, equal to 9 MW, the efficiency of the monocrystalline silicon panels, 21%, and the latter reference standard data for solar radiation, using the following eq. (31), the area of the photovoltaic field is easily obtained:

$$A = \frac{W_{pv,nom}}{G_{stc} * \ \eta_{pv}} \tag{31}$$

In the examined case, the determined area corresponds to an area of 42'857,14 m$^2$. With the use of this data, it is possible to calculate the power produced by the photovoltaic system, hour by hour, using the following eq. (32):

$$W_{pv} = G * A * \eta_{pv} * PR \tag{32}$$

The only missing piece of data is the Performance Ratio (PR), a dimensioned variable that is used to compare photovoltaic systems that use different technologies. It is given by the ratio between $E_M$ [kWh/m$^2$], the monthly energy output from fix angle of PV panel, and $H_M$ [kWh/m$^2$], the monthly plane irradiation for fix angle. PR is calculated month by month and used in Eq. (32), based on the calculation month. The following table 9 shows the values obtained during the calculation phase:

| Em [kWh/m2] | Hm [kWh/m2] | PR |
|---|---|---|
| 95,20 | 113,7 | 0,8373 |
| 99,47 | 119,58 | 0,8318 |
| 130,41 | 159,86 | 0,8158 |
| 149,33 | 186,71 | 0,7998 |
| 165,69 | 211,44 | 0,7836 |
| 163,05 | 212,98 | 0,7655 |
| 175,65 | 232,36 | 0,7559 |
| 171,18 | 225,54 | 0,7590 |
| 143,41 | 184,85 | 0,7758 |
| 127,76 | 160,95 | 0,7938 |
| 103,62 | 127,02 | 0,8157 |
| 92,62 | 111,17 | 0,8332 |

*Table 9 - PR monthly calculation*

Once this last piece of data has been determined, using eq. (32), the power value generated by the photovoltaic system is calculated for each hour. Furthermore, with the same procedure used and described in the previous paragraph “3.1.1”, the power value is used to calculate the total annual energy produced. In the end, the total amount of energy produced in the case in question corresponds to approximately 14.356 GWh, corresponding to a total annual amount of 1595 hours of active production in 2018.

A second level of more refined modelling has been then applied, [77], [78], [79], involving the use of additional formulas, in order to provide more reliable data as output for a more precise energy analysis of the PV system. This second modeling does not consider the panel always at the same temperature, but at its real temperature, eq. (33), depending on the irradiance value to which it is subject. This is important because as the temperature of the panel increases, its efficiency and therefore its power produced decreases.

$$T_{cell} = T_a + \frac{G_{tot}}{800} * (NOCT - T_{cell,STC}) \tag{33}$$

$T_a$ is the air temperature, [°C]; $T_{cell\_STC}$ is the standard temperature of the panel, equal to 20 °C, to which the previous modeling referred; 800 is the reference solar radiation, in W/m$^2$; NOCT is the Normal Operating Cell Temperature, which assumes a tabulated value based on the reference geographical position. For Menfi (AG) 48 °C is used. Finally, $G_{tot}$ is the total solar radiation reaching the photovoltaic panel.

$$G_{tot} = G_{b,n} * \cos(\theta) + G_{d,h} * F_{c,s} + G_{t,h} * \rho_g * (1 - F_{c,s}) \tag{34}$$

Eq. (34) reports the formula used to calculate the total solar radiation incident on the photovoltaic panel. It is given by the contribution of direct, diffuse and reflected radiation that are provided directly by the PVGIS software. g is the albedo, which is a dimensionless variable that expresses the ability to reflect sunlight. An albedo of 0.2, [80] is considered for the crystalline silicon panel. Finally, θ, that is the angle of incidence of sunlight on the photovoltaic panel. This variable needs further formulas to be calculated, below are the formulas necessary for its determination:

$$\cos(\theta) = \cos(\beta)\cos(\theta_z) + \sin(\beta)\sin(\theta_z)\cos(\gamma_s - \gamma) \tag{35}$$

$$\cos(\theta_z) = \cos(\phi)\cos(\delta)\cos(\omega) + \sin(\phi)\sin(\delta) \tag{36}$$

$$\delta = 23.45\sin(360\frac{284 + n}{365}) \tag{37}$$

$$\omega = (h - h_{culm})\frac{360}{24} \tag{38}$$

$$h_{culm} = 12 + \frac{L_{toc} - L_{ref}}{15} - \frac{EOT}{60} + DST \tag{39}$$

$$\begin{aligned} EOT = 229.2(&0.000075 + 0.001868\cos(B) - 0.032077\sin(B) \\ &- 0.014615\cos(2B) - 0.04089\sin(2B) \end{aligned} \tag{40}$$

$$B = \frac{(n-1)360}{365} \tag{41}$$

$$\cos(\gamma_s) = \frac{\cos(\theta_z)\sin(\phi) - \sin(\delta)}{\sin(\theta_z)\cos(\phi)} \tag{42}$$

$$F_{c,s} = \frac{1 + \cos(\beta)}{2} \tag{43}$$

With the exception of eq. (43), which reports the formula for the calculation of the collector sky view factor, $F_{c,s}$, which indicates the portion of the sky visible from the observation point of view of the panel and is of fundamental importance to quantify the portion of diffuse and reflected radiation perceived by the panel, all the remaining equations serve to determine θ. Starting from eq. 35, the one that allows to determine the angle by applying the arc of the indicated function, shows further variables: β is the optimal inclination of the panel, equal to 32°; $\theta_z$ is the zenith, the angle between the parallel line from the observation point and the plane parallel to the surface of the solar panel; γ is the surface azimuth equal to 3° in this specific case of work and $\gamma_s$ the solar azimuth, i.e. the angle that is formed between the line that hypothetically joins the panel to the sun, and the horizontal plane of the earth's surface.

Eq. (36) is used to calculate the zenith, having available the latitude, ϕ, the inclination of the Earth's axis, φ, equal to 23°27' and the hour angle, ω, an astronomical parameter that represents the angle between the plane passing through the Earth's axis and the zenith, and the plane containing the Earth's axis and the zenith. φ can actually be calculated more accurately by using eq. (37), where n is simply the day of the year in which the calculation is being performed. Eq. (38), on the other hand, is the formula used to calculate the hour angle, where h is the standard time and $h_{culm}$ is the noon time, calculated by eq. (39). In this last equation, the difference between $L_{toc}$ and $L_{ref}$ is the difference in longitude between the observer's meridian and the longitude of the meridian in the local time zone, while EOT eq.(40) represents the Equation Of Time in minutes and DST the Daylight Saving Time, equal to 1 if it is considered or 0 if not. Eq. (42) is used to calculate the solar azimuth, using the variables just described, and finally eq. (41), complementary for the calculation of EOT, in which n is the number of the day considered for the calculation.

After the calculation of formulas above described, thus once the total radiation and the real temperature of the panel have been calculated, it is possible to use a final formula, eq. (44), from which the real power produced by the cell is calculated, [81]:

$$W_{pv\_real} = f_{pv} * \frac{W_{pv,nom} * G}{G_{stc}} \left[1 + \Omega\left(T_{cell} - T_{cell,STC}\right)\right] \tag{44}$$

Where $f_{pv}$ is the derating factor, a parameter that serves to quantify the use of an electronic component, and therefore, based on its use, how much it's preserved and how much it's consumed, taken equal to 82% [75]. Ω is the temperature coefficient, which allows to numerically quantify the effect of temperature on the power produced, equal to -0.3 %/K, [76]. All other parameters are known and have already been explained.

Considering all the formulas listed above, as expected, a reduction in the annual energy produced by the photovoltaic field was obtained, operating a number of hours lower than the previous case, equal to 1339 hours, and passing from approximately 14.356 GWh, to 12.053 GWh, leaving uncovered a portion of electricity equal to (33.975 – 12.053) = 21.922 GWh. Therefore, known the consumption required by the urban city, calculated in paragraph “3.1.1”, and quantified the producibility of the photovoltaic system, the missing share of electricity that must be integrated through SOFC is identified by difference. These two primary quotas are reported on a monthly basis in the following fig. 15, which allows to better visualize and recognize the quantities and trends involved in this first energy analysis. As expected, the producibility of the renewable plant is greater in summer, when the hours of light during the day are superior.

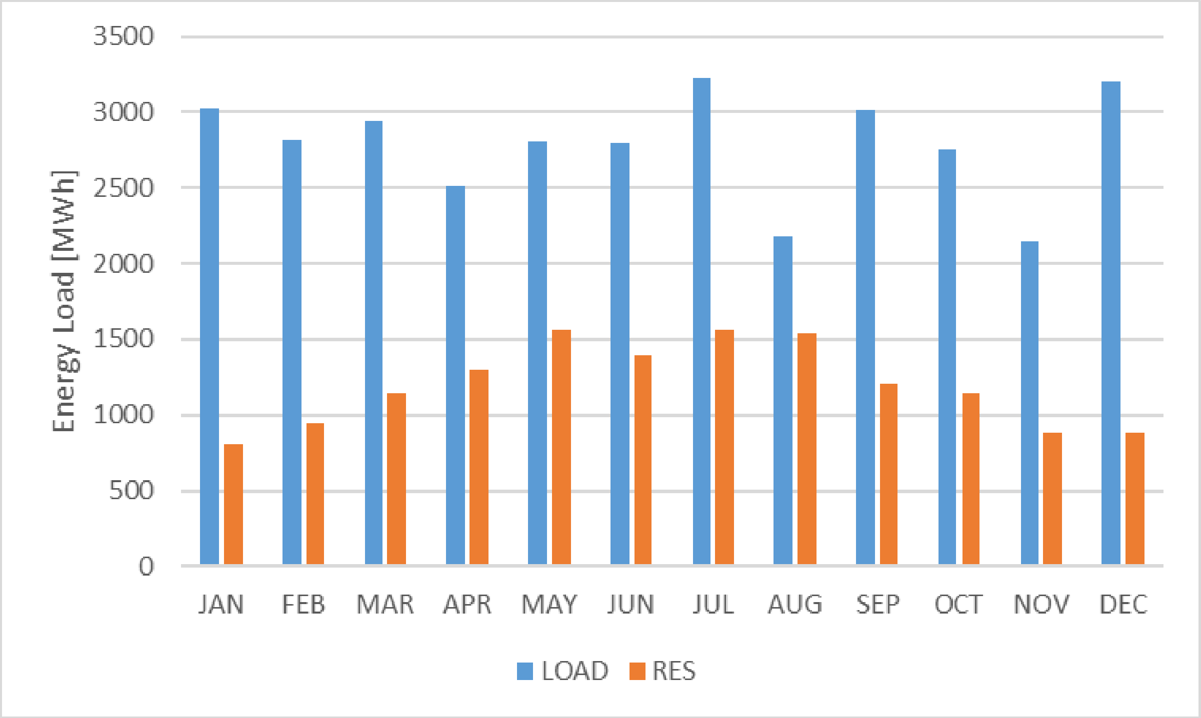

*Figure 15 - comparison between electrical input from urban load and electrical output of PV field*

From the next paragraph the main component of greatest interest for the plant will become specifically relevant: the reversible Solid Oxide Cell.

## 3.2 Physic behaviour of rSOC

This following chapter provides a detailed description of the physics involved in rSOC operation and of the approaches that can be followed for its modelling. Specifically, as a first hypothesis, a 0D model is assumed for the formulations and description of the phenomena involved in the rSOC. This model in zero dimensions represents a simplification compared to reality or to more detailed models, as for example occurs in the work of Yu Luo et al [82], who adopts a 2D approach using a FEM (Finite Element Method) for a much more precise and exhaustive CFD (Computational Fluid Dynamic) analysis from a scientific and physical point of view. Despite this, for the purpose of this thesis work, the 0D model has sufficient validity and completeness.

As already mentioned in “2.2”, the rSOC system is an electrochemical device. By analyzing this compound word it can be stated that, with the prefix “electro” the ability of the device to produce or absorb power is meant, working as SOFC or SOEC respectively. Therefore, the two typical variables that characterize an electrical object become predominant, namely the intensity of the current and the voltage. The latter, for both modes of operation, has a positive value, while the convention imposes, for the variable that represents the displacement of electrical charges over time, a positive sign if it works as a galvanic cell, while a negative sign if it works as an electrolyzer. These statements can be found in the next fig. 16, which directly reports the trend and dependence between these two electrical variables: the characteristic curve.

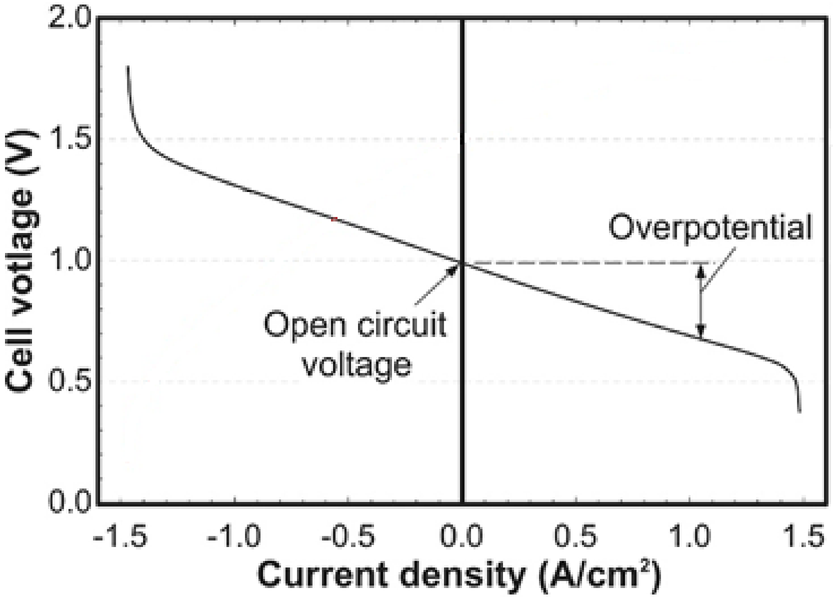

*Figure 16 - Polarization curve for both SOEC and SOFC mode [89]*

The curve allows to visualize and mathematically understand the potential of a specific electrochemical device. In fig. 16 the specific case of interest for the thesis work is reported, for a generic rSOC, which is the union of the trend from SOFC, which occurs in the right part, and the SOEC, on the left section.

Moreover, the curve allows a comparison between different electrochemical devices. This is simplified by the fact that, as seen in the abscissa axis of the graphic, the dependence of the voltage as a function of the current density is reported. The current density [A/cm$^2$] is the ratio between the current intensity [A] and the cell surface [cm$^2$]. Its use allows a better comparison, because it is more equitable, as an electrochemical device tends to generate a greater power in proportion to its size. In fact, considering the constant voltage variable, as the useful surface of the cell increases, the current produced also increases because there are physically more points, the tpb (see paragraph "2.2.2"), in which it is possible to carry out the electrochemical reactions.

The fundamental variables that characterize the polarization curve are explained in detail in the following rSOC modeling paragraphs.

Finally, in the word electrochemical reported above, the suffix "chemical" refers to the fact that the device is characterized by chemical reactions, which take place inside it and which generate electrical phenomena. In fact, the voltage that characterizes the cell is due to a change in potential that is generated between the anode and cathode, due to the different intensity between the electric fields produced by the reactions mentioned. The current intensity, on the other hand, is the direct cause of the motion of electrons in the external circuit that connects the two electrodes, also produced as a result of chemical reactions.

### 3.2.1 Open Circuit Voltage – OCV

The first variable that is analyzed and modeled is the so-called reversible voltage or Nernst voltage or Open Circuit Voltage (OCV). To prove the formula, it is necessary to start by carrying out a thermodynamic analysis of the herewith studied closed system rSOC.

The first hypothesis that is made upstream is to consider the system in equilibrium conditions, a definition that also coincides with the ideal case of thermodynamic reversibility. This condition specifically implies that the change in entropy, defined with the variable ΔS, which always occurs following a thermodynamic transformation, is ideally zero. In physical terms, this statement means that both the system and the environment do not undergo any variation or change, allowing the transition of state from the initial to the final conditions and vice versa.

The second hypothesis is stationarity. All dynamic behaviours and variations that would occur in reality are therefore neglected, and all physical variables subject to analysis, such as temperature, pressure, flow rates, etc. are considered constant. Basing on these hypotheses and finally considering the cell as a closed box, i.e. without specifying what is inside it, an energy balance is carried out.

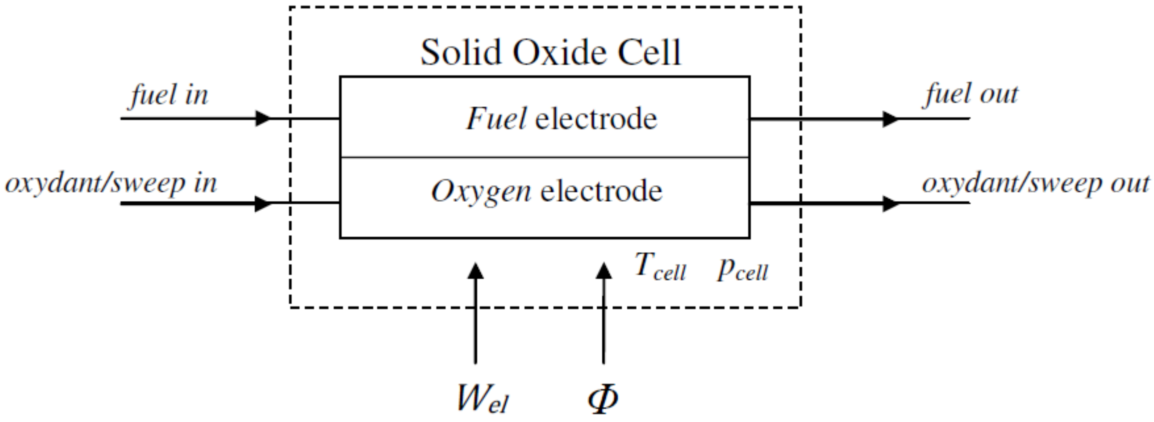

*Figure 17 - Energetic balance of rSOC*

The setting of the thermodynamic analysis is carried out using fig. 17 as a reference, in order to represent the control volume and the mass and energy streams involved. According to the first law of thermodynamics, eq. (45), the difference between thermal power $\phi_{th}$ [$W_{th}$] and electrical power $W_{el}$ [$W_{el}$] is assumed as the variation of energy generated between products and reactants, which in the case under consideration correspond respectively to products, fuel and oxydant. This energy variation is expressed as the product of the molar flow rate $\dot{n}$ [mol/s] and the specific molar enthalpy $\hat{h}$ [J/mol]:

$$\phi_{th} - W_{el} = \dot{n}_{prod}\hat{h}_{prod} - \dot{n}_{fuel}\hat{h}_{fuel} - \dot{n}_{oxydant}\hat{h}_{oxydant} \tag{45}$$

$$\hat{h} = f(T, p_i) \rightarrow \hat{h}(T, p_i) \tag{46}$$

On the other hand, from the second law of thermodynamics, eq. (47), it can be deduced that the ratio of the heat flux to the temperature, with the contribution of the irreversibility generated during the thermodynamic process $\Sigma_{irr}$ [W/K], is equal to the entropic variation generated between products and reagents:

$$\frac{\phi_{th}}{T_{rSOC}} - \Sigma_{irr} = \dot{n}_{prod}\hat{s}_{prod} - \dot{n}_{fuel}\hat{s}_{fuel} - \dot{n}_{oxydant}\hat{s}_{oxydant} \tag{47}$$

$$\hat{s} = f(T, p_i) \rightarrow \hat{s}(T, p_i) \tag{48}$$

As illustrated by eqs. (46) and (48), the specific molar enthalpy and entropy values are a function of the cell temperature and partial pressures. To better understand this last variable, it is stated that the total pressure of the rSOC is equal to the pressure value measured in the electrodes, which is constant and identical for both, deriving from the sum of the partial pressures exerted by the components that make up the inlet streams. Considering the contemporary literature, most of the studies present rSOC operating at ambient pressure, as can be seen in the works of Y.Lee [83], D. Ferrero [89] and R.K. Akikur [93]. This pressure value allows to obtain very low consumptions, above all electrical ones, as regards the auxiliary components, as for example it could happen in the operating case of a fuel cell, for the compression operation of the input stream composed of a high quantity of $H_2$. As already stated in "2.1.1", this element has one of the highest specific heats present in the materials used in the production of energy.

In addition to electricity consumption, examples could also be provided for the thermal case, as well as for the entire water pre-heating line which, starting from ambient temperature values, must usually heat up, evaporate and overheat before entering the rSOC. Despite these positive assumptions, with the continuous evolution of this innovative technology thanks to increasingly targeted research and studies, and above all to the development and advancement of knowledge for the construction materials used, studies at high pressures are also starting to be present in the literature. Among them S.H. Jensen [87] should be mentioned, who presents an experimental research where the main characteristics of the cell are tested as the pressure varies, reaching values of 25 bar. Further interesting theses are those of A. Rendine [84 ], M. Scaltritti [85], A. Calvo [86] and E. Giglio [90], in which studies of hypothetical polygenerative systems at about 30 bar are conducted, very similar in ethics to the work of this master thesis, which uses an rSOC operating at 33.1 bar. Although at first the consumption of some of the auxiliary systems increases their negative energy contribution due to the high pressure values, overall the system gets a general upgrade. The performance of the rSOC improves markedly as all its physical phenomena involved in the electrochemical reactions are improved, producing a chain effect on all components and systems connected downstream and obtaining higher global efficiency values. For example, considering the methanation section that follows the electrolysis phase, the reactors work at approximately the same pressure as the SOEC, at 32.4 bar, allowing to save considerable quantities of electrical energy to compress the stream leaving the electrolysis section which is characterized by a high amount of $H_2$.

Continuing with the thermodynamic analysis, once the equations that apply the first and second principles of thermodynamics on the system in question have been set, all the terms for the molar flow rate of the fuel are normalized, thus dividing everything by $\dot{n}_{fuel}$, the following is obtained:

$$q_{th} - l_{el} = v_{prod}\hat{h}_{prod} - \hat{h}_{fuel} - v_{oxy}\hat{h}_{oxy} = \Delta\hat{h}_{reac} \tag{49}$$

$$\frac{q_{th}}{T_{rSOC}} = v_{prod}\hat{s}_{prod} - \hat{s}_{fuel} - v_{oxy}\hat{s}_{oxy} = \Delta\hat{s}_{reac} \tag{50}$$

Where, $q_{th}$ is the molar heat J/mol, $l_{el}$ is the molar work J/mol and $v_{(i)}$ is the stoichiometric coefficient for a generic reactants and product, dimensionless. As can be seen in eq. (50), the contribution of irreversibility, $\Sigma_{irr}$, is neglected thanks to the first hypothesis expressed at the beginning of the paragraph in which the equilibrium condition was stated. Finally, the contribution of molar heat is made explicit in eq. (49) and is replaced in eq. (50) obtaining eq. (51):

$$l_{el} = T\Delta\hat{s}_{react} - \Delta\hat{h}_{reac} = -\Delta\hat{g}_{react} \tag{51}$$

In paragraph "2.2.1.1" the Gfe is explained in detail. Eq. (51) therefore indicates that the molar work is equal and opposite to the variation of Gfe between products and reagents. This result also explains the fact that for a fuel cell, characterized by a negative Gfe variation, there is an electric power production ($l_{el}$> 0), while for an electrolyser, characterized by a positive Gfe variation, there is an absorption of electrical power ($l_{el}$ <0).

The next equation which allows to continue the proof of the OCV is Faraday's Law, as illustrated by eq. (52). This formula allows to quantify an electric current, associating it with a molar flow. In this relation two elements are introduced: the Faraday constant, F, of value 96’487 [C/mol], which derives from the product resulting from the Number of Avogadro, $N_a$, equal to $6.02214076*10^{23}$ [particles per mol] and the charge of an electron , $q^{e-}$, with value -$1.60217663*10^{-19}$ [C]; the second element is the variable $Z_r$, which is called charge number and represents the number of electrons exchanged (delivered by oxidation or gained by reduction) in the electrochemical reactions of the species $(-)_r$:

$$\dot{n}_r = \frac{I}{Z_r F} \tag{52}$$

Finally, considering what happened in the previous steps, when eqs. (45) and (47) were normalized, the electric power term was divided by the molar flow rate of the fuel and the molar work was obtained. Taking advantage of this formulation and simultaneously substituting for the term of the molar flow rate present in the denominator, the fraction deriving from eq. (52), for the term of electrical power present in the numerator, the product of voltage and current, and finally for the term of molar work eq. (51), the final desired equation is obtained, representing the OCV (eq. (53)). In fact, by rearranging the equation obtained, making the voltage explicit, the OCV is obtained. The procedure just described is shown below:

$$\begin{cases} W_{el} = I * V \\ l_{el} = \dfrac{W_{el}}{\dot{n}_{fuel}} \\ eq.52 \end{cases} \rightarrow \begin{cases} l_{el} = \dfrac{I * V}{\dfrac{I}{Z_r F}} \\ eq.51 \\ V = OCV \end{cases} \rightarrow OCV = -\frac{\Delta\hat{g}_{react}}{Z_r F} \tag{53}$$

The first and most important parameter of the polarization curve is the OCV, represented in the previous fig. (16) by the origin of the axes. It represents the voltage that would be measured when the cell is operating as an open circuit, without any current that flows in the external circuit. It means that transport phenomena (that will be analyzed successively) do not occur, without any generation of entropy, as expressed in the initial hypotheses. By applying the ideal gas model, Eq. (53) can be decomposed, obtaining the following Eqs. (54) and (55):

$$OCV_{SOFC} = -\frac{\Delta g_{react}(T, p_0)}{Z_r F} + \frac{RT}{Z_r F} \ln\left[\frac{\prod_i^{\#react}\left(\frac{p_i}{p_0}\right)^{v_i}}{\prod_i^{\#prod}\left(\frac{p_i}{p_0}\right)^{v_i}}\right] \quad (54)$$

$$OCV_{SOEC} = +\frac{\Delta g_{react}(T, p_0)}{Z_r F} + \frac{RT}{Z_r F} \ln\left[\frac{\prod_i^{\#prod}\left(\frac{p_i}{p_0}\right)^{v_i}}{\prod_i^{\#react}\left(\frac{p_i}{p_0}\right)^{v_i}}\right] \quad (55)$$

As already mentioned, the formula of OCV is also named Nernst equation thanks to Walther Hermann Nernst who discovered and formulated it first. Specifically, eq. (54) describes the fuel cell behaviour, while eq. (55) the electrolyser mode. Basically, the differences between the two formulas, as already mentioned for eq. (51), are the Gfe variation. Regarding the electrolyser mode, the variation is positive, because of the chemistry nature of the reactants involved. In fact, the chemical reactions involved in this modality are non-spontaneous reactions, it is necessary to supply electrical power to make them happen. In the specific case of this thesis work, this peculiarity is exploited precisely to store excess energy from the photovoltaic field, in the form of a chemical product. Regarding the other mode, the Gfe assumes a negative value, distinguishing the chemical reactions involved as spontaneous reactions, therefore without any need for external inputs, providing the electrical power produced by the SOFC as output, for the case analyzed in this thesis work.

The second different aspect of the formulas is related to the variable pressure. As previously announced for Eqs. (46) and (48), enthalpy and entropy are sensitive to temperature and pressure values, a statement that is also valid for Gfe. In fact, in eq. (54) and (55) this dependence is directly indicated, where $p_0$ is equivalent to the reference pressure, 1 bar, while the remaining part of the formula, and specifically the logarithm argument, allows to represent the contribution of the components that make up the incoming and outgoing streams from the rSOC system. Between the two modes, the arguments of the logarithm are reversed, this due to analytical considerations.

Like pressure, temperature also affects these thermodynamic parameters. The following figures 18 and 19 represent this concept: they report the trend of Gfe, enthalpy and entropy as a function of the temperature and operating voltage of the cell, for $H_2/H_2O$ e $CO/CO_2$, the chemical elements mainly involved in electrochemical reactions:

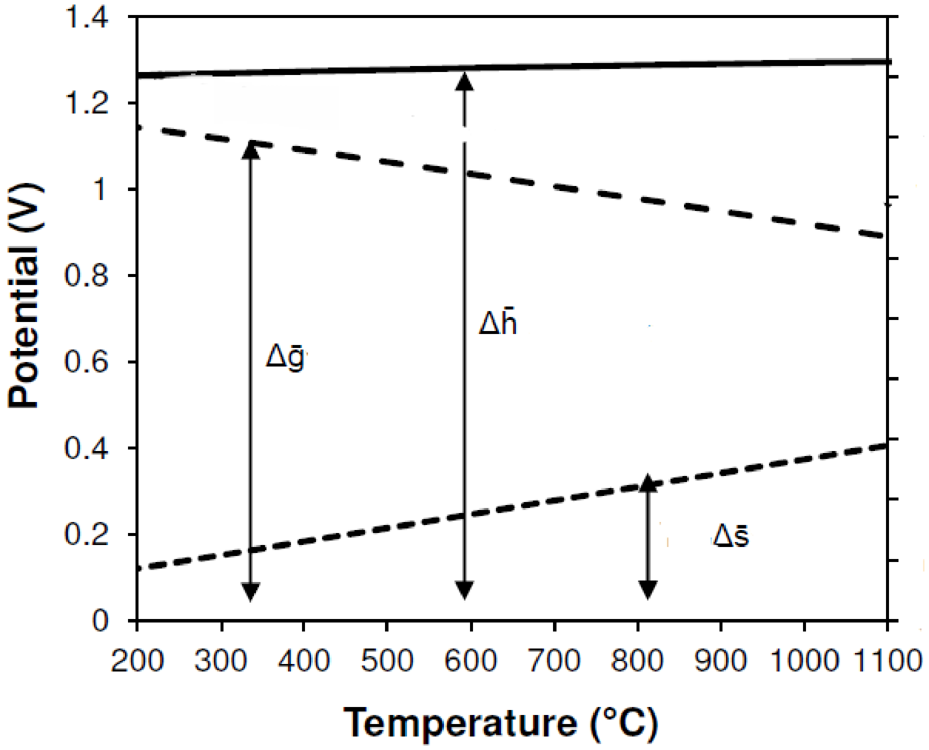

*Figure 18 - Hydrogen and Water dependency*

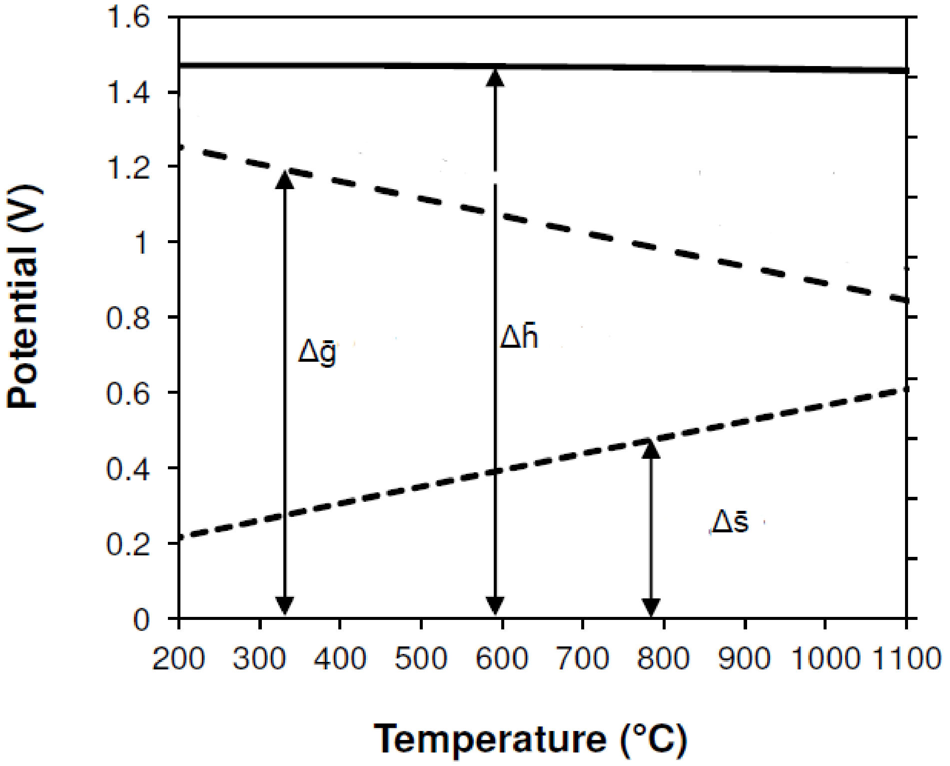

*Figure 19 - Carbon monoxide and dioxide dependency*

The ordinate axes of fig. 18 and 19 refer to the voltage values exerted by the cell. The difference in the values reported on these axes is due to the fact that the thermodynamic variations involved in the $H_2$ / $H_2O$ reactions are different from those that occur in the case of CO / $CO_2$. Consequently, one would expect different values of OCV, but in practice and with a good approximation to what really happens in reality, in the case in which these elements are present at the same time within the rSOC, the final values of OCV turn out to be identical, a cause of the WGS reaction, eq. (4) of paragraph “2.1.2.1”. Therefore, referring to the work of D. Ferrero [89], by considering the redox reaction $H_2$ / $H_2O$ (eq. (56)) and the CO / $CO_2$ reaction (eq. (57)), it can be shown that, at the equilibrium, the voltage variation between these two pairs of chemical compounds is zero (eq. (61)):

$$H_2 + \frac{1}{2} O_2 \leftrightarrow H_2O \tag{56}$$

$$CO + \frac{1}{2} O_2 \leftrightarrow CO_2 \tag{57}$$

$$E_{H_2/H_2O} - E_{CO/CO_2} = \frac{\Delta \hat{g}_{H_2/H_2O}(T, p_0)}{2F} - \frac{\Delta \hat{g}_{CO/CO_2}(T, p_0)}{2F} + \frac{RT}{2F} \ln \left[\frac{p_{H_2O} p_{CO}}{p_{H_2} p_{CO_2}}\right] \tag{58}$$

$$E_{H_2/H_2O} - E_{CO/CO_2} = \frac{(\hat{g}^0_{H_2O} - \hat{g}^0_{H_2} - \hat{g}^0_{CO_2} + \hat{g}^0_{CO})}{2F} + \frac{RT}{2F} \ln \left[\frac{p_{H_2O} p_{CO}}{p_{H_2} p_{CO_2}}\right] \tag{59}$$

$$\Delta \hat{g}_{WGS} = \hat{g}^0_{H_2} + \hat{g}^0_{CO_2} - \hat{g}^0_{H_2O} - \hat{g}^0_{CO} + RT \ln \left[\frac{p_{H_2} p_{CO_2}}{p_{H_2O} p_{CO}}\right] = 0 \tag{60}$$

$$E_{H_2/H_2O} - E_{CO/CO_2} = \frac{\left(\hat{g}^0_{H_2O} - \hat{g}^0_{H_2} - \hat{g}^0_{CO_2} + \hat{g}^0_{CO}\right)}{2F} - \frac{\Delta \hat{g}^0_{WGS}}{2F} = 0 \tag{61}$$

Eq. (58) indicates the potential variation that occurs between the two redox pairs, directly proportional to the Gfe values. In order to demonstrate that its value is zero, eq. (60) represents the variation of Gfe for the reaction of WGS, eq. (4) of paragraph "2.1.2.1", consisting of its contribution of variation under conditions environment / reference ($\Delta \hat{g}^0_{WGS} = \hat{g}^0_{H_2} + \hat{g}^0_{CO_2} - \hat{g}^0_{H_2O} - \hat{g}^0_{CO}$) and the contribution of the partial pressures. Furthermore, with the fuel equilibrium condition, this variation is considered to be zero, as reported in eq. (60). Finally, by replacing eq. (60) inside eq. (59), eq. (61) is obtained and its null value is shown.

It can be stated that, for the specific case of the thesis work, the calculation relating to the OCV variable was carried out only considering the redox chemical reaction $H_2$ / $H_2O$, explained in the previous eq. (56), despite the presence of the CO / $CO_2$ couple. This allows to calculate the OCV value only once and to use it for both cases: for example, considering the rSOC operating in electrolysis, this mode can operate in steam-electrolysis or co-electrolysis, but independently from this, even if these two modes of operation foresee the use of $H_2$ / $H_2O$ and $H_2$ / $H_2O$ & CO / $CO_2$, the OCV value will be the same.

Next equations report the specific formula used in the calculation:

$$OCV_{\mathrm{H2/H2O}} = OCV^{0}_{\mathrm{H2/H2O}} + \frac{RT_{cell}}{2F} \ln\left[\frac{\gamma_{H_2}\sqrt{\gamma_{O_2}}}{\gamma_{H_2O}}\right] + \frac{RT_{cell}}{2F} \ln\left[\sqrt{\frac{p_{rSOC}}{p_0}}\right] \tag{62}$$

$$OCV^{0}_{\mathrm{H2/H2O}} = 1.253 - 2.4516 * 10^{-4} * T\ [K] \tag{63}$$

Eq. 62 differs from the basic formulation reported in eq. (54) and/or (55) in that the product that generates the partial pressure ($\mathrm{p}_i = \mathrm{p}_{tot}\ \gamma_i$ in which $\gamma_i$ represents the mole fraction of the considered component) is made explicit, exploiting the properties of logarithms. eq. (63) is an equation obtained from experimental data and adopted in many scientific articles, as in [83], [86], [91] and [93], which allows to obtain the standard value of OCV for the redox $H_2$ / $H_2O$.

At the end, considering the inlet reactants' molar fractions in the device and the operating rSOC's conditions, 850 °C and 33.1 bar, the final value obtained for the OCV value is **0.916** [V].

### 3.2.2 Electrochemical model: the formulation of the rSOC operation voltage

As explained in the previous paragraph, the OCV is the ideal voltage to which the rSOC is subjected in case the external circuit, which connects the two electrodes and which has an attached load in the middle, is disconnected: circuit condition open. Theoretically we have a voltage applied to the device but not a current produced. The main characteristic of this ideal voltage is that, as the name implies, it does not ideally consider all those loss phenomena, which would penalize the performance of the rSOC. Therefore, it can be said that the OCV is the voltage limit value that characterizes the two operating modes of the rSOC: as regards the SOFC mode, the goal is to produce electrical power. In fact, for this case the OCV represents the maximum voltage value. Considering the losses of the operating phase, lower voltage values would be obtained, thus producing lower values of generated electrical power. As for SOEC, the goal is to produce chemicals by absorbing electrical power to cause electrochemical reactions, therefore, the OCV value in this case corresponds to the minimum, allowing it to consume the least amount of electricity. All other voltage values for the electrolysis operation are greater. Obviously, these statements about the power produced and absorbed are purely theoretical, since, as the current is zero in open circuit conditions, the product between OCV and current would always be zero. What has been said regarding the voltage values is reflected in fig. 16, which represents the polarization curve, directly proportional to the voltage and current density values.

It is of primary importance to explain the complete cell voltage formula, shown in the following eq. (64):

$$V_{cell} = OCV \pm \eta_{act,an} \pm \eta_{act,cat} \pm \eta_{ohm} \pm \eta_{diff,an} \pm \eta_{diff,cat} \tag{64}$$

The terms named with $\eta_{(x)}$ represent the losses of the system and are called overpotential losses. The sign is positive or negative based on the cell operation. As just stated, the fuel cell mode, as the current increases, or rather the current density, decreases the voltage values. Consequently, the negative convention is used for the SOFC. On the other hand, for SOEC, the positive convention is used because, as the current density increases, its voltage values increase.

As shown by eq. (64), there are three types of overpotential losses characterized by the subscript -act, -ohm and -diff, each of which indicates a direct consequence to a specific physical phenomenon. Furthermore, they are graphically reflected in the three different slopes of the polarization curve, which as a final result obtains that typical elongated s-shape and rotated by - 90 ° (as observed in the previous fig. 16). Therefore, the three characteristic traits are reported:

- The first section is characterized by the charge transfer phenomenon. It refers to the kinetic behaviour of electrochemical reactions both for the fuel and oxygen electrode, graphically represented by the first non-linear stretch just after the OCV in the polarization curve;
- The second is the charge conduction phenomena which refers to the resistance of pass through the electrolyte layer and in the external circuit, for ions and electrons respectively, graphically represented by the second trait. It's the most representative of the cell and easily identifiable as it is the linear part of the polarization curve;
- The third, the mass diffusion, refers to molecule diffusion in both electrodes, graphically represented by the last non-linear section of the polarization curve.

A further brief description of each of these terms is reported below, although a simplifying hypothesis of linearity will then be made, in which only the contribution of overpotential losses deriving from the charge conduction phenomena will be considered predominant.

#### 3.2.2.1 Activation overpotential – $\eta_{act,an|cat}$

The voltage of the cell is affected by the kinetic of both half electrochemical reactions, which take place in the two electrodes separately. Each reaction has its own kinetic, a proper characteristic time, strictly related to its rate of reaction. Usually, when a chemical formula is reported, it refers to the main reactants and products that are required and obtained respectively to carry out this reaction. In reality, as far as complex reactions are concerned, there are intermediate reactions that follow each other in a chain and that allow the global reaction to take place as it is then briefly reported in conclusion. For this reason, the global rate of reaction is obtained as the average of the kinetics involved in all the process reactions.

It depends on many factors such as reactants' utilization, the concentrations of the chemicals involved in the process and on the constant rate. The latter is a kinetic parameter calculated by the Arrhenius equation, which gives a correlation between the activation energy of the reaction-step and the temperature involved ($k = Ae^{-\frac{E_a}{RT}}$). The lowest value of the constant rate determines the "Rate determining step", that determines the speed (rate) at which the overall reaction proceeds.

Considering usually a general chemical reaction, the rate of reaction only depends on temperature, while, in an electrochemical reaction, the rate of reaction depends on the temperature and also on the potential gradient in the electrodes, ω. It is an electrical parameter which affects the kinetic of the reactions involved and modifies the energy level of reactants or products. This advantage, divided between positive effect at reactants and at products, is expressed by the symmetry factor β.

Therefore, starting from the equation of the electrochemical rate of reaction ($\acute{\Gamma}(T, \omega) = k(T)e^{\frac{\alpha F}{RT}vz\omega}$), Butler and Volmer formulate another expression which states the relationship between the current density ($i$) and the potential gradient ($\eta_{act}$), inside the electrode, due to charge transfer phenomena taking place when the reaction has been activated. It is called Butler-Volmer equation, and it is represented in the next eq. (65). Combined with the definition of hyperbolic sin, the activation overvoltage formula is achieved in eq. (66):

$$i = i_0 \, [\exp\left(\frac{(1-\beta)F\eta_{act}}{RT}\right) - \exp\left(\frac{\beta F\eta_{act}}{RT}\right)] \tag{65}$$

$$\eta_{act} = \frac{RT}{\beta F} * \sinh^{-1}(\frac{i}{2i_0}) \tag{66}$$

Almost all the constitutive variables of the formulae have already been described, as the symmetry factor $\beta$, the Faraday constant F, the universal molar constant of gas R and the temperature of operation T. $\eta_{act}$ is the voltage drop [V] generated by the electrochemical reactions. Instead, $i_0$ is the exchange density current, an important parameter which expresses the capacity, for each electrode, to cause the reaction to take place. It is influenced by the amount of tpb, the temperature and the amount of catalyst distributed in the electrodes: a larger value of tpd means larger areas where the reactions can take place, thus a larger $i_0$; indeed, an electrode with a fine-grain structure will perform much better than a coarse grained one.

#### 3.2.2.2 Diffusion overpotential – $\eta_{diff,an|cat}$

The second loss in the formulation of the cell voltage is the diffusion overpotential ($\eta_{diff}$). When the streams of reactants composed of fuel and oxygen agents are sent to supply the electrochemical reactions in both the electrodes, two different conditions of these streams can be noticed. The initial condition, named bulk condition, refers mainly to the concentration assumed by the stream in the supply channel, before interacting with the electrode. Then, the gas flows across the electrode, reaching the point of activation determining the effective reactant concentration condition, the second one. The physical process of gas' molecular diffusion, strictly affects the total amount of reactants (more precisely, their concentration) in the point of reaction.

$$D_i^{eff} = D_i \left(\frac{\varepsilon}{\tau}\right)^n \tag{67}$$

The effective diffusive coefficient of the i-specie, $D_i^{eff}$, is the best parameter to identify the real concentration condition of the gas reactant in the point of reaction. It takes into consideration the starting diffusive coefficient in bulk condition, $D_i$, coupled with the porosity of the electrode, $\varepsilon$, and the flow gas tortuosity, $\tau$. As already mentioned, the diffusive coefficient in bulk condition describes the concentration of the gas species before any interaction with the electrode of interest. If the effective diffusive coefficient assumes the same value of the bulk condition one, it will be an ideal condition, where the diffusive phenomenon doesn't produce any loss. In reality the losses are present, and they derive from the porosity of the electrode material, so the void space inside it where the gas flow is able to pass (thus, this coefficient is strictly depending on the material which it is made). Then the tortuosity, the pathway configuration followed by the stream of gas inside the electrode. The more complicated the path, the higher the tortuosity, which causes a lower diffusive coefficient. Lastly, in eq. (67), the coefficient "n" is a fitting parameter.

Therefore, it is clear that diffusion phenomena are linked to the reagents' concentration in the tpb of the electrodes. Considering a normal operation condition of rSOC, when it requires larger current, higher number of reactions are necessary in the reaction points. To drive this process correctly, a proper number of molecules are needed in this region. Their amount grows with the increment of the current and, in this situation, the mechanism of molecular diffusion in the porous structure of the electrodes may become too slow to replace rapidly enough the molecules which have reacted over the electrode surface, causing the molecule storage phenomenon. This is why the reactant concentration drop rises in the reaction point, producing the overpotential loss in terms of cell voltage. Physically, this diffusion phenomenon does not produce directly a potential drop, but rather it indirectly achieves it, reducing the reactant concentration in the reaction point which is strictly related to voltage through a Nernstian effect. Therefore, a proper model is fundamental to approximate the diffusion phenomenon effect related to the voltage drop. Srikanth S. et al [35] observed that the Fick's Model, the Stefan-Maxwell Model and the Dusty Gas Model (DGM) are commonly used for modelling the mass transport in SOC. An overview of the performance of the three different models is presented by Suwanwarangkul et al. [94]. The Stefan-Maxwell model is significant for operations of rSOC in a low pressure regime from 1 to 3 bar, therefore, for the present thesis work it is not a good choice because the methanation section and the rSOC work in pressure at 32.4 and 33.1 bar respectively. The DGM is the most accurate model, but it is difficult to implement in an analytical way, as it requires a numerical solution that is expensive in terms of time and effort. Thus, the Fick's law model is the best choice, in one-dimension (1D) coordinate, in order to have a compromise between accuracy and costs. Through it, a 1D transport equation can be approximated, linking the molar flow rate of the chemical species with the product of the cross-section surface of electrode, the diffusivity coefficient in bulk condition and the variation of the chemical concentration on electrode's thickness. The final result of the model finds the density current parameter expressed in the next eq. (68):

$$i = 2FD_i \frac{C_i^{\infty} - C_i^{tps}}{L_{elec}} \tag{68}$$

$$i_l = 2FD_i \frac{C_i^{\infty}}{L_{elec}} \tag{69}$$

The variables appearing in eq. (68) and (69) are the final results as already mentioned previously. The common components are F, which is the Faraday constant, $D_i$, the diffusive coefficient in the bulk condition and L, the thickness of the electrode

Regarding the numerator of the fraction, $C_i^{\infty}$represents the concentration of the i-specie in the bulk condition, while $C_i^{tpb}$ is the concentration of the i-specie in the tpb inside the electrode. The eq. (69) is the limit behaviour of the density current found with the Fick's law, because the maximum current achievable is obtained when the concentration of the chemical species is null in the activation point inside the electrode. Both current parameters assume different values between cathode and anode, because different are the chemicals involved and different is the length of the electrodes.

Finally, in order to determine the diffusion overpotential formula, it is necessary to introduce a new version of the Nernst equation. This variant uses the concentrations of the reagents and products and not the classic partial pressures, eq. (70), because it is herewith more practical to help calculations for diffusion overvoltage. Subsequently, by subtracting this new version of the OCV formula in the operating conditions of the electrode (tpb) and in the bulk condition, the final desired formula, eq. (71), is obtained:

$$OCV^{tpb\ or\ \infty} = \pm \frac{\Delta g_i(T, p_0)}{Z_r * F} + \frac{R * T}{Z_r * F} * \ln\left[\frac{\prod_i^{\#r|\#p} C_i^{v_i}}{\prod_i^{\#p|\#r} C_i^{v_i}}\right] \tag{70}$$

$$\Delta V_{tpd-\infty} = OCV^{tpb} - OCV^{\infty} = \eta_{diff} = \frac{RT}{2F} \ln \left(\frac{C_i^{tpb}}{C_i^{\infty}}\right) \tag{71}$$

Considering the huge difficulty related to a constant monitoring of the diffusion inside the tpb, the equation can be reformulated in order to simplify it, using the previously obtained eqs. (68) and (69):

$$\eta_{diff} = |\frac{RT}{2F} \ln \left(1 - \frac{i}{i_l}\right)| \tag{72}$$

Eq. (72) is the final formula used to calculate, for both cathode and anode, the diffusion overvoltage. It is mathematically derived from the combination of eq. (71), (69) and (68), in order to consider not the concentration but the density current which is extremely easier to track and manage. The result is expressed in absolute value because $i_l$ is always bigger than $i$, due to its limited behaviour. This means obtaining an argument of natural logarithmic between zero and one which is always negative. The absolute value needs to correct this analytical issue.

### 3.2.2.3 Cross-over effect

Before proceeding with the last overpotential losses and to be through, the cross-over effect will be debated, which is an indirect phenomenon that should be considered in the calculation of the cell's voltage. Differently from the overpotential losses, it is not accounted directly in the formula as a distinct variable, but its effect adds a fictitious current $i_{cross}$ in the equation of the polarization curve, in particular, correcting the diffusion and activated overvoltages (it does not interact with the OCV part). The next two equations are going to show the modifications performed:

$$\eta_{act} = \frac{RT}{\beta F} * \sinh^{-1}\left(\frac{i}{2i_0}\right) \rightarrow \frac{RT}{\beta F} * \sinh^{-1}\left(\frac{i + i_{cross}}{2i_0}\right) \tag{73}$$

$$\eta_{diff} = \left|\frac{RT}{2F} \ln\left(1 - \frac{i}{i_l}\right)\right| \rightarrow \left|\frac{RT}{2F} \ln\left(1 - \frac{i + i_{cross}}{i_l}\right)\right| \tag{74}$$

The cross-over effect derives from a real consideration. In the hypothetical condition, the electrolyte layer should be totally impermeable to the passage of molecules and electrons across it, permitting only the passage of ions due to its chemical composition, as expressed in paragraph "2.2.2.1". However, in reality the effect doesn't occur as just mentioned, even if the amounts are low, they produce a decrement of cell efficiency:

- The molecules diffusivity allows the transport through electrolyte of fuel molecule, which react with the oxygen agent or viceversa, producing a reactants concentration reduction and, considering for instance the reaction between methane and oxygen or hydrogen and oxygen, cause an high amount of heat in the electrode, obstructing the thermodynamic stabilization of the cell;

- The electrons conductivity allows the conduction of electrons in the electrolyte layer producing an increment of the ohmic losses.

Therefore, when decreasing the thickness of the electrolyte layer, the cross-over effect will be enhanced, whereas oppositely, when increasing the thickness, the cross-over effect reduces. But on the other hand, increasing too much the thickness directly implements the ohmic overvoltage, which is going to be described in the next paragraph “3.2.2.4”. In fact, a thicker electrolyte layer means higher effort for charge transport: ions diffuse with more difficulty through it. For this reason, the cross-over phenomena is a trade-off between the two effects. Specific studies must be conducted on the design phase, in order to guarantee the lowest cross-over losses.

#### *3.2.2.4 Ohmic overpotential*

Finally, the last loss phenomenon will be described, the ohmic overpotential loss $\eta_{ohm}$. It accounts for the voltage drop due to the charge transport effects of the electrons that flow in the external circuit, but also by the ions which pass through the electrolyte layer.

Current knowledge of this topic, as expressed for example by M. Santarelli in his teaching at the Polytechnic of Turin [30], affirms that the effect of the voltage drop, associated with the phenomenon of electron circulation, is clearly more effective than that of ions. This is scientifically demonstrable by considering the conservation of charge in the rSOC. Regardless of the mode of operation, it can be said that the amount of current produced by the transport of electrons is the same as that associated with the phenomenon of ions. According to Ohm's law, the voltage or, in this case, the voltage drop can be expressed as the product of current and associated electrical resistance. This last variable is inversely proportional to the electrical conductivity. Therefore, with the help of contemporary literature, thanks to the theoretical and experimental researches conducted, it is known and affirmed that the conductivity associated with electrons is about a million times greater than that of ions. Consequently, the voltage drop associated with the phenomenon transport of electrons is about one million times smaller than that of ions. It is deduced that the ohmnic drop effect can only be represented by this last phenomenon, which refers to the thickness of the electrolyte layer, because, the greater the thickness of this component, the greater the voltage drop associated with the transport phenomenon of the ions:

$$\begin{cases} I_{ions} = I_{e^-} \\ \Delta V \cong \dfrac{I}{\sigma} \\ \sigma_{e^-} \cong 10^6 \sigma_{ions} \end{cases} \rightarrow \Delta V_{ions} \gg \Delta V_{e^-}$$

This useful demonstration therefore expresses the importance of the length of the electrolyte layer. The following eq. (75) reports the formula used to calculate the ohmic overpotential losses $\eta_{ohm}$:

$$\eta_{ohm} = i * ASR_{\Omega} \tag{75}$$

The formulation unmistakably follows Ohm's law, in fact the analogy predicts $\eta_{ohm}$ as voltage drop [V], i as current density [I/cm$^2$] and finally the variable $ASR_{\Omega}$ as the electrical resistance, expressed however not in [Ω] but in [Ωcm$^2$]. This last variable is called Area Specific Resistance, expressed as the resistance associated with the transport phenomenon of ions and electrons (which has been proven to be negligible without leading to large approximation errors).

At this point, the most important approximation of all the thesis work is introduced: as described above, for accurate and detailed studies, the determination of the operating voltage of the cell requires the explicit calculation of all overpotential losses. It is therefore stated that, for simplistic reasons, with which in any case valid results are obtained from a scientific point of view, without compromising the research work, the only effect of electrochemical loss considered is that of the ohmnic overpotential, consequently neglecting the others. This assumption involves a linearization of the polarization curve. Furthermore, exploiting the theoretical knowledge of this last loss, a further hypothesis expressed by the following eq. (75.1) is made:

$$ASR_{\Omega} = (L_{el}\rho_{el} + L_{an}\rho_{an} + L_{cat}\rho_{cat}) + ASR_{int} \tag{75.1}$$

From eq. (75.1) it is noted that the term of ASR does not refer only to the associated resistance of the electrolyte layer, but ideally to the entire rSOC, considering the resistive contribution of the two electrodes and also of the interconnector, the auxiliary structural component which connects the cells to each other. This formulation is found in many contemporary studies such as [83] and [85]. Therefore, for the calculation of the ASR the lengths reported in table 10 are considered:

| $L_{el}$ | 10 | µm |
|---|---|---|
| $L_{an}$ | 500 | µm |
| $L_{cat}$ | 60 | µm |
| $L_{int}$ | 1500 | µm |

*Table 10 – Geometric data of a single cell*

$L_{el}$, $L_{an}$, $L_{cat}$ and $L_{int}$ correspond to the dimensions of the elements that make up a single cell. They were chosen considering contemporary literature, using average values, with the aim of reporting a real situation as faithfully as possible. Instead, for the calculation of resistivities, empirical formulas deriving from experimental data were used, represented by the following eqs. (76) to (79), obtained using the aid of scientific articles present in the literature, as [83], [95] and [96]:

$$\rho_{el} = 2{,}94 * 10^{-5} * \exp\,(\frac{10350}{T_{cell}}) \tag{76}$$

$$\rho_{an} = 2{,}98 * 10^{-5} * \exp\,(-\frac{1392}{T_{cell}}) \tag{77}$$

$$\rho_{cat} = 8{,}114 * 10^{-5} * \exp\,(\frac{600}{T_{cell}}) \tag{78}$$

$$\rho_{int} = 1{,}68 * 10^{-2} \exp\left(-\frac{413{,}5}{T_{cell}}\right) \tag{79}$$

Considering the usual cell temperature equal to 850 °C, the following values were obtained:

| | | |
|---|---|---|
| $\rho_{el}$ | 0,295 | Ωm |
| $\rho_{an}$ | $8{,}629*10^{-6}$ | Ωm |
| $\rho_{cat}$ | $1{,}384*10^{-4}$ | Ωm |
| $\rho_{int}$ | 0,012 | Ωm |

*Table 11 - Resistivity results*

Finally, using eq. (75.1), the sought value of ASR equal to **0,304** Ω$\text{cm}^2$ was obtained.

### 3.2.3 Thermoneutral voltage – $V_{TN}$

The last variable of fundamental importance for the modeling of the rSOC is the thermoneutral voltage. Before delving into this topic, an introduction to thermodynamic behaviours relating to the exchange of energy in the rSOC is of primary importance. It is now known that this electrochemical device allows to operate in two different modes, SOFC or SOEC. The choice of mode depends on the contribution of electric power to be managed. In the case of produced power, the mode is that of SOFC. In the thesis work, this method uses natural gas as fuel, taking it from the local distribution network. In reality, as illustrated later, all this fuel is considered free cost as both the methanation section and the CCS section provide for the production of SNG. Unfortunately, the use of a stream with a high percentage of $CH_4$ entails many drawbacks, a problem that is bypassed by transforming this component into $H_2$ and CO through the reactions of methane reforming, eq. (3) and eq. (5), paragraph “2.1.2.1 ”, which can occur internally in the electrochemical device or externally in another component. Thus, it is clear how the thermal behaviour of the SOFC is totally exothermic: the electro-oxidation reactions that take place in the anode, treated in paragraph "2.2.1.1", produce heat.

The behaviour of the other mode that absorbs electrical power, SOEC, is different. In this case, based on the voltage value of the device, it can assume an exothermic or an endothermic behaviour, because the reactions involved in the SOEC cathode, eq. (15) and eq. (16) in paragraph “2.2.1.1”, are endothermic. Hence, they need heat to take place. At the same time, as happens in the SOFC, irreversibility occurs inside the cell, caused by the physical phenomena that occur during the operational phase. Those directly responsible for these irreversibility are the overpotential losses analyzed in detail in the previous paragraph "3.2.2". Therefore, considering this information, it is clear that there is a situation in which the heat necessary for the electrochemical reactions equals that produced exothermically by the irreversibility. This point is marked as a thermoneutral condition, characterized by the thermoneutral voltage, which is of primary importance for electrolyser operations because it allows to obtain an electrical efficiency of the device of 100%. It will therefore be essential to try to operate at a voltage value as close as possible to it. For the moment the formula of the thermoneutral voltage is demonstrated and the value is obtained in the specific case of the thesis work.

Therefore, an energetic analysis of the SOEC is set up by exploiting the first principle of thermodynamics, eq. (45). The molar capacities can be reformulated with the help of Faraday's law, eq. (52). Both proposed equations are present in paragraph “3.2.1”. Successively, the molar specific enthalpy values are associated with the reactions involved in the device, which are the previous eqs. (14), (15) and (16) of paragraph "2.2.1.1", and with the secondary chemical reactions of WGS, eq. (4) of paragraph "2.1.2.1", and the inverse of the SMR or the methanation reaction that exploits carbon monoxide, eq. (18) of paragraph "2.2.1.1", obtaining the following energy balance:

$$\phi_{th} - W_{el} = -\frac{I}{2F}\Delta\hat{h}_{H_2O|H_2} + r_{wgs}\,\Delta\hat{h}_{wgs} + r_{mr\_co}\,\Delta\hat{h}_{mr\_co} \tag{80}$$

In eq. (80), the variable $r_{wgs/mr\_co}$ indicates the rate of chemical reaction for the secondary reactions. The presence of these two reactions will make it possible to distinguish the thermoneutral voltage of co-electrolysis from that of steam-electrolysis, since the use of $CO_2$ as fuel at SOEC generates CO, which in turn, being in the operating conditions of the cell of 850 °C and 33.1 bar, interacts with the other chemical compounds generating the secondary reactions. Their presence is essential to take into account the effect of pressure. In fact, considering only the contribution of enthalpy, being a thermodynamically variable influenced only by temperature, for any pressure value, its value does not vary much. On the other hand, with the presence of these secondary reactions, working at a high operating pressure, the kinetics of the reactions increases, because the rate of reaction is very influenced by this variable, obtaining a different thermoneutral voltage value.

Taking this into account, eq. (80) can be modified. The electrical power is considered as the product of the voltage of the cell $V_{cell}$ and the current required by the SOEC for its electrolysis operations. The thermal flux $\phi_{th}$ is zero if the cell voltage corresponds to the thermoneutral voltage. Consequently, the following is obtained:

$$\begin{cases} \phi_{th} - V_{cell}I = -\frac{I}{2F}\Delta\hat{h}_{H_2O|H_2} + r_{wgs}\,\Delta\hat{h}_{wgs} + r_{mr\_co}\,\Delta\hat{h}_{mr\_co} \\ \phi_{th} = 0 \leftrightarrow V_{cell} = V_{tn} \end{cases} \tag{81}$$

$$V_{tn} = \frac{\Delta\hat{h}_{H_2O|H_2}}{2F} - \frac{r_{wgs}\,\Delta\hat{h}_{wgs} + r_{mr_{co}}\,\Delta\hat{h}_{mr_{co}}}{I} = V_{tn\_H_2O|H_2} - \Delta V_{chemicals} \tag{82}$$

As can be seen from eq. (82), the thermoneutral voltage in the case of co-electrolysis is given by the contribution of two factors: the thermoneutral voltage of steam-electrolysis and a potential drop introduced by the secondary reactions. Going into the details of the calculations, the first contribution is determined with the following equations:

$$2H_2O \rightarrow 2H_2 + O_2 \tag{83}$$

$$\Delta\hat{h}_{H_2O|H_2} = 2\hat{h}_{H_2} + \hat{h}_{O_2} - 2\hat{h}_{H_2O} \tag{84}$$

$$\hat{h}_{H_2} = \hat{h}^0_{H_2} + \int_{T_0}^{T_{cell}} cp_{H_2}(T)dT \tag{85}$$

$$cp_{H_2}(T)dT = 27{,}28 + 0{,}0036T + \frac{50200}{T^2} \tag{86}$$

$$\hat{h}_{O_2} = \hat{h}^0_{O_2} + \int_{T_0}^{T_{cell}} cp_{O_2}(T)dT \tag{87}$$

$$cp_{O_2}(T)dT = 29{,}96 + 0{,}00418T - 16700T^2 \tag{88}$$

$$\hat{h}_{H_2O} = \hat{h}^0_{H_2O,(l)} + \int_{T_0}^{513.15} cp_{H_2O,(l)}dT + \Delta\hat{h}_{EVA} + \int_{513.15}^{T_{cell}} cp_{H_2O,(g)}(T)dT \tag{89}$$

$$cp_{H_2O,(l)} = 75{,}44\ [\frac{J}{molK}] \tag{90}$$

$$cp_{H_2O,(g)}(T) = 30 + 0.01071T + \frac{33500}{T^2} \tag{91}$$

Starting from the water electrolysis reaction, eq. (83), the equation for calculating the change in enthalpy produced, eq. (84), is formulated. The equations ranging from (85) to (91) are complementary to the calculation of $\Delta\hat{h}$. Among them we find the integrals for the determination of the enthalpy values of the specific chemical component, eqs. (85), (87) and (89), in which the term $\hat{h}^0$ corresponds to the enthalpy value in the reference conditions, 298.15 K and 101.325 kPa. For the $H_2$ and $O_2$ element, the integrals can be calculated directly between the reference temperature and the cell temperature, since, in this temperature range, no changes in state take place, and both chemical elements remain in the gaseous state. While in the case of water, it is noted that there is a change of state, from liquid to gaseous. In fact, 513.15 corresponds to the evaporation temperature, in K at a pressure of approximately 33.1 bar. Finally, the entropy change value associated with the change of state must be considered. To carry out the resolution of the integral, the specific heat values are also reported for each chemical element, which depends on the temperature. All these complementary formulas, with the exception of integrals, but also including numerical values, have been obtained from [97]. In the end, the thermoneutral voltage value for the case of steam-electrolysis, in the operating conditions of the cell, is obtained, equal to **1.288** V.

Instead, as regards the second contribution, the voltage drop associated with the secondary reactions that take place in the SOEC, reference was made to the following equations:

$$r_{wgs} = k_{wgs}(p_{H_2O}p_{CO} - \frac{p_{H_2}p_{CO_2}}{K_{wgs}}) \tag{92}$$

$$k_{wgs} = 0{,}0171\exp(-\frac{103191}{RT_{cell}}) \tag{93}$$

$$K_{wgs} = \exp(-0{,}2935Z^3 + 0{,}6351Z^2 + 4{,}1788Z + 0{,}3169) \tag{94}$$

$$Z = \frac{1000}{T[K]} - 1 \tag{95}$$

$$r_{mr\_co} = k_{mr\_co}(p_{CH_4}p_{H_2O} - \frac{p_{CO}\left(p_{H_2}\right)^3}{K_{mr\_co}}) \tag{96}$$

$$k_{mr\_co} = 2395\exp(-\frac{231266}{RT}) \tag{97}$$

$$K_{mr\_co} = 1{,}0267 * 10^{10}\exp(-0{,}2513Z^4 + 0{,}36651Z^3 + 0{,}581Z^2 - 27{,}134Z + 3{,}277 \tag{98}$$

The above formulas were obtained after the analysis of contemporary literature, taking as a reference [82], [91] and [98]. These texts report mathematical models deduced and formulated over time after various experimental tests. In reality there are further formulations which vary according to the degree of precision and the data available. Among the many other articles available, [59], [99] and [100] are reported as valid alternatives for the formulation of these physical variables. Analyzing the above formulas, from eq. (92) to (98), the importance of pressure for these reactions is affirmed and reiterated, in fact, the formulas are characterized by the partial pressure values of the chemical elements present in the reactions involved. In the two formulas of the global rate of reaction, eq. (92) and (96), two other variables that characterize the kinetic behaviour of the reactions appear: the rate constant, eq. (93) and (97), and the equilibrium constant, eq. (94) and (98). The first is a variable that characterizes the kinetics of the reaction with the chemical concentration of its reactants, while the second is used to take into account how much the chemical reaction differs from the equilibrium situation.

Finally, having performed the calculations by solving eq. (82), a value of **1.211** V is obtained for the thermoneutral voltage in the co-electrolysis operation. As expected, different values were obtained for the two electrolysis cases. Co-electrolysis has a lower value of thermoneutral voltage, because the secondary reactions that occur within the cathode of the SOEC are endothermic, they require heat to take place, decreasing the thermal energy available for the main reactions. In conclusion, three behaviours can be distinguished for a generic electrolytic cell:

- When $V_{TN} > V_{cell}$ the electrolyte has an endothermic behaviour, so the reactions need heat to be supplied;
- When $V_{TN} = V_{cell}$ the electrolyte has a null flux, so no exchange of energy between the system and the outside environment;
- When $V_{TN} < V_{cell}$ the electrolyte has an exothermic behaviour, so the reaction involved in the electrolyte produces heat that must be removed in order to not compromise the next operations.

### 3.2.4 rSOC design

Once the characteristic parameters of the rSOC have been determined, it must be dimensioned in order to proceed with the simulations on Aspen Plus. This topic is dealt with specifically in the future chapters relating to the analysis of the polygenerative plant. Cell sizing means attributing geometric dimensions and energy characteristics to the electrochemical device. Just as it was possible to establish the size of the photovoltaic system, paragraph "3.2.1", by exploiting the hourly demand for electricity required by the urban load made up of 30 thousand people, paragraph "3.1.1", it is possible to do the same thing for the rSOC.

Therefore, from the energetic point of view, the rSOC was sized considering its SOFC mode, because the main purpose of the polygenerative plant is to meet the urban electricity needs. Considering the maximum power required, equal to about 5.65 MW, a SOFC size of 6 MW was chosen in the case of continuous power produced (DC). In fact, as it must be sent to the grid in the form of alternating current, using a conventional efficiency of an inverter equal to 96%, an alternating power produced of 5.76 MW is obtained. Hence, the SOFC operating at 100% of its capacity will always be able to meet the electrical demand.

Regarding its complementary part of SOEC, considering a power ratio between the two modes of 5, a maximum absorbable DC power of about 30 MW is obtained. It is already known a priori that the choice adopted will imply a slight oversizing of the electrolyser part, even if, by switching off and on the modules that make up the SOEC, it will be possible to make it operate with maximum efficiency, exploiting an operability range between 20 and 80%.

The mentioned modules are the elements that make up the rSOC system. Each module is made up of a set of stacks, each of which is in turn made up of a set of blocks. The set of elementary cells, studied in detail (from an electrochemical and material point of view) form a block. The following fig. 20 shows a representation of what has been stated, facilitating its understanding:

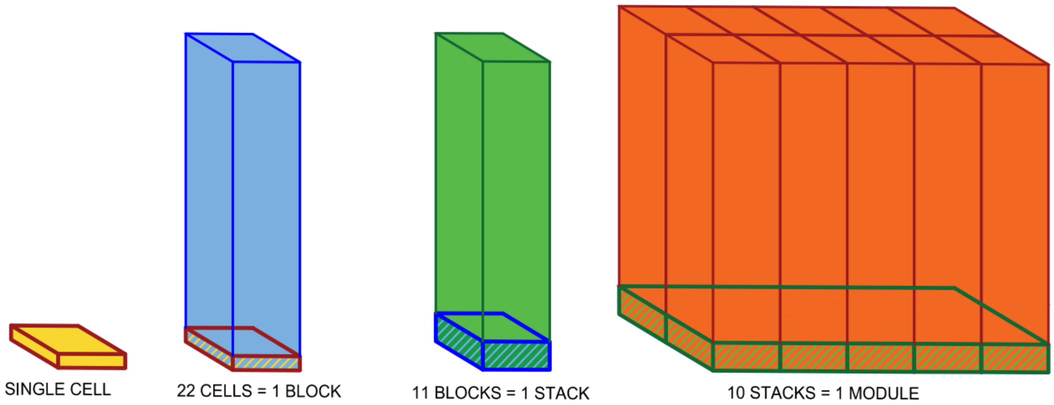

*Figure 20 – Configuration of rSOC*

Once the size of the rSOC is known, the determination of the power values associated with each part that constitutes this device is immediate. In the thesis work a rSOC of size 6|30 MW was therefore designed in the case of SOFC|SOEC respectively. The rSOC consists of 12 modules, each of which has a characteristic power of 0.5|2.5 MW. Each module consists of 10 stacks, for a total of 120 stacks, each of which has an associated power of 50|250 kW. Each stack is composed of 11 blocks, for a total of 1320, with a characteristic power of about 454.5 W. Finally, each block is composed of 22 cells, for a total of 29’040 cells, each of which has a power of about 20.66 W.

As for the characteristic dimensions, it has been opted for a unit cell with dimensions of 300 cm$^2$. This value was chosen after a careful analysis of the literature, as these devices are not available in large quantities, resulting in still niche products. This implies the difficulty of choice as there are various types of dimensions. Considering the model of the Solid Oxide Cell, the dimensions chosen were 15x20 cm$^2$.In order to conclude the rSOC study, it is necessary to determine the actual lengths of the overall dimensions of this device. As was done for the determination of the lengths of the electrodes, the electrolytic membrane and the interconnector reported in the previous table 10 of paragraph "3.2.2.4", the same thing is done for the complementary characteristic quantities. [83], [101] and [102] are examples of scientific articles which inspired the choice of dimensions. Finally, the following table 12 summarizes the values that have been adopted:

| | | | |
|---|---|---|---|
| Cell thickness | lc | 0,207 | cm |
| stack end plate thickness | lep | 4,5 | cm |
| stack space for manifolds | lstack | 2 | cm |
| insulation thickness | lins | 30 | cm |
| inactive cell space | linact | 2,5 | cm |
| Length single cell | length | 15 | cm |
| width single cell | width | 20 | cm |
| Active area of a single cell | Aact | 300 | cm2 |
| depth of module | L1 | 569,94 | cm |
| heigth of module | L2 | 349,525589 | cm |
| width of module | L3 | 323,205081 | cm |

*Table 12 - Geometrical information about rSOC*

The last three lines, $L_1$, $L_2$ and $L_3$, respectively the transversal dimension, the height and the depth of a module, were obtained a posteriori using the eqs. (99), (100) and (101), obtained from the reference texts, such as [102].

$$L_1 = n_c l_c + 2l_{ep} + 2l_{ins} \tag{99}$$

$$L_2 = n_b * \left(\sqrt{A_{ACT}} + 2 \; * l_{inact} + 2 * l_{stack}\right) + 2 * l_{ins} \tag{100}$$

$$L_3 = n_s * \left(\sqrt{A_{ACT}} + 2 \; * l_{inact} + 2 * l_{stack}\right) + 2 * l_{ins} \tag{101}$$

Table 12 therefore shows the dimensions that refer to:

- $l_c$, the thickness of the cell;
- $l_{ep}$, the thickness of the end plate, i.e. of the interconnector that allows to obtain a repetition of cells;
- $l_{stack}$, the space attributed to the cell that allows the passage of the feeding channels or removal of the reagents / products;
- $l_{ins}$, the thickness of the insulation that allows to reduce heat dissipation inside the device, stabilizing the processes of electrochemical reactions;
- $l_{inact}$, a length that refers to an inert part of the cell that allows it to be electrochemically isolated from the rest of its components and, above all, unable to react with adjacent materials.

At this point the rSOC is completely identified from every point of view. The only missing data, of primary importance for future simulations relating to the rSOC system with its complementary components, called Balance of Plant (BoP), concerns the determination of the actual polarization curve of the device analyzed in the thesis work. As reported in the following paragraph “4.2”, “4.3” and “4.4”, through the curve it will be possible to determine, for a specific power required, the current and voltage values necessary to obtain it.

Therefore, with the help of the MatLab software, it was possible to develop a code capable of representing both this important characteristic curve and the power trend, for both rSOC modes, as the number of modules switched on varies, and therefore the number of active cells. This second curve demonstrates the power ratio present between the two modes.

The code implements some previously calculated variables: first the OCV, which is the same for the two modes, as well as the ASR, necessary to represent the resistance of the passage of the charges inside the device. ASR reflects in the slope of the curve, which will have a linear trend due to the linearity approximation which allowed to neglect all the overpotential losses with the exception of the ohmnic one. In the end, knowing the number of cells which allows to express the number of active modules during operations, and by creating a current vector, it is possible to first obtain a current density vector, then the voltage vector of the cell and finally the power of the cell. A small excerpt is given here only as an example:

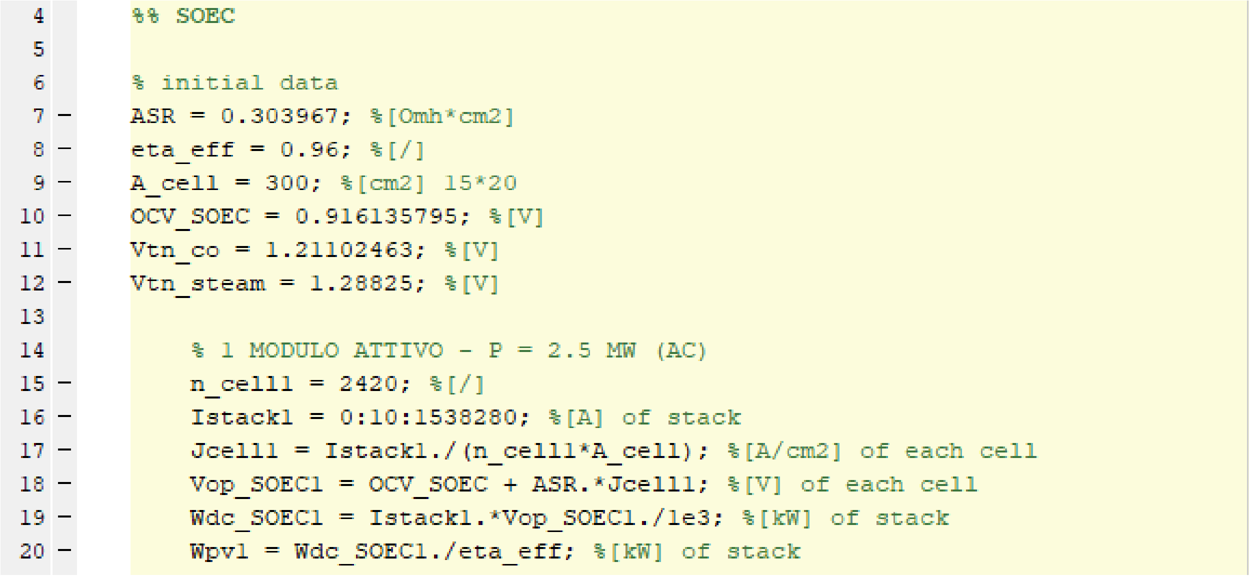

```
%% SOEC

% initial data
ASR = 0.303967; %[Omh*cm2]
eta_eff = 0.96; %[/]
A_cell = 300; %[cm2] 15*20
OCV_SOEC = 0.916135795; %[V]
Vtn_co = 1.21102463; %[V]
Vtn_steam = 1.28825; %[V]

    % 1 MODULO ATTIVO - P = 2.5 MW (AC)
    n_cell1 = 2420; %[/]
    Istack1 = 0:10:1538280; %[A] of stack
    Jcell1 = Istack1./(n_cell1*A_cell); %[A/cm2] of each cell
    Vop_SOEC1 = OCV_SOEC + ASR.*Jcell1; %[V] of each cell
    Wdc_SOEC1 = Istack1.*Vop_SOEC1./1e3; %[kW] of stack
    Wpv1 = Wdc_SOEC1./eta_eff; %[kW] of stack
```

*Figure 21 - Excerpt of MatLab code for Polarization curve*

Finally, the final graphics obtained by the program are reported:

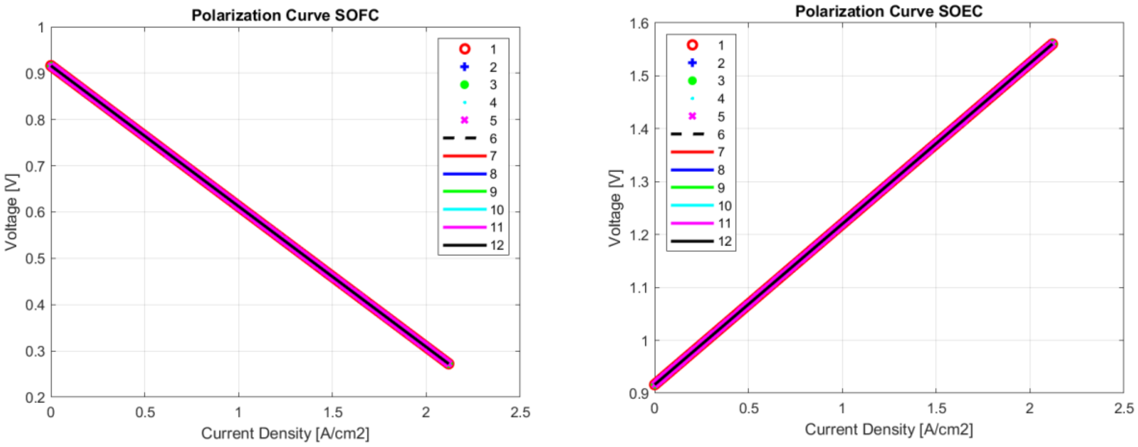

Figure 22 - Polarization curves

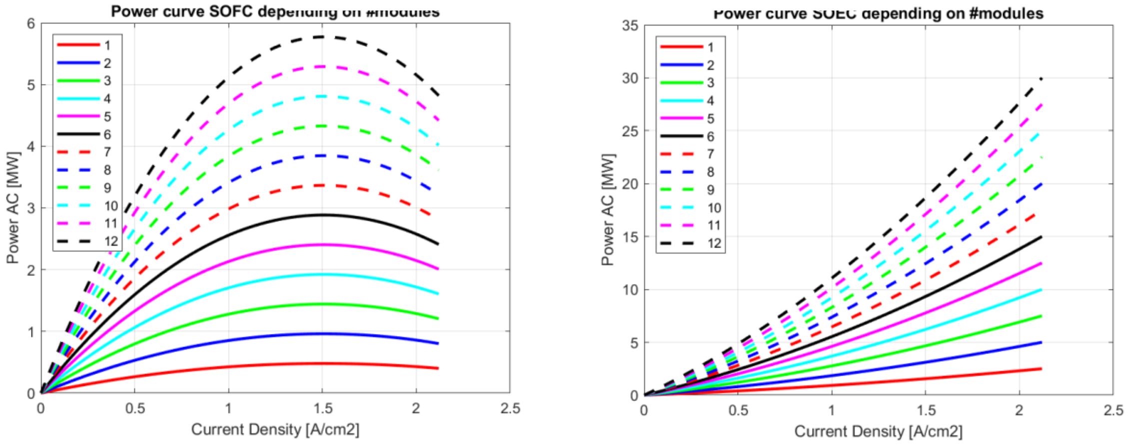

Figure 23 - Power Curve for both modalities

Each plot's legend shows the number of active modules. As it can be seen, the graphics reflect the trends expected in the design phase, in particular for the electric powers in the two modes: continue increment of power absorbed by SOEC mode with rising of current, while for SOFC, higher power produced until its maximum point of work, then a rapid decreament in function of the increment of the current.

## 3.3 $CO_2$ removal process using MEA: thermodynamic model

The removal of carbon dioxide is a contemporary topic that is drawing the attention of the scientific community, improving both the processes and the materials involved year by year. Governments around the world are also starting to take it into consideration, appraising it as the cornerstone of the eco-sustainable transition, of fundamental necessity. The state of the art of this technology, previously discussed in paragraph "2.4", anticipated which type of CCS is adopted in this thesis work. The type is that of post-combustion, which has been seen to be very advantageous as it allows it to be implemented both in new and old projects, through a sort of extraordinary maintenance called retrofitting.

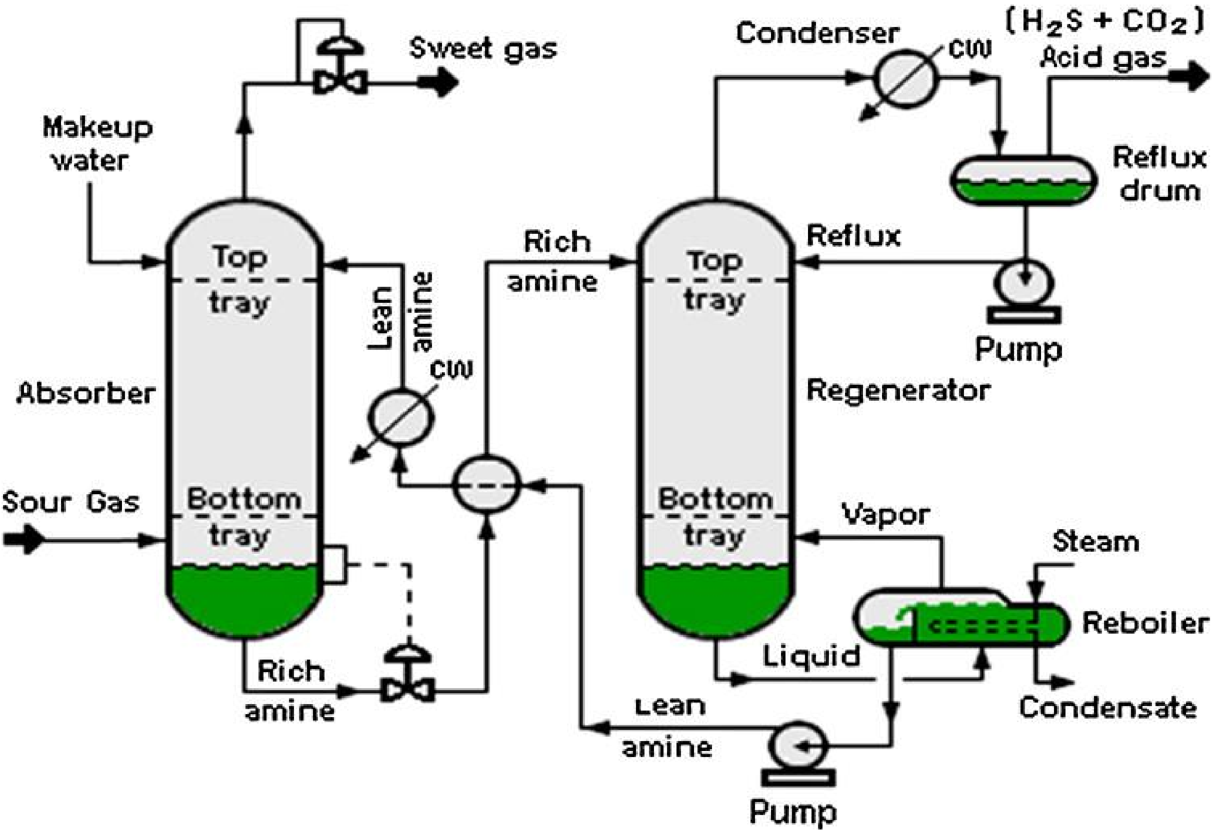

*Figure 24 - CCS section scheme [103]*

Fig. 24, taken from reference [103], represents a plant design very similar to that used in the thesis work, which can therefore be taken into consideration for this first modeling phase. This scheme is based on what has already been explained in “2.4”, i.e. that in the absorbent column, the removal of $CO_2$ occurs through a counter-current circulation through the chemical absorption process. On the other hand, in the stripper column the reverse desorption process occurs, thus purifying the substance that allowed the pollutant to be removed. Specifically, as regards the first column, the carbon dioxide present in the acid gas to be cleaned / purified, usually exhaust gas from industrial or energy processes, comes into contact with a liquid solution of water and solute, which chemically reacts with the acidic substance ($CO_2$), removing it.

The exhaust gas, purified of its acid component, is expelled from the top of the absorbent column, while the liquid solution, which has become acid, descends by gravity and exits from the lower part. The opposite occurs in the regenerative column. The liquid rich in the pollutant must be purified, consequently it is dropped from top to bottom, inside this column, coming into contact with inert materials that will allow the separation of the two phases. Below, due to gravity, the purified solution comes out: it consists of water and solute, not in the initial proportions. On the contrary, the acid gas is expelled from above and is filtered. Finally, to further improve the purity of these two streams, the liquid solution is passed inside a heat exchanger, the reboiler, which, by providing heat, further improves the desorption process, removing and recirculating a small part of acid gas that was still contained within the liquid. The outlet gas from above passes inside a cooler, which allows part of the liquid solution to condense by removing heat, especially water, further purifying the acid stream leaving the system.

In this modeling phase, the treated aspect concerns the physics-chemistry involved in the absorption / desorption processes. From a theoretical point of view, it was decided to operate with MEA as a solute. In fact, both the pertinent literature and above all the Aspen Plus program, used after sizing to carry out the simulations, refer to the complete libraries inherent to this substance, where all the properties of interest are reported. Despite this, the reactions used by Aspen to determine the values of the fundamental physical parameters will be analyzed in the next paragraph "4.5 Aspen model: Carbon Capture and Sequestration".

As a matter of fairness, as previously stated, the knowledge regarding the materials involved in CCS are improving, in fact new ones with better properties are being discovered. Among these, the Ionic Liquids (ILs) deserve a mention. They facilitate the process efficiencies, such as greater compatibility with the acid substances to be removed (higher gas-liquid mass transfer rates) or a lower regeneration energy required by the reboiler. At the same time, they bring also economic advantages, such as the use of a smaller quantity of solution, [104].

Despite the advantages, also present in other innovative substances, the CCS section of the thesis work uses an aqueous solution of MEA. Although its characteristics are not generally the best, this solution has excellent properties, such as the rapid reaction rate, the low cost of the solvent, appropriated thermal stability, low molecular weight and thus high absorbing capacity on a mass basis, and relatively low solubility of hydrocarbons in the solution [106], [107] and [108]. Above all it has a consolidated status, as all its characteristic parameters are now known, due to the numerous studies on this substance / process. Therefore, in table 13, referring to the literature [104], the average values of some very important variables which characterize this substance are reported:

| Property | Aqueous amines | Units |
|---|---|---|
| Molecular wright | 60-250 | g/mol |
| Density | 0,65-1,2 | g/cm3 |
| Viscosity | <7-460 | mPa*s |
| Boiling point | 111-350 | °C |
| Flash point | 14-380 | °C |
| Melting point | -65 to 25 | °C |
| Freezing point | -46 to 110 | °C |
| Vapor pressure | <0,001-11 | mmHg |
| Water solubility | <10-100 | % |
| Thermal stability | 100-251 | °C |
| Physical state | liquid | - |
| CO2 solubility | <50-85 | m3/m3 |
| ΔHvap | <50-528 | kJ/mol |
| ΔHabs | -36 to 100 | kJ/molCO2 |

*Table 13- MEA properties*

However, the aqueous solution of MEA has also some disadvantages such as the low $CO_2$ loading capacity (i.e usually one mol of $CO_2$ for each two mol of MEA is absorbed), high energy content for the reboiler duty caused by high enthalpy of reaction involved with $CO_2$, high degradation of the column's materials with the formation of secondary component as carbon oxysulfide (COS) or oxygen-bearing gases, and finally higher corrosiveness than those of many other amines [104], [105] and [109].

Finally, the reactions involved in the absorption / desorption phases, between the liquid solution and the acid substances, will be described hereafter, although for the thesis work only $CO_2$ is considered as a substance to be removed, neglecting the presence of other pollutants (such as sulphates, like $H_2S$, COS, etc.). In fact, biogas is considered as the gaseous stream that must be purified in the CCS section, which has a composition chosen upstream of the design equal to 65%$CH_4$, 34%$CO_2$ and 1%$N_2$. This composition was chosen as the average value, considering other studies in the literature (see [92] and [110]), simplified as compared to reality: in fact the smaller percentages (order of ppm or in any case < 1%) relative to other compounds, usually highly polluting, should always be removed. The set of reactions that occur inside the columns are:

$$2H_2O \leftrightarrow H_3O^+ + OH^- \tag{102}$$

$$H_2O + HCO_3^- \leftrightarrow H_3O^+ + CO_3^{-2} \tag{103}$$

$$H_2O + MEA^+ \leftrightarrow H_3O^+ + MEA \tag{104}$$

$$H_2O + MEACOO^- \leftrightarrow MEA + HCO_3^- \tag{105}$$

$$2CO_2 + 2H_2O \leftrightarrow HCO_3^+ + HCO_3^- \tag{106}$$

The eqs. from (102) to (106) are the main reactions involved during the phenomenon of chemical absorption. The production of ionic compounds allows the various elements to bind and react in the redox listed above.

### 3.3.1 Physico-chemical properties

The thermodynamic analysis of the CCS section, in particular of the physical and chemical reactions that occur within the two columns, can be conducted with different degrees of accuracy. The model considered for the thesis work is the equilibrium-based model, which assumes the condition of equilibrium between the liquid and the gaseous phase. This model allows various assumptions. Being the simplest model, the hypotheses simplify the discussion of the topic, causing a lower degree of accuracy of the results. Nevertheless, it can be stated with proven certainty that the final result appropriately reproduces reality. The hypotheses ([105] and [111]) foresee:

1. All the considered reactions take place in equilibrium conditions, even those within the reboiler and condenser;
2. The interface between the liquid phase and the vapor phase is in equilibrium;
3. Negligible degradation of the solvent;
4. Negligible thermal losses and pressure drops in all parts of the column;
5. $N_2$ is inert and never takes part in chemical reactions.

Through the model, it is possible to derive the parameters involved and which serve to characterize the absorption phenomenon. The Aspen Plus software used in the subsequent simulation phase, allows to use this model, and, through its libraries, the execution of calculations: all the variables and constants necessary for the calculation and execution of the formulas are known and quantified. These formulas are reported in the equations below:

$$lnk_i = A + \frac{B}{T} + ClnT + DT \tag{107}$$

$$lnP_i^V = C_{1i} + \frac{C_{2i}}{T + C_{3i}} \tag{108}$$

$$c_{pi} = C'_{1i} + C'_{2i}T + C'_{3i}T^2 \tag{109}$$

$$V_m^l = \frac{RT_{ci}[Z_i^{*,RA}(1 + d_i(1 - T_r)]^{[1+(1-T_r)^{\frac{2}{7}}]}}{P_{ci}} \tag{110}$$

$$lnn_i = A_i + \frac{B_i}{T} + C_i lnT \tag{111}$$

$$\sigma_i = C''_{1i}\left(1 - \frac{T}{T_{ci}}\right)^{(C''_{2i}+C''_{3i}T_{ri}+C''_{4i}T_{ri}^2+C''_{5i}T_{ri}^3)} \tag{112}$$

$$\lambda_i = D_i + D_{ii}T + D_{iii}T^2 \tag{113}$$

A, B, C, D, $C_{1i}$-$C_{3i}$, $C'_{1i}$-$C'_{3i}$, $C''_{1i}$-$C''_{5i}$, $Z_i^{*,RA}$, $d_i$ and $D_i$-$D_{iii}$ are all known constants via the Aspen software databank Plus. From eq. (107) to (113), the formulas relating to the rate of reaction's constant ($k_i$), vapor pressure ($p^V$), liquid heat capacity ($c_p$), molar volume ($V_m$), viscosity (n), surface tension (σ) and thermal conductivity are reported. It is clear how all the physicochemical properties depend on the temperature (T). Having known the values of these variables, the Aspen Plus software is able to apply the model to simulate the behaviour of the two streams within the main components of the CCS.

## 3.4 Design of methanation reactors

The modeling of the polygenerative plant ends with the methanation section. This part of the plant, as extensively described in the previous chapters, allows the syngas produced in the SOEC operation phase to be transformed into SNG, increasing its exergetic value, subsequently introducing it into the national distribution network, taking into account its standards.

In the literature, for the modeling of the fundamental components of the methanation section, various models can be adopted, which differ according to the level of detail required. For example, if a thermofluidodynamic model were adopted in several dimensions, it would be possible to determine the conditions inside the reactor at each point. For the thesis work there is no need to adopt a complicated model, as it is sufficient to consider the methanation reactors (the characteristic elements to be modelled in this operational section) as closed boxes, as done previously regarding the model of the rSOC. Consequently, a 0D model is chosen, in which it is necessary to know only the main values such as temperature and / or pressure and flow rates that flow into and out of these reactors. All data relating to the dimensions of the methanation reactor are therefore exempt and not necessary either in the modeling phase or in the simulation phase.

This solution will be implemented by the Aspen Plus program during the simulation phase, which will determine the parameters necessary to fully describe the processes that take place in the methanation reactors.

Regarding the 0D approach, a very compatible model is used: the equilibrium model. As a first point, it does not require the knowledge and therefore the determination of many variables, on the contrary, just as stated previously, it only refers to temperature, pressure, flow rates of the fluids involved and their molar fractions. Furthermore, the study is conducted in stationary conditions, with the main assumption that all the chemical reactions involved have a very fast kinetics that can always be considered in equilibrium conditions. There is no transient or any dynamic situation, so the variable time in the formulas is never present. Taking into account the equilibrium model and its simplifying assumptions / hypotheses, it is possible to carry out the simulations at a later time. As will be seen, a special chapter will deal with the simulations of the methanation section using the Aspen Plus software.

Inside the methanation reactors, the characteristic reactions are mainly three:

1. CO methanation, eq. (17), already expressed in paragraph "2.2.1.1", in which methane is produced using hydrogen and carbon monoxide as reactants favourite by a ratio H/C=3;
2. WGS, eq. (4), paragraph “2.1.2.1”, the characteristic reaction of the conversion between carbon monoxide and carbon dioxide;

3. $CO_2$ methanation, eq. (18), paragraph "2.2.1.1", the last reaction that describes the chemical process of methane formation with the exploitation of carbon dioxide.

To assume only these three reactions to describe the phenomena of conversion of syngas into SNG, neglects secondary ones. Among them, those which occur between primary substances, such as CO, $CO_2$, $CH_4$, $H_2$ and $H_2O$, and other elements, especially impurities such as sulphates, very present in the exhaust gases of industrial and energy processes. Neglecting these elements precludes the use of different components and therefore investment and operating costs which should be considered for a more detailed analysis, as these elements are harmful to health and to the components of the system, and must be removed from the system and insulated, so that they can be disposed of safely.

All three reactions have already been reported and described in the previous paragraphs, but a very important aspect not yet considered is that relating to their kinetics. The importance of these reactions is therefore related both to their kinetics, which expresses the rates at which these reactions occur, but also to the reactants and products involved in such reactions. Although the Aspen plus program neglects much of the kinetics of the processes due to the stationary model chosen, and in particular it does not consider those variables such as the rate reactions, useful for evaluating the characteristic times of reactions, the formulas for the constants of balance are still described. These variables are part of the kinetic field, but they express a quantitative characteristic, that is the dependence of the concentrations of products and reactants, which is fundamental for the 0D model adopted. The formulas relating to the equilibrium constants are therefore reported:

$$K_{CO\_meth}(p) = \frac{Y_{CH_4} Y_{H_2O}}{Y_{CO}\left(Y_{H_2}\right)^3}\sqrt{p_{tot}} \tag{114}$$

$$K_{WGS}(p) = \frac{Y_{CO_2} Y_{H_2}}{Y_{CO} Y_{H_2O}} \tag{115}$$

$$K_{CO_2\_meth}(p) = \frac{K_{CO\_meth}(p)}{K_{WGS}(p)} \tag{116}$$

$$K_{CO\_meth}(T) = e^{(0.2513Z^4 - 0.3665Z^3 - 0.581Z^2 + 27.1337Z - 3.277)} \tag{117}$$

The formulas show that the first three are a function of pressure, in fact the term Y is the mole fraction of the compound considered, while the last formula depends on the temperature. For those as a function of temperature, only the equilibrium constant of CO methanation is reported, since that of the WGS reaction has already been described by eq. (94). Instead, that of $CO_2$ methanation is expressed as a function of the other two, both in the case of dependence on temperature and pressure.

Lastly, the Z is expressed by the previous eq. (95). These formulas are frequently found in the literature related to the kinetics of methanation reactions, such as in [59] and [115], and are very important as they determine the final concentrations obtained downstream of the methanation reactor. Hence, they express how many reactants have reacted and how many products have formed. Their degree of importance is not the same, eq. (18) (CO methanation) is privileged compared to eq. (17) ($CO_2$ methanation), because, from the kinetic point of view, it takes place at a higher speed. This implies, in the real case, a shorter residence time inside the reactor, with lower operating costs. Furthermore, $CO_2$ methanation has the disadvantage of forming two moles of water, increasing its quantity. The greater the quantity of water, the more WGS reactions will be, which do not produce methane, and at the same time decrease its formation because they convert the CO molecule into $CO_2$. Therefore, a good design involves the intensive exploitation of the first to the detriment of the other two.

In the thesis work, the methanation process that can be referred to is HICOM (High CO Methanation). Unlike its rival TREMP (Topsol REcycle Methanation Process), it involves that all three reactions described above are exploited in methanation reactors, without the need to remove compounds (in addition to sulphates, $CO_2$), in such a way to have a specific H/C at the entrance. It is therefore a process with less restriction, which has the disadvantage of obtaining a slightly lower concentration of $CH_4$ at the end of the methanation process, compared to the rival process.

The operating conditions of pressure and temperature chosen for the methanation reactors refer to the literature. Referring the work of T. James at al [116], who conducted several experiments, testing different reactors made of different materials, the optimized temperature and pressure values were identified for each type of reactor. It can therefore be said that, for the nickel catalyzed reactors, adopted in the methanation section of the thesis work, the best operating conditions are about 220 °C and 32.4 bar. James er al. state that for these values, the production of methane is maximized, while for lower or higher values, in addition to the smaller quantity of methane, there are undesirable effects such as corrosion and deterioration of the components due to reactions that are triggered. The coupling with the SOEC under pressure is very advantageous: at the outlet of the electrolyser, the syngas can be cooled from 850 to 220 °C, recovering useful heat for other plant processes. Furthermore, the pressure levels between the two operating sections are almost identical, consequently there is no need to compress the syngas, avoiding high electrical consumptions that would have occurred. As a matter of completeness, it is useful to mention that in the thesis work a syngas storage was considered, in such a way as to allow the methanation section to operate continuously at a constant flow rate, avoiding switching on and off the reactors, which is very expensive operation in terms of energy and with long lead times.

Once the operating conditions of the reactors are known, it is fundamental to know what is the maximum temperature to which the system can be subjected. This is very important because, as reported in “2.2.1.1”, the methanation reactions are exothermic. Therefore, their processes produce heat, increasing the temperature. Consequently, the only constraint that had to be respected was to consider the maximum outlet temperature from the first reactor, equal to 700 °C. For higher values, the deterioration of nickel occurs with a clear decrease in the kinetics of reactions and the formation of harmful compounds. To prevent the temperature from reaching values higher than the limit value, a recirculation between the first and second reactor was opted for, in order to control the composition of the syngas stream at the inlet of the first reactor.

The goal of the methanation section is to convert the syngas into SNG, a compound with a high percentage of $CH_4$. Based on the type of process considered, SNGs are obtained with a high concentration of methane which usually varies from 95 to 99%. Exploiting a single methanation reactor is unthinkable: the exothermic reactions of methanation would increase the temperature too much, shifting the equilibrium from the production of the desired compound to the reactants. Furthermore, the continuous increase in temperature would converge to too high values, which would make these temperatures incompatible with most of the materials used. Consequently, the structure of the methanation section, especially for the thesis work, is based on a series of four methanation reactors, with a cooler interposed between them (for a total of three), so as to bring the temperature back to the optimal value and at the same time exploit this heat obtained at high temperatures for other thermal processes of the system.

The remaining BOP of the methanation section includes separators, in order to further filter the substances, and finally a mixing with nitrogen, the inert substance which regulates some properties of the SNG. In fact, the purified and methane-rich flow, before being introduced into the national distribution network, must necessarily comply with standards. Specifically, with the three parameters listed below:

- Gas Gravity, GG [no dimension]. This parameter allows a gas with an appropriate density to be introduced into the network, in order to avoid accumulations or leaks from the pipes, very important problems that must never occur as they could increase the risk of fires (explosions, fires, etc.). The GG therefore represents the density of the SNG normalized to that of the air;

$$GG = \frac{\rho_{sng}}{\rho_{air}} \tag{118}$$

  To be injected into the network, the gas must have a GG value between 0.5 and 0.8;

- High Heating Value, HHV kJ/kg or kJ/m$^3$. This is a usual thermodynamic variable used for fuels. In fact, it represents the amount of thermal energy stored within a substance, in terms of mass or volume. To be introduced into the network, the gas must have an HHV between 35 and 45;

- Wobbe Index, WI kJ/kg or kJ/m$^3$. It represents the relationship between the two variables listed above (GG / HHV). To be input into the network, the gas must have a WI value between 47 and 52.

In the following chapter, these design bases will be applied within the Aspen Plus environment, a software that is able to perform component simulations and gives as output all the data relating to the physical properties (temperature, pressure, composition, flow rates, etc.) and the values of energy flows (such as electrical or thermal powers) required / produced. It will then be possible to analyze in detail the behaviour of the system, knowing the initial conditions calculated in the modeling paragraph above.

# 4 Analysis and results of the polygeneration plant

The purpose of this chapter is to obtain a complete description, hour by hour, of the polygenerative plant for a total duration of one year. Chapter 3 allowed to model the composing sections of the plant, investigating which physical and electrochemical processes could be implemented. In fact, once these processes are known, it is possible to use them in such a way as to obtain the data that describe the behaviour of the global system, allowing very useful considerations to be made when compared to alternative systems.

As already mentioned, the thesis work is almost totally composed (with the exception of the photovoltaic panel technology, nowadays mature and commercialized on a large scale) of innovative elements, appointed to solve the environmental problems widely discussed in the first chapter. In fact, with increasing incidence, the technologies of methanation, the capture of carbon dioxide and above all the rSOC electrochemical device, are technological innovations that are not yet fully integrated in the industrial field and in the production of energy. The reason for this slow upgrade of the systems currently used derives precisely from the fact that they are contemporary technologies. The materials of which these devices are made, are not directly taken from nature, but, as for instance in the case of the electrodes or the electrolytic membrane of the rSOC, they must be modified / altered in dedicated processes, which still appear to be more of a niche. This aspect can also be noted, for example, in the absorbent fluids used in the CCS section. As described above, the plant uses an aqueous solution of MEA, but in the literature new more performing and less expensive materials are emerging day after day. Therefore, the initial condition in which most of these technologies are found today does not favour their use. Fortunately, it can be said with extreme certainty that, like any technology still in the research phase or in any case not very advanced, in the future there will be more innovations that will make the technology economically competitive. This thesis, therefore, tends to inform about the potential of these indispensable technologies for the development of a society with an eco-sustainable footprint.

The simulation of the plant is therefore of primary importance to investigate the benefits that can be drawn from this system, but above all, it allows to take note of the negative aspects that will have to be improved and studied in greater detail to further promote the technologies and make them competitive in their sectoral market.

Before describing the simulation phase in detail, it is necessary to report and analyze the logic scheme implemented. The main function of the plant is to meet the urban electricity needs of a built-up area of 30’000 people. This request is met by exploiting, respectively, approximately one third of the technology of photovoltaic panels and for the remaining fraction the innovative solid oxide system. The common denominator of these two technologies is their ability to produce electricity as an alternative to conventional power plants, which exploit fossil fuels, emitting a large amount of pollutants into the atmosphere, causing the greenhouse effect. The photovoltaic field uses the energy of the sun, converting it directly into electricity. Being a technology strictly dependent on atmospheric conditions, it is coupled to an rSOC in such a way as to compensate for the fluctuations that occur during the day. In moments of energy deficit, the operating mode of SOFC makes it possible to make up for this lack, using $CH_4$, CO and $H_2$ as fuel, producing $H_2O$ and $CO_2$. On the other hand, in the energy surplus phase, the SOEC operation allows to store the energy that would be wasted in the form of $H_2$ and syngas. In support of the rSOC key section there are two other very interesting technologies from an environmental point of view. The first, the CCS, has the primary benefit of purifying the exhaust fumes of industrial processes, or, as in this case, biogas and the products of the SOFC section (hypothesis that will be analyzed in the future), therefore fluids with a high quantity of GHG substances, in such a way as to make them inert towards the environment. At the same time, a further important benefit is the production of an almost totally pure stream of $CO_2$ by filtering these GHGs, which can be disposed of inside the electrolyser, transforming it from polluting waste into syngas. As already seen, this compound consisting mainly of $H_2$ and CO, is attracting more and more attention thanks to its ability to store carbon dioxide, transforming it, downstream of further processes, into commonly used products such as biofuels, nourishment for plant cultures and much more. Finally, the second and last technology coupled to the rSOC, which precisely exploits the syngas produced by it, is the methanation section. From a technological point of view, this part of the plant is more mature than the other two previously reported. Unfortunately, it is not widely used as it involves the exploitation of substances that have not yet penetrated much into the market today, namely syngas. Fortunately, coupled with SOEC and also considering the previous section of CCS, an extremely interesting circular system is created: with CCS a polluting stream is purified, following the processes of current technologies. The rSOC exploits the removed pollutant by storing it in a compound, allowing the generation of a biofuel (SNG) in the methanation section, which can be exploited in conventional processes. This closed scheme has the benefit of avoiding the depletion of resources and environmental reserves and at the same time decreases the environmental impact caused by the release of these pollutants.

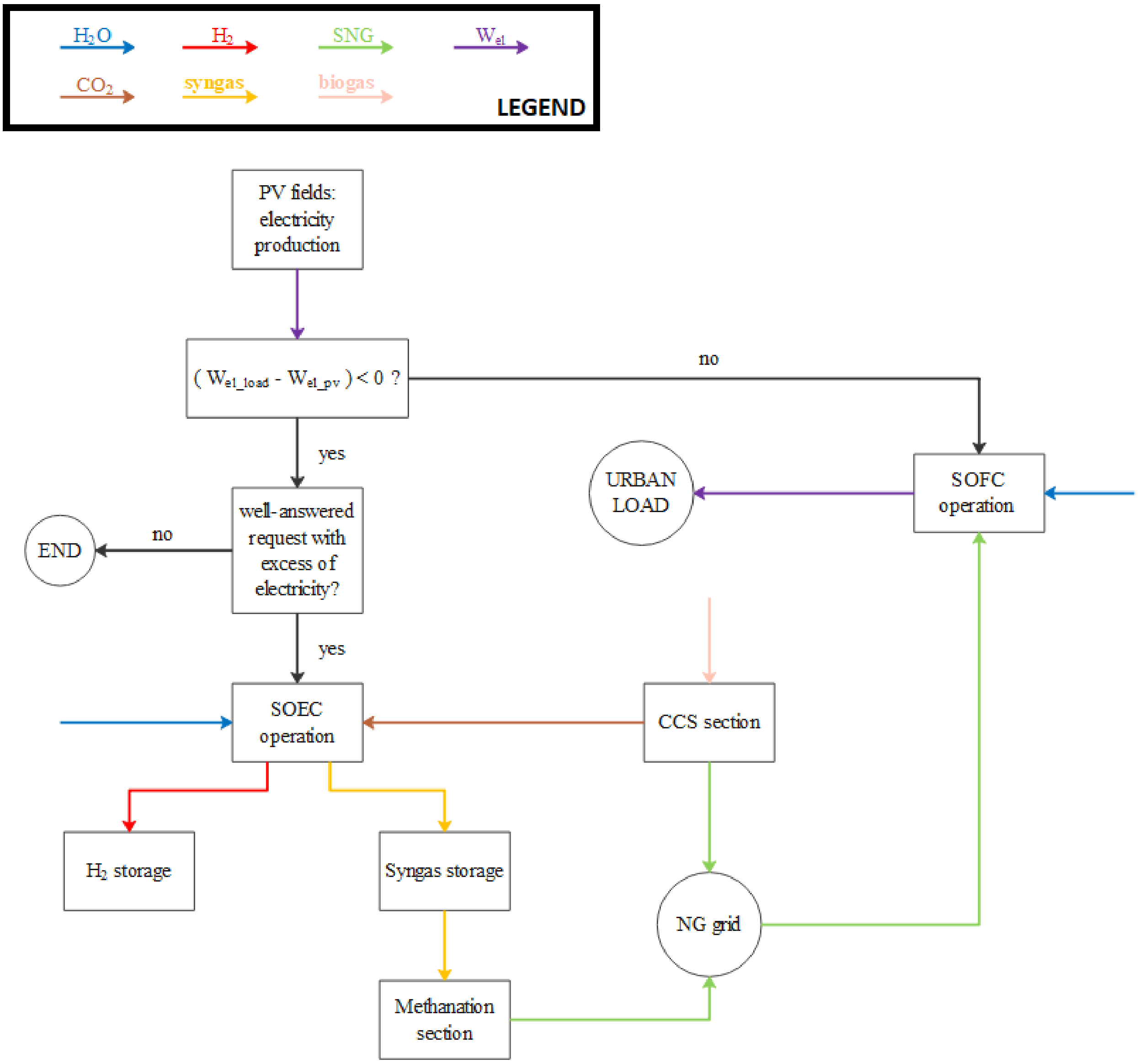

*Figure 25 - Logic scheme*

Fig. 25 above reflects the operations that are carried out in the system. Downstream of the SOEC there are two storage units: one for hydrogen and one for syngas. As explained later in detail, the accumulation systems have the function of accumulating these two important streams in such a way as to reuse them afterwards, allowing more convenient operations from an economic and operational point of view. At the moment it is important to specify that when $H_2$ is produced there is no production of syngas, and vice versa, as the SOEC is operating respectively in steam or co electrolysis.

The simulation with the use of Aspen plus was performed for each section of the system. In chapter 4 the settings, components and complementary formulas used (in addition to those foreseen in the modeling phase) for the simulation will be reported in detail.

Therefore, once the Aspen program has been set, i.e. made able to reproduce the process in question with high accuracy, the results obtained will correspond to the physical and chemical properties of each streams and each component. In general, a discrete map of the simulated plant section is obtained, which describes it in detail with reference to the setting conditions. Repeating this process for different settings will result in a series of discrete maps. By carrying out these simulations for each section and reporting this information in an Excel table, then interpolating the missing data that occur between one map and another, a final continuous map is obtained for each section which describes the behaviour. Having drawn up these continuous maps, which are independent between one section and another, with the use of a Matlab code, it will be possible to unify their information and to determine, hour by hour, all the data associated with each component / stream of the entire polygenerative plant. Finally, it will be possible to calculate all the performance parameters. The latter are the final variables that directly measure the performance of the system in terms of efficiencies, thermal and energy consumption, quantities of materials produced and other intrinsic variables of each section. The analysis of these parameters, grouped and reprocessed within the final tables and graphs, will allow to judge the performance of the system, in such a way as to visualize the pros and cons of the coupling of these innovative technologies.

## 4.1 Simulation through Aspen Plus environment

Advance System for Process Engineering (ASPEN) is a simulation software developed by Dr. L. Evans at the M.I.T Cambridge, Massachusetts. Al-Malah et al wrote a text [117] in which they describe in detail the various functions and operations that can be performed using this program. In general, Aspen Plus is based on a flowsheet simulation, in which it is possible to represent a model of a chemical process. Of this process it is possible to choose / set any of its characteristics: in its libraries there are icons that allow to consider within the process input and output of material streams, input and output of energy streams, input and output of electrical / mechanical signals and many industrial components. Based on the element to be considered, the software offers a wide range of possibilities: for devices such as reactors, circulation pumps, compressors etc. (the physical elements of which the industrial plant consists of), icons are available that can be positioned on the sheet. These components are then connected by flows of matter represented with simple lines. Intrinsically to these two elements, it is possible to proceed both with the setting of their chemical-physical properties and with the description of the processes / reactions / transformations that occur during their interactions. In fact, Aspen Plus allows to set up all the engineering relations necessary to simulate the process in question. Quoting directly from [117], ASPEN is able to reproduce the following physical phenomena:

- Balance equations of extensive thermodynamic properties, such as mass, mole and energy;
- Thermodynamic relationships for reacting and non-reacting medium, such as phase and chemical equilibrium;
- Rate correlations for momentum, heat and mass transfer;
- Reaction stoichiometry and kinetic data;

- Physical constraints imposed on the process.

Going into more detail, without specifying any formula and always referring to [117], the following are the settings that can be implemented, so as to represent reality as accurately as possible:

1. Specify the chemical components in the process using the Aspen Plus databanks or introducing by myself into the platform;
2. Specify thermodynamic models to represent the physical properties of the components and mixtures in the process, building into Aspen Plus;
3. Define the process flowsheet setting the unit operations, the process streams that flow into and out of the unit operations, select the models from Aspen Plus Model Library to describe each unit operation or chemical synthesis and place them onto the process flowsheet, label each unit operation model (i.e, blocks) as part of the process flowsheet and connect the blocks via process streams;
4. Specify the component flow rates and the thermodynamic conditions (temperature, pressure and composition) of all the streams;
5. Specify the operating conditions for the unit operation models, as the blocks.

Therefore, by setting the necessary information expressed in points 1 to 5 in Aspen, it is possible to virtually represent the process in question. Calculator blocks and design specifications are tools present in the Aspen Plus environment, in which it is possible to implement some of the above points while configuring the process. In the properties section, instead, it is possible to choose the necessary thermodynamic and electrochemical models.

After the above general introduction to Aspen plus, it is necessary to describe which hypotheses can be implemented for the simulation in the specific case of the thesis.

The first hypothesis concerns the stationarity of the simulated process. This means that all dynamic phenomena such as reaching the temperatures of the streams of matter inside the components, the chemical, physical reactions and the electrical phenomena involved are neglected: all transients are not considered. This first hypothesis is very important as it helps simplifying the treatment of the problem, adopting simpler models, characterized by a lower number of iterations to achieve the desired final result (therefore with a lower computational cost).

The second hypothesis regards the adiabatic nature of the components: this ideal condition allows to consider the physical devices used within the flowsheet as perfectly isolated from the external environment. This is a very important assumption because it means that all the thermal losses that would actually occur are neglected. If considered, Aspen plus calculates the thermal power produced in a specific component (heat exchanger, reboiler, etc.), which can be used in a heat exchange process as recovered heat. In the thesis work, this has always been counted in the calculation of the performance parameters in which it appeared (e.g.

Efficiencies), bringing a benefit if the component is characterized by an exothermic behaviour (heat production), or as a loss in the case endothermic behaviour (heat demand). In reality, the optimization of internal heat exchanges in the system should be envisaged through a specific thermal analysis study, the pinch analysis. This methodology was not foreseen in the thesis work as it refers to a single case examined. Unfortunately, if it had been done in this work, it would have had to be implemented for each simulation, making the treatment extremely complex and time-consuming.

The third hypothesis is that of negligible pressure drops: similar to the second one, as it is considered an ideal situation aimed at not contemplating thermal losses, in this case any type of pressure loss is excluded. In reality, the circulation of a fluid in a pipe, duct or component, is hindered by various physical phenomena such as its viscosity and the path to be followed (length of sections, curves, fittings, etc.), which cause a decrease of pressure and therefore of force with which the fluid is pushed to the final goal. In the thesis work it is therefore assumed that the circulation does not cause any pressure loss, and that the presence of devices such as pumps and compressors have the sole function of increasing the pressures to the operating values of the subsequent components, without the need to take into account no compensation for pressure drops.

The fourth and final hypothesis is another simplification that neglects the real dimension: size independence. Closely related to the type of model used, the dimensions of the components are extremely important, for example in a 2D study, the shape of the device plays a crucial role both from a thermodynamic (as there will certainly be favoured areas and areas disadvantaged in heat exchange), and economic point of view (devices with particular shapes must be made with specific equipment and machinery, increasing the cost of production). The only exception made in the thesis work concerns the absorber and the stripper present in the CCS section. For these two elements, in fact, Aspen requires the dimensions relating to the diameter and height of the pipes. The absence of this data would not have allowed the calculation by the software, always reporting an incomplete setting error.

From the next paragraph both the flowsheets adopted for the simulations and the results (performance parameters) will be analyzed in detail.

## 4.2 Aspen model: SOEC steam-electrolysis

In order of importance, the first operational section that is described and analyzed is that of SOEC. As seen in the general introduction of chapter 4, the electrolysis envisaged in the thesis work can be used for the production of hydrogen or syngas, exploiting the excess electricity produced by the photovoltaic field. This decision was taken during the design phase of the polygeneration plant, taking into consideration the Power-to-X (PtX) model on which it is based. From the point of view of the future potential, these two flows of matter are fundamental for an eco-sustainable development. In fact, as previously described in the state of the art, they constitute one of the best alternatives to conventional systems that are used today. Furthermore, their use is becoming increasingly popular in modern civilization, such as in the case of green transport with hydrogen engines. The purpose of this thesis, similar in ideological terms to many others, is to support this path, demonstrating, among the various alternatives, what the potential could be in the industrial field for these materials.

The choice of producing hydrogen or syngas in a differentiated manner within a polygenerative plant is purely for demonstration purposes. In the current literature there is still not much research proposing an industrial system, as the focus is still on trying to improve individual technologies. Known the potential of these products, it was very interesting to carry out a demonstrative study of this system, which will also be analyzed from an economic point of view, in order to get a more precise idea on the current conditions and, above all, on the convenience that would be nowadays if these technologies were really adopted. The logic that has been taken into consideration is the following: the first two days in which the rSOC operates in electrolyser mode were set for the production of hydrogen via steam-electrolysis. In fact, it is known that on the basis of the reagents considered and sent as input to the electrochemical device, it is possible to choose which products to obtain. To make the system more stable, the hydrogen produced is stored inside a suitably sized storage, paragraph "4.6", in order to transport it afterwards to refilling stations to power the transport of hydrogen vehicles. This last part is exempt from the thesis work, which stops at the stock of $H_2$ in the storage. For the sake of completeness, what may be a valid solution for transporting hydrogen to the refilling station (tube-trailer) is mentioned below. On the other hand, co-electrolysis is used for the production of syngas, carried out in the remaining days of the week in which the rSOC operates as SOEC. Also in this case, a suitably sized syngas storage will be provided, paragraph "4.8" with the aim of allowing the operation of the methanation section in stationary conditions (at constant flow), thus avoiding switching on and off, which would be factors of system loss.

Following the ethics on which the SOEC section is based, the model implemented in the Aspen Plus environment is described in detail. The first operation to be carried out is the setting of the properties on which the electrolyser section is based. The general setup foresees the specification of the measurement units of the physical variables. The unit sets outlined for the flowsheet are consistent with the international measurement system (SI), in which temperatures are expressed in [°C], pressures in [bar], mass flows in [kg/s], volumetric in [$m^3/s$], the molar ones in [mol/s], the powers in [W] and the energies in [J]. Subsequently, the chemical elements present in the operations of the plant engineering section must be specified. For steam-electrolysis, water, hydrogen, oxygen and nitrogen were considered. Aspen has a large database that allows, once the chemical components have been chosen, to determine the values of their physical variables, as long as they are specified within the "Property Sets" section. For instance, by choosing the "QVALNET" property from the list in the section just mentioned (as it was actually done), it is possible to determine for each element or compound its calorific value, excluding the need to explicitly specify it numerically. In addition to this property, there was no need to set any other property, as it was the only one necessary to fulfill the calculations of the plant operations. The last step for the complete setting of the properties of the flowsheet involves the choice of a method, used by Aspen, to carry out all the calculations for the determination of the thermodynamic properties. The method chosen for this section is that of “Peng-Robinson”. It is the recommended method because it allows to simulate in an optimal way, without producing anomalous behaviours, processes involving high temperatures and pressures, exploiting mixtures containing hydrocarbons or light gases such as carbon dioxide and hydrogen.

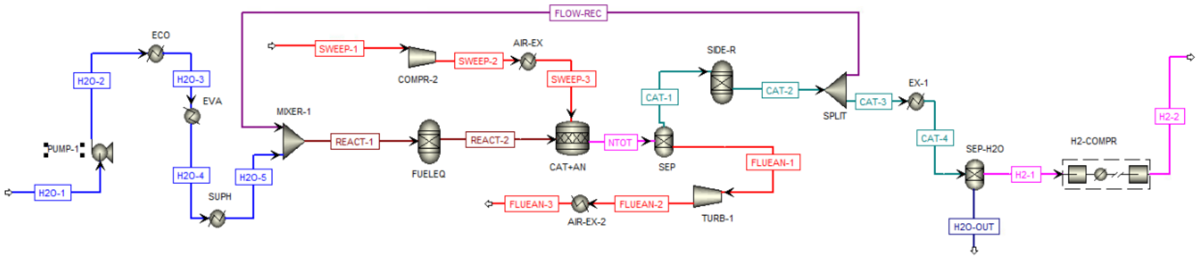

*Figure 26 - SOEC steam-electrolysis plant on Aspen Plus*

Circulation pumps, compressors and turbines require as input the output pressure of the component and its efficiency. The first component of the system, "PUMP-1", has the function of increasing the pressure of the pure stream of incoming liquid water, bringing it from the ambient value of 1 to 33.1 [bar], which is the operating pressure of the electrolyser. As previously stated in the hypotheses of paragraph “4.1”, it is reiterated that, for this component and in general for each component used to represent the systems, there are no physical phenomena of pressure and temperature losses. As for efficiency, the second parameter characterizing the pump, the expression of the ratio between the useful power and the absorbed power has been set to the chosen value of $\eta_{pump}$ = 80%. It should be noted that this value has been considered not only in relation to this specific component, but in general for each pump element present in each section of the polygenerative system. This is a further hypothesis considered in the thesis work because actually the choice of a component refers to a specific product of a specific supplier. This implies that the efficiencies should not all be the same.

Like the pump, also the compressor “COMPR-2” and the three compressors in the “H2-COMPR” block have been set by imposing the same efficiency, equal to $\eta_{compressor} = 70\%$. The first increases the ambient air pressure level to be sent to the anode for the reduction reactions. Taken from the outside at atmospheric conditions, it is increased until it reaches 33.1 bar of the electrochemical device. Its composition assumed as 79.05% $N_2$ and 20.95% $O_2$ therefore does not require the use of an oxygen separator. It is in fact known that a pure stream of $O_2$ operating in the anode would lead to a decrease in the efficiency, due to higher tension of operation (only for SOFC mode it is a benefit), moreover it increases the investment and operating costs. Despite this, the outside air was used, since a "TURB-1" turbine was provided, capable of generating additional electricity. Furthermore, it will also be possible to recover heat through the “AIR-EX2” component, exploiting its high exergetic content deriving from operations in the SOEC at 850 °C.

Instead, the other three compressors are part of an alternating refrigeration and compression system, essential for correctly modifying the physical conditions of the hydrogen produced during steam-electrolysis operations. The goal is to alter the conditions from the initial values of 850 °C and 33.1 bar to 20 °C (cooling effect of the intercoolers) and 250 [bar] (pressure increase by the compressors). These storage conditions will be explained in paragraph “4.7”, which refers to the design of hydrogen storage. To ensure the production of pure hydrogen, it is necessary to remove water, the second component present in the waste products of steam-electrolysis. The "SEP-H2O" separator performs this function, allowing the liquid phase to be separated from the gaseous one by setting the split fraction or directly the flow rate in the Aspen environment, known the pressure of the outgoing fluids.

Lastly, the "TURB-1" component previously mentioned, and in general each turbine of the polygeneration plant, is characterized by an efficiency equal to $\eta_{turb} = 75\%$, chosen consulting notes from “complementi di macchine”, “thermal design and optimization”, “complementi di energetica”, and so on, of Politecnico di Torino.

The heat exchangers in the system are very important components. Their function is to modify the temperature of the mainstream indicated at the inlet and outlet, increasing its temperature to reach the level required for the correct operation of the process, or decreasing it by recovering heat. This last thermal power brings benefits in the efficiency of the system as it is ideally exploited in its entirety, without considering any type of losses. Furthermore, as already mentioned in the previous paragraph, the management of the thermal powers exchanged by the heat exchangers should take place following the optimization process of the pinch analysis, which has not been considered because it is not fundamental for the purpose of the thesis work, and above all because of the enormous complications it would have introduced.

The heat exchangers of the water supply line to the cathode of the SOEC are the most expensive in terms of energy. This is strictly dependent on the high specific heat of the water.

In addition, the heat consumption increases further considering the high flow rates required for SOEC operations. "ECO", "EVA" and "SUPH" are respectively the economizer, with the purpose of increasing the liquid water temperature, making it almost reach the change condition phase; the evaporator, in which occurs the transition of state from liquid water to steam, and finally the superheater, which allows the temperature level of the steam to be raised until the required 850 °C temperature is reached. The use of these components for the water supply line is a conventional choice as they are always used in energy generation systems in which water at high temperatures is involved, such as Rankine plants.

Further heat exchangers are those of the air line, necessary to feed the anode side. “AIR-EX” and “AIR-EX2” are designated for this role. The first one allows the temperature to be raised, and the second one allows the recovery of the thermal power associated with the final products. Finally, the last heat exchangers are "EX-1", used to recover the heat present in the steam leaving the cathode, the same function of the intercoolers present in the "H2-COMPR" section which also have the function of controlling the temperature during the $H_2$ compression process. In general, in the Aspen plus environment, the heat exchanger component can be set by simply setting two parameters. The first one is the phase of the stream that flows inside, such as 'vapor-liquid' in "ECO" or "EVA" and 'only-vapor' inside "SUPH". The second one is the temperature or the pressure drop (based on which of the two is known upstream). With the use of these settings, it is possible to uniquely determine the thermodynamic quantities of the output stream. Specifically for the thesis work, considering the hypothesis of zero pressure losses, a temperature will always be set.

In the electrolyser system there is a recirculation downstream of the electrochemical device, a strictly necessary choice for this operating mode. It is necessary to guarantee at least a percentage equal to 10 $\%_{mol}$ of $H_2$ at the inlet of the fuel electrode in order to maintain a reductive atmosphere, avoiding the re-oxidation of the nickel catalyst in contact with water vapour. The “SPLIT” component separates the flow of matter leaving the SOEC’s cathode in a controlled manner, guaranteeing this minimum molar percentage. The flow then ends up in the “MIXER” which allows to mix the recirculated flow with the inlet reagents.

The last and most important component, "CAT+AN", represents the electrodes of the SOEC, although the reproduction of the complete electrochemical device requires the presence of two other auxiliary components, "FUELEQ" and "SIDE-R". After analyzing them in Aspen, the former was chosen as a stoichiometric reactor, with which it is possible to simulate the electrochemical reactions which take place inside it. The actual reduction and oxidation reactions that occur are entered directly as a global reaction, describe by the next eq. (119):

$$H_2O \rightarrow H_2 + \frac{1}{2}O_2 \tag{119}$$

Furthermore, it is necessary to set the reactor temperature and pressure values, also specifying the phase of the reactants involved in the chemical process, in such a way as to allow the simulation to obtain all data: physical variables of the output products and thermal power absorbed/released by the process. The two auxiliary components, on the other hand, are used to obtain a more accurate simulation, for compliance with the equilibrium condition necessary for chemical reactions. Indeed, to guaranteed the equilibrium, "FUELEQ" and “SIDE-R” are considered, representing respectively the inlet and outlet surface of the fuel electrode, hypothetically. On Aspen, Gibbs’ reactors were used, in fact this component allows to evaluate the product in terms of chemical composition and temperature, calculating them through the energy and mass conservation equations, minimizing the Gfe.

### 4.2.1 CB and DS of SOEC steam-electrolysis’ section

Once all the components have been reported, connected to each other through special streams and the initial data set, it is necessary to set the spreadsheets that Aspen uses to conduct the simulation. These elements must be filled in following the modeling that took place as a previous step in the elaboration of the thesis.

In general, the design specifications (DS), allow to calculate a specific value to be obtained for a given variable. Aspen is able to obtain this result with various degrees of accuracy based on the tolerance value set. To do this, it is possible to vary a second variable, which can be any of those considered in the project, for example a temperature value, the quantity of flow rate in a certain component, the chemical composition of a certain constituent element of the compound, and so on. Furthermore, to direct the program in the right direction, equations can be set that lead to the calculation of the project specification, with the use of a sheet (subsection of the DS) called fortran. A calculator block, on the other hand, is a section of the Aspen program that allows to perform a specific calculation, choosing the input variables that the program must use for the calculations, obtaining export variables that are overwritten to the value previously set. With the use of these two tools, Aspen is able to simulate the process by performing a series of iterations, to reach convergence dictated by compliance with all the specifications set.

Two DSs and two CBs were used to simulate the steam-electrolysis process. The first DS has the objective, already stated above, to obtain as a specification a value equal to 10 $\%_{mol}$ of hydrogen in the "REACT-1" stream, visible in the system plant of fig. 26. The convergence of the result is obtained from the percentage variation of recirculated flow “FLOW-REC”, downstream of the operations performed by the “SPLIT” component. In addition, the variation in flow rate also optimizes the flow rates at the cathode and anode inlet. The second DS, on the other hand, is more complex and has the objective of determining the alternating power required by the SOEC, produced by the photovoltaic field and necessary for the activation of the electrochemical reactions. The setting of the DS’ Fortran starts setting the constant values known from literature:

- Faraday's constant, F equal to 96’485;
- Inverter efficiency, $\eta_{inv}$ equal to 96%, used for the conversion of power from direct (the one actually exploited by the SOEC) to alternating (coming from the photovoltaic section);
- Fuel utilization, FU set to 0.786.

While further variables deriving from the results obtained in the previous modeling phase:

- Cell's area, equal to 300 $cm^2$;
- ASR equal to 0.304 $\Omega$ $cm^2$;
- Number of the cell, $n_{cell}$;
- Oper Circuit Voltage, OCV equal to 0.916 V;
- Thermoneutral voltage, $V_{TN}$ equal to 1.288 V;
- Current of the entire SOEC, $I_{stack}$.

Most of the variables reported above have already been described previously, consequently the missing ones are now explained. The fuel utilization is a very important variable as it guarantees values of the acceptable partial pressures of the reactants. The flows of matter are thus considered in their real conditions, starting from their stoichiometric conditions, ideal because, according to the theory, they are the minimum necessary to make chemical reactions take place.

$$FU = \frac{\dot{n}_{fuel,st}}{\dot{n}_{fuel,real}} \tag{120}$$

The number of cells is updated with each simulation based on the number of active modules operating in steam-electrolysis. This consideration is fundamental because it allows the electrolyser to operate at the maximum possible efficiency value, taking into account that its operability can vary in a range between 20% and 80% of its size (30 MW). As seen in “3.2.4”, the rSOC is made up of 12 modules, each of which, for the electrolyser mode, absorbs a power of 2.5 MW. By simulating the behaviour of the cell for each of its modules, for different values of absorbed power, it is possible to obtain a series of very detailed continuous maps. Their analysis with the help of a Matlab code allows to associate the values of all the variables of the system to a certain condition (power actually supplied to the SOEC, given by the difference between the urban load demand and the power produced by the PV). By adopting this algorithm only for modules that fall within the operability percentage and by choosing the case in which there is the greatest efficiency, the final values sought can be obtained.

Last but not least: the total current absorbed by the SOEC. Once the polarization curves of the device are known, for a certain absorbed power it is possible to identify the current value required through the Matlab file described in "3.2.4". If it is set on the DS Fortran, Aspen is able to carry out all the necessary complementary equations:

$$V_{op} = OCV + ASR \frac{I_{stack}}{n_{cell} A_{cell}} \tag{121}$$

$$W_{DC} = FU \; H_2O_{in} \; V_{op} \; 2 \; F \tag{122}$$

$$W_{pv} = \frac{W_{DC}}{\eta_{inv}} \tag{123}$$

$$P_{out} = G_{H_2} LHV_{H_2} \tag{124}$$

$$BOP_{el} = W_{PUMP} + W_{COMPR-2} + W_{H_2-COMPR} \tag{125}$$

$$\eta_{el} = \frac{P_{out}}{W_{DC}} \tag{126}$$

$$\eta_{el,net} = \frac{P_{out}}{W_{DC} + BOP_{el}} \tag{127}$$

$$Q_{rel} = \left(V_{TN} - V_{op}\right) I_{stack} \tag{128}$$

$$BOP_{th} = Q_{ECO} + Q_{EVA} + Q_{SH} + Q_{AIR-EX} + Q_{AIR-EX2} + Q_{EX1} + Q_{H_2-COMPR} \tag{129}$$

$$\eta_{CHP,exo} = \frac{P_{OUT} + |Q_{rel}|}{W_{DC}} \tag{130}$$

$$\eta_{CHP,endo} = \frac{P_{OUT}}{W_{DC} + |Q_{rel}|} \tag{131}$$

$$\eta_{CHP,net,exo} = \frac{P_{OUT} + |Q_{rel}|}{W_{DC} + BOP_{el} + BOP_{th}} \tag{132}$$

$$\eta_{CHP,net,endo} = \frac{P_{OUT}}{W_{DC} + |Q_{rel}| + \; BOP_{el} + BOP_{th}} \tag{133}$$

The first variable to be calculated is the value of the cell's operating voltage, eq. (121). This formula derives from the assumptions made in "3.2.2.4" relating to the linearization approximation. In fact, the fraction that multiplies the ASR represents the current density [A/cm$^2$], and together they form the overpotential losses which through the linearization approximation allow to represent all the losses phenomena present during the operations of the electrolyzer.

$H_2O_{in}$ represents the molar flow rate of the water component of the "REACT-2" stream, since, thanks to the previous DS specification, a hydrogen content of 10%$_{mol}$ is set. It follows that the remaining part will be 90[%$_{mol}$ of water. In the calculation of the continuous power required by the SOEC, WDC, only the contribution of water was considered as that of hydrogen does not take part in the steam-electrolysis reactions, maintaining an inert behaviour in relation to SOEC operations. Once the variable has been associated with its reference component, Aspen is able to derive its value, using it in the calculation of the eq. (122), to obtain the continuous power necessary to activate the electrochemical reactions. Once this value has been determined, the program proceeds with the execution of the remaining equations, in particular eq. (123), relating to the calculation of the receiving alternating power from the PV section, $W_{pv}$. This series of operations is repeated in the iterative process that ends when convergence is reached: that is, obtaining an alternating power value that falls within the specific value +/- the tolerance.

The complementary equations reported above, from (124) to (133), allow to calculate important parameters useful for the classification of SOEC in terms of efficiency. Two types of efficiencies are considered, electrical and combined. The first one, $\eta_{el}$, takes into account the conversion between the electrical power required by the SOEC for proper operation and the useful effect, in terms of thermal power producible by the products of the SOEC estimated by the LHV. Instead the second efficiency, $\eta_{chp}$, takes into account both this useful effect, but also considers the contribution of the heat produced or absorbed by the device itself, $Q_{rel}$. Furthermore, both can be gross or net (marked with the subscript net), based on whether the auxiliary components (BOP), which allow the electrochemical device to function correctly, are also considered. Therefore, the first step for their determination consists in calculating the thermal power associated with the stream of hydrogen produced, $P_{out}$ of the eq. (124), obtained from the product between the mass flow rate of this streams, “CAT-3” and its net calorific value, LHV, already mentioned in “2.1.1” because it is made of $H_2$. The second thermal variable of fundamental importance is the heat exchanged between the cell and the environment, eq. (128). As already known, when the SOEC is in operation, a certain operating voltage value can be attributed. When this variable has a value greater than the thermoneutral voltage, its behaviour is exothermic with the production of heat towards the environment. In the opposite case in which it is lower, there is a heat absorption due to the prevalence of the endothermic behaviour. In the first case, the thermal power contribution produced is considered at the numerator, eq. (130), because it can be considered as an increase in efficiency if it is recovered and exploited. Otherwise, eq. (131), the required thermal power passes to the denominator, highlighting the negative contribution it makes, as heat must be produced to ensure the occurrence of the electrochemical reactions. All the efficiency equations described above refer to the gross case, in which only an imaginary control volume is considered that includes only the electrochemical device. By widening this boundary and taking into account the ancillary components it is possible to determine an efficiency that has a more significant impact in describing and classifying the SOEC. Eq. (125) shows the auxiliary components that produce a useful or negative effect in terms of electrical power. The considered $BOP_{el}$, in fact, reports the powers required or produced by the pump, the compressors and the turbine. Its contribution is considered for the determination of the net electrical efficiency, $\eta_{elnet}$, as can be seen in eq. (127). Instead, the thermal contributions of the other components, such as heat exchangers, are considered in eq. (132) or (133) within the $BOP_{th}$ variable.

Unlike the DSs adopted for the simulation of the electrolyser section, the CBs were created in order to verify the fundamental variables taken for granted because they were derived from the modeling work. In fact, once the iteration convergence was reached, the program was forced to perform the calculations expected in the CBs, calculating for instance OCV and $V_{TN}$, in order to prove if they were consistent with the initial values entered. For the verification of the open circuit voltage, the formula of the modeling step wasn't applied, eq. (62) in paragraph “3.2.1”. This formula refers to the partial pressures of the reagents and products of the cathode. However, considering the condition of chemical equilibrium in the electrodes, an alternative formula was used that exploits the logarithmic ratio between the partial pressure of oxygen in the anode and cathode:

$$OCV = \frac{R(T_{cell} + 273{,}15)}{4F} \ln \left( \frac{p_{O_2,SWEEP3}}{p_{O_2,REACT2}} \right) \tag{134}$$

An alternative formula was also used for the thermoneutral voltage with the same purpose of verifying the consistency of the initial values entered. It is known that electrical power is given by the product of current and voltage. Using the inverse formula, it is possible to obtain the voltage value as a function of the other two variables:

$$V_{TN} = \frac{W_{DC}}{I_{stack}} \tag{135}$$

Using the inverse formula of Faraday's Law, eq. (52) in paragraph "3.2.1", the value of the current absorbed by the SOEC is determined as a function of the difference in molar flow between reactants ($\dot{n}_{O2,sweep1}$) and products ($\dot{n}_{O2,fluean1}$) of the anode considering only the oxygen component:

$$I_{stack} = \left(\dot{n}_{O_2,FLUEAN1} - \dot{n}_{O_2,SWEEP-1}\right) 4F \tag{136}$$

The calculation of the continuous power produced, on the other hand, is performed considering the product between molar flow and molar specific enthalpy between products and reagents of the electrodes, considering all the elements of these streams:

$$W_{DC} = \dot{n}_{FLUEAN1} h_{FLUEAN1} + \dot{n}_{CAT1} h_{CAT1} - \dot{n}_{SWEEP3} h_{SWEEP3} - \dot{n}_{REACT2} h_{REACT2} \tag{137}$$

Both checks executed by CBs have always reported similar values compared to the reference variables, positively ascertaining the data used in the setup phase of the simulation.

### 4.2.2 Performance parameters, results of SOEC steam-electrolysis' section

Downstream of the Aspen program setting, a series of simulations were performed for each module in order to obtain as many discrete maps. These maps trace the behaviour of all the descriptive parameters of the streams and components present in the plant section. To obtain the missing data between one simulation and another, the linear interpolation method was adopted, which made it possible to determine, for all cases dependent on the number of active modules, a continuous summary map of SOEC operations between 20 and 80 % of its size. These final maps were exported to Matlab and analyzed through a specially created code with the aim of obtaining, hour by hour, the values of all the components and streams. As mentioned above, the creation of continuous maps was drawn up for each section, in order to obtain a description of the overall behaviour of the entire polygeneration plant.

The analysis of the steam-electrolysis section's results shows that the first data of great interest is its operating time. Downstream the simulation, considering the electric power values produced by the PV section (according to the weather conditions obtained from PVGIS online software), and the electric powers absorbed by the urban civil loads, the total time dedicated for electrolyser operations was 1746 hours, of which 483 available for steam-electrolysis. Of these, only 435 were sufficient for the purposes, as the difference between the two durations represents the hours in which the powers are below or above the operating range, set between 20 and 80 %. The short period of time taken for the steam-electrolysis operations fully reflects the logistics set in the design phase: only the first two days of energy surplus were used for the production of $H_2$. The results shown in the following table 14, also report the total quantity of flow produced in the reference year. As for hydrogen, referring to the literature, [89], [118] and [119], it is possible to associate its value with a small production plant. They are characterized by a production that varies between 30 and 100 kg$H_2$ per day, with a weekly value between about 150 and 500 kg$H_2$ (considering operating conservatively, five days a week).

| **Process Parameter** | **Result** | **Unit** | |
|---|---|---|---|
| $I_{SOEC}$ | 1,1119 | **MA** | **ARITHMETIC MEAN** |
| $J_{cell}$ | 1,2554 | **A/cm2** | |
| $V_{op}$ | 1,2977 | **V** | |
| $key_{SOEC}$ | 35,0827 | **kWh/kg$_{H2}$** | |
| $G_{H2O-1}$ | 223,558 | **tons$_{H2O}$/y** | **SUM** |
| $G_{H2}$ | 20,430 | **tons$_{H2}$/y** | |
| $G_{SWEEP1}$ | 40,479 | **tons$_{air}$/y** | |
| $G_{FLOWREC}$ | 8,941 | **tons$_{flowrec}$/y** | |

*Table 14 – mass flow rate & electric parameters for steam-electrolysis*

Although the quantity of $H_2$ produced is sufficient to guarantee the weekly supply of 392.888 $kgH_2$ for a refilling station dedicated to heavy transport (a topic that will be dealt with in greater detail in the following paragraph relating to hydrogen storage), in relation to the quantity of water needed for its production, it appears that only the useful effect alone is equal to approximately 9%. This problem implies the need for a high quantity of water for these types of plants. From the point of view of the initial capital, it does not present a disadvantage, but from the point of view of operating costs it does, due to the high energy expenditure necessary to increase the temperature and pressure of the water, from the environmental conditions to the operating ones of the SOEC. Furthermore, it is extremely worrying from an environmental point of view as its uncontrolled overexploitation would cause a rapid depletion of water reserves. For this reason, careful and controlled management of this resource must be contemplated, considering this purpose as important as the reduction of GHG release into the atmosphere. In fact, among the various benefits, the presence of an internal recirculation allows to reduce the quantity of reagents to be introduced into the plant section. It also allows to stabilize the internal conditions of the streams, as for example in this case, ensuring a fixed molar percentage of $H_2$ for the flow rate entering the SOEC cathode. Moreover, considering the stream "H2O-OUT", it could be implemented a dedicated recirculation system able to reduce drastically the amount of inlet water "H2O-1", reducing the stream at the right amount consumed in the previously SOEC operation.

Finally, unlike the high flow rate of water required, that of air is much lower, and is learned to be about double that of $H_2$ produced. Fortunately, this environmental resource is widely available in nature and its operating costs are also low, mainly due to the low specific heat capacity. The flow rates were analyzed in terms of annual sums in order to give them greater significance from the point of view of use in the SOEC section. In reality, also for the other sections, the flow rates will always be reported considering their total annual quantities.

In table 14, however, there are other data that make it possible to represent the system if referred to the annual average values: the electrical parameters. It is noted that on average, the SOEC tends to assume an operating voltage value greater than that of thermoneutral voltage: 1.298 > 1.288 [V]. This average exothermic behaviour implies that there are more moments in which the SOEC produces heat to be removed to keep the operating conditions stable, avoiding all sorts of degrading phenomena, compared to the time necessary for the endothermic behaviour, in which the activation and maintenance of the reactions electrochemical requires heat. Having known this detail, as a result of an additional sensitivity study, not envisaged in this thesis, it would be possible to further optimize the total efficiencies of the system by properly exploiting this heat with a high exergetic content. Unlike the average values of current and current density which allow especially to have an idea of the high values present during the operation of the SOEC, there is an important parameter, reported as $key_{SOEC}$, which is very interesting in order to describe the production capabilities of hydrogen. In fact, this variable represents the amount of electricity needed to produce one kilogram of hydrogen in the operating conditions of the cell, 850 °C and above all 33.1 bar. Its value was obtained as the annual average of the hourly values obtained from the ratio between the continuous power absorbed during the hour of operation of the SOEC and the hourly mass flow of hydrogen produced. The average value obtained settles on 35.0827 $kWh/kg_{H2}$, or, by converting it as a function of the volume under standard conditions and therefore considering a density of about 0.089 $kg/Sm^3$, a specific volume consumption of about 3.122 $kWh/Sm^3_{H2}$ is obtained. Comparing the value of this important variable, which characterizes electrolysers in terms of performance, is in agreement with values in the literature [30]. Furthermore, this is in line with the data transcribed and reported in table 14. As can be seen, the amount of water required is significantly higher than the amount of hydrogen produced, resulting in a high energy consumption for the production of a modest amount of fuel. This peculiarity with negative features, in reality, can be exploited in an advantageous way. In fact, as the polygenerative plant intends to operate, by coupling the production of hydrogen with the production of electricity from RES, this surplus can be easily stored, which would otherwise be wasted. Furthermore, considering both conventional energy production systems such as gas turbines or especially innovative fuel cells, it is possible at a later time to convert the high chemical potential of this element back into electricity. And this aspect is much more interesting if we consider the electrochemical device, since, if it is possible to operate in conditions close to the thermoneutral condition, the electrical and generally global efficiencies of the system are extremely high, reaching ranges between 50 and 80 %.

Finally, the following fig. 27 allows to draw conclusions with respect to the electrical and thermal powers exchanged. Both are measured in MW, and each of their components refers to a total annual value, given by the sum of the hourly values obtained. The sign convention, on the other hand, is used to determine the type of flux: positive values indicate a power produced and outgoing from the system, while negative values indicate an absorbed power. The graph positioned in the upper part of fig. 27, shown below, corresponds to the electrical powers involved in the steam-electrolysis section. Among them, the continuous and alternating power necessary for the electrochemical reactions from the SOEC and finally the net electric power of the components that make up the $BOP_{el}$ of the electrochemical device can be found. As reported in eq. (124), this last variable considers the compensation between the electricity absorbed by the pump "PUMP-1" and by the compressor "COMPR-2" for their correct functioning, and the electricity produced by the turbine "TURB-1" which receives the waste products of the anode: mainly nitrogen and excess oxygen. As can be seen in the figure, its value is practically negligible, slightly lower than zero, meaning that net of the electricity of the auxiliary components, the absorption contribution is slightly greater than the positive production one. From the point of view of efficiencies, the gross electrical efficiency value does not differ much from the net one, if not for a very small decrease. As for the other two powers considered, $W_{AC}$ and $W_{DC}$ the difference is simply dictated by the performance of the inverter, the electronic device that allows the conversion between one and the other. The negative values are in line with the theory of SOEC, as it is the operation of the electrochemical device that absorbs electricity to store it in the chemicals created.

The part below of the graph, on the other hand, shows all the thermal powers of greatest interest present in the plant engineering section considered. The first value that catches the eye is that relating to the thermal power associated with the flow of hydrogen produced, $P_{out}$. Its value does not differ much from that of the electrical power, highlighting the high electrical efficiency available to SOEC. This peculiarity depends on the physical phenomena present in the SOEC: unlike conventional systems, the conversion of electricity into chemicals and vice versa (for SOFC) exploits a direct conversion, avoiding major losses such as, for example, the phenomenon of friction. This allows to obtain net yields higher than those of classical systems such as gas turbines and/or Rankine turbines. Furthermore, as mentioned before, one of its advantages connected to this is the high rate of conversion from chemicals to power (Power-to-Gas-to-Power), which allows to use electricity in times of need or possibly resell it during the hours of the day when there is a greater demand (to increase the selling price).

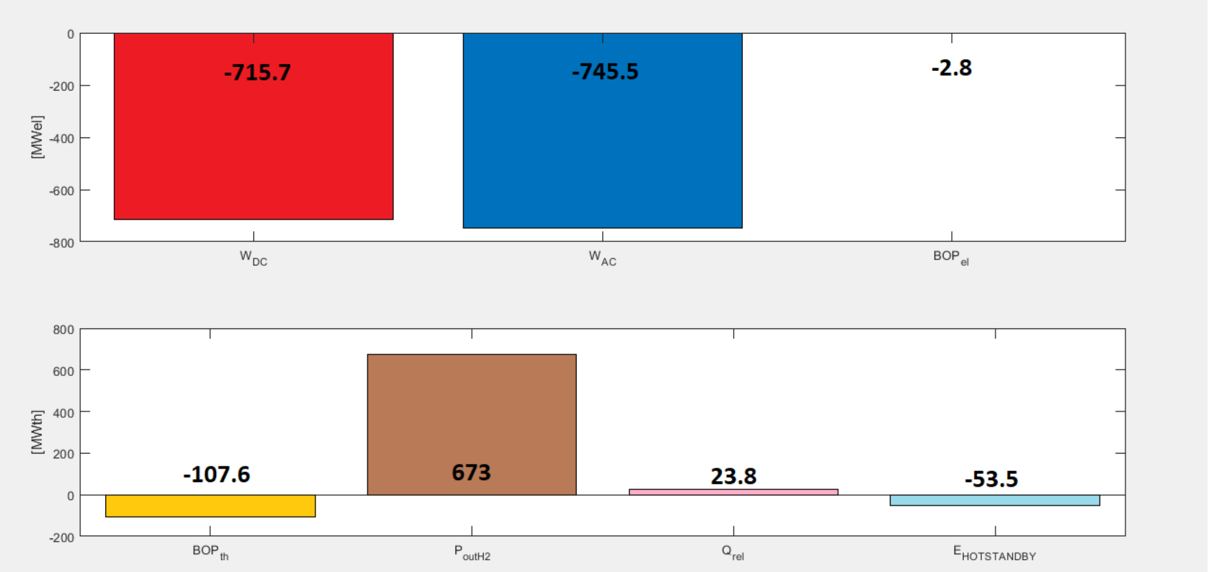

*Figure 27 -Energetic flux characteristic of the steam electrolysis section*

Continuing the analysis of fig. 27, the thermal power associated with the variable $BOP_{th}$ expresses the overall value of the thermal powers of the auxiliary components, as expressed in eq. (128), consisting mainly of heat exchangers and water line heaters. The first produce both a positive effect, recovering heat from the product streams leaving the electrochemical device, and a negative one, as the gas sweep flow rate entering the anode requires heat to reach the desired temperatures. In addition, there is only the negative contribution of the water line, which, unlike the air, has significantly higher thermodynamic characteristics, resulting in a huge heat consumption. Furthermore, as can be seen in tab. 14, the amount of water consumed in a year of plant operation is an order of magnitude greater than the other carriers. The final value obtained expresses a negative net balance, equivalent to a decrease in the combined net yield of the system considered.

Subsequently, visualizing the thermal power exchanged between the cell and the environment, $Q_{rel}$, it is possible to notice how its value is relatively low, tending to zero. This behaviour is consistent with what was set in the modeling phase: one of the main objectives, in fact, was to operate in conditions as similar as possible to the thermoneutral situation. Furthermore, the result obtained is in line with what is reported in table 14, because as already mentioned, the average operating voltage value is slightly higher than the thermoneutral voltage value. In fact, it is indicated with a positive sign, thus expressing a flow trend outgoing, from the system to the environment (exothermic behaviour).

Finally, in order to better explain the last variable, the hot-standby heat, it is necessary to consider what has been said in the design section of the SOEC, or rather, of the entire electrochemical device. Therefore, an arrangement comprising 12 modules is known. To operate in the condition with the maximum possible efficiency (the thermoneutral condition), a modulation of the powers managed by the cell has been adopted by activating the switching off or switching on of these modules. In the event that the SOEC has modules that are off, they are not completely deactivated, but kept hot, ready to guarantee their operation in the event of future accension. In order to determine this thermal power, the insulation thermal conductivity value associated with the rSOC was first calculated, [101]:

$$\lambda_{SOEC} = 1{,}875 * 10^{-8} * T_{SOEC}^{2} + 7{,}488 \ * 10^{-6} * T_{SOEC} + 0{,}0224 \qquad (138)$$

This variable measures the ability of heat to interact with rSOC materials in terms of heat conduction. In reality, the empirical formulation reported, obtained by following numerous experiments conducted, [120], allows to obtain an approximate value that describes its general behaviour, avoiding the determination of the variable for each single material constituting the device. Thanks to its application, a final value equal to 0.037642 W/mK has been obtained, considering the 850 °C (+273.15 for conversion to K) of the operating phase as $T_{SOEC}$.

$$E_{hot-standby} = \frac{k_{SOEC}}{l_{ins}} \, A \, (T_{air} - T_{SOEC}) \qquad (139)$$

Eq. (139) obtains the final value of energy necessary to maintain the temperature at the value of the device, in such a way as to be able to avoid a long transient necessary to reach the operating condition if it is at room temperature ($T_{air}$). Within the formula there is $l_{ins}$, which represents the thickness of insulation present in the rSOC, data previously provided in paragraph "3.2.4", equal to 30 cm. Finally, variable A comes into play to determine the incidence of the module numbers. It represents the total external area of all the modules, and is derived from the following eq. (140):

$$A = 2 \, n_x * (L_1 L_2 + L_2 L_3 + L_3 L_1) \qquad (140)$$

Referring to paragraph "3.2.4", which shows the reference values of the lengths that characterize the rSOC, it is possible to determine the total value of the area, including not only the areal extension of the electrodes, but also all the auxiliary components such as insulators, end plates and the inactive cell space. Instead, $n_x$ represents the number of modules considered. Thanks to them it is therefore possible to effectively associate the necessary heat to the number of inactive modules.

The last data reported are the most important, which allow to better describe the behaviour of the steam-electrolysis section: the efficiencies. However, in order to have a better visualization, the values of the steam-electrolysis and co-electrolysis efficiencies have been considered together, reporting the overall behaviour of the SOEC. They will be reported in the next paragraph on the second electrolysis mode.

## 4.3 Aspen model: SOEC co-electrolysis

The second Aspen model analyzed concerns the section of the SOEC used for co-electrolysis. In this case, the electrochemical device receives as input reagents not only water, but also a 99.99% pure stream of carbon dioxide, coming from the complementary section of CCS, so as to be able to produce the desired syngas. From the plant engineering and setting point of view of the Aspen model, there are no substantial differences compared to its steam-electrolysis counterpart. In reality they are very similar, with the exception of some details that allow the correct functioning of the operations.

The unit of measurement chosen to quantify the parameters, as in each plant section of the polygeneration plant, is that of the SI, abundantly explained in "4.2". As regards the Property Sets, however, as in the steam-electrolysis, a single variable was set to which the physical property QVALNET was associated, available in the software database. This allows to directly determine and associate the net calorific value for a given stream, without any need to set it manually. Finally, the substantial difference that characterizes this setup compared to that of steam-electrolysis are the chemical compounds considered. In fact, it is necessary to consider not only the chemical elements previously listed in "4.2", but also carbon dioxide, carbon monoxide, methane and MEA.

As previously mentioned, the electrochemical device requires both water and carbon dioxide to be able to carry out the co-electrolysis operations. The acid gas flow comes from the CCS section, where it is removed from a biogas stream with the intention of purifying it and producing biomethane to be introduced into the national natural gas network. This connection makes it possible to obtain a production line that starts from a waste ($CO_2$), namely an element that constitutes a cost in a production system, enhancing it and subsequently converting it into syngas. From an economic point of view, a cost is transformed into a profit. Furthermore, there is also an environmental advantage because it avoids the release into the atmosphere of a pollutant responsible for the greenhouse effect. As regards carbon monoxide and methane, on the other hand, they are considered as they are the elements produced by co-electrolysis. In reality, methane is generated indirectly due to the elements present in the cathode of the electrolyser, as will be shown in detail below, resulting in a benefit in the case that the syngas is processed in methanation reactors for the SNG production. Finally, the solute MEA contained in the acid stream of $CO_2$ entering the co-electrolysis section is present as a small residual trace of the CCS operations. Its quantity is negligible compared to that of the other components, in fact, during the operations of the electrolyser it disperses without interacting with any other molecule present in the system. It has been reported more as a matter of congruence between exit from CCS and entry to co-electrolysis.

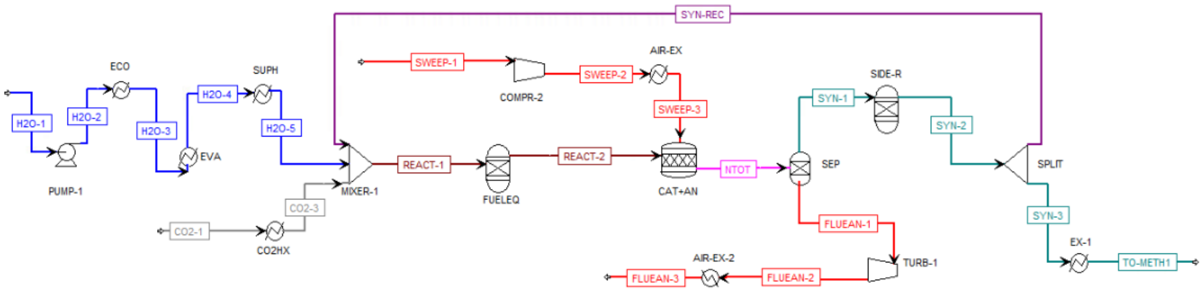

*Figure 28 - SOEC co-electrolysis plant on Aspen Plus*

Fig. 28 shows the plant design of the co-electrolysis section implemented in the Aspen Plus environment. Comparing it with fig. 26, depicting the plant of the steam-electrolysis counterpart, it is noted how the plant remains identical to the previous, except some differences that can already be identified at the graphic level, but not only.

The first difference is related to the presence of the carbon dioxide supply line. The “CO2-1” stream is the flow of carbon dioxide produced and sent by the CCS section at the conditions of 35 °C and 33.1 bar. The pressure value is directly in agreement with the operating value of the electrochemical device, excluding the presence of a compressor. On the other hand, from the point of view of temperature, the incoming sour gas must be further heated, passing through the “CO2HX” heat exchanger, in such a way as to reach the necessary 850 °C. From the point of view of efficiencies, the absence of the compressor leads to a decrease in electricity consumption, on the other hand, the necessary high temperature jump requires a large amount of heat. Furthermore, by reiterating the hypotheses expressed in "4.1", all the phenomena of loss of pressure and temperature are neglected, due to the adiabatic nature of the components thus zero pressure drops during their operations. Still considering the carbon dioxide supply line, a further hypothesis is made: there is no need for $CO_2$ storage between the CCS and the electrolyser because the gas flow is supplied at the exact moment of the electrochemical device request, resulting in a perfect functional coupling between the two plant sections.

Therefore, considering the flows of the streams, there are two supply lines, one for water and one for carbon dioxide. Downstream of the components that allow to obtain the required thermodynamic conditions, they are conveyed inside a mixer, "MIXER-1", which also receives the recirculation flow of the cathode products. As in the case of steam-electrolysis alone, this recirculation is essential to obtain the reagent entering the cathode of the SOEC with an initial molar composition equal to 10% of hydrogen, which, as already seen, is of primary importance to avoid the damage to the electrode. "FUELQ" and "SIDE-R" are the same components already analysed: they are Gibbs reactors that respectively allow to obtain an input and output stream in equilibrium conditions. The setup of the “CAT+AN” component embodies the second difference with respect to steam-electrolysis. Since it is the representation of the physical place in which the electrochemical reactions take place, therefore choosing a stoichiometric reactor, it is necessary to set the second electrolysis reaction that occurs inside it. Specifically, the global electrochemical reaction of electrolysis of carbon dioxide, expressed by the following eq. (141):

$$CO_2 \rightarrow CO + \frac{1}{2}O_2 \tag{141}$$

This equation, together with that of water electrolysis, eq. (119) in “4.2”, allows to obtain as a product a compound characterized by a high percentage of hydrogen and carbon monoxide: syngas. The oxygen necessary for the reactions is sent by the air supply line, which is also equipped with a compressor and heat exchanger in order to reach the right conditions. Downstream of the stoichiometric reactor, the “NTOT” stream is obtained at first, ideally containing the products of both electrodes. In reality, the products of the electrodes are separated, since the places where the partial electrochemical reactions take place are physically distant. Therefore in this case, the electrodes were not considered separate but together, resulting in their subsequent subdivision through the separator, "SEP". Inside it has been declared a quantity of 100% separation for the oxygen and nitrogen flow rates, so as to simulate the behaviour of the electrochemical device in an alternative way to reality. In fact, two flows branch off from it, the one represented by "FLUEAN-X" represents the waste products of the anode, consisting of nitrogen and a higher amount of oxygen than the initial one. Just as in steam-electrolysis there is the presence of a turbine, "TURB-1", which exploits the high mass flow out of the gas sweep generating electricity. The second flow, on the other hand, is the product of the cathode, or the desired syngas, “SYN-X”. The "SPLIT" component allows to recirculate a part of this compound, guaranteeing the molar percentage of hydrogen at the SOEC inlet, while "EX-1" is the heat exchanger which acts by decreasing the temperature of the final stream, "TO-METH1 ". The latter flow is very important because, as we will see in the CBs section, it will have to respect certain parameters in order to be introduced into the national distribution network, and by acting on the temperature, it is possible to change the density, a very important variable for these parameters.

In carrying out the simulations, Aspen follows this path just described. As known, the final result obtained is a discrete map of all the parameters of the streams and components examined. Considering different input powers to the electrochemical device, with the same number of modules turned on, as many discrete maps are obtained. Through linear interpolation it is possible to fill the absent operating conditions, obtaining in the end a continuous map representing the performances of the SOEC with the number of active modules fixed. By repeating this procedure for all operational configurations of the SOEC, 12 continuous maps are finally obtained. Once consulted through a specially created Matlab code, the maps allow to obtain the annual trend which describes the behaviour of the device operating in co-electrolysis. Therefore, taking into consideration the hourly data available, it is possible to make an average composition of the "TO-METH1" stream, obtaining:

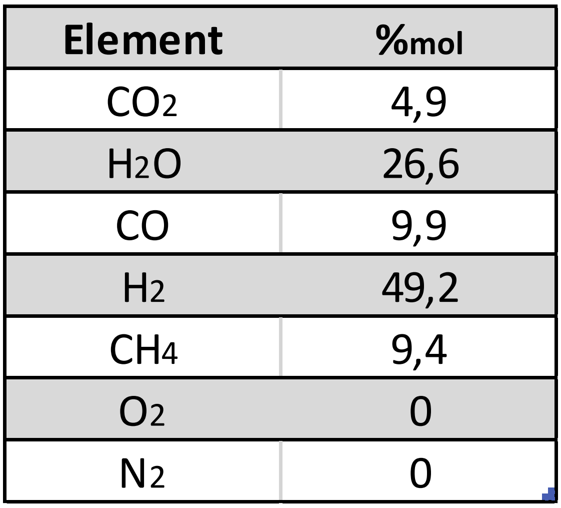

| Element | %mol |
|---|---|
| $CO_2$ | 4,9 |
| $H_2O$ | 26,6 |
| CO | 9,9 |
| $H_2$ | 49,2 |
| $CH_4$ | 9,4 |
| $O_2$ | 0 |
| $N_2$ | 0 |

*Table 15- - average molar composition of syngas produced*

Comparing the values obtained with the work of E. Giglio et al. [92], it can be said that the result is in line with the theory. The presence of water and carbon dioxide derives from the fact that the FU used for the calculations is not 100% but lower, equal to 78.6%. This implies that for 21.4% of the reactants, it is not affected by electrolysis phenomena, remaining inert and therefore present in the waste products.

Compared to steam-electrolysis, the quantity of hydrogen is significantly lower, due to the presence of carbon monoxide, produced by carbon dioxide. These elements, in addition to characterizing the syngas stream, are directly responsible for the quantity of methane present inside the cathode of the SOEC: in fact, the simultaneous presence of $H_2$ & $CO_2$ and $H_2$ & CO in the same environment, under the operating conditions of the SOEC, cause the methanation reactions, eq. (18) and (19). The percentage of methane at the outlet is directly proportional to the operating pressure, as the quantity increases by increasing it, reaching approximately 10 [%] for values of 30 [bar]. This statement is confirmed in many studies in contemporary literature, such as in the reference work by E. Giglio [90], and is nowadays taught in courses that deal with this topic, [30]. The following fig. 30 shows the molar concentrations trend for the cathode flow during co-electrolysis operations. Most of them have an almost constant trend as the operating pressure varies, while methane and hydrogen are more involved. The decrease in the molar percentage of hydrogen is precisely due to the methanation reactions, favored by increasing pressure, consume the light gas for the production of methane.

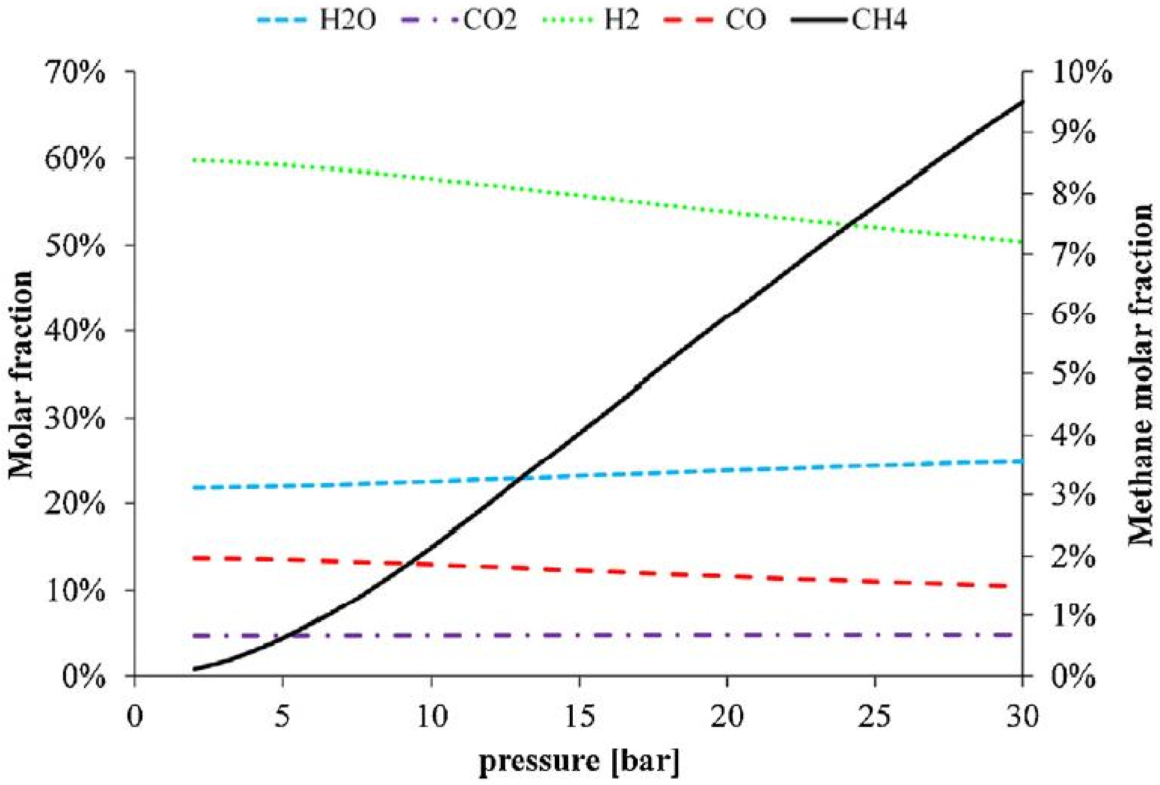

*Figure 29 - concentration of methane in function of pressure [90]*

As already analyzed in "2.2.1.1", the methanation reactions are characterized by an exothermic behaviour, producing heat and increasing the cathode temperature of the SOEC, leading two very important effects:

1. From a thermodynamic point of view, an increase in temperature leads to a decrease in the enthalpy of the reactions involved. The high temperature is in fact generated by the heat released by the reactions, meaning a lower internal energy content. In terms of the operating parameters of the electrochemical device, this lower energy content translates into a lower thermoneutral voltage or a lower thermoneutral current, decreasing the productivity of the electrochemical device because exothermic behaviour increases. The previously mentioned thermoneutral current is, as the name implies, the value assumed by the operating density current of the device when it is in thermoneutral condition. It is summarized in the following demonstration.

$$V_{cell} = V_{TN} \rightarrow \frac{\Delta h}{zF} = \frac{\Delta g}{zF} + ASR * i_{TN} \rightarrow i_{TN} = \frac{\Delta h - \Delta g}{ASR * zF} \tag{142}$$

   Thus, thermoneutral condition can be expressed in terms of current or voltage.

2. The second effect is related to the transport phenomena involved in the cell. An increase in temperature favours the kinetics of electrochemical reactions, increasing the speed with which they occur. In addition, it also improves the diffusivity of the

reactant streams in the electrodes, up to the activation point of the reaction (tpb), allowing overall to obtain a greater number of electrochemical reactions. Finally, also from the point of view of resistivity there are advantages, in fact the increase in temperature decreases the ability of the electrolyte layer to oppose the passage of ions, allowing the passage of more electrical charges in the connected external circuit. Overall, this results in better productivity.

The two effects are conflicting, the first causes a deficit in the performance of the SOEC, while the second causes benefits. Considering the contemporaneity of the two effects, the first prevails over the second, marking a net decrease in performance. Consequently, cathode heating must be avoided by exporting a greater amount of heat in order to maintain the temperature at operating conditions. In the specific case of the thesis work, it is the incoming air flow which, when increased, allows to manage the thermal flows deriving from the exothermicity of the methanation reactions present in the SOEC.

### 4.3.1 CB and DS of SOEC co-electrolysis' section

The setting of the algorithms followed by Aspen to simulate the behaviour of the SOEC operating in co-electrolysis is very similar to the case of steam-electrolysis, differing only in some values and parameters dictated by the presence of carbon dioxide and its derivative products/components.

The first DS analyzed sets the molar fraction of hydrogen in the stream entering the cathode of the SOEC equal to 10%$_{mol}$. As already described above, this quantity must always be guaranteed in order to avoid any possible re-oxidation reactions between the nickel present as a catalyst in the fuel electrode (cathode) and the water vapour, keeping a reducing atmosphere. In order to guarantee the correct molar quantity of hydrogen, the amount of recirculated stream, "SYN-REC" between the SOEC outlet and inlet, is then varied through the "SPLIT" component.

The second DS necessary for a correct simulation has the purpose of setting an important parameter called H/C, which is fundamental for the subsequent methanation step since the quantity of methane that can be produced depends on its value. This variable is the expression of the ratio between the molar quantity of hydrogen with respect to the carbonaceous substances present (CO and $CO_2$):

$$H/C = \frac{\%_{mol}H_2 - \%_{mol}CO_2}{\%_{mol}CO + \%_{mol}CO_2} \tag{143}$$

The molar fractions reported in eq. (143) refer to the syngas produced by the cell, specifically to the "SYN-2" stream. The achievement of the desired value, equal to 3, was obtained by controlling through the DS the amount of water entering the co-electrolysis section, by varying the "H2O-1" stream, in such a way as to ensure the optimal quantity of hydrogen produced by the electrolysis reactions of water. H/C value of 3 means that, CO-methanation reactor, characterized by this ratio between hydrogen and carbon monoxide reagent molecule, is favored compared to the other.

The third and last DS is the one that allows to calculate the amount of electrical energy necessary for the co-electrolysis reactions, setting the excess power produced and sent by the photovoltaic field as a technical specification. To obtain the desired value, the incoming quantity of carbon dioxide is varied on Aspen. The equations needed to calculate the required electrical power are roughly those set in the steam-electrolysis section, with the exception of some parameters. In the initial setting phase, the first data entered are the known ones, deriving from constants and values obtained during the modeling phase:

- Faraday's constant, F = 96'485;
- Fuel utilization, FU = 0.786, representative of the amount of reactants involved in electrochemical reactions;
- Inverter efficiency, $\eta_{inv}$ = 0.96;
- Net area of the cell, $A_{cell}$ = 300 $cm^2$, the one considered for the calculation of the electrochemical parameter as the current density;
- Number of the cell, $n_{cell}$;
- Operation current of the entire SOEC, $I_{stack}$;
- ASR = 0.304 Ω $cm^2$;
- OCV = 0.916 V;
- $V_{tn}$ = 1.211 V.

Regarding the number of the cell, it is different for each simulation because it represents the number of activated modules, during operation. As for the $n_{cell}$, the intensity of the current must be modified each different simulation, obtaining its value by the power curve, fig. 23 of paragraph "3.2.4", finding the right value on the Matlab's code created for that curve. As for the electrochemical parameters, which are identical to the steam-electrolysis section and equal to those calculated during the modeling phase. All with the exception of the thermoneutral voltage, whose value differs from the case of steam-electrolysis due to the electrochemical reactions of carbon dioxide as explained in "3.2.3". The rest of the equations used are identical to those previously reported in "4.2.1" by eq. (121) to (133), except eq. (122) and (124), respectively for the calculation of the electric power in direct current and the thermal power of the output stream. They are replaced by the following equations:

$$W_{DC} = F\left(CO_{2,in} + H_2O_{in}\right)V_{op}2FU \tag{144}$$

$$P_{out} = G_{syngas}LHV_{syngas} \tag{145}$$

Eq. (144), unlike (121), reports the molar flow rate of carbon dioxide as an additional term because this substance is also involved in the electrolysis processes. Eq. (145), on the other hand, has the same configuration as (124), what changes is the substance considered, which is no longer a stream of pure hydrogen but syngas. The calorific value varies, and downstream of the simulations it was possible to attribute an average value of 18.19 $MJ/kg_{syngas}$, obtained by using the QVALNET variable set in the Aspen properties section. As previously mentioned, the rest of the equations do not change between steam and co-electrolysis, as the electrochemical device always operates in electrolyser mode, so the physical phenomena involved are always the same, while the only variants depend on the type of fuel used.

As for the CBs instruments, the same ones of the steam electrolysis section have been implemented. Their function always provides for the verification of the values used in the settings of the electrochemical parameters of the SOEC using alternative formulations to those adopted in the modeling phase. Therefore, also in this case, the checks were conducted for the value of the open circuit voltage (OCV), using the eq. (134), and for the thermoneutral voltage, with eqs. (135), (136) and (137). Downstream of the simulation, the consistency of the results between the data implemented at the beginning and the data obtained subsequently has always been verified, reporting almost identical values.

### 4.3.2 Performance parameters, results of SOEC co-electrolysis' section

The last paragraph necessary to provide a detailed description of the simulation of the co-electrolysis process ends with the analysis of the hourly results obtained. As for the alternative section of steam-electrolysis, the final hourly data, covering a period of one calendar year, were obtained by applying the algorithm created on the Matlab program, capable of managing and filtering the necessary data among all available data to describe the work. The positive difference between the electricity supplied by the photovoltaic and that required by the urban load (surplus) has determined the SOEC mode for the rSOC device. The first two days of the week in which this condition occurred were dedicated to the production of hydrogen, while the remaining days for the production of syngas. The choice of data necessary to describe the co-electrolysis process, for the current time that is being calculated, has been made by choosing the best configuration (number of modules turned on), using the efficiency of the device as a comparison parameter. Compliance with the power limits was set in the program, discarding all operations in which the surplus power supplied was less than 20% or greater than 80% of the rated power. This check was carried out for each configuration, and at the end the results that allowed to obtain the greatest efficiency were chosen.

The first fundamental data from which it is possible to draw some opinions is the operating time in co-electrolysis. Unlike its alternative mode, in which there were 48 hours per year of input power that did not fall within the limit range constraint, for the case of co-electrolysis the problem does not occur, since it was able to operate all 1263 hours of surplus that he could exploit. Overall, the gross hours in which the rSOC is used as SOEC are 1748, of which 1700 net, obtaining a global utilization factor of 19.4%. As presented later, the portion of missing hours will be filled by SOFC operations. The value obtained is in line with the modeling phase because the primary purpose of the thesis system is to satisfy the electricity needs of the urban network considered, exploiting the electricity produced by the photovoltaic field coupled to a fuel cell, in order to drastically reducing the consumption of greenhouse gases, typically produced in conventional energy production systems. The size of the photovoltaic field is the direct consequence of rSOC's operational hours. The compromise that was adopted in the design phase was to produce at least 1/3 of the electricity through a photovoltaic field, and the remaining part with the complementary device. This is due to the large spaces occupied by the panel technology, which would have subtracted useful land surface suitable for other purposes.

The further data obtained from the analysis of co-electrolysis simulations are shown in table 16 below. The optimal description of the plant section requires knowledge of the electrical parameters that characterize it, of the total annual flow related to main streams (those entering and leaving the system) and, in the case of the electrolyser, specific consumption, a parameter of primary importance to classify the device in terms of performance.

| Process Parameter | Result | Unit | |
|---|---|---|---|
| $I_{SOEC}$ | 1,3183 | **MA** | **ARITHMETIC MEAN** |
| $J_{cell}$ | 1,2559 | **A/cm2** | |
| $V_{op}$ | 1,2979 | **V** | |
| $key_{SOEC}$ | 5,61 | **kWh/kg$_{syngas}$** | |
| $G_{H2O-1}$ | 548,04 | **tons$_{H2O}$/y** | **SUM** |
| $V_{CO2-1}$ | 4807,32 | **m3$_{CO2}$/y** | |
| $G_{SWEEP-1}$ | 33,19 | **tons$_{SWEEP-1}$/y** | |
| $G_{syn-rec}$ | 73,24 | **tons$_{synrec}$/y** | |
| $V_{tometh}$ | 17956,80 | **m3$_{tometh}$/y** | |

*Table 16 - main flow rates & electric parameters for co-electrolysis*

Among the electrical parameters, the most interesting is certainly the average operating voltage value of the cell. As can be seen from the result obtained, in this case the value is higher than that of the thermoneutral voltage (about 1.211 V), attributing an exothermic behaviour to the SOEC operating in co-electrolysis. Considering the syngas production system, high amount of water, carbon dioxide and air to be heated from room temperature or approximately (35 °C for inlet stream of carbon dioxide) to the SOEC's operating temperature, consumes a huge amount of heat. To optimize the combined net efficiency, it was therefore considered the exploitation of the excess heat produced by the electrochemical device to heat these streams at the entrance to the system. Logically, the actual optimization should have been the result of the pinch point analysis, in order to establish that the temperatures of the sources and thermal wells were consistent in terms of exergy. Therefore, as already mentioned in the introduction of Aspen simulations, this hypothesis was made in such a way as to consider all the heat flows of the system components usable. In the end, the average cell operating voltage result is justified. The coherence of the voltage implies the coherence of the average current of the device, because the two variables are linearly dependent and linked by the values of the polarization curve: for a given voltage there is a specific current and vice versa. Consequently, once the voltage value is accepted, the current value is also justified and the current density value is justified in cascade, linked to the latter by two constants: the number of cells and the net cell area.

The flow rates in table 16 are evaluated as annual sum. Only for the incoming carbon dioxide "$V_{CO2-1}$", and for the syngas produced "$V_{tometh}$", are reported as volume flow rate, because it is conventional for these elements to be compared in terms of volume. While the remaining are in terms of mass. The first, the acid gas stream introduced into the SOEC cathode, is considered under the CCS outlet conditions, 35 °C and 33.1 bar. As also described in the CCS results, there will be congruence between the quantities of $CO_2$ exiting the filtering section of the acid gas and that of the electrolyser. Converted in terms of mass, in standard condition, the management of the carbon dioxide flow in the SOEC avoids the release of about 273.28 $tons_{CO2}$ every year. In order to make a more concrete comparison, the globally valid WLTP (Worldwide harmonized Light vehicles Test Procedure) standard is considered, which came into force in 2017 and applied to new vehicles produced. According to the standard, each car manufacturer must indicate the value in grams of carbon dioxide produced for each kilometer traveled. By consulting the newspaper "Il sole 24 ore", specifically the article dated 10 December 2020, an average value of 109.19 [$g_{CO2}$/km] can be used, considering the various car manufacturers. According to the ICDP (International Car Distribution Program) in Italy, an average motorist travels 12000 km in a year. Taking these data into consideration, the carbon dioxide savings produced by SOEC alone can be represented as having avoided the circulation, for one year, of 208 cars.

The stream of syngas produced "$V_{tometh}$", shown in tab. 16, is at the operating conditions of storage and methanation section, 20 °C and 32.4 bar. The temperature value is decreased from the operating conditions of the SOEC to the designated ones by circulating the outgoing syngas inside the "EX-1" heat exchanger present in the final section of the co-electrolysis plant. The removed heat will contribute positively to the calculation of the combined net efficiency. The syngas produced is stored inside a specially sized storage to allow continuous and stationary operation of the methanation section. It is useful to mention that these two sections are characterized by an overall efficiency that reports the conversion efficiency from carbon dioxide to SNG. From the point of view of pressure, the peculiarity of making the electrochemical device operate at the same operating pressure of the methanation section (in reality with a slight difference equal to 0.7 bar), allows to obtain mainly two advantages: the first involves the reduction of operating costs deriving from the compression of the syngas, which, being made up of a good percentage of hydrogen (in the specific case of the thesis work 49.9% reported in table 15), would involve a large expenditure of electricity for the compressor. The second, on the other hand, is the increase in the overall efficiency of the system caused by the high initial percentage of methane present in the syngas stream leaving the electrolyser section (in the specific case of the thesis work: 9.4%, reported in tab. 15).

The remaining streams shown in tab. 16 are the same already considered in the steam-electrolysis section. The longer time of co-electrolysis mode, results in the fact that the flow rates treated are higher as expected, with the exception of air one, whose value is slightly lower. The presence of the carbon dioxide line requires heat to bring the fluid to operating conditions. This necessary thermal power is provided by the SOEC, characterized by a high exothermic behaviour. The net result is a decrease in excess air, which, in the absence of the acid gas line, would have fulfilled the heat removal avoiding overheating of the electrochemical device.

Finally, the last parameter of tab. 16 analyzed is that of the specific consumption, a variable which allows to classify the device in terms of efficiency. Its value is obtained from the ratio between the total annual energy absorbed by the SOEC and the total mass quantity of syngas produced in the year. The final value obtained is 5.61 kWh needed to produce 1 kg of syngas.

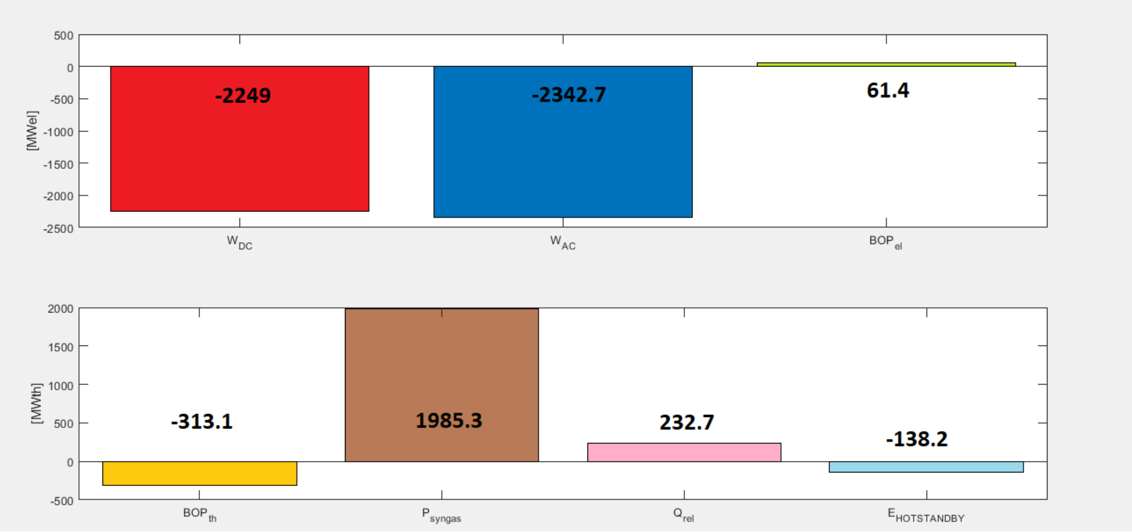

*Figure 30 - Energetic flux characteristic of the co-electrolysis section*

Fig. 30 shows the summations for each energy flow exchanged in the co-electrolysis section. The electric power in direct current, $W_{AC}$, is the surplus electricity produced by the photovoltaic field used for the electrochemical reactions to take place. Overall, this power amounts to -2342.7 $MW_{el}$. The negative sign indicates, according to the adopted convention, that it is an input power to the system. The continuous power value, $W_{DC}$, whose annual sum is equal to -2249 $MW_{el}$, differs by a small amount of electricity, dissipated because of the efficiency losses due to conversion by inverter, from alternating to direct power. The last variable relating to the electrical powers is the one that expresses the electrical value of the BOP. The final value of 61.4 $MW_{el}$ expresses that the positive contribution of electricity produced in the “TURB-1” turbine in fig. 28 is greater than the negative one of the “PUMP-1” and “COMPR-1” components respectively to increase the pressure level of the water and air stream entering the electrochemical device.

The lower part of fig. 30 shows the values of the thermal flows involved in the system under analysis. First of all, "$P_{syngas}$" corresponds to the intrinsic thermal power of the syngas leaving the system. Its high value of 1985.3 $MW_{th}$ is a sign of the high electrical efficiency of the system because, due to the low transformation losses characterizing the electrochemical device, it is possible to store a greater amount of energy inside the chemical product. As regards the $BOP_{th}$, i.e. the auxiliary devices that allow the correct operation of the SOEC, the quantity of net thermal power is equal to -313.1 $MW_{th}$. According to the sign convention adopted, the negative value indicates a global endothermic behaviour, i.e. that most of the auxiliary components, in order to function, need thermal energy. This information is consistent with the plant because the supply lines (water, carbon dioxide and air) require a large amount of heat to be able to reach the operating conditions, while only the heat recovery units present on the product output lines do not equal the thermal contribution. Among them, the predominant component is the water line, as the high sensitive and above all latent heat greatly increase the heat required by the auxiliary device.

The final positive value is "$Q_{rel}$" with a value of 232.7 $MW_{th}$. This parameter indicates the global thermal behaviour of the SOEC operating in co-electrolysis. The positive value suggests that its behaviour is mainly exothermic, information already known since the operating voltage exceeded the thermoneutral one. According to how the heat flows were managed in the thesis work, the amount of heat produced by the SOEC compensates in its entirety that required by the auxiliary thermal components. The end result is a decrease in the consumption of thermal power required by external sources, even if the combined net efficiency value is affected, decreasing its value. The last heat flow to be considered is that necessary to keep ready the modules switched off in case of future accension, with a value of -138.2 $MW_{th}$, which also contributes negatively to the combined net efficiency.

As mentioned in the final paragraph of "4.2.2", to conclude the electrolyser performance parameters section, the final results relating to efficiencies are reported. The trend of electrical efficiency, eq. (126), is shown in the following fig. 31, while that of net electrical efficiency, eq. (127), that takes into account the $BOP_{el}$, in the next fig. 32. The annual trend of values varies from 81.37 % to 113.76 % for gross electricity, while from 83.47 % to 113.27 [%] for net. The high efficiency values derive from the fact that the electrolyser has been designed to operate as close as possible to thermoneutral conditions. Moreover, in these conditions the electrical efficiency value assumes a value equal to 100 %. Indeed, for voltages below this threshold it is possible to reach electrical efficiencies higher than 100 %. Vice versa, for gradually higher values, the efficiency decreases.

Finally, the combined efficiency trend, eq. (130) and (131), which also takes into account the heat exchanged between SOEC and the environment, is shown in the following fig. 34, while that of the combined net efficiency, eq (132) and (133), which also reports the consumption of the entire BOP of the system, is shown in fig. 33. In this case, the annual trend of the values varies from 97.28 % to 97.74 % for the first, and from 83.91 % to 89.65 % for the second. The values decrease compared to the electrical efficiency because in the thermal powers come into play non-negligible parameters, which affect by lowering the combined net efficiency. It is the most represented parameter for the electrochemical device due to it takes into account every component of the section under examination.

In the following tab. 17 the annual average values obtained downstream of the analysis of the results are displayed.

| **SOEC EFFICIENCIES [%]** | |
|---|---|
| ηel | 94,16 |
| ηel,net | 96,01 |
| ηchp | 98,23 |
| ηchp,net | 87,18 |

*Table 17 - SOEC average efficiencies*

The figures which report the trends in efficiencies show that, during the summer period, the operations in electrolyser mode occur more frequently than in winter. This is justified by the fact that the energy arriving at the SOEC is produced by the photovoltaic field, which during the summer produces a greater amount of energy surplus, thanks to the long days and low rainfall frequencies. The electrical efficiency, a characteristic of the electrochemical device alone, shows a more fluctuating trend, demonstrating a greater dependence on the fluctuations produced by renewables. On the other hand, the combined efficiency has a much more static trend during the course of the year due to the energy flows produced by the BOP of the system, which, being mostly endothermic, allow to stabilize the production of heat deriving from the exothermic behaviour of the SOEC.

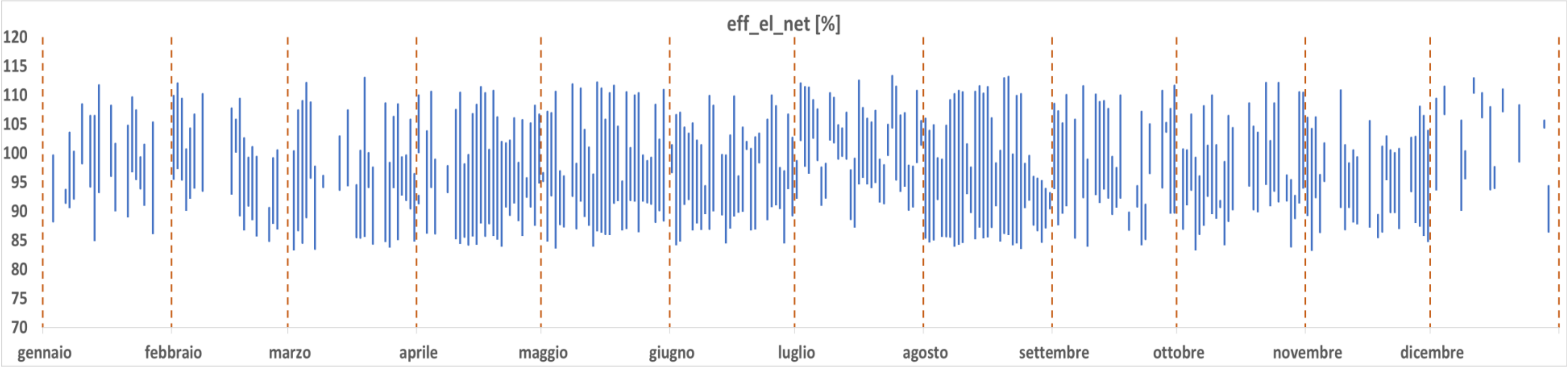

*Figure 32- SOEC Net Electrical Efficiency*

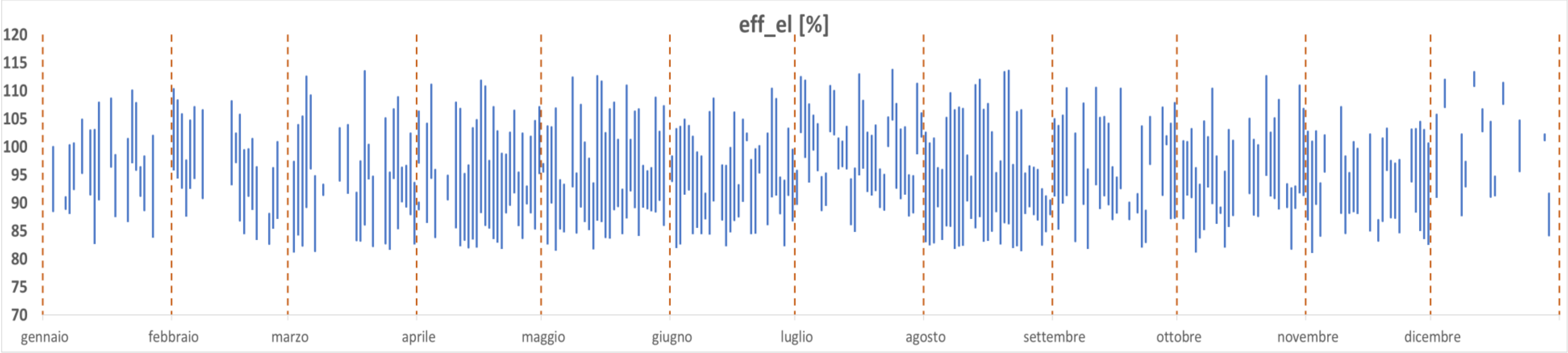

*Figure 31 - SOEC Electrical Efficiency*

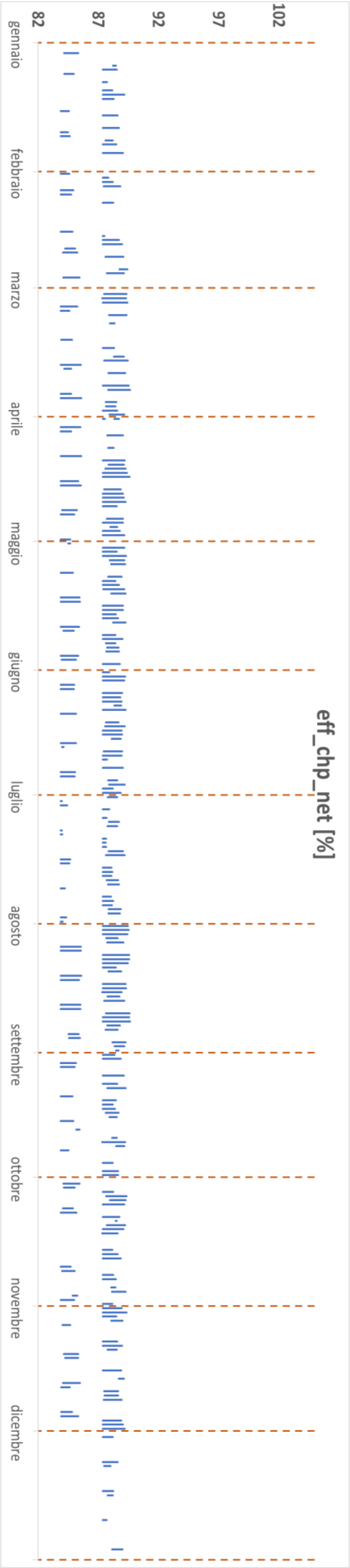

*Figure 33 - SOEC Net CHP Efficiency*

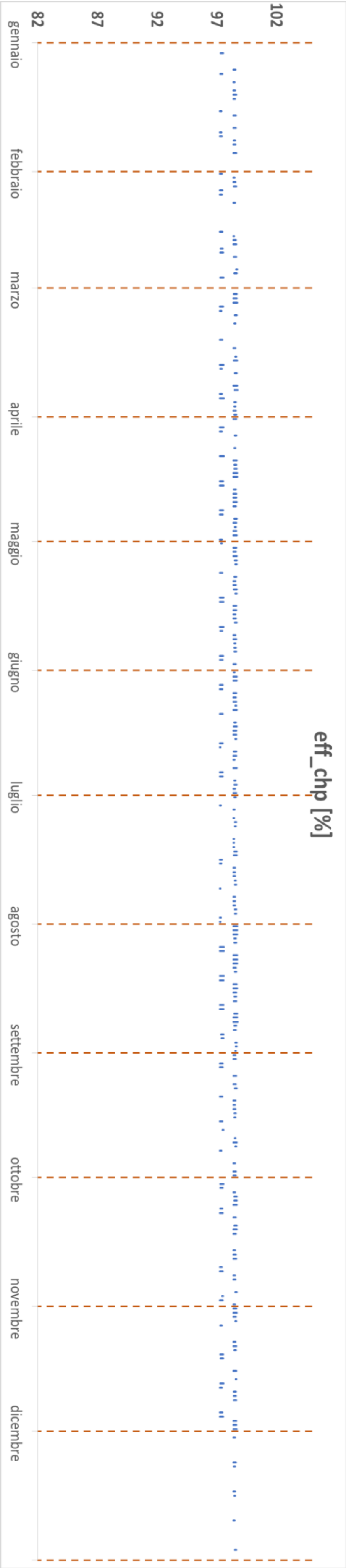

*Figure 34 - SOEC CHP Efficiency*

## 4.4 Aspen model: SOFC

The third Aspen model described is the last one necessary for the complete description of the operations carried out by the rSOC. The SOFC mode is activated every hour in which energy deficit problems occur, in order to compensate for the missing amount of electricity that the PV field would not be able to supply, exploiting the natural gas taken from the national distribution network. Moreover, the particular operation of the device allows to avoid the release into the atmosphere of polluting gases, a highly sensitive problem nowadays in all conventional cogeneration plants, fulfilling the environmental goals set for 2030 regarding the reduction of polluting atmospheric emissions.

The implementation of the model, on Aspen, begins as always with the setup of the properties necessary to describe the physical and electrochemical phenomena involved in the plant processes. Like all simulations carried out in this thesis work, the units of measurement considered are those belonging to the SI, such as [°C], [bar], [s], [J], [W], [kg] and [$m^3$]. As regards the chemical molecules involved in the electrochemical processes, $H_2O$, $O_2$, $H_2$, $N_2$, $CH_4$, $CO_2$ and CO are specified. In fact, the streams at the entrance of the plant are methane, the water and, thanks to the presence of an external pre-reformer, hydrogen, while the air drawn from the surrounding environment for the cathode feed line. Downstream of the reactions involved in the SOFC there are the air depleted of oxygen and the stream of the anode products, at the outlet, consisting mainly of water and small percentages of hydrogen, carbon dioxide, carbon monoxide and methane. In the last paragraph in which the results are analyzed, the precise percentages referring to the annual average values obtained will be reported.

As in the case of the electrolyser, the method chosen and implemented is that of PENG-ROB, which allows the program to use equations of state able to determine the properties of chemical compounds containing hydrocarbons or light gases, such as carbon dioxide and hydrogen. The method will be applied by the program, with the exception of the pre-reforming reactor where the minimum Gfe model will be followed, directly applied by the component. Finally, the last subsection to be programmed is that relating to property sets, i.e. those properties that can be obtained directly from the program database. The list below describes what these properties Aspen has by default, improve the information each program updating, base on scientific discoveries:

- CPMX, determines the specific heat at constant pressure of a mixture of gases or liquids;
- HMW, determines the specific enthalpy of a gaseous or liquid mixture;
- SMX, determines the specific entropy of a gaseous or liquid mixture;
- KMX, determines the thermal conductivity of a gaseous or liquid mixture;
- MUMX, determines the viscosity of a gaseous or liquid mixture.

After the description of the basic properties necessary for the correct simulation, the system is reported on the flowsheet of the Simulation section, considering the streams and the components involved. The following fig. 35 shows the final result obtained:

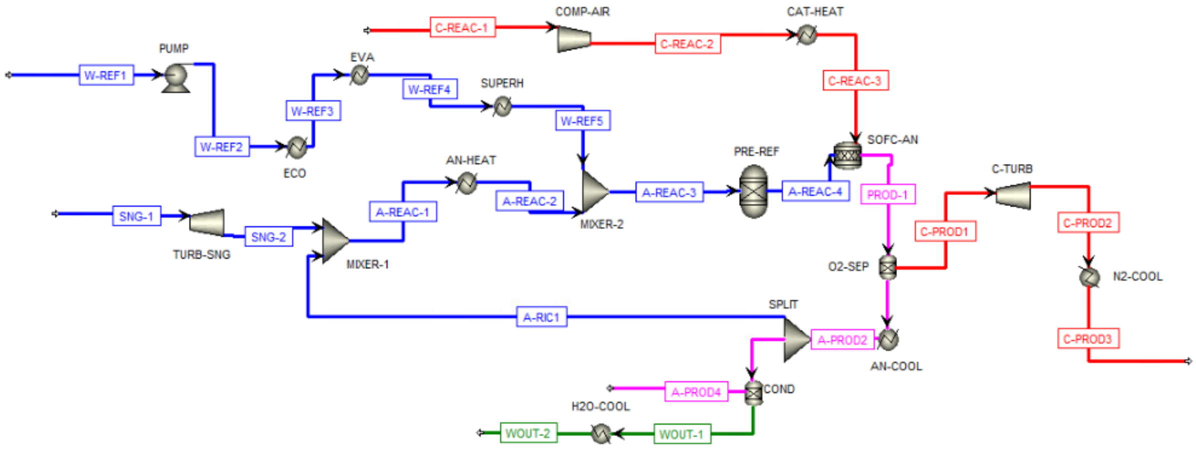

*Figure 35 - SOFC plant on Aspen Plus*

"SNG-1" is the natural gas stream entering the system at the initial conditions of 25 °C and 60 bar, with a chosen composition of 97.45 $\%_{molCH_4}$, 0.15 $\%_{molH_2O}$, 1 $\%_{molCO_2}$ and 1.4 $\%_{molN_2}$. This composition differs from the average composition of the natural network because, in this case, it was chosen to operate with an incoming carbon stream that has the same composition as that produced in the CCS and methanation section. The "TURB-SNG" component, characterized by an efficiency of 75 %, allows to change the pressure level of the inlet flow, 60 bar, bringing it to the operating level of the SOFC, equal to 33.1 bar, while producing electricity. At the turbine outlet, the natural gas is mixed in "MIXER-1" with the recirculated anode products, and conveyed to another mixer, "MIXER-2", where water vapor is added. The presence of recirculation allows the system to increase efficiencies because there is a high percentage of water in the products leaving the anode. Therefore, the recovery of this water makes it possible to reduce the supply flow rate, decreasing the heaters' thermal load. Furthermore, there is also the benefit of recirculating, albeit in a reduced percentage, a small amount of elements necessary for the production of electricity in the SOFC ($H_2$ and $CH_4$).

In order to avoid irreparable damage to the SOFC due to possible carbon deposition (a concept explained in paragraph "2.2.2.2"), the high carbon content present in the stream entering the anode is converted into hydrogen by using the reforming reaction, eq. (3) and (5) in "2.1.2.1". This process occurs initially outside the electrochemical device, at the "PRE-REF" component, and later also inside the device itself, due to the operating conditions and the chemical elements present. In order to ensure correct conversion, compliance with an important parameter is required, the Steam to Carbon (S/C) ratio set to 2 for the “A-REAC-3” stream. In Aspen, the component chosen to represent the pre-reforming reactor is the Gibbs reactor, on which the model of the minimum Gfe is applied, in order to ensure the equilibrium conditions of the reforming reactions. Such reactions are characterized by an endothermic behaviour and, coupled with the SOFC, they form a thermal system in which the heat necessary for sustaining the reforming reactions is supplied by a part of the heat produced by the electrochemical reactions of the SOFC, characterized by an exothermic behaviour. Therefore, to obtain the optimal thermal coupling, the flows entering the pre-reformer are pre-heated until they reach the temperature of 800 °C and the operating pressure of the device of 33.1 bar. They will consist of the inlet water, "W-REF1", at the initial conditions of 20 °C and 1 bar which initially passes through the "PUMP" pump, characterized by the usual electrical efficiency of 80 %, in such a way as to guarantee the pressure level. Successively they pass into the heated components "ECO", "EVA" and "SUPERH" which provide the heat necessary for the change of state and the achievement of the desired 800 °C. The second, the flow of matter consisting of the high carbon content, "A-REAC-1", characterized by an average temperature of 91 °C, passes inside the "AN-HEAT" heat exchanger, requiring a large amount of energy to reach the necessary temperature value. The mixing of the two fluids allows to obtain "A-REAC3", at the inlet of the "PRE-REF", in which as many reforming reactions will take place as necessary to obtain the temperature of 700 °C set for the output, relative to the stream "A-REAC4". This stream in mention will constitute the fuel of the anode and together with the air, which is also treated in its supply line, will be sent to the SOEC inlet. Specifically, the air is composed of 79.05 $\%_{molN2}$ and 20.05 $\%_{molO2}$ and initially at atmospheric conditions of 20 °C and 1 bar, it is compressed in the compressor " COMP-AIR” characterized by an efficiency of 70 %, and then heated up to 750 °C. It is not necessary that the injection temperatures of the fuels at the electrodes correspond exactly to the operating value set in “SOFC-AN”, equal to 850 °C. This is due to the thermal integration with the pre-reformer envisaged and implemented by the program, which will allow a number of electrochemical reactions necessary to meet the required thermal and electrical power to take place.

As in the case of the electrolyser, in the component representing the SOFC, expressed in Aspen as a stoichiometric reactor, it's not the partial electrochemical reactions which are specified (previously described by eq. (9) in eq. (13) in "2.2.1.1"), but the global ones reported below:

$$H_2 + \frac{1}{2}O_2 \rightarrow H_2O_{(g)} \tag{146}$$

$$CO + \frac{1}{2}O_2 \rightarrow CO_2 \tag{147}$$

As shown by eq.s (146) and (147), the partial electrochemical reaction of methane, eq.s (148) and (149) reported below, which constitutes the main compound of the anode fuel, does not appear among those implemented in the “SOFC-AN” component, but only those of hydrogen and carbon monoxide.

$$A: CH_4 + 4\,O_2^{2-} \rightarrow 2H_2O_{(g)} + CO_2 + 8e^- \tag{148}$$

$$C: 2O_2 + 8e^- \rightarrow 4\,O_2^{2-} \tag{149}$$

This behaviour derives from the fact that, as previously mentioned, the presence of methane, water vapor and carbon dioxide in the SOFC anode, under operating conditions, gives rise to internal reforming reactions ($CH_4 + H_2O \rightarrow 3H_2 + CO$; SMR) ($CH_4 + CO_2 \rightarrow 2H_2 + 2CO$; DMR). Furthermore, the presence of water and carbon monoxide produces a third reaction, that of WGS ($CO + H_2O \rightarrow H_2 + CO_2$). Under the operating conditions of the cell, these last three reactions are characterized by a kinetics clearly superior to that of the electrochemical reaction of methane. Consequently, it can be stated with high accuracy that, considering the electrochemical reactions of hydrogen and carbon monoxide, they can replace that of methane. From the electrical point of view, the performances are not altered because, observing the reactions, one mole of methane generates 8 electrons, as well as three moles of hydrogen and one of carbon monoxide (SMR) or two moles of both hydrogen and carbon monoxide (DMR).

Initially, SOFC's products are mixed. This ideal configuration is corrected by introducing the "SEP-O2" component, dividing the streams of the anode products from those of the cathode. To obtain this result, 100 % of the oxygen and nitrogen flow rate of the "PROD-1" stream is separated and sent into the "C-PROD1" stream, constituting the section leaving the cathode, while the remaining part will be that of the anode with the stream “A-PROD1”.

In the cathode product line there is a "C-TURB" turbine from which it is possible to carry out an electrical recovery by exploiting the high flow rate of depleted air leaving the system, decreasing the pressure value from 33.1 bar of the stream "C-PROD1" to the environmental one. Finally, "N2-COOL" is the exchanger that allows to recover the high quality thermal power from the products leaving the cathode "C-PROD2" initially characterized by a temperature of 850 °C. "C-PROD3" will be the cathode products brought back to atmospheric conditions of 1 bar and 20 °C, in such a way as to be able to introduce them into the atmosphere without any environmental danger or, considering the chemical composition depleted of oxygen, to exploit them in a nitrogen extraction system.

Regarding the anode products, most of them are recirculated within the system by the "SPLIT" splitter, resulting in a significant recovery in terms of energy and mass. However, before being separated, heat recovery takes place thanks to the "AN-COOL" component, which takes advantage of the high temperature difference between 850 and 220 °C. This last temperature was set to this value in such a way as to obtain, downstream of the first mixer, a stream with a temperature of 91 °C. With regard to non-recirculated products, they are sent inside a condenser in order to remove the vapor present by liquefying it. "W-OUT1" is the liquid stream at 33.1 bar that is obtained, which is further cooled from 220 to 20 °C and recirculated in the water supply line. Even the final “A-PROD4” waste is not wasted, in fact it is recovered in the CCS section due to its methane and carbon dioxide content. Considering its quantity significantly lower than that of the incoming biogas, the hypothesis is made that the biogas’ chemical composition is not changed by the presence of the recirculated flow, remaining constant and equal to the values set by the project.

The table below expresses the average compositions of the streams of greatest interest for the SOFC plant section, in order to provide a better understanding of the process described above.

| | MOLAR FRACTION [%] | | | | | | |
|---|---|---|---|---|---|---|---|
| | **H2O** | **O2** | **H2** | **N2** | **CH4** | **CO2** | **CO** |
| **A-REAC3** | 56,76 | 0,00 | 1,96 | 0,09 | 28,37 | 12,48 | 0,36 |
| **A-REAC4** | 39,67 | 1,10E-20 | 24,78 | 0,07 | 17,47 | 12,98 | 5,03 |
| **PROD1** | 28,91 | 6,26 | 1,16 | 47,12 | 8,15 | 8,17 | 0,23 |
| **A-PROD4** | 0,00 | 0,00 | 6,53 | 0,00 | 46,02 | 46,13 | 1,33 |
| **A-RIC1** | 62,02 | 0,00 | 2,48 | 0,00 | 17,48 | 17,52 | 0,50 |

*Table 18 - chemical composition for important streams*

### 4.4.1 CB and DS of SOFC' section

Once the analysis of the system implemented on the simulation flowsheet is concluded, the description of the tools designed to allow the program to obtain results that reflect reality is reported. Among them, four DSs and a CB can be found.

SOFC is able to produce direct current by exploiting the electrochemical reactions within its electrodes. The electricity produced in this way can be sent to the grid by converting it into alternating phase with the use of an inverter. The first DS, in fact, has the purpose of obtaining a specific electrical power in alternating current produced. The convergence of this result takes place, allowing the program to vary the quantity of natural gas withdrawn from the distribution network. In the fortran subsection of the DS under consideration, the equations necessary for convergence are defined. The first data that are entered, as always, are the known initial conditions. Among them:

- The inverter efficiency, $\eta_{inv}$ equal to 96 %;
- The fuel utilization factor, FU, set for the SOFC section at 80 %. This variable is very important because it declares the quantity of reactions that actually take place with respect to the stoichiometric condition, eq. (120) in "4.2.1";
- Faraday's constant of value 96'485;
- Number of cells, $n_{cell}$;
- Active area of a cell, $A_{cell}$;
- Area Specific Resistance, ASR equal to 0.304 $\Omega cm^2$, representing all SOFC loss phenomena thanks to the linearization hypothesis;
- Open Circuit Voltage, OCV equal to 0.916 V, fundamental parameter to characterize the behaviour of the electrochemical device. It is the ideal current value that the cell would assume if it were disconnected from any load (open circuit);
- Current produced by the SOFC, $I_{SOFC}$.

Considering the modeling adopted, the SOFC is composed of 12 modules, each of which consists of 2420 cells and capable of producing 500 $kW_{el}$. The logistics on which the operations of the device are based foresees to use a range of operability from 0 to 100 %. Therefore, to identify the optimal number of cells, uniquely corresponding to the number of modules that must remain on, once the electrical power to be produced has been chosen, a series of simulations are carried out in the operating ranges, for each possible configuration: 1 module on and 11 off, 2 modules on and 10 off, until 12 modules on and 1 off. For each simulation, the configuration dependent on the number of modules accessed is set by entering the correct value of the number of cells and the value of the current intensity. This last variable can be easily identified by consulting the Matlab program with which the polarization curve of the electrochemical device was determined, because, through the linearization approximation it will be possible to determine, for a specific power value, the associated values of current and voltage: to a current value corresponds one and only one voltage, for each modular configuration. By doing so, the current value necessary to describe a specific value of alternating power to be acquired for a given number of modules is obtained. By adopting this scheme it was possible to allow the program to determine the optimal value of input natural gas flow rate. The complementary formulas for obtaining convergence are then reported:

$$V_{op} = OCV - ASR\frac{I_{SOFC}}{n_{cell}A_{cell}} \tag{150}$$

$$I_{H_2} = 2F\dot{n}_{H_2O} \tag{151}$$

$$I_{CO} = 2F\dot{n}_{CO_2} \tag{152}$$

$$W_{AC} = FU\left(I_{H_2} + I_{CO}\right)V_{op}\eta_{inv} \tag{153}$$

Eq. (150) reports the equation for calculating the operating voltage for the linearization hypothesis. This parameter has been extensively investigated in paragraph “3.2.2”. Eq.s (151) and (152) represent the inverse formula of the Nernst formula, an equation that allows to attribute, for a known molar flow rate, the associated current intensity value. The scalar constant 2 reported is the explicit value of the number of electrons exchanged during the electrochemical reaction, and it is the same for both the partial electrochemical oxidation reaction of hydrogen and carbon monoxide, as can be verified in greater detail from eqs. (10) and (11) respectively of paragraph "2.2.1.1". Finally, Eq. (153) gives the final formula for the calculation of the alternating power. The program compares the result with the value set in the specification and, if included in the tolerance between +/- 1 %, confirms the convergence.

The second DS implemented is very similar to the first, because it is based on the same specification. In this case, by always setting a certain value of alternating electrical power produced, the flow of air entering the system is varied. This is possible because the electricity produced depends on the amount of fuel sent to the electrodes, and the exploitation of this feature allows the program to identify the optimal configuration. The initial data to be reported are the same as the first DS, with the exception of the FU. In fact, in the case of the gas sweep entering the cathode, the actual flow rate condition is not expressed as a function of FU but of Air Utilization (AU). The concept is the same, what changes is the stream of matter considered. In the case of the thesis work, it was chosen to operate with an AU equal to 0.5, i.e. with an excess of real air double compared to the minimum stoichiometric condition. This high excess of air allows to manage the heat flows involved in the SOFC, keeping the temperature constant at 850 °C. Below, the second and last formula is reported, which presents some differences compared to the previous case:

$$W_{AC} = \dot{\mathrm{n}}_{O_2} V_{op} 4F\ AU\ \eta_{inv} \tag{154}$$

Eq. (154) is a different formulation for calculating alternating power. The variable $\dot{\mathrm{n}}_{O2}$ represents the molar flow, referring only to the oxygen component, of the stream "C-REAC-3". In fact the scalar constant 4 takes into account the number of electrons exchanged by the partial electrochemical reduction reactions that take place in the cathode and involve oxygen. These two parameters multiplied by Faraday's constant express the associated current intensity value and, if they're multiplied by the voltage value, the continuous power produced is obtained. Finally, by finding the product with the efficiency value of the inverter, the conversion into alternating phase is obtained and thanks to the multiplication by AU, the final value is brought back to the real situation.

Both the last two DSs foreseen in the simulation sheet have the purpose of obtaining for the stream "A-REAC-3" an S/C ratio equal to 2, in such a way as to allow a high conversion of the methane inside the pre -reformer, avoiding future carbon deposition problems. Its value is calculated from the ratio between the water molar flow rate and that of methane in the “A-REAC-3” stream. At a thermodynamic level, the percentage of carbon produced drastically increases with increasing temperature, consequently it is very important to control its value due to the high operating temperatures of the SOFC. The hypothetical case of deposit would mean a decrease in the catalytic performance of the nickel catalyst in the electrodes of the electrochemical device, compromising its performance. Therefore, to intervene on this problem, with the third DS the flow of water entering the supply line is varied, in such a way as to have sufficient water available. The fourth DS, on the other hand, acts simultaneously with the other, varying the flow rate of the recirculated stream "A-RIC1" of the anode products, which have a high percentage of water, as can be seen in the tab. 18 above. By carrying out the simulations, based on the values set at the input relating to the initial flow rate of water, air or natural gas, the program reports two types of convergence. The first type made it possible to obtain absolute convergence by acquiring greater inlet water flows and smaller quantities of recirculation; to the contrary, in the second one the recirculated flow drastically increases. For the purposes of the most performing configuration, the second type was chosen, decreasing the heat consumption expected in the water supply line, and decreasing the flow of natural gas to be withdrawn from the network as part of it could be reintegrated by recirculation as shown in tab. 18.

The only CB has the function of verifying some data entered. In fact, in terms of algorithm, this tool is operated at the end, post convergence of all DSs. Basically, the verification involves the calculation of the FU and AU, using the following equations reported, [127]:

$$FU = \frac{\dot{n}_{H_2,AREAC4} + \dot{n}_{CO,AREAC4} - \dot{n}_{H_2,PROD1} - \dot{n}_{CO,PROD1}}{\dot{n}_{H_2,AREAC4} + \dot{n}_{CO,AREAC4}} \tag{155}$$

$$AU = \frac{\dot{n}_{O_2,CREAC1} - \dot{n}_{O_2,PROD1}}{\dot{n}_{O_2,CREAC1}} \tag{156}$$

The molar discharge values referring to the specific chemical element are obtained as input from the system. The fuel utilization factor, in the anode, is calculated as the ratio between the difference in flow rates of the elements affected by the electrochemical reactions, hydrogen and carbon monoxide, and the flow rates referred to the same elements at the initial conditions only. “A-REAC-4” constitutes the initial chemical composition to refer to, while “PROD-1” the final composition. The same applies to the air utilization factor, whose only difference is the initial reference flow rate, no longer referred to the stream entering the anode but to the cathode, "C-REAC-1".

## 4.4.2 Performance parameter, results of SOFC section

The final paragraph of the rSOC plant engineering section, relating to the fuel cell mode, reports the final results obtained from the simulation. As in the other sections of the system previously described, the continuous map generated with the data obtained from the simulations on Aspen was analysed in the Matlab file to obtain the hourly values of our interest.

The first explicit result concerns the operating time of the plant, equal to 7014 hours per year, with a consequent utilization factor of about 80.06%. The high value is reflected in the fact that, due to the way the management of urban loads was set up, all night-time electricity consumption would certainly have been covered by the SOFC due to the lack of solar radiation and therefore the impossibility of the PV plant to produce electricity.

| | | |
|---|---|---|
| Total electricity required by Urban Load | 33,975 | GWh/y |
| Total electricity produced by Photovoltaic plant | 12,053 | GWh/y |
| Total electricity produced during SOFC operation | 21,922 | GWh/y |

*Table 19 . Annual electricity input and output of the polygeneration plant*

The tab. 19 expresses the annual electricity balance of the entire plant. The amount of electricity produced during SOFC operations corresponds to 21.922 GWh/y, equivalent to

64.53 % of the total electricity required by the urban load of 30 thousand people, while the remaining part of 35.47 % is satisfied by the PV. The results are reflected in the logic behind the modeling phase: to avoid the depletion of a large portion of the territory to be used for the location of photovoltaic panels, which for the case in question of 9 MW corresponds to about 42 km$^2$, a compromise between the amount of energy produced by the PV and SOFC. The compromise of quotas of 1/3 and 2/3 respectively, obtained downstream of various simulations conducted, has given excellent results both in the energy-environmental and in the economic fields, an aspect examined in the final chapter 5 of the thesis work.

| Process Parameter | Result | Unit | |
|---|---|---|---|
| $I_{stack}$ | 4,8171 | **MA** | **ARITHMETIC MEAN** |
| $J_{cell}$ | 0,5634 | **A/cm2** | |
| $V_{op}$ | 0,7449 | **V** | |
| $spec_{prod}$ | 4,4557 | **kWh/kgSNG-1** | |
| $G_{SNG}$ | 5536,119 | **tons/y** | **SUM** |
| $G_{WREF-1}$ | 4449,400 | **tons/y** | |
| $G_{CREACT-1}$ | 92834,000 | **tons/y** | |
| $G_{ARIC1}$ | 35432,000 | **tons/y** | |

*Table 20 - main flow rates & electric parameters for SOFC*

Table 20 reports the characteristic parameters of the electrochemical device and its BOP. SOFC is characterized by an annual average operating voltage of 0.7449 V and an annual average current density of 0.5635 A/cm$^2$. The point on the polarization curve, fig. 22 in “3.2.4”, which is determined by exploiting these variables as coordinates, shows that, on average, the operations in SOFC affect the upper part of the polarization curve. This portion of the curve is characterized by operating conditions with medium-high voltage values and medium-low current values, presaging a high efficiency of the device due to the low energy dissipations and parasitic currents that could be created for high current values. The linear approximation with which the polarization curve was calculated does not take into account the conditions of efficiency drops attributed to high currents, due to the secondary physical phenomena that arise in these situations. However, even if this aspect had been considered, there would have been no major problems or in any case, these situations would have occurred rarely, thus attesting to the good operability of the device. Such result is obtained thanks to the control of the number of modules turned on during operations, in such a way as to always try to operate in conditions of maximum efficiency.

The “$spec_{PROD}$” variable is very important as it characterizes the device operating in fuel cell mode, determining the amount of electricity it can produce using one kilogram of natural gas taken from the network. Its net value of 4.4557 kWh/$kg_{SNG}$ was obtained from the average of the hourly ratios between the electrical power produced in the alternating phase and the hourly mass flow rate of the gas entering the system. A kilogram of natural gas, composed of 60 %$CH_4$ and 40 %$CO_2$ has an average content of 9.84 kWh/$kg_{SNG}$, a data obtained as an average of the values available on the internet by consulting UniFI, LuceGas.itSelectra and metropolitan city of Bologna. Furthermore, according to the official document of the Italian government released by ISPRA on 2 April 2019, the average Italian electricity efficiency stands at 41.5 %. Consequently, the net energy value, in terms of electricity, produced on average in Italy using natural gas as a resource, is 4.0836 kWh/$kg_{SNG}$. The comparison of the two values shows a correspondence, since the net electrical efficiency of the device, shown in tab. 21, has a value 5.7 % higher than the national average. This increase in efficiency is evident in the increase in energy that can be produced considering one kilogram of natural gas. The incongruity of the comparison resulting from the difference in the chemical compositions of natural gas is neglected, since, during the electrochemical processes, the composition of the fuel changes, thus validating the comparison made.

| SOFC EFFICIENCIES [%] | |
|---|---|
| ηel | 63,03 |
| ηel,net | 47,20 |
| ηchp | 87,06 |
| ηchp,net | 87,08 |

Table 21 - SOFC average efficiencies

The last data reported in tab. 20 show the quantities of streams involved in the SOFC system. The recirculated flow rate, as already expressed above, allows to reduce the amount of water in the supply line, increasing the combined efficiencies of the system, which has an average net value of about 87 %. The high amount of air introduced into the system is caused by the low utilization factor of this gas, equal to 0.5. The choice of this value also derives from the fact that the temperature control of the SOFC takes place by removing the incoming air, which acts as a thermal well. Overall, the plant consumes 5536.12 tons of natural gas during one year of operation.

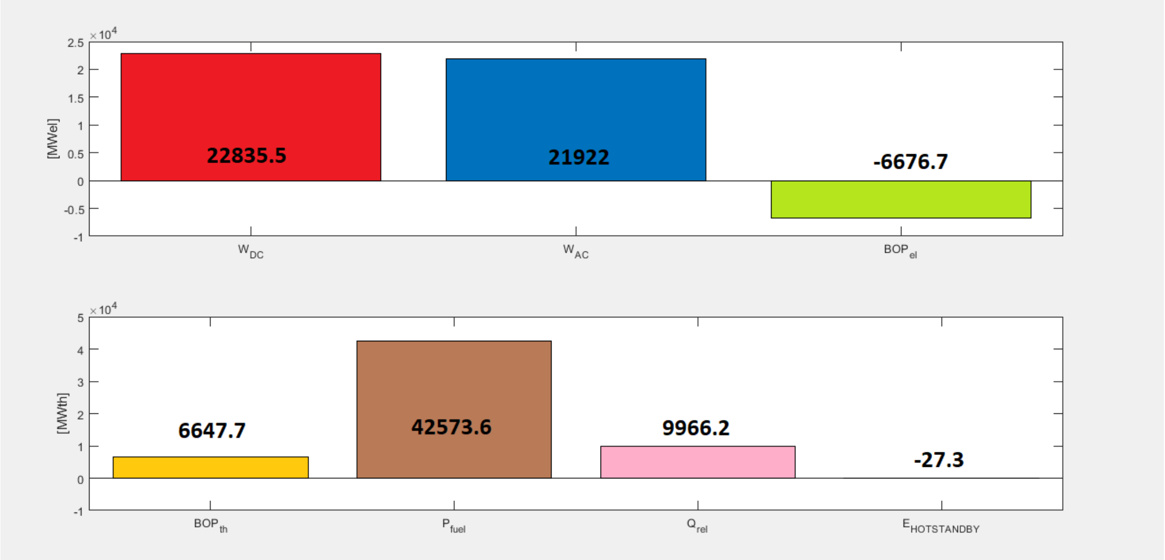

Figure 36 - Energetic flux characteristic of the SOFC section

Fig. 36 illustrates the energy balances of the entire plant section. The total electrical power value in the continuous phase differs from that of the alternating phase due to the efficiency of the inverter equal to 96 %. As for the other flows, the equations below list the formulas adopted, with the exception of the thermal energy exchanged between the device and the environment, $Q_{rel}$, which refers to eqs. (128) in "4.2.1".

$$BOP_{el} = W_{PUMP} + W_{TURB-SNG} + W_{COMPR-AIR} + W_{C-TURB} \tag{157}$$

$$\begin{split} BOP_{th} = Q_{ECO} + Q_{EVA} + Q_{SUPERH} + Q_{CAT-HEAT} + Q_{AN-HEAT} + Q_{PRE-REF} \\ + Q_{O_2-SEP} + Q_{N_2COOL} + Q_{COND} + Q_{H_2O-COOL} \end{split} \tag{158}$$

$$P_{FUEL} = \dot{n}_{H_2} LHV_{H_2} + \dot{n}_{CO} LHV_{CO} \tag{159}$$

In the $BOP_{el}$ all devices that use electricity to produce a useful effect on pressure are considered, such as the two turbines, the compressor and the pump in the system. Its final total value of -6676.6 $MW_{el}$ indicates that the auxiliary electrical components consume more electrical energy than they produce. Specifically, it has been identified that the electrical energy needed to compress the incoming air, "COMP-AIR", is the main energy-consuming source, due to the high flow rate involved. Its contribution clearly exceeds the benefit of the cathode products turbine, “C-TURB”, due to the quantity of oxygen reacted in the electrochemical processes which determines the reduced flow of depleted air.

The $BOP_{th}$, on the other hand, was calculated taking into consideration all the components in which heat exchanges take place. It was possible to make this assumption by considering all the thermal flows involved as valid, neglecting their exergetic characteristics. A more in-depth analysis, not the subject of the thesis in question, would require the application of pinch analysis in order to verify the congruence of the heat exchanges between the internal components of the system. The positive value obtained indicates that the set of net heat flows of the auxiliary components is exiting the system, making a useful contribution to the calculation of the combined net yield, opposite to that of the electrical components which tend to decrease efficiency.

The useful power, $P_{FUEL}$, is the annual sum of the amount of energy stored within the "A-REAC-4" component. Its value of 42’573.6 $MW_{th}$ was obtained by adding the product between the flow rate referring only to the hydrogen component contained in the stream in question, for its lower calorific value, $LHV_{H2}$ equal to 248.2 kJ/mol, and the flow rate referred only to the carbon monoxide component of the stream under examination, due to its lower calorific value $LHV_{CO}$ of value 282.0 kJ/mol. The intrinsic energy content values were taken from the work of Giovanilton F da Silva et al., [128].

Lastly, the final heat flow considered is the one necessary to keep the inactive modules of the SOFC hot. Its value of -27.3 $MW_{th}$ is small compared to the other thermal powers involved. The result is confirmed by considering its average operating conditions. As previously described, the electrochemical device tends to work in the upper part of the polarization curve, in the presence of a medium-low current and low operating voltage values. The low current values can be interpreted thanks to the possibility of the device to modulate its power by activating or switching off the modules. In fact, by operating with a high number of modules it is possible to lower the current content. These operations with a high number of modules therefore involve a low contribution of thermal energy necessary for hot standby.

The last parameters to be described are the most important: the efficiencies of the device. In tab. 21 annual average values were reported. The values are confirmed when compared with the reference texts, [89] and [110]. As expected, the SOFC technology confers an electrical efficiency with a significantly higher value than that of conventional systems, reaching 63 %. Due to the high value of the $BOP_{el}$, its net value, the one that considers the components involved in electricity exchanges, drops dramatically to the value of 47.2 %. In the case of gross combined efficiency, its value takes into account the heat exchanged with the cell. Considering the hypothesis of being able to make full use of it, the plant manages to reach a value of approximately 87 %. Furthermore, considering both the values of the electrical and thermal BOP, a final average value, representative of the SOFC plant section, is obtained, equal to 87 %. The values of the combined gross and net efficiency differ by a very small percentage, just 0.01 % because the energy contributions of the auxiliary systems (always BOP) have a practically equal value but with the opposite effect, so they are balanced. The equations used to calculate the four efficiencies are reported below. Comparing the eq. (160) relating to the electrical efficiency in the SOFC, with respect to eq. (126) of the electrolyser, it is noted that the terms of the fraction are reversed.

In the fuel cell, the useful effect is to produce electricity, $W_{DC}$, by exploiting the energy content of the fuel. In the case of the electrolyser it is the opposite. The useful effect is the energy content contained in the hydrogen stream produced, obtained by absorbing electricity. Keeping this in mind, when it is necessary to add the effect caused by the rest of the components or the heat exchange that directly affects the electrochemical device, the value of electrical power produced or absorbed needs to be changed. Consequently, both BOP and $Q_{rel}$ contributions will appear in the numerator for SOFC and in the denominator for SOEC. In reality, for the electrolyser, the heat exchange of the electrochemical device towards the environment will be counted in the denominator only in the case of endothermic behaviour, when this heat source must be produced externally and sent to the SOEC, while it will be placed in the numerator in the case of exothermic behaviour in such a way as to consider its contribution in a positive way, because it is heat produced by the SOEC towards the environment. The equations from (160) to (163) are those relating to the SOFC, while those of the electrolyser section are the eqs. (127), (127), (130), (131), (132) and (133) of "4.2.1".

$$\eta_{el} = \frac{W_{DC}}{P_{fuel}} \tag{160}$$

$$\eta_{el,net} = \frac{W_{DC} + BOP_{el}}{P_{fuel}} \tag{161}$$

$$\eta_{chp} = \frac{W_{DC} + Q_{rel}}{P_{fuel}} \tag{162}$$

$$\eta_{chp,net} = \frac{W_{DC} + Q_{rel} + BOP_{th} + BOP_{el}}{P_{fuel}} \tag{163}$$

The last graphs shown are those of the following figs. 37, 38, 39 and 40, representing the trends of the four efficiencies obtained during the annual simulation of the SOFC section, in which the annual trend of the values varies from 42.24% to 76.94% for gross electricity, and from 26.83% to 61.46% for the net. For the combined energy efficiency, however, it varies from 64.86% to 101.77% for the gross and from 64.62% to 101.59% for the net.

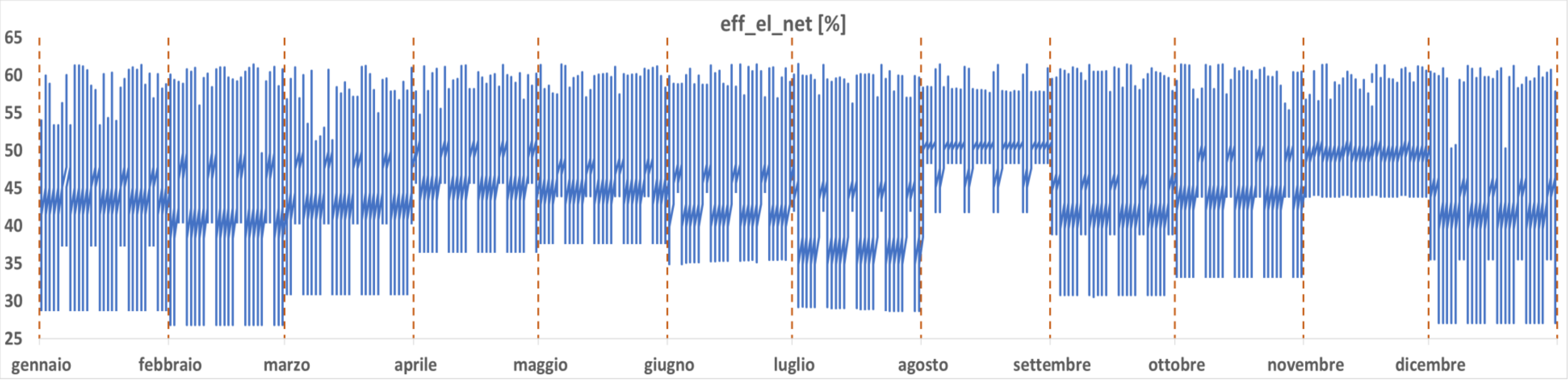

*Figure 37-SOFC Net ELectrical Efficiency*

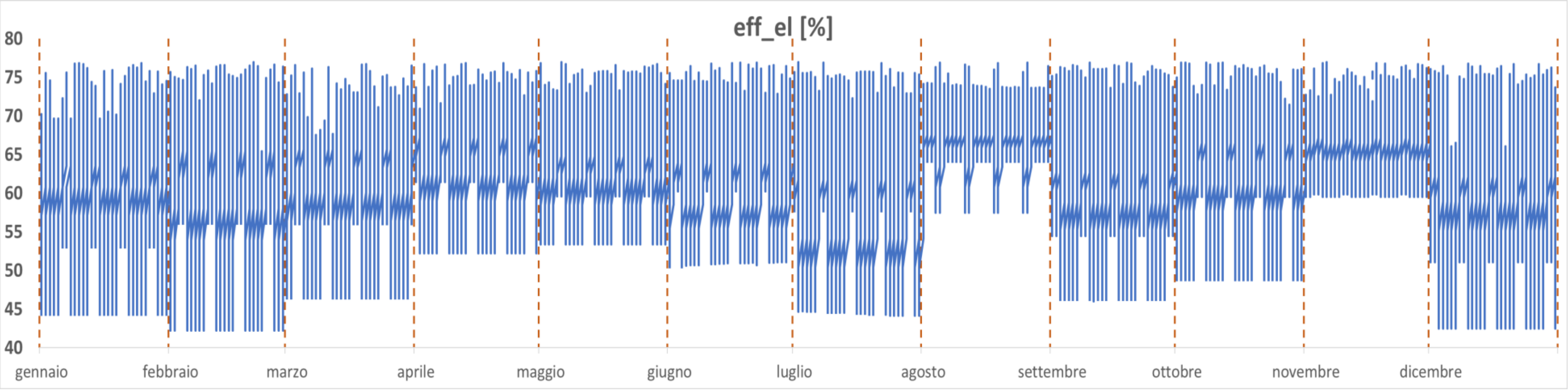

*Figure 38 - SOFC Electrical Efficiency*

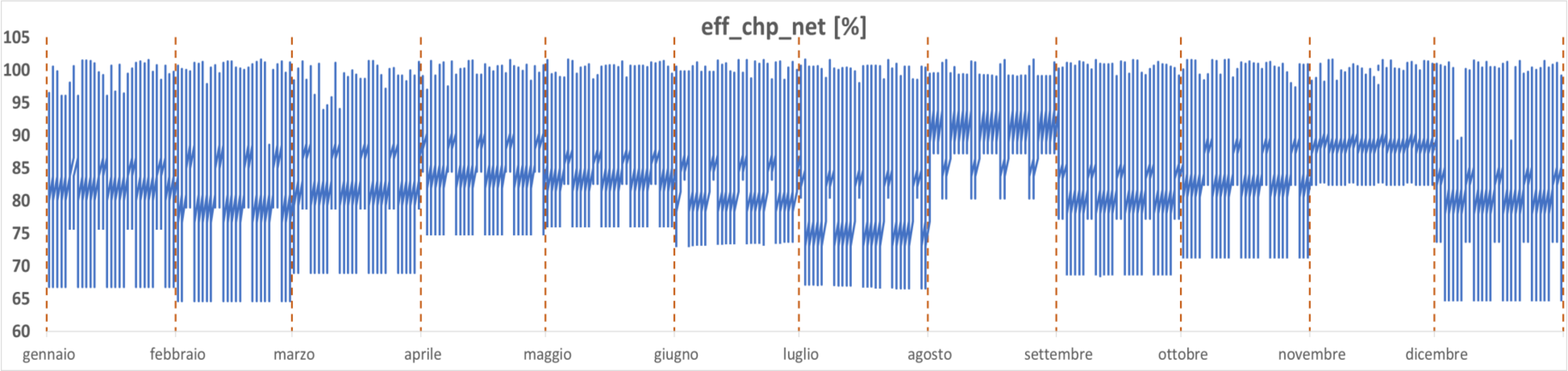

*Figure 39 - SOFC Net CHP Efficiency*

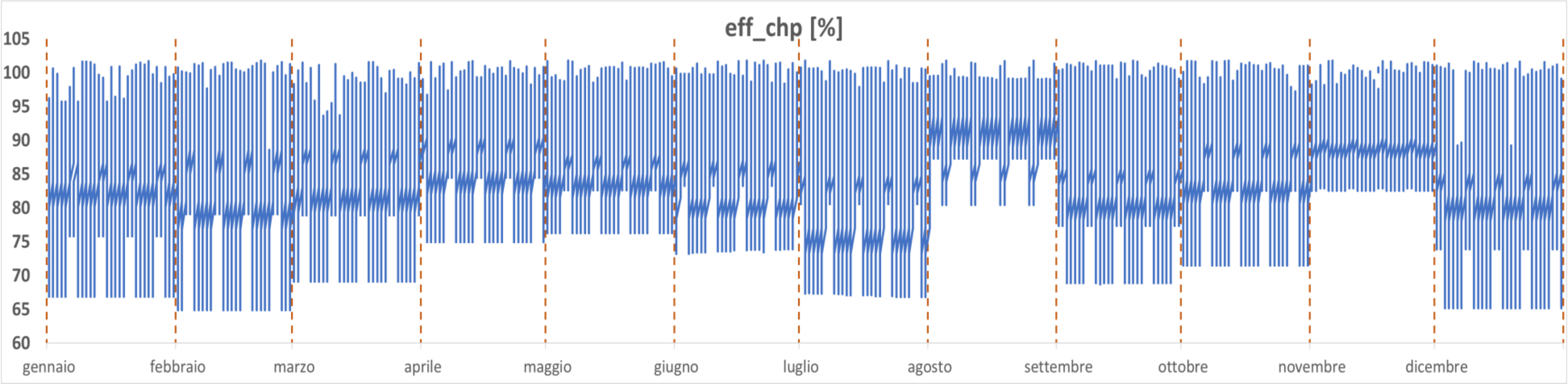

*Figure 40- SOFC CHP Efficiency*

## 4.5 Aspen model: Carbon Capture and Sequestration

The carbon dioxide removal plant allows to fully reach the goals set for 2030 for the abatement of GHG emissions. The 450 $ppm_{CO2}$ threshold, at this point, is close if the current rate of atmospheric pollution is maintained, consequently the inversion of the curve that measures the concentration of carbon dioxide in the atmosphere must take place. In general, the way of thinking about future plants must be based on circular systems, taking into account every phase of the entire life cycle, especially by designing a connection between waste and new product. This last aspect which can be represented by recycling or, even better, by reuse is precisely the concept on which the CCS section is based. The technology on which CCS section is based is in fact that of post-combustion, which manages the polluting gases after their production, filters dangerous substances and transforms them into usable and above all non-polluting products.

The representation of the plant on Aspen Plus begins with the setting of the properties on which the program will refer. The units of measurement used are as usual those of SI, [°C], [bar], [s], [J], [W], [kg] and [$m^3$], those of greatest interest for the simulation.

The setup of the chemical elements present in the system is very important. The Carbon Capture and Sequestration plant, in fact, is based on the absorption process, using specific aqueous solutions, whose optimal structure has been and is still being studied in recent years, in which the solvent plays the primary role of absorbent of the absorbed substance ($CO_2$). In the thesis work an aqueous solution is considered, whose solvent is MEA, present with a quantity of 30 $\%_{mol}$. Therefore, the chemical components to consider in the property setup are the following molecules: MEA, $H_2O$, $CO_2$, $CH_4$ and $N_2$. Furthermore, it is also necessary to specify the presence of the ions that are created and interact in the chemical reactions of the system: $MEA^+$, $H_3O^+$, $MEACOO^-$, $HCO_3^-$, $OH^-$ and $CO_3^{2-}$. The chemical reactions involved are presented in paragraph "3.3" and expressed by eqs. (102) to (106).

In order to ensure the correct simulation of the absorption process, Henry's law is set within the component section. In this way Aspen is able to determine Henry's constant and correctly set the physical equations for calculating the solubility of carbon dioxide that interacts with the aqueous solution of MEA. Many studies have been conducted using the Aspen database to manage the absorption processes between carbon dioxide and aqueous solution of MEA, such as the work of Akinola T.E. et al., [105], on which the modeling section of the CCS of the thesis work is mainly based. The notions implemented by Akinola T.E. et al. are reported both regarding the chemical processes involved and the creation phase of the Aspen model on which the simulations are based. Furthermore, the validation of the parameters in the Aspen database have been verified by the work of Huang Y. et al., [121].

The thermodynamic model chosen in Aspen plus is the Electrolyte Non-Random Two Liquid model (ELECNRTL). It is characterized by great versatility because it determines the chemical-physical interaction of the absorption process with high accuracy, accepting a wide range of solute concentration within the absorbent solution. Such model is perfect for the case of thesis work as the concentration of 30 $\%_{mol}$ is classified as a high concentration (because it is higher than the threshold of 15 $\%_{mol}$, [67]). The accurate results obtained from the model are possible thanks to the database present in Aspen, which presents the correct values of the binary molecular interaction parameters, fundamental variables to describe the absorption process of the aqueous solution based on MEA. As expressed by the work of Ravichandra A. et al. [122], for each binary mixture, the interaction parameters are expressed in terms of molecular size and strength of interactions, which are in turn calculated from molecular simulations.

The last setting realized to obtain the coherent and complete section of the properties for the CCS system involves the insertion of the stream properties. As in the case of the electrolyser, in which the program was required to calculate, through the databank at its disposal, the value of the lower heating value, also in this case it is possible to exploit the intrinsic knowledge of the program to obtain important data for the purposes of analysis, thus excluding their manual entry. This also reduces the probability of a human error that could occur if the entered data is not completely valid to represent the simulated reality. The properties entered are:

- PH2OTDEW, the dew point temperature, calculated as a function of its partial pressure within the solution it is part of. This thermodynamic condition is very important because it allows the biomethane produced by the purification action of the CCS to be dried at the right relative humidity conditions;
- RHOMX, which allows to directly calculate the density of a mixture;
- FAPP, the apparent mole flow rates for only electrolytes systems produced by the carbon dioxide, water and MEA chemical reactions;
- WAPP, the apparent mass flow rates for only electrolytes systems, produced by the carbon dioxide, water and MEA chemical reactions;
- XAPP, the apparent component mole fraction for only electrolytes systems, produced by the carbon dioxide, water and MEA chemical reactions;
- QVALGRS, for the calculation of the high and low heating value in term of mass.

After describing the properties section, the flowsheet work is analyzed, which shows the CCS plant, represented by the following fig. (41).

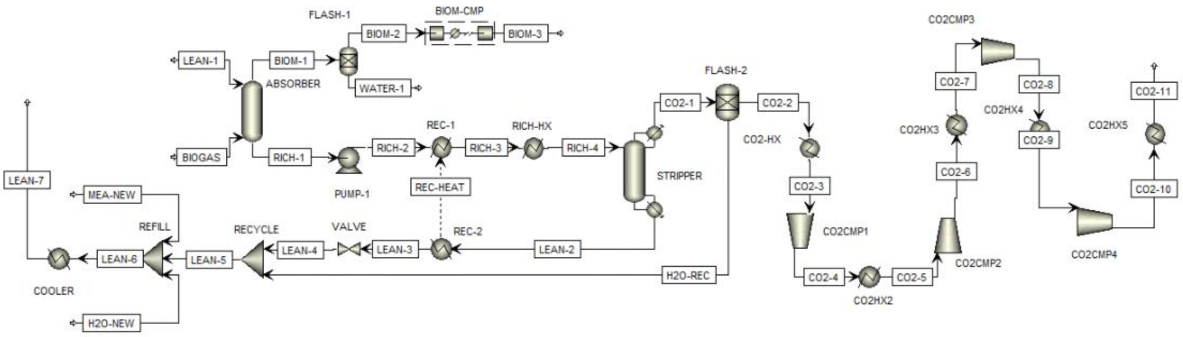

*Figure 41 - CCS plant on Aspen Plus*

The carbon dioxide removal system revolves around the two fundamental components, the absorbent column "ABSORBER" and the desorbent column "STRIPPER". The “BIOGAS” gaseous stream is the initial stream that must be purified, characterized by an initial composition of 65 $\%_{molCH4}$, 34 $\%_{molCO2}$ and 1 $\%_{molN2}$. It is sent to the lower section of the absorbent column, in such a way as to chemically react, in counter-current, with the aqueous solution "LEAN-1", composed of 30 $\%_{molMEA}$ and 70 $\%_{molH2O}$. The thermodynamic conditions of the incoming streams are for both 1.1 bar, a slight overpressure to avoid infiltration in the supply pipes, and at a temperature of 40 °C and 30 °C respectively. The pressure of the solution must be kept approximately at the atmospheric level, since, for values higher than 2 bar, degradation phenomena come into play which would sharply decrease the performance of the absorption reactions. Vapor-liquid are the valid phases managed by the “ABSORBER”. Geometrically it was set by choosing a geometric ratio between height and diameter equal to 10. Specifically, an absorbent column was set, with a section packed height of 6 [m] and a section diameter of 0.6 m, for a total of six sections. Furthermore, the set packing characteristics provide for the specification of packing type, of the vendor, the type of construction material used and the type of packaging. The following fig. (42) reports the Mallapack 250Y typology implemented in the thesis work.

*Figure 42 - Packing MALLAPACK 250Y [123]*

This model is globally widespread in the field of absorption and desorption processes, thanks to its unique characteristics that give it a low pressure drop, between 0.3-1 mbar, at minimum liquid load approximate to 0.2 $m^3/(m^2h)$ and a maximum liquid load up to more than 200 $m^3/(m^2h)$, data provided by the Sulzer Chemtech company ™.

The "STRIPPER" desorbent column has the same packing characteristics: Packing MALLAPACK 250Y. Like the absorber, an H/ø ratio of 10 was chosen, with different geometric characteristics. In fact, during the design phase, a section packed height of 5 m with a section diameter of 0.5 m was chosen, for a total of 9 section. The choice of the different dimensions is due to the fact that the desorption reactions are characterized by different kinetics, consequently the number of sections in which the chemical reactions are favored has been increased, obtaining acceptable purity values in the output streams. For this purpose, the component is directly connected to two heat exchangers, a reboiler located in the lower part and a condenser, in the upper one, with the function of further increasing the purity of the outgoing streams by evaporating the $CO_2$ residuals linked to the MEA and due to the regeneration and by liquefying the residual water of the outgoing carbon dioxide stream.

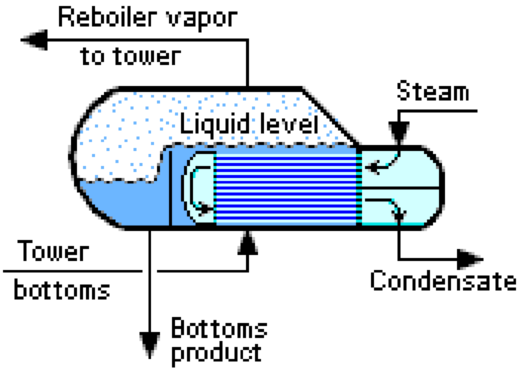

*Figure 43 - Kettler reboiler, GFDL*

Fig. (43) represents the Kettler reboiler implemented in the thesis system. The regenerated aqueous solution coming out of the lower head of the tower enters the reboiler, absorbs heat from a stream of steam introduced into a tube bundle and undergoes a change of state becoming liquid. This heat exchange involves the evaporation of excess carbon dioxide which is recirculated inside the stripper, while the aqueous solution of MEA, "LEAN-2", continues its path. Instead, the process on which the condenser is based is exactly the same, with the only difference that the secondary thermofluid stream (usually water as in the reboiler), removes heat from the primary (the acid gaseous flow of carbon dioxide), evaporating and allowing to condense the residual water.

Known the characteristics of these two components in which the chemical reactions of absorption/desorption take place, it is possible to describe the behaviour of the plant section, because the remaining part of the BOP consists of the classic components already analyzed in the operational sections of the rSOC. Downstream of the absorption reactions in the

"ABSORBER" component, two streams of matter are obtained. From the top there is the outlet of the biogas purified by carbon dioxide "BIOM-1" in the conditions of 39 °C and atmospheric pressure ($\Delta p = 0.1$ bar), consisting mainly of methane, a small percentage of water, about 1 $\%_{molN2}$, and the residue of carbon dioxide, also in the order of 1 $\%_{molCO2}$. Before being fed into the national distribution network, the water still present is further separated, using the "FLASH-1" component. It is a reactor of the fluidized bed family that allows, by exploiting high input speeds, the possibility of carrying out chemical reactions which separate some of the chemical components present in the input stream into different phases: in this case gaseous biomethane "BIOM-2 "and liquid water" WATER-1 ". The biomethane is further processed within a compression process with intercooling in such a way as to reach the conditions suitable for introducing it in the network (35 °C and 15 bar), while the pure distilled water is collected and reused within the plant, such as in the rSOC section.

In the lower part of the absorber, the aqueous solution comes out, rich in the removed acid substance "RICH-1" at 54 °C and 1.1 bar, and it's conveyed to the line leading to the stripper where its physical conditions are modified in order to optimize the desorption process, favored at 110 °C and 2.6 bar. Considering the literature, [67], [68], [105], [121] and [123], the optimal values of the absorption process involving MEA as a solvent are around 50 °C, while those of the desorption of 120 °C, positively affirming the validity of the data obtained/used. To alter the pressure value, the acid liquid passes inside a pump, "PUMP-1", characterized by an efficiency of 80 %. The material of the device is not specified, although, in a more detailed analysis, the possibility of the formation of carbonic acid from the chemical reaction of water and carbon dioxide, a corrosive compound for many metals, should certainly be considered. Reaching the designated temperature, on the other hand, occurs in two stages. The first uses a heat exchanger that recovers heat directly from the regenerated flow leaving the stripper, "REC-1", while the second phase involves an additional heat exchanger, "RICH-HX", capable of bridging the missing heat difference .

As for the streams exiting the stripper, the pure flow of carbon dioxide exiting from the top of the regenerative column is initially sent into a flash reactor, "FLASH-2", which further removes the last residual fraction of water present, obtaining in output a $99.99\%_{molCO2}$ pure stream, “CO2-2”. The stream of acid gas is finally circulated in a compression and inter-refrigeration system, in such a way as to increase its pressure level up to the operating conditions of the next electrolysis section. The extracted water, "H2O-REC", is recirculated and mixed with the regenerated solution, "LEAN-2", coming out from the bottom of the stripper. Before mixing, this last flow of matter which is at the conditions of 134 °C and 2.6 bar, is passed into the "REC-2" recovery exchanger to decrease its temperature, releasing heat to the stream rich in carbon dioxide (“REC-1” and “REC-2” are the same exchanger, it has been split because the heat recovery takes place in the same system). Successively, it passes inside a lamination valve "VALVE", a throttle component, since it has a sudden section change capable of losing pressure by converting it into friction, obtaining the "LEAN-4" stream. This stream, mixed in the "RECYCLE" mixer with the recovered water, forms "LEAN-5", which is sent to the input of another mixer, "REFILL", together with the external water "H2O-NEW" and the new “MEA-NEW” solvent, in such a way as to obtain an output stream, “LEAN-6”, which has the same chemical composition as the absorbent solution initially introduced into the absorber. The complete regeneration of the stream allows its reuse in a new absorption cycle. The final “COOLER” heat exchanger allows the temperature level to be brought back to the initial level of “LEAN-1”.

### 4.5.1 CB and DS of CCS’ section

For the correct simulation of the carbon dioxide removal process of the acid biogas stream, four DSs and two CBs were implemented. Thanks to the software and to the set up of the simulation file, the equations that are used to describe the absorption/desorption processes are directly managed by the program. Consequently these tools will have the main task of managing the incoming streams to the system.

The first DS peculiarity is to obtain a net removal of carbon dioxide equal to 98 $\%_{mol}$ with a tolerance of +/- 1 %. To obtain the result, the mass flow rate of the inlet MEA-based aqueous solution is varied.

$$98 = \frac{CO_{2,BIOGAS1} - CO_{2,BIOM1}}{CO_{2,BIOGAS1}} * 100 \tag{164}$$

Eq. (164) is the one set in the definition section of the specification. "BIOGAS-1" is the acid flow entering the absorbent column that must be purified, while "BIOM-1" is the biomethane generated after the absorption process. The numerator of the fraction indicates the molar percentage of carbon dioxide removed in the absorber, while the denominator indicates the initial molar fraction.

The second DS has the purpose of obtaining an aqueous solution based on MEA leaving the CCS plant, "LEAN-7", with the same chemical composition as the one at the inlet, "LEAN-1", except an expected tolerance of 1 %.

$$\frac{CO_{2,LEAN7}}{MEA_{LEAN7}} = \frac{CO_{2,LEAN1}}{MEA_{LEAN1}} \tag{165}$$

The presence of carbon dioxide in the absorbent solution entering the absorber is due to the fact that this DS overwrites the input of the composition initially set at 30 $\%_{molMEA}$ and 70 $\%_{molH2O}$, because the regeneration processes are not 100 % efficient. In view of a recirculated flow, there will be small traces of carbonaceous substances both at the inlet and outlet. To obtain the congruence dictated by the DS, the thermal power exchanged in the reboiler is varied.

The third DS aims to obtain a biomethane leaving the CCS section, “BIOM-3”, characterized by a dew point equal to -5.01 °C with a tolerance of +/- 0.1%. This result, in addition to entailing a low water content in the outgoing gas and therefore an increase in efficiencies in case it is treated within a conventional cogeneration system for the production of electricity and heat, is a fundamental requirement for biomethane produced, placing on the distribution network. Indeed, annex 11/A of the Decree issued by the Ministry of Economic Development on 19 February 2007, provides the definition of the chemical-physical characteristics of natural gas transported in Snam Rete Gas pipelines. Such legislation establishes that natural gas or biomethane introduced into the network has to comply with the criteria of HHV, WI and GG, already explained in paragraph "3.4", and imposes a dew point of the water contained in the stream, lower or equal at -5 °C. Obtaining this result is ensured by varying the amount of water removed by the "FLASH-2" component.

The fourth and last DS aims to obtain a fixed temperature difference equal to 15 °C between the stream "LEAN-3" and "RICH-2", varying the amount of heat recovered by the "REC-1”|”REC-2”. This approach is based on the method of pinch analysis, a criterion that allows to optimize the management of thermal flows. In fact, the determination of the temperature difference between the streams involved in a heat exchanger system is one of the results of the pinch analysis. In the specific case of the thesis work, as previously stated, this optimization was not carried out, consequently the value of the thermal jump was chosen on the indicative basis of the absorber and stripper temperatures and validated with experiments carried out by launching simulation with the program.

As regards the CBs, the first one which was analyzed allows to calculate the quantity of solute water, "H2O-NEW", and solvent MEA, "MEA-NEW", to be fed into the "REFILL" mixer inlet to obtain the optimal chemical composition for the second DS.

$$\dot{n}_{MEANEW} = Y_{MEA,BIOM1}\dot{n}_{BIOM1} + Y_{MEA,CO2-2}\dot{n}_{CO2-2} \tag{166}$$

$$\dot{n}_{H2ONEW} = Y_{H2O,BIOM1}\dot{n}_{BIOM1} + Y_{H2O,CO2-2}\dot{n}_{CO2-2} \tag{167}$$

The coefficient Y reported in eqs. (166) and (67) represents the molar fraction of the chemical element considered, MEA or H2O, for the streams in question, "BIOM-1" or "CO2-2". As can be seen from the equations, the amount of solute and solvent to be integrated in the final mixer is equal to the amount lost in the output streams. The terms present at the first member of the two equations are the final molar flow rates which constitute the variables exported from the CB, overwriting the previous value.

Finally, the second CB has the function of calculating for the outgoing biomethane stream, "BIOM-3", the parameters that allow it to be fed into the network. As a first step, the molecular mass of the substance, consisting mainly of methane and traces of nitrogen, carbon dioxide and water, is calculated by multiplying the mole fraction of the element by its specific weight value:

$$MW_{BIOM3} = 16 * Y_{CH_4} + 28 * Y_{N_2} + 44 * Y_{CO_2} + 18 * Y_{H_2O} \tag{168}$$

The second variable to be calculated is the molecular mass of the air, using a formula similar to eq. (168). A value equal to 28.55 g/mol is obtained with a composition of 79.05 $\%_{molN2}$ and 20.05 $\%_{molO2}$. Once the molecular masses are known, the remaining functions are set, taking into consideration that the density and the higher calorific value in terms of mass of the biomethane are determined respectively by the RHOMX and QVALGRS properties.

$$GG = \frac{MW_{BIOM3}}{MW_{air}} \tag{169}$$

$$HHV_{vol} = \mathrm{HHV}_{mass} * \rho_{BIOM3} \tag{170}$$

$$WI = \frac{HHV_{vol}}{\sqrt{GG}} \tag{171}$$

The Gas Gravity (GG) variable, eq. (169), had been previously calculated in Eq. (118) of paragraph “3.4” with an alternative formula. Refer to the chapter mentioned for an explanation of all the parameters and their acceptability ranges.

In conclusion, at the end of the CCS’plant simulations, the mean values obtained downstream are 36.784 MJ/Sm$^3$, 48.783 MJ/Sm$^3$ and 0.569 for HHV, WI and GG respectively.

### 4.5.2 Performance parameters, results of the CCS’ section

The final paragraph of the CCS plant section reports the final results obtained from the simulations. As in the other sections of the system previously analyzed, the continuous map generated with the data obtained from the simulations on Aspen was managed in the Matlab file to obtain the hourly values of our interest.

The first result to be discussed concerns the operating time of the plant, equal to 1263 hours per year, i.e. an utilization factor of approximately 14.42 %. The figure fits perfectly with the hours of use of the SOEC operating in co-electrolysis, because the two systems work in symbiosis: it has been considered the hypothesis of the carbon dioxide removal plant providing the supply of carbon dioxide at the exact moment in which the rSOC would operate in co-electrolysis, without the insertion of a storage interposed between the two sections. This hypothesis can be justified by the fact that, although this has not been considered in the current thesis plant, by monitoring the atmospheric conditions it is possible to make very accurate metereologic forecasts in the short term, in such a way as to reduce the operating costs that would have been affected by inserting a storage.

The following table (22) shows the most interesting results that allow conclusions to be drawn on the CCS plant section, especially by making comparisons with the reference scientific articles, such as the study by Akinola T.L et al. [105] and that of Huang Y. [121], both conducted also using MEA as a solvent for the removal of carbon dioxide.

| Process Parameters | Results | Units | |
|---|---|---|---|
| Lean/Biogas | 3,6869 | $kg_L/kg_B$ | ARITHMETIC MEAN |
| $CO_2$ Lean loading | 0,2899 | $kmol_{CO2}/kmol_{MEA}$ | |
| $CO_2$ rich loading | 0,4306 | $kmol_{CO2}/kmol_{MEA}$ | |
| Reboiler heat duty | -3,6169 | $GJ/tons_{CO2}$ | |
| Reboiler temperature | 133,9 | °C | |
| Rich solvent temperature | 54,0 | °C | |
| Condenser heat duty | 0,8886 | $GJ/tons_{CO2}$ | |
| Lean solvent cooling | 2,1244 | $GJ/tons_{CO2}$ | |
| Pump duty | -0,0104 | $GJ/tons_{CO2}$ | |
| Recover heat | 4,7300 | $GJ/tons_{CO2}$ | |
| Biogas treated | 522,12 | $tons_{biogas}/y$ | |
| Lean solvent | 1925,00 | $tons_{MEA}/y$ | SUM |
| Biomethane produced | 249,36 | $tons_{biom}/y$ | |
| $CO_2$ produced | 4810,05 | m3/y | |

*Table 22- key parameters result summary of CCS section*

Overall, the simulation of the plant made it possible to purify by transforming an acid stream of incoming biogas, initially composed of 34 $\%_{mol}$ of carbon dioxide, into biomethane with a final content of the acid component reduced to 1 $\%_{mol}$. To obtain this result, the quantity of solvent required, in terms of mass, to purify one kilogram of biogas is quantified. The reference variable is Lean/Biogas, with a value of 3.6869 $kg_L/kg_B$, obtained from the annual average of the ratios between the mass flow rate of "LEAN-1", referring only to the MEA component of which it constitutes 30 $\%_{mol}$, and the mass flow of “BIOGAS” entering the absorber, finding confirmation in the results of the reference articles. This variable is influenced by the absorption capacity of the solvent, a chemical parameter widely investigated in past and current research. In fact, the studies conducted to date try to reduce the amount of solvent necessary for removal, by carrying out experiments that are based on the modification of the concentration of MEA, or on the use of innovative materials such as IL, trying to identify the solution with the best carbon dioxide absorption capacity. The mole fraction of 30 % derives from studies of this kind, [125].

$CO_2$ Lean Loading and $CO_2$ Rich Loading are two very important variables for the behaviour classification of the absorber. The first represents the ratio between the molar fraction of carbon dioxide and that of MEA in the "LEAN-1" solution at the entrance to the absorbent column, eq. (172). The second represents the same ratio but for the “RICH-1” stream, eq. (173), the solution which has become acidic downstream of the removal processes.

$$CO_2\ Lean\ Loading = \frac{Y_{CO_2,LEAN1}}{Y_{MEA,LEAN1}} \tag{172}$$

$$CO_2\ Rich\ Loading = \frac{Y_{CO_2,RICH1}}{Y_{MEA,RICH1}} \tag{173}$$

The values are respectively 0.2899 $kmol_{CO2}/kmol_{MEA}$ and 0.4306 $kmol_{CO2}/kmol_{MEA}$ and also in this case they are in line with what is reported in the reference scientific articles. As in the case of L/G, these variables are strictly dependent on the absorption capacity of the aqueous solution based on MEA. In addition, also the influence of $CO_2$ absorption reaction kinetics is a very important parameter for the absorber because the residence time inside the component derives from the speed with which the reactions occur. High absorbing capacity of the system allows to obtain shorter times, resulting in high advantages in energy and economic terms, [126]. A longer residence time would imply an absorber characterized by a higher fraction active area, therefore a higher investment cost. Furthermore, thanks to the possibility of operating for a longer period, operating costs would also be affected. To obtain a better absorption capacity, in addition to acting on the chemical composition of the solution, it is possible to intervene on some parameters of the system:

- Increment of the solution circulation, not recommended due to the increase in operating costs;
- Increment of the solution temperature to improve the absorption kinetics, not recommended because it would involve an increase in the heat to be supplied and therefore in operating costs;
- Considering the absorber structure, the supply of the solution at the highest possible point of the column to increase the residence time with the same geometry, a recommended intervention since it does not involve any additional cost.

As for the stripper, the most important parameters are the Reboiler heat duty and Condenser heat duty. These variables make it possible to draw conclusions on the energy consumption of the regeneration processes, which constitute the largest share of the operating costs of the entire CCS plant. The first of the two, whose average value obtained downstream of the annual analysis is -3.6169 $GJ/ton_{CO2}$, is the thermal energy used in the reboiler to purify the outgoing stream of carbon dioxide, characterized by an average temperature of 133.9 °C. The thermodynamic parameter of reference in this case is the heat of absorption, i.e. the thermal indicator of the amount of energy that is required to break the chemical bonds that bind the MEA and the acid substance. The greater the heat absorption, the greater the amount of energy to be supplied to regenerate the solution. The value is coherent with the reference scientific texts, so this variable can only be substituted with an absorbent substance that establish chemical bonds with a lower energy resistance.

The heat duty Condenser, on the other hand, assumes an average value of 0.8886 $GJ/ton_{CO2}$. The same considerations that were made for the component present at the bottom of the stripper also apply to the condenser, unlike the amount of energy represented by the variable is that released during the liquefaction process of the condensing water. The sign convention used in tab. (22) is that provided by Aspen, in which a positive energy indicates that it has been produced and is leaving the system, while a negative energy indicates the opposite, that is has been absorbed and entered the system.

The energy characterization of the CCS system can be carried out on additional components. The unit of measurement to which they refer is always the energy necessary for their proper functioning compared to a ton of carbon dioxide produced. Among them we find Lean solvent cooling, which energetically characterizes the “COOLER” component with a value of 2.1244 GJ/ton$_{CO2}$. Despite the high energy content corresponding in terms of absolute value to 58.73 % of the heat duty Reboiler, in terms of exergy it struggles to find use because of the low temperatures involved. The initial temperature, which on average sets on 69 °C, is decreased until it reaches the initial values of the incoming solution, 30 °C for its reuse. Therefore, the thermal jump at low temperatures could only be used for a pre-heating of liquid water before introducing it into the economizer, for instance. The next component is the Pump Duty, whose value averages -0.0104 GJ/ton$_{CO2}$. It quantifies the amount of electricity needed by the pump "PUMP-1" to compress the flow of solvent rich in acidic substance from the value of 1,1 [bar] inside the absorber, to the 2.6 bar necessary for stripper operations. Finally, the last component whose energy footprint was calculated is the "REC-1" or "REC-2" heat recovery unit. Analyzing the hourly data of the component, an average value of 4.73 GJ/ton$_{CO2}$ was identified for the Recover heat variable. The high amount of heat is directly recovered in the system between the regenerated solution line and that sent to the stripper for regeneration. The following equations report the formulas that were used for the calculation of the energy variables:

$$Lean\ solvent\ cooling = \frac{Q_{COOLER}}{\dot{\mathrm{m}}_{CO_2-11}} \tag{174}$$

$$Pump\ duty = \frac{W_{PUMP-1}}{\dot{\mathrm{m}}_{CO_2-11}} \tag{175}$$

$$Recover\ heat = \frac{Q_{REC-1}}{\dot{\mathrm{m}}_{CO_2-11}} \tag{176}$$

The last information on the CCS system shown in tab. (22) concern the sum of the main flows entering and leaving the system. During the whole year, considering the 1263 [h/y] of plant operation, 522.12 tons$_{BIOGAS}$/y of biogas are treated, which, expressed in standard volumetric conditions, corresponds to 479’632 Sm$^3_{BIOGAS}$/y. The chemical absorption action allows to produce in the reference year 249.36 tons$_{BIOM}$/y of biomethane, characterized by an average chemical composition comprising 97.45 %$_{molCH4}$, 0.15 %$_{molH2O}$, 1 %$_{molCO2}$ and 1.4 %$_{molN2}$. Consequently, the stream of carbon dioxide produced, composed of 99.99 %$_{molCO2}$ and of remaining traces of water, methane and nitrogen, will be equal to 272.6 tons$_{CO2}$/y. By comparing the value obtained with that expressed in “4.3.2” of the co-electrolysis section, where the saving of carbon dioxide emitted was discussed, a comparison is identified that reports an error committed of 0.269%. The comparison can also be highlighted by comparing the total volume flow value of $CO_2$ at the conditions of 35 °C and 33.1 bar present in table 22 equal to 4810.05 m$^3$/y, and the one reported in table 16, which expressed the total volume value, under the same conditions reported above, of the carbon dioxide entering the co-electrolysis system equal to 4807.32 $m^3/y$. The coincidence between the results of the CCS output section and the co-electrolysis input section demonstrate the correctness of the data. Finally, the last flow rate analyzed during the year was that of the MEA solvent used in the plant, which a total value in mass terms equals to 1925 $ton_{MEA}/y$.

## 4.6 Aspen model: Methanation

The methanation section is the last sub-system of the polygeneration plant analyzed. The purpose of this part of the plant is to further increase the energy quality contained in the syngas, converting it into SNG and introducing it into the national distribution network. This process concludes the cycle that involved the use of a stream of carbon dioxide, filtered and removed by a gas that contained it in large quantities (biogas), transforming it into a useful product with a high energy content. In addition, the resulting considerable environmental benefit avoids the release of GHG substances into the highly harmful atmosphere, a concept in line with the objectives set for 2030 and which revolves around the circular management of the carbon dioxide life cycle.

As for any other section of the polygeneration plant, the setting of the Aspen sheet begins by setting the values of the Properties. The SI is the definition basis of the measurement units, using the classic [°C], [bar], [s], [J], [W], [kg] and [$m^3$].

The chemical components of interest to the methanation section are the same as those foreseen in the co-electrolysis section, i.e. $H_2O$, $CO_2$, $H_2$, CO, $O_2$, $CH_4$ and $N_2$. These two plants are closely dependent on each other, and connected with the interlude of a syngas storage. In fact, this gas, containing 99.99 % of carbon dioxide captured in the biogas, is sent by the co-electrolysis section, stored in the period of inactivity of the methanation, and subsequently sent into it for its conversion into SNG and injection of natural gas into the network. As further discussed in the paragraph concerning storage, it allows the methanation section to operate in stationary conditions with a constant flow rate.

As regards the setting of the properties, as in the case of the electrolyser (in general rSOC), the method chosen and implemented is that of PENG-ROB. This method allows the program to use the most appropriate equations of state to determine the properties of chemical compounds containing hydrocarbons or light gases such as carbon dioxide and hydrogen. The method will be applied by the program with the exception of methanation reactors, in which the minimum Gfe model will be followed, directly applied by the components.

Finally, the setting of the properties necessary to simulate the methanation process ends with the explanation of the physical parameters directly obtained from the Aspen databases:

- GMX is the Gfe in kJ/kmol calculated directly for a gaseous mix. It is fundamental for the case in question because the methanation reactors used in the Aspen flowsheet, as in the analogous case of the SOFC pre-reformer, will be based on the concept of minimum Gfe, in such a way as to supply the gas stream in equilibrium conditions;
- QVALGRS, a parameter that determines the high heating value of a gaseous or liquid compound, expressed in MJ/kg.

Once the properties have been set, the system is represented directly on the simulation sheet, reporting the control unit diagram in which all the components and streams concerned appear, represented by the next fig. 44.

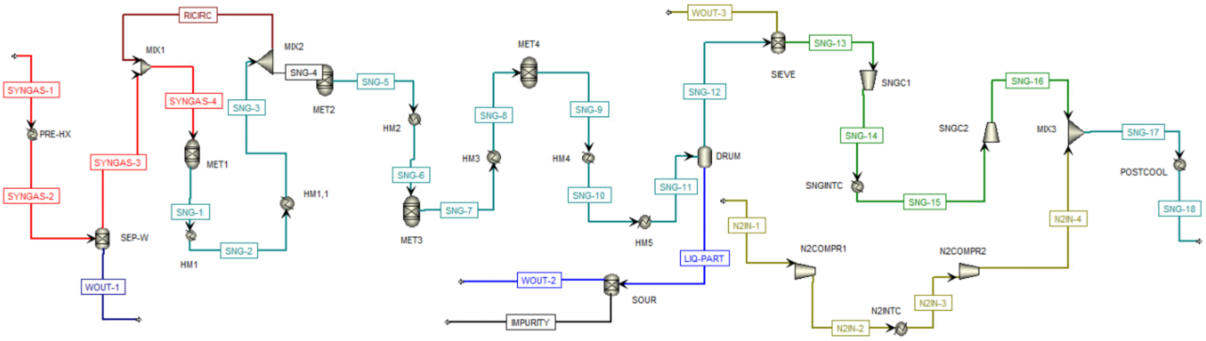

*Figure 44 - Methanation plant on Aspen Plus*

The methanation section process begins with the injection of syngas, "SYNGAS-1", by the storage, initially at the storage conditions of 20 °C and 32.4 bar, chemically consisting of $26.62\%_{molH_2O}$, $4.92\%_{molCO_2}$, $49.2\%_{molH_2}$, $9.87\%_{molCO}$ and $9.39\%_{molCH_4}$, obtained from the co-electrolysis operations. The presence of carbon dioxide and carbon monoxide, reacting with hydrogen, cause methanation reactions. Considering the thermodynamics of the reactions, explained in detail in "2.2.1.1", the higher percentage of CO compared to $CO_2$ allows a better performance, avoiding the energy waste of breaking down that additional oxygen atom, an element that distinguishes the chemical composition of the two compounds, resulting in an exothermic reaction with a higher heat content. Referring to the contemporary literature, [30], [59], [90] and [129], it is known that these reactions are favored at the operating conditions of 220 °C and 32.4 bar. As seen previously, the pressure value, similar to that of the operation of the electrolyser, in addition to favoring the methanation reactions, allows to obtain already in the electrolysis phase a percentage of about 10 $\%_{mol}$ of methane, increasing the system production efficiency. Furthermore, it facilitates a considerable electrical saving by avoiding the compression of the syngas, characterized by a high hydrogen content (high specific heat). As for the temperature, the value of 220 °C was obtained considering both the optimization of the kinetics of the reactions involved, and the system limit temperatures, especially that of the first methanation reactor. Since the reactions are exothermic, therefore producing heat, the syngas at a temperature of 220 °C allows to obtain a maximum outlet temperature from the first reactor of 700 °C. This limit temperature prevents the degradation of the nickel catalyst, a constituent material of methanation reactors.

The “SEP-W” component separates a certain amount of water vapor from the incoming stream, in order to adjust the H/C ratio, whose value allows to obtain a better or worse conversion of methane. The amount of water separated will depend on the recirculation downstream of the first methanation reactor and on the limit temperature of 700 °C: in order to respect all the system conditions, the separator varies the water content in the inlet stream, favouring the optimal H/C ratio equal to 3 thanks to the chemical composition of the "RICIRC" recirculation mixed in the "MIX1" mixer and able to carry out a suitable number of methanation reactions in compliance with the maximum temperature. Although the methanation reactors are not of the TREMPT type, but HICOM, an H/C ratio of 3 favours the methanation reactions of carbon monoxide, an element that is present in the initial stream of syngas in double quantities compared to the analogous $CO_2$.

"SYNGAS-4" is the stream obtained after mixing with recirculation, characterized by a composition of $15.61\%_{H_2O}$, $5.83\ \%_{CO_2}$, $52.15\ \%_{molH_2}$, $9.65\ \%_{molCO}$ and $16.75\ \%_{molCH_4}$. It is sent to the first methanation reactor, where the first conversion phase takes place, by varying the temperature from the initial 220 °C to the final 700 °C expected, obtaining at the output the "SNG-1" stream, characterized by composition $30.20\%_{H_2O}$, $5.29\%_{CO_2}$, $31.23\%_{H_2}$, $3.41\ \%_{CO}$ and $29.87\%_{CH_4}$. Percent quantities of components vary as expected from methanation reactions ($3H_2 + CO \rightarrow CH_4 + H_2O$, carbon monoxide methanation) ($4H_2 + CO_2 \rightarrow CH_4 + 2H_2O$, carbon dioxide methanation), eq. (17) and (18) of paragraph "2.2.1.1". The comparison of the two streams chemical compositions inherent to the methanation processes that take place in the first reactor, shows that the quantity of methane and water in the outlet stream increases, leading to a decrease in the percentages of the reactants, especially hydrogen, as 3 moles are needed for CO-methanation and 4 moles for CO2-methanation, but also carbon monoxide and carbon dioxide which use only one mole.

As extensively discussed in the descriptive chapters of the methanation process "2.3.1", the conversion into methane must be divided into several reactors, with intercoolers interposed between them, in such a way as to introduce a stream of matter characterized by an optimal temperature of 220 °C, in order to avoid any phenomenon of thermal degradation of the materials constituting the methanation reactors (nickel). “HM1” and “HM1.1” are the first exchangers placed downstream of the first reactor. Their cooling thermal load that they must guarantee is the highest because the methanation reactor network system is designed in such a way as to have the maximum temperature of the flow of material leaving the former. The high exergetic content of this amount of removed heat can be exploited in any other section of the entire polygeneration plant. As already stated, in the thesis work there is no optimization of the management of heat flows due to the lack of pinch analysis, consequently each heat flow was hypothetically considered as recovered.

As displayed in fig. 44, the block consisting of methanation reactor and intercooler is repeated several times, for a total of four methanation reactors and six intercoolers, following the same process previously described. Table 23 below adds complementary information to the methane conversion processes, reporting the chemical compositions of the stream at the inlet and outlet of the various methanation reactors, as well as the reference temperatures.

| Component [$\%_{mol}$] | Storage Syngas | Inlet Met1 "SYNGAS-4" | Outlet Met1 "SNG-1" | Outlet Met2 "SNG-5" | Outlet Met3 "SNG-7" | Outlet Met4 "SNG-9" | SNG to grid "SNG-18" |
|---|---|---|---|---|---|---|---|
| **H2O** | 26,62% | 15,61% | 30,20% | 44,00% | 51,60% | 51,60% | 0,00% |
| **CO2** | 4,92% | 5,83% | 5,29% | 2,97% | 0,62% | 0,62% | 0,41% |
| **H2** | 49,20% | 52,15% | 31,23% | 12,26% | 2,28% | 2,28% | 1,23% |
| **CO** | 9,87% | 9,65% | 3,41% | 0,19% | 0,00% | 0,00% | 0,00% |
| **O2** | 0,00% | 0,00% | 0,00% | 0,00% | 0,00% | 0,00% | 0,00% |
| **CH4** | 9,39% | 16,75% | 29,87% | 40,59% | 45,50% | 45,50% | 97,83% |
| **N2** | 0,00% | 0,00% | 0,00% | 0,00% | 0,00% | 0,00% | 0,52% |
| Temperature [°C] | 20 | 220 | 700 | 519 | 332 | 238 | 25 |

*Table 23 - Molecular composition of the main streams in the methanation section*

From the point of view of temperatures, the results obtained show that the maximum value corresponds to the stream leaving the first reactor, as expected. The methanation processes end with the "SNG-9" stream, composed of $51.60\%_{H2O}$, $0.62\%_{CO2}$, $2.28\%_{molH2}$, about $0,00\%_{molCO}$ and $45.50\ \%_{molCH4}$. The values obtained are in line with the chemical compositions of the reference works by D. Ferrero [89] and E. Giglio [90], in which the chemical compositions of the streams entering and leaving the reactors are reported, allowing a direct value comparison. The initial content of $H_2$, CO and $CO_2$ decreases drastically compared to the initial conditions, making way for $CH_4$ and $H_2O$. The last steps necessary for placing the SNG produced into the network initially involves the complete removal of the water content, increasing its energy content, because, in the event of combustion, a compound with a high water content drastically decreases its performance due to the absorbed heat that would be used for the evaporation of water instead of being used for the activation of combustion reactions. Finally, a quantity of nitrogen is added through a dedicated supply line, in order to obtain the appropriate values of WI, GG and HHV necessary for the correct insertion into the network.

Water separation occurs with the adoption on Aspen of a flash unit component, "DRUM", present downstream of the methanation processes in the reactors. This component receives at the input the "SNG-11" stream which is characterized by a liquid-vapor phase due to the lowering of temperature occurred in the last heat exchanger, "HM5", which brings it to the conditions of 25 °C at a constant pressure of 32.4 bar. Inside the drum component, represented by the below fig. 45, the two-phase mixture undergoes partial vaporization processes, passing inside a series of rolling valves with variable section. This process allows the separation of the phases by producing the concentrated SNG, "SNG-12", towards the top and liquid water with impurities from below. The stream of the lower line passes inside a filter, "SOUR", implemented on Aspen as a separator component, in such a way as to produce a stream of pure "WOUT-2" water and "IMPURITY" impurities consisting of a reduced stream of $CH_4$, $CO_2$ and $H_2$. Hypothetically, this almost negligible final stream rich in methane is recirculated at the inlet of the methanation section, mixing with the "SYNGAS-1" stream without changing its composition. The distilled water, on the other hand, is reintegrated inside the rSOC section in the water supply line.

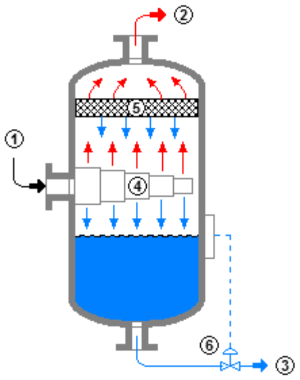

*Figure 45 - Drum, flash unit by MbeyChok*

The upper line stream continues its journey up to the "SIEVE" component, represented on Aspen as another separator unit. In fact, it has the task of removing the last residues of water from the SNG stream, obtaining a stream free, “SNG-13”, at conditions of 25 °C and 32.4 bar. This stream, belonging to the SNG line, joins the nitrogen line through the "MIX3" component which allows the mixing of the two substances.

Before reaching the mixer, the SNG stream is fed into a series of components consisting of two compressors, "SNGC1" and "SNGC2", characterized by a mechanical efficiency of 70 %, and a heat exchanger, "SNGINT", interposed between them. The aim is to reach an operating pressure of 60 bar in two steps, maintaining a low temperature in order to avoid self-ignition problems resulting from high temperatures and above all from the high content of flammable material. Mixing with $N_2$ has precisely this safety function, also decreasing the energy content (HHV) contained.

For the nitrogen line, it was hypothesized that the input stream "N2IN-1" is composed entirely of nitrogen. Therefore, all oxygen separation processes are neglected. The approximation is validated by the fact that, from the rSOC section (for both operating modes), streams of depleted air are produced, i.e. with a significantly reduced percentage of oxygen due to electrochemical reactions. Consequently, the operating costs that would have to be considered in the purification of the depleted air for the production of pure nitrogen as well as the investment cost relating to the machinery used for the separation are neglected, and the presence of a nitrogen storage is excluded. The methanation operations were managed in such a way as to operate with a constant flow rate for the entire period from July to December 2018. Returning to the nitrogen line, it is introduced at atmospheric conditions of 25 °C and 1bar. It is compressed in two steps, up to 60 bar and cooled between one compression and the next in order to recover heat and avoid overheating of the compressor components.

In the "MIX3" mixer, the two lines are mixed in such a way as to obtain an SNG with the characteristics necessary to enter the network. The last step involves its temperature decrease, up to 25 °C, in order to avoid fires and explosions in the distribution line.

### 4.6.1 CB and DS of Methanation' section

The plant was designed to represent the behaviour of the methanation section through a single simulation. Basing on the calculations that will be discussed in the paragraph relating to the sizing of the syngas storage, the operations will be carried out with a constant volume flow of 4.4272 $m^3/h$, referred to the operating conditions of the storage. This affects the setting of the DS and CB, clearly simplifying the problem. Specifically, only two DSs were needed to obtain a complete and rigorous description of the system.

The first DS had the sole purpose of varying the recirculated fraction "RICIRC" until the temperature convergence at the outlet of the first methanation reactor, set at 700 °C. Without recirculation, the mole fraction of methane would have been insufficient for an optimization of the methanation processes, reaching outlet temperatures of the first reactor below the target value. This aspect is also shown in tab. 23, in which the molar percentage of methane in the syngas in the storage is 9.87 %, while that at the inlet of the first methanator (mix with recirculation) is higher than 16.75 %.

On the other hand, the second and last DS aims to obtain an SNG at the output, referring to the "SNG-18" stream, characterized by a GG value of 0.555. The Gas Gravity variable, as known from Eq. (169) of paragraph "4.5.2", derives from the ratio between the molecular mass of the SNG that is intended to be introduced into the network and the molecular mass of the air. To obtain the required target value to be respected, imposed by the Italian legislation, the flow of pure nitrogen introduced into the system is varied. This stream is inert in the classic combustion processes. Consequently, in the event that the SNG stream undergoes heating, the greater the quantity of nitrogen, the greater will be the share of heat absorbed and wasted. It is common practice to increase the nitrogen share to decrease the higher calorific value (HHV), but also, as in this case, to modify the molecular mass / density of the SNG. Therefore, by controlling the nitrogen it is possible to obtain a SNG flow that respects all the input characteristics.

### 4.6.2 Performance parameters, results of the Methanation' section

The final paragraph of the methanation section reports and analyzes the results obtained from the simulation. Unlike the other sections of the system previously discussed, only one simulation was required to represent its behaviour. This operating mode derives from the fact that, considering the possibility of storing the syngas produced by the co-electrolysis section, it was decided to operate in stationary conditions in the methanation plant, without interruptions, from July to December 2018. The planned operation of 24 hours a day in the foreseen months has made it possible to minimize the operating costs of the plant and to optimize its production, avoiding all transients relating to switching on and off, which would have caused a portion of heat to be supplied to keep the plant components in hot stand-by conditions.

The operating time of the plant already expected in the modeling phase, is confirmed by the results proposed by Matlab, operating 4056 hours per year, represented by a utilization factor of approximately 46,3 [%].

| Process Parameters | Results | Units | |
|---|---|---|---|
| Input Syngas | 391,99 | tons/y | **SUM** |
| | 17971,44 | m3/y | |
| Output SNG | 126,65 | tons/y | |
| | 2891,29 | m3/y | |
| $BOP_{th}$ | 308,592 | $MW_{th}$ | |
| $BOP_{el}$ | -4,805 | $MW_{el}$ | |
| Wobbe Index | 49,54 | [/] | **ARITHMETIC MEA** |
| Gas Gravity | 0,555 | [/] | |
| $HHV_{SNG}$ | 36,90 | MJ/kg | |
| $LHV_{SNG}$ | 778,96 | kJ/mol | |
| Global Efficiency (co-el+METH) | 82,03 | % | |

*Table 24 - key parameters result summary of Methanation section*

Table 24 shows the most important process parameters. Firstly, the annual mass or volume flow rate of the treated syngas, respectively of 391.99 t/y and 17’971.44 m$^3$/y, calculated at the storage conditions of 20 °C and 32.4 bar. This stream is produced in the co-electrolysis section, stored in the suitably sized storage and finally sent to the methanation section, referring to the storage operating conditions indicated above. By comparing the value of the annual volume flow with the one of the co-electrolysis section, a perfect congruence is obtained. In fact, in the case of the electrolyser, the value obtained under the same physical conditions corresponded to 17’956.8 m$^3$/y, referred to in table 16 in "4.3.2", committing an error of 0.081%] compared to the one calculated for the methanation section.

The second flow is the output of the SNG produced. Also in this case its value is reported referring to the mass, equal to 126.65 t/y, and to the volume, 2891.29 m$^3$/y. In this case, the volumetric flow rate is significantly lower, due to the pressure of 60 bar of which it is characterized. From a mass point of view, instead, it can be stated that 32.31 % of syngas is converted into SNG. The percentage may appear low but the high initial content of water present in the syngas must be considered, as well as the nitrogen flow rate that has been added to normalize the input variables to the values suitable for the introduction into the distribution network. Moreover, it is also necessary to consider the small losses of useful methane which are recirculated in the system, through the “IMPURITY” stream. Overall, the value obtained is considered more than acceptable, also because, thanks to the methanation reactions, about 96 % of carbon dioxide and carbon monoxide are converted into biomethane, avoiding their release into the atmosphere.

The powers are quantified by the variables $BOP_{th}$ and $BOP_{el}$. They consider all the components present in the system, divided solely on the basis of their thermal or electrical behaviour. The thermal contribution of the system is equal to 308.592 $MW_{th}$ and is uniquely represented by the heat exchangers. Its positive value indicates that, overall, the amount of heat present in the methanation section must be removed, especially in the refrigeration exchangers interposed between the methanation reactors, resulting in a useful effect if this heat is exploited. On the other hand, the electrical contribution of -4.805 $MW_{el}$ deriving from the compressors is obviously negative, thus decreeing a net consumption of electricity. Fortunately, the value necessary for the compression operations is not very high when compared with the thermal gain.

Among the parameters represented as average value (actually directly corresponding to the simulation value due to the operability in stationary conditions), there are the final values of GG, WI and HHV that characterize the "SNG-18" stream to be entered in network. By comparing the values with the acceptability ranges expressed in paragraph “3.4”, the validity of the data obtained is demonstrated. The energy value in molar terms of the calorific value has also been reported, equal to 778.96 kJ/mol. Such value is of primary importance for the determination of the variable described below.

The last variable shown in the table is the most important, since it represents the overall efficiency of the system. The global term derives from the fact that a more extensive system is considered, including both the co-electrolysis section and the methanation section, in such a way as to consider the entire life cycle of the syngas, from its formation to its conversion into SNG. The efficiency used to evaluate the performance of the two combined plants is calculated using the following eq. (177):

$$\eta_{globale} = \frac{LHV_{SNG18}}{\Delta h_{globale}} \tag{177}$$

The efficiency value is calculated using the useful effect of the energy contained in the SNG output stream on the numerator, and on the nominator the amount of energy required for the production of the gas. This is represented in terms of enthalpy change, and is calculated according to the following eq. (178):

$$\Delta h_{globale} = \Delta h_{co-electrolysis} + \Delta h_{methanation} \tag{178}$$

Obviously, the global enthalpy variation takes into account the energy variations that occur in both sections. In the case of the electrolyser, the change in energy can be calculated as the enthalpy difference between products and reactants of the global co-electrolysis reaction, eq. (180), i.e. the one that takes into account in a single chemical reaction both the electrolysis of water and the electrolysis of carbon dioxide, eq. (179):

$$3H_2O + CO_2 \rightarrow 3H_2 + CO + 2O_2 \tag{179}$$

$$\Delta h_{co-electrolysis} = 3h_{H_2} + h_{CO} + 2h_{CO_2} - 3h_{H_2O} - h_{CO_2} \quad (180)$$

The specific enthalpy values for each component were obtained from the textbook [97], considering the operating temperature of the SOEC equal to 850 °C. In the end, an endothermic positive value of 1140.50 kJ/mol was obtained.

As regards the enthalpy variation of the methanation section, the enthalpy variations of the methanation reactions come into play. In fact, the final value was obtained considering the reference enthalpies present in the literature and previously reported in eqs. (17) and (18) of paragraph "2.2.1.1", according to a proportion of 2/3 for CO-methanation and 1/3 for $CO_2$-methanation. These proportions were obtained considering the molar fractions relative to the two compounds in the “SYNGAS-1” stream entering the methanation section, obtaining a final value of -190.87 kJ/mol, an indicator of the exothermic behaviour of this section.

By adding the two contributions, a net value of approximately 949.63 kJ/mol is obtained and, applying eq. (178), an overall efficiency value of 82.03% is obtained. This value indicates the level of thermodynamic affinity between the two plant sections. Furthermore, the high value prefigures an excellent match, avoiding the fact that in the future, plants of this kind can be built in place of the extraction of new fossil fuels, thus avoiding the depletion of environmental resources.

## 4.7 Modelling and results of $H_2$ storage system

The steam-electrolysis section of the plant considered allows the production of hydrogen, operating the first two days of energy surplus of the photovoltaic field. The storage of excess energy in the form of chemicals is a very important concept for stabilizing the fluctuation of renewables. To optimize this aspect, the hydrogen energy vector produced is stored, so that it can be resold at a later time.

From the point of view of storage sizing, considering the dependence on the fluctuation of solar radiation, the resulting weekly production is calculated, visible in the following fig. 46. The timing chosen derives from the fact that, to avoid an excessive size of hydrogen gas, the storage was discharged weekly to supply a refilling station.

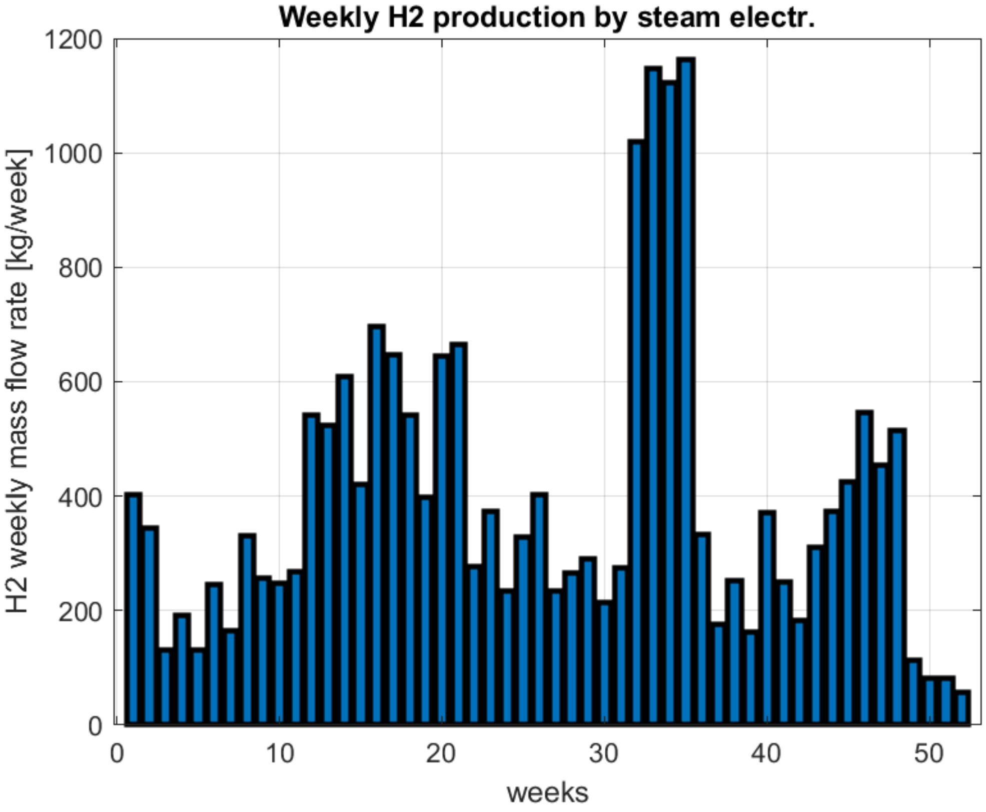

*Figure 46 - Weekly $H_2$ production by the steam-electrolysis*

The trend shows a lower weekly production in the first and last weeks of the year, and a high production during the summer months, specifically from the 32nd to the 35th week (the month of August), producing globally in a year 20.430 $t_{H2}$/y, as also reported in table 14 in "4.2.2". By dividing the total production value by the 52 weeks of the year, a weekly mass flow rate of 392.88 $kg_{H2}$/week is obtained, which will be emptied from the storage section and transported to the refilling stations. Due to the low production in the first weeks it is necessary to consider an initial quantity of hydrogen, which allows to always have a positive quantity or at least null of substance stored. From the calculations carried out and as shown in the following fig. 47, a minimum initial quantity of 1607.9 $kg_{H2}$ is required. Since the mass balance between the input and output of hydrogen is zero during the year, the final quantity of hydrogen present in the storage on the last day of the year will correspond to the initial one on January 1st. Consequently, this initial quantity should only be considered as an additional cost of the first year for an economic analysis.

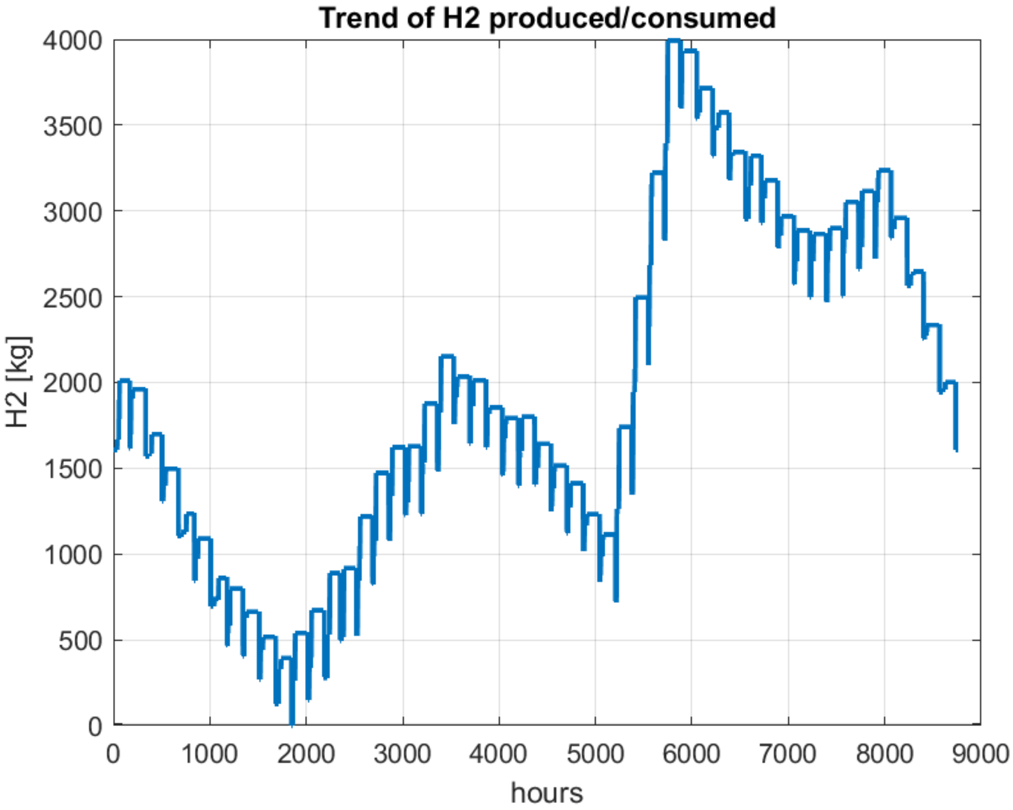

*Figure 47 - Mass balance in H2 storage*

Fig. 47 is the final result obtained from modeling by using an algorithm created specifically on Matlab. As can be seen, the size of the hydrogen storage, in the conditions of compressed gas at 20 °C and 250 bar, will be equal to 4000 kg. The storage pressure was obtained by consulting the contemporary literature, especially the work of A. Calvo [86], who reports a study of an electrolyser coupled to a hydrogen refilling station for heavy public transport (bus).

As regards the transport of the hydrogen produced, the Tube-Trailer mode was used, basing on the reference [130], a text in which the available techniques for the transport of hydrogen in the current state of the art are described with high accuracy. The Tube-Trailer technology involves the transport of hydrogen inside pressurized pipes at different values with the use of heavy trucking. By increasing the storage pressure of the pipes, the quantity of hydrogen stored increases but also the transport costs significantly increase. Therefore, the weekly frequency chosen to load the trucks used derives from a trade off that takes into consideration the cost of storage, the cost of transport and the environmental effect deriving from the exhaust fumes of road haulage.

Basing on text [130] it was possible to choose the most appropriate configuration for transporting hydrogen from the storage section to the refilling station, a device that allows cars to refuel with hydrogen. The following list summarizes the features of the implemented Tube-Trailer:

- It was decided to operate with trucks capable of transporting four steel tubes with a diameter of 26 inc (66.04 cm) at a storage pressure of 250 bar;
- The maximum $H_2$ payload for this configuration is 250 kg, that is the maximum payload that each tube could carry;
- Maximum percentage of $H_2$ volume occupied in the ISO container is the 20% of the maximum payload, therefore in each pipe pressurized at 250 bar it is possible to transport a maximum of 50 $kg_{H2}$;
- Maximum 200 miles delivering from the production facility;
- Cost of transportation for $H_2$ storage at 250 bar is 245 $/kg. This economic data is reported in order to complete the information provided on the technology, but it is redundant for the purposes of the thesis as the economic part does not take into account transport, a cost that would be borne by the owner of the refilling stations.

In the examined case, the chosen configuration is optimal: by considering to unload the 392.88kg of hydrogen produced inside eight pipes (thus using two trucks of the chosen configuration), the following quantity of hydrogen per pipe would be obtained: 392.88 / 8 = 49.11 $kg_{H2}$. Comparing the data obtained with the maximum capacity of 50 $kg_{H2}$, it can be deduced that 98.22 % of the available space is used, thus optimizing the quantity of hydrogen transported.

## 4.8 Modelling and results of Syngas storage system

The last polygeneration plant section analyzed in the thesis concerns the syngas storage section. The presence of this device allows an optimal coupling between the co-electrolysis section and the methanation section, allowing the latter to operate in stationary conditions at a constant flow rate.

Therefore, the sizing of the storage takes into account the maximum volumetric flow rate of syngas produced in the co-electrolysis section, equal to 17’956.8 $m^3$/y at the conditions of 20 °C and 32.4 bar, exactly those coming out of the syngas from the co-electrolysis section. By choosing to operate continuously, 24 hours a day, from the beginning of July to the end of December, and assuming that in this period no malfunctions or failures occur, which would cause a temporary shutdown of the plant, the Matlab program allows to obtain a value of 4056 annual operating hours. By dividing the two data, the constant volumetric flow rate is obtained, equal to 4.4272 $m^3_{SYNGAS}$/h sent hourly from the storage to the methanation section during the period considered.

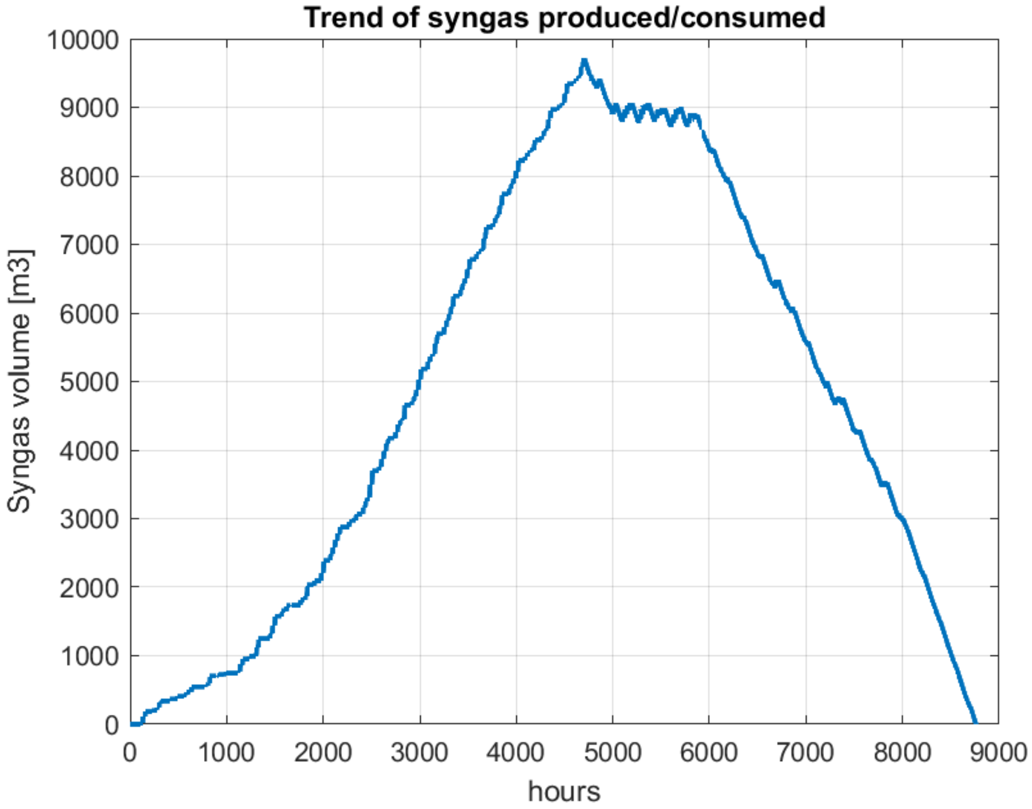

*Figure 48 - Mass balance in syngas storage*

Figure 48 shows the final result obtained by the algorithm created specifically on Matlab to define the size of the storage, which is 9’718 m$^3$, rounded up to 10000 m$^3$. The proposed trend follows the perspective in which the positive flow entering the storage is that of the co-electrolysis section, which grows strictly more, until it reaches its peak on the last day of June. Subsequently, the mass balance is carried out where, in addition to the portion produced, the portion taken and sent to the methanation section is also considered. As can be seen, the sizing of the storage allows to obtain a zero net annual budget, without investment costs related to an initial supply of syngas.

# 5 Economic Analysis

To conclude the thesis work, once the technical part is completed, the system is analyzed from an economic point of view, in order to provide information on the actual realization.

The information necessary for the quantification of costs will be obtained from the literature, using as main reference Richard Turton's text [131], a cornerstone for the technical and economic description of chemical processes in general. The use of this source allows to estimate the investment cost of the components, CAPEX. Furthermore, reference will be made to external texts such as scientific articles, or technical data sheets of companies for the determination of operation&maintenance (OPEX) and replacement costs (REPL).

## 5.1 Methodology of Net Present Costs

The economic description provided for the thesis plant is very basic, it is based on the concept in the Net Present Cost (NPC), i.e. the determination of the total expenses attributable to a plant during the entire duration of its life referring to the present. This data is the basis for the determination of other different economic indicators and, is the very useful for the comparison between different plants, managing to compare different technologies with each other. For instance, five different NPCs are calculated for the thesis work, one for each section of the plant (photovoltaic, rSOC but also SOFC, methanation and CCS) quantifying them in current-year dollar [$\$_{2018}$].

$$NPC = CAPEX_0 + \sum_{j=1}^{T}\left[\frac{OPEX_j}{(1+d)^j} + \frac{REPL_j}{(1+d)^j}\right] \tag{181}$$

Eq. (181) represents the general formula of the NPC and the following list summarizes the terms that compose it:

- T is the analysis period, in years, corresponding to the plant's lifetime;
- d is the corrected discount rate, considering an expected inflation rate. It represents the economic interest to which a certain component is subject, in case of its value must be carried forward to a year different from the reference year (today) or vice versa, bringing a future value back to the present value, hence by calculating its real cost;
- $CAPEX_0$ are the capital expenditures (including transport and installation costs) due to investments performed at the beginning of the analysis period (i.e., j = 0);
- $OPEX_j$ represents the costs attributable to the operational phase of the reference component such as the heat necessary to reach the operating temperature levels, the consumption of electricity and so on. But it also takes into account the maintenance costs necessary to keep it running properly

(including ordinary and extraordinary maintenance). The subscript j indicates that it refers to the j-th year;

- $REPL_j$ are the replacement costs. They refer to the periodic reinvestment/regeneration to maintain reliable the operation of the system. It includes all related transport and installation costs of the new/regenerated units.

As stated in the introduction, knowing the investment, operation, maintenance and replacement values, using eq. (181) it can be easily calculated the associated cost value. The difficulty lies in identifying the correct value, sometimes due to too many options available and sometimes to the difficulty in finding the information.

In order to extend the economic analysis to the entire life of the plant is used the discount rate variable, d, obtainable directly from banking sources in the event that the economic analysis is a real case, or, as in this thesis work, it can be calculated through an economic formulation, expressed by the following eq. (182), also used in references [86] and [132]. In this way it is possible to determine any future cost at the present value:

$$d = \frac{d^{I} - ir}{1 + ir} \tag{182}$$

It's a compound value, resulting from the use of other economic variables such as the nominal discount rate d' and the inflation rate *ir*. The values chosen are respectively 7% and 2%, following the indications of the reference scientific papers [86] and [132], obtaining a final value equal to 4.9%. The inflation variable represents the effect of the price increase of an asset in general, while the nominal discount rate allows to convert the cost into an annuity for a reference year, without taking into account the effect of inflation.

Usually, when calculating an investment cost (CAPEX), it refers to a reference size. To change the purchase cost obtained, depending on the size of the device, the scale dependency formula must be performed, represented by the following eq. (183):

$$cost = \left(\frac{S}{S_{ref}}\right)^{n} * \frac{cost_{ref} * S_{ref}}{S} \tag{183}$$

The components of the equation are:

- cost [\$/unit] is the specific CAPEX of the equipment in the real size condition;
- S [unit] is the size of the equipment;
- $cost_{ref}$ [\$/unit] represents instead the specific CAPEX of the same equipment with reference size $S_{ref}$ [unit];

- n is an exponent that expresses the increase in cost as the size increases. It is not known a priori, therefore the six-tenths-rule will always be used, an empirical formulation that gives a value to n of 0.6.

The last effect that is imperative to mention, as it occurs with high frequency, is the effect of time on purchased equipment cost. In these cases, it must be taken into account that, depending on the reference text used, the information on the purchase cost of the component could refer to a different time period than the current-value considered. Consequently, as in the case of the size of the component, the cost must be brought back to the current time using a general formulation represented by the following eq. (184):

$$\frac{C_1}{C_0} = \frac{I_1}{I_0} \tag{184}$$

The components of the above equation are:

- $C_i$ is the purchansing cost, 1 means that is referred to the time when the cost is desidered, while 0 is referred to base time when cost is known;
- $I_i$ is the index cost, the subscripts are referred to the same time of above.

The index costs are variables that allow to perform the time conversion, determined by archives such as the Marshall and Swift Equipment Cost Index (MSECI) or the Chemical Engineering Plant Cost Index (CEPCI), which have been drawn up by government agencies in collaboration with experimental data obtained from companies over the years.

| Year | MSECI | CEPCI |
|---|---|---|
| 2001 | 1094 | 393 |
| 2018 | 1457 | 511 |

*Table 25 - Index Costs for Polygeneration Plant*

Table 25 shows the indices used, filtered between the various years available. The year 2001 derives from the fact that Turton's text [131] reports costs derived from the year 2001. 2018, on the other hand, is the reference year to which all the real costs obtained will have to be converted.

Once the explanation of real costs at current time is concluded, in the next paragraph is specified the references chosen to identify the CAPEX, OPEX and REPL economic variables.

## 5.2 Polygeneration component costs estimation

The cost determination of the component was carried out in order to find its specific reference cost value. Subsequently, the value was modified according to the scale and time dependency, known the size and the reference date, for each related plant.

Consequently, this parameter is going to indicate, one per sub-paragraph, the values obtained for the calculation of the reference cost.

### 5.2.1 Photovoltaic plant

The costs attributed at the photovoltaic section are obtained by following the reference text [133], in which the price expressed derives from a trend cost analysis of the last 40 years. In fact, it demonstrates how the cost referring to the module component alone has drastically decreased from 24-26 [€/$W_p$] in 1980, to 0.29 [€/$W_p$] in 2018, due to the increase in the production of this technology. It was estimated that the price dropped by 24% with each doubling of production capacity and, as can be seen from the costs reported, in the last 38 years this process has occurred more than six times, without any inversion or stabilization of the trend in the future, making therefore presage a further decrease in the years to come.

Taking into consideration the data available in [133], an overall investment cost of 1300 [$/kW] was estimated, consisting of actual 800 [$/kW] with a breakdown of the costs represented in next table 16, and a percentage equal to 70% of the CAPEX for Engineering Procurement & Construction (EPC), which express the costs necessary for all the engineering services responsible for carrying out the design, the procurement costs of materials and those relating to the construction and supervision of the work.

| COMPONENT | SHARE OF TOTAL COST |
|---|---|
| Module | 51% |
| Inverter | 11% |
| Substructure and fence (steel) | 11% |
| BOP | 9% |
| Construction & Transport cost | 16% |
| Transformer | 2% |

*Table 26 - PV CAPEX costs share*

The cost reported refers only to CAPEX, for a plant characterized by modules with an efficiency of 21% and a lifetime of 25 years. Considering the high level of quality achieved for this technology, it is assumed that both OPEX and REPL costs are neglected. For photovoltaics, the operation costs are significantly lower than maintenance costs such as cleaning the panels or checking the electrical components by a specialized technician. However, considering the high quality of the component, as mentioned, they can be neglected. The same applies for the replacement costs, which do not need to be taken into account also because the calculations of the NPCs are carried out considering the Polygeneration plant lifetime of 25 years.

The following table 27 shows the costs that have been attributed to this technology.

| CAPEX [$/kW] | OPEX [$/kW] | REPL [$/kW] | LIFETIME [y] | REF. |
|---|---|---|---|---|
| 1300 | negl. | negl. | 25 | [133] |

Table 27- PV system economic information

## 5.2.2 Reversible Solid Oxide Cell

The electrochemical device is the heart of the entire polygeneration plant, as it communicates with every other plant's section. Studies relating to this modern technology are becoming increasingly frequent, giving the possibility for further improvements, in view of a future increase in production deriving from the conditions of technological maturity. In addition to studies based on the physical aspects of the electrochemical device, those based on economic analysis are also gaining ground. Unfortunately, since the technology is too recent, it is not present on the Turton [131], but by consulting the contemporary literature it is possible to obtain a modest number of data. It is difficult to identifying the information necessary for a pressurized rSOC, operating both in electrolysis and as a fuel cell, due to a lack of available data. It is much easier to identify formulas for quantifying the costs associated with only one of the two operating modes. For instance, in the study by Proost et al [134] the specific cost [€/kW] is reported as a function of the operating power that a fuel cell is able to product, eq. (185):

$$c_{spec,FC} = 23364 P_N^{-0,404} \tag{185}$$

On the other hand, in the work of Marocco et al. [132] an alternative formula is given to quantify the specific cost [€/kW] of a PEMFC with a size of 10 kW. Despite the electrochemical device differs from the one used in this thesis work, as it is characterized by low operating temperatures and especially by dynamic rather than stationary behaviour (better as engine than generator, for instance), it is nevertheless reported in the following eq. (186), in order to provide a broader analysis of the costs of these important devices. The formula uses the size of the device to find the cost:

$$c_{spec,FC} = 3947 \frac{10}{P_N} \left(\frac{P_N}{10}\right)^{0,7} \tag{186}$$

In the document by Roland B. [136], a series of tabulated values are reported as a function of the power produced by the SOFC. Taking into consideration an interpolated value between those available of 5 and 10 MW, a value equal to 2000 [€/kW] was obtained, a specific cost which is supported by the work of Julich F. [143].

With regard to OPEX costs, including device maintenance, the article by Marocco et al. [132] provides as indication a value equal to 3% of the costs obtained from the CAPEX. This percentage finds support in a large number of scientific articles in the literature, such as [138] and [139]. The consulting firm Tractebel and Hinicio wrote a report [140], in which it is possible to find a formulation, eq. (187), of these costs carried out by partializing different contributions:

$$OPEX = 4\%CAPEX * \left(\frac{1}{3} + \frac{2}{3} * \frac{h_{real}}{8760}\right) \quad (187)$$

The formulation attributes to the operation and maintenance costs a value equal to 4% of the CAPEX, adjusting fixed costs by one third, while variable costs for two thirds, depending on the actual operation time of the plant (utilization factor).

As for the REPL, the article by Marocco et al. [132] gives a cost equal to 35% of the CAPEX, finding support in the text proposed by the Hinicio agency, [140]. The work of Kalici et al. [141] uses the same concept of determination, but with a percentage of 27% referred to CAPEX, as for the study conducted by Santos M. et al. [142] which attributes a value of the percentage equals to 26.27% [(2 * 0.4 / 3)*100] of the CAPEX.

Finally, the choice of rSOC component's lifetime is discussed. Basing on the works cited above and, taking into consideration also other rSOC studies such as the work of Ferrero D. [89], it is possible to identify 40 thousand operating hours. Considering that in the Thesis work, the electrochemical device operates all the 8760 hours of the years, each year (thanks to a simplifying hypothesis), the replacement intervals could be approximate equals to 5 years.

| CAPEX [$/kW] | OPEX [$/kW] | REPL [$/kW] | LIFETIME [y] | REF. |
|---|---|---|---|---|
| 2000 | - | - | - | [136],[143] |
| - | 3%CAPEX | - | - | [132],[138],[139] |
| - | - | 35%CAPEX | - | [132],[140] |
| - | - | - | 5 | [89],[119],[132] |

*Table 28 - rSOC system economic information*

Table 28 shows the final values chosen to represent the costs of the rSOC, downstream of the economic investigations conducted and reported above. Considering a future perspective, it is still intended to report the notions deriving from the scientific study by Schimidt O. et al. [137], who states that in 2030, the SOC technology (specifically speaking of the SOEC mode) will significantly increase its production, reaching investment costs between 1050 and 4250 [€/kW].

### 5.2.3 Absorber and Stripper

The absorption and the desorption columns are the main components for the CCS section. According to [144], for the estimation of these cost of equipment there are basically three paths to follow. The best with the highest degree of accuracy is to have the price and various information relating to operation and maintenance costs available directly from a supplier.

The second choice involves obtaining costs using similar systems. The third and less accurate choice lies in the use of texts in which correlations or descriptive graphs of the component are reported.

In this case, it was chosen to follow the third way basing on Turton [131] as a reference text, in which it is possible to find a vast collection of data for many components used in chemical processes. According to the reference text, the investment cost of the component can be obtained by applying a formula, shown in the following eq. (188):

$$CAPEX = C_p(B_1 + B_2 F_M F_P) \tag{188}$$

Both columns are categorized as Vertical Process Vessel. The determination of its initial investment cost is based on the Material Factor ($F_M$) and on the Pressure Factor ($F_P$), two variables that can be calculated from case to case, and on two constants, $B_1$ and $B_2$, which have fixed values that depend on the type of component.

Proceeding in order, all the parameters are describe keeping in mind that these formulas implemented by Turton [131] are used not only for these components, but also for many other different equipment types.

According to Turton [131], the term $C_P$ corresponds to the equipment cost data, which takes into account only the size variation of the component respect to the reference value, which is the volume [$m^3$] for vertical process vessel, calculated according to the following eq. (189):

$$\log_{10}(C_P) = K_1 + K_2 \log_{10}(A) + K_3[\log_{10}(A)]^2 \tag{189}$$

The variable A corresponds to the size of the component, characterized by its unit of measurement. $K_1$, $K_2$, $K_3$ are constants that can be obtained from the Turton tables [131] by choosing the specific type, for instance in the case in question, the component is a Process Vessel, and its specific characteristic is Vertical (there are also parameter values for the Horizontal case). In the event that the size of the component, A, belongs within the validity range of the formula, it can be implemented directly. If A's size is superior or less, it is necessary to calculate the equipment cost data for one of the two limits, and then apply the formula of the scale dependency, eq. (183), bringing it back to its real size.

The calculation of the pressure factor $F_P$ aims to consider in economic terms the effect of the pressure to which the component is subjected. As the operating pressure level increases, the cost increases because it will be necessary to use a more complex component from the design point of view and therefore with a lower but more controlled production. In the case of vessel components, the pressure factor is calculated with a specific equation that can be used only for these equipment types, expressed by the following eq. (190):

$$F_{P,vessel} = \frac{\frac{(P+1)D}{2[850-0,6(P+1)]}+0,00315}{0,0063} \tag{190}$$

The empirical formulation reported by Turton [131] allows the calculation of the pressure factor, known the pressure of the device P and the diameter of the vessel D.

As regards the material factor $F_M$, this variable has the function of taking into account the material with which the component was built. Rarer and more precious materials obviously increase the price of the considered device. Therefore, the value is obtained directly from the tables, with the only requirement to know the construction material which, for the case in question of the absorber and stripper, is stainless steel.

The last data required to obtain the cost of the CAPEX, referring to the year 2001, are the constants of the Bare Module Factor, $B_1$ and $B_2$. Their value is simply determined in the same way as the other constants $K_1$, $K_2$ and $K_3$, i.e., with the use of a special table which only requires knowledge of the specific type of component (vertical process vessel).

| $K_1$ | $K_2$ | $K_3$ | $F_p$ | Material | $F_m$ | $B_1$ | $B_2$ |
|---|---|---|---|---|---|---|---|
| 3,4974 | 0,4485 | 0,1074 | 0,62 | SS | 3,1 | 2,25 | 1,82 |

*Table 29 - Vertical Process Vessel constants' value (Absorber & Stripper)*

Table 29 shows the values of the constants obtained for the calculation of the CAPEX. The last step consists in converting the value of the investment cost obtained and bringing it back to the value for the year 2018 in question. The time dependency formula is therefore used, eq. (184).

Regarding the determination of OPEX, it is not possible to refer to Turton [131], consequently a review of scientific articles of the literature was made in order to identify appropriate values from projects in which very similar components were present. According to the text by Akinola et al. [105], the value of the OPEX derives from the sum of the costs attributable to the maintenance and operations of the component, for a value respectively equal to 3% and 1% of the CAPEX. The study by Bassano C. [145], on the other hand, defines the OPEX value of an absorbent/desorbent column equal to the sum of the Fixed Operating Cost (FIX) and Variable Operating Cost (VOC), attributing a value respectively equal to 4% and 1.2% of the CAPEX, adding more a percentage equal to 50% FIX, attributing it to the cost of personnel assigned to the management of the components. Overall, a value equal to 7.2% of the CAPEX is obtained:

$$OPEX = FIX + VOC + WORKES = 7{,}2\%CAPEX \tag{190}$$

Lastly, for the calculation of replacement costs (REPL), the scientific article written by Mulet A. [146] is referred to, which considers a total value approximated by excess to 14% of the CAPEX, attributable for a 10.63% by shell cost and 3.35% for the platform cost.

| CAPEX [$/kW] | OPEX [$/kW] | REPL [$/kW] | LIFETIME [y] | REF. |
|---|---|---|---|---|
| Eq.(188) + eq.(183) | - | - | - | [131] |
| - | 7,2%CAPEX | - | - | [145] |
| - | - | 14%CAPEX | - | [146] |
| - | - | - | 10 | [105], [144] |

*Table 30 - Absorber and Stripper economic information*

The final table 30 summarizes the values adopted for the economic analysis related to this component. The useful life of the components has been set at 10 years, which is equivalent to two replacements in the 10th and 20th years of the polygeneration plant.

## 5.2.4 Methanation Reactor

Methanation reactors are the main components of the methanation section. The determination of the CAPEX takes place in the same way as for the absorber and stripper, since even the methanation reactors belong to the type of vertical process vessel. Unlike the components of the CCS, whose length and diameter were known, for the adiabatic reactors of methanation the data is not available. Consequently, the work of Giglio E. [135] is considered, which relates to the useful database in the scientific report [147] determining the amount of initial catalyst (nickel) fills inside the methanation reactor. This data is obtained from the interpolation between the values of catalyst volume and methane flow rate. The final value obtained is increased by a further 50%, in order to obtain the fictitious volume of pressurized vessel which contains the catalyst.

As previously stated, once the volume is obtained, the procedure explained in "5.2.3" is followed to the letter, with the use of the same formulas, finally obtaining the following constant values:

| $K_1$ | $K_2$ | $K_3$ | $F_p$ | Material | $F_m$ | $B_1$ | $B_2$ |
|---|---|---|---|---|---|---|---|
| 3,4974 | 0,4485 | 0,1074 | 1,138776 | Ni alloy clad | 3,6 | 2,25 | 1,82 |

*Table 31 - Vertical Process Vessel constants' value (Methanation reactor)*

The operating and maintenance costs for the case in question are determined by the sum of fixed and variable costs. Following the indications of Gorre J. [148], the FIX are calculated, in turn, as the sum of 5% CAPEX and the cost attributed to the catalyst present in the reactor:

$$FIX = 5\%CAPEX + C_{catalyst} \tag{191}$$

The cost of the catalyst is calculated as its specific cost of 440 [$/ft$^3$] (approximately 15’538.468 [€/m$^3$]), reported by the work of Giglio E. et al. [135], for the reactor volume in ft$^3$. As regards VOCs, however, their cost is neglected because, according to [148], their value would be attributable to the auxiliary components which are already monetized separately.

Finally, the REPL costs, currently unavailable in the contemporary literature, have been obtained assuming they have the same cost as another Gibbs reactor (their component representation on Aspen), or a pre reformer. In this case, using Morocco et al. [132], a complete replacement is considered, i.e. a REPL value equals to 100% of the CAPEX.

| CAPEX [$/kW] | OPEX [$/kW] | REPL [$/kW] | LIFETIME [y] | REF. |
|---|---|---|---|---|
| Eq.(188) + eq. (183) | - | - | - | [131] |
| - | FIX + VOC | - | - | [148] |
| - | - | 100%CAPEX | - | [132] |
| - | - | - | 20 | [148] |

*Table 32 - Methanation reactor economic information*

Table 32 shows the final summary values of the economic parameters adopted for these components. The lifetime is set to 20 years, needing a single replacement intervention during the 25 years of polygeneration plant’s life.

### 5.2.5 $H_2$ and Syngas Storage

In the plant analyzed in this thesis work there are two storage devices downstream of the electrolyser processes, with the aim of storing the chemicals produced and reusing them in more convenient situations, optimizing the connection between different sections of the system.

Hydrogen storage allows this substance to be stored in the form of compressed gas at 250 bar and 20 °C. Both the pressure increase and the temperature control at an environmental value allow to decrease the hydrogen volume, in such a way as to decrease the cost of the tank due to higher storage capacity. Considering the operating methods of hydrogen production (first two days of energy surplus by PV section are dedicated to steam-electrolysis), the reference value obtained is an hourly average production equal to 41.82 kg/h, converted on a weekly scale equal to 392.88 kg/week. Considering that production falls into medium-low capacity plants, the pressure of 250 bar chosen for the storage section was the most convenient technical-economic compromise.

In his study on the costs and transport systems of hydrogen, Wade A. Amos [150] reports a series of graphs from which it is possible to obtain the specific cost per kilogram attributable to the hydrogen storage section, also depending on the amount of time the device has to perform its storage duties. Taking into consideration the pressure value and the average hourly mass flow rate, a specific investment cost of 1.1 [$\$_{1998}/kg_{H2}h$] is obtained, which, multiplied by the total annual operating time 485 hours of steam-electrolysis operation, gives a value of 531.3 [$\$_{1998}/kg_{H2}$].

The scientific study by Weinert et al. [149], on the other hand, reports a direct formulation for the calculation of its investment cost, depending on the total size, in kilograms, of the storage. The formula is shown in the following eq. (192):

$$CAPEX = \frac{1000}{1,2}\left(m_{H_2,storage}\right)^2 \tag{192}$$

In addition to investment costs, the same study states that operating costs can be calculated as 2% of CAPEX, as well as replacement costs, considering an average storage life of 20 years. The following table 33 summarizes the values used for the various economic variables.

| CAPEX [$/kW] | OPEX [$/kW] | REPL [$/kW] | LIFETIME [y] | REF. |
|---|---|---|---|---|
| 531,3 | - | - | - | [150] |
| - | 2%CAPEX | - | - | [86],[149] |
| - | - | 2%CAPEX | - | [86],[149] |
| - | - | - | 20 | [86],[149] |

*Table 33 - $H_2$ storage economic information*

On the other hand, the intermediary syngas is produced by the SOEC when it operates in co-electrolysis for the remaining days of energy surplus in the week. Considering the high pressure operations in the electrolyser section, to reduce operating costs, it was decided to store the syngas at the same pressure value of 32.4 bar but at a temperature of 20 °C, in order to avoid the expansion of the gaseous syngas caused by the kinetic content which would increase with increasing temperature. As can be seen in fig. 28 in “4.3.1“, which represents the co-electrolysis plant scheme, the “EX-1” component has the function of cooling the stream of syngas produced, so as to introduce it into the storage section under the established conditions.

The economic variables of this component are reported basing on the works of Cau G. [151] and of Cocco D. [152], in which a formula for estimating the investment cost of the storage including transport and installation is adopted. In the mentioned texts, the component belongs to the section shown by the acronym of SSS (Syngas Storage System), including not only the pressurized tank but also an auxiliary compressor capable of increasing the pressure level to the desired one. In the case in question, the part of the equation relating to the last component is neglected. The final formulation obtained is reported, expressed by the following eq. (193), whose CAPEX value is expressed in [$\$_{2011}$]:

$$CAPEX = 80000 + 65V_{syngas,storage} \tag{193}$$

$V_{syngas,storage}$ expressed in eq. (193) represents the total volume occupied by the gas at storage conditions: 20 °C and 32.4 bar, corresponding to 9718 $m^3$ i.e. the maximum size of the component.

According to the above studies, a value of operating costs is reported, which also refers to a constant with the addition of a cost, which in this case derives only from the mass flow treated in the compressor. Neglecting this last additional and unavailable cost, a value of 300 thousand [$\$_{2011}$] per year is used for OPEX. Finally, replacement costs are completely neglected even if the average life span of the syngas storage component is 20 years.

Table 34 shows the summarized values used for the economic variables:

| CAPEX [$/kW] | OPEX [$] | REPL [$/kW] | LIFETIME [y] | REF. |
|---|---|---|---|---|
| Eq. (193) | - | - | - | [151],[152] |
| - | 300000 | - | - | [151].[152] |
| - | - | negl. | - | [151],[152] |
| - | - | - | 20 | [151],[152] |

*Table 34 - Syngas storage economic information*

## 5.2.6 Turbine

The turbine expander components, in the thesis work, are not determined with the help of Turton [131] but rather by taking advantage of the data provided by the NETL (National Energy Technology Laboratory), [153]. The American research group has produced a report from which it is possible to determine the costs for many mechanical components used in industrial processes (as chemical process). The purchase costs for gas turbines, which are adopted within the plant sections, are calculated with the help of a graph. Once the type of turbine has been selected, the cost, in 1998 dollars, is directly associated with the maximum power that the component can produce, in horsepower (1 kW = 1.35962 CV).

The following figure 49 shows the graph adopted to obtain the investment cost of the component.

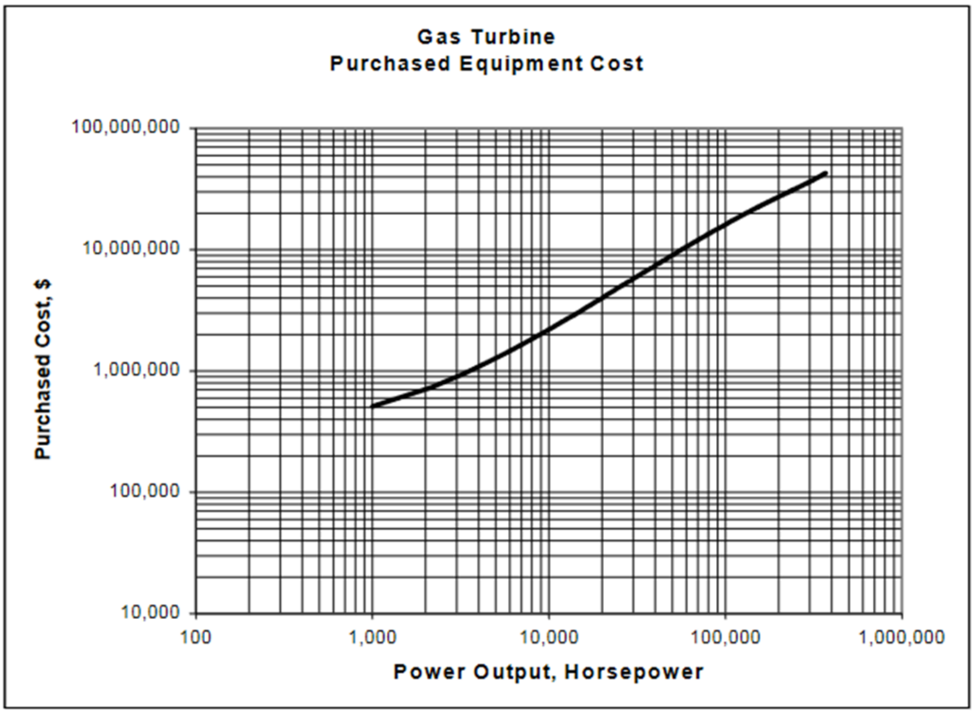

*Figure 49 - CAPEX turbine component*

Since turbines are consolidated components in the industrial field, various companies are available such as © 1995-2021 Sargent & Lundy, LLC and © Sulzer Ltd 2021 from which it is possible to obtain the value of the average useful life for gas turbines equal to 12500 total hours. Considering the three turbines that are used in the polygeneration plant, "TURB-1", operating with the anode products of the electrolyser (both co and steam electrolysis) for a total of 1746 hours per year, has a life expectancy equal to 71 years rounded down. The “C-TURB” and “TURB-SNG” turbines, operating in the SOFC section for a total annual 7014 hours, would instead have an expectation equal to 17.8 years, rounded down to 17 years.

As for the operation and maintenance costs, OPEX, to be associated with the component, it is possible to use the work by various government and/or research agencies. According to the Danish Energy Agency, their value corresponds to 11% of the CAPEX. This result is supported and confirmed by other agencies such as the IEA and the Electric Power Research Institute (EPRI). Alternatively, according to the work of Aurecon [154], the value can be obtained by making explicit the contribution of variable and fixed costs. The former would depend on the maximum power value MW capable of being produced by the gas turbine, while the latter, the fixed ones, would instead refer to the value of energy produced MWh. The two energy flows are distinguished according to a different specific cost, as can be seen from the following eq. (194), which reports the formulation adopted:

$$OPEX = 10{,}9 \left[\frac{\$}{MW\ y}\right] P_{turb} + 3{,}7 \left[\frac{\$}{MWh\ y}\right] Q_{turb} \tag{194}$$

Finally, the costs arising from the replacement of the turbine component are mentioned, which are set equal to 80% of the CAPEX, a value obtained from the research carried out in the literature and reported in the textbook of Gulen C.S. [160].

Table 35 below shows the summary economic parameters for turbines:

| CAPEX [$/kW] | OPEX [$/kW] | REPL [$/kW] | LIFETIME [y] | REF. |
|---|---|---|---|---|
| Fig. 49 | - | - | - | [153] |
| - | 11%CAPEX | - | - | Danish EA, IEA, EPRI |
| - | - | 80%CAPEX | - | [160] |
| - | - | - | 71 \| 17 | Sargent & Lundy ©, Sulzer © |

*Table 35 – Turbine economic information*

## 5.2.7 Compressor

In the economic analysis conducted, the investment cost of the compressor was calculated using the information available in the Turton textbook [131]. Depending on the value of the flow rate treated in the component, its type can essentially vary between centrifugal or rotary compressors, both belonging to the family of rotary compressors in which the increase in the pressure of the gas involved derives from the rotational movement of the impeller. The first centrifugal type was adopted for the higher flow rates involved, such as in the compressors of the air lines, while in the others, where the flow rates were reduced, the rotary type was applied.

Referring to the previous subsection concerning absorber and stripper, the calculation of the equipment cost $C_P$ is the same as reported in the paragraph mentioned by eq. (189). The reference unit of measurement is the power delivered by the compressor. The investment costs of the CAPEX component, however, are calculated according to an alternative formulation respect to eq. (188) of absorber and stripper paragraph. It is represented by the next one:

$$CAPEX = C_p F_{BM} F_P \tag{195}$$

$F_{BM}$ (Bare Module Factor) is a constant calculated thanks to the tabulated values present in the economic reference text, [131], according to the type of compressor (centrifugal or rotary) and the material used for its construction. Steinless Steel (SS) is chosen for centrifugal compressors and Carbon Steel (CS) for the other type, as the former usually operates at higher flow rates and pressures, and therefore requires a more resistant and consequently more expensive material.

Instead, as regards the calculation of the pressure factor $F_P$, the effect of the pressure to which the component is subjected in monetary terms is taken into account, using a formulation very similar to that of the equipment cost adopted in "5.2.3". Next eq. (196) represents the formula of pressure factor:

$$\log_{10}(F_P) = C_1 + C_2 \log_{10}(P) + C_3[\log_{10}(P)]^2 \tag{196}$$

As it can be seen, the setting is identical to eq. (189) except that P corresponds to the pressure value in which the component operates. $C_1$, $C_2$, $C_3$ are constants obtained from the Turton tables [131], exactly like $K_1$, $K_2$ and $K_3$ in eq. (189), known the pressure range and the type of compressor. In the case in question, the values of the constants are always zero for each type of compressor, thus producing a pressure factor always equals to one.

| $K_1$ | $K_2$ | $K_3$ | $F_P$ | Material | $F_{BM}$ |
|---|---|---|---|---|---|
| 0 | 0 | 0 | 1 | SS | 5,75 |
| 0 | 0 | 0 | 1 | CS | 2,8 |

*Table 36 – Centrifugal and Rotary Compressor constants' values*

The literature reports alternative formulas for the calculation of CAPEX. For instance, the references [135] and [157] show that this cost can be approximated at the value of 4500 [$/kW$_{el}$], where the electric power is the one needed to sustain the compressor operations.

For the calculation of the OPEX, related to the maintenance costs and to the expenses necessary to keep the component in operation, a value equal to 2% of the CAPEX was used, also reported by the literature, [135], [156]; the same references were used to set the REPL costs value equal to 100% of the CAPEX and the average useful life of 20 years (only one replacement during the life of the system).

The following table 37 summarizes the equations/formulas implemented for the calculation of the economic variables of the compressors.

| CAPEX [$/kW] | OPEX [$/kW] | REPL [$/kW] | LIFETIME [y] | REF. |
|---|---|---|---|---|
| Eq. (195) | - | - | - | [131] |
| - | 2%CAPEX | - | - | [135],[156] |
| - | - | 100%CAPEX | - | [135],[156] |
| - | - | - | 20 | [135],[156] |

*Table 37 - Compressor econimic information*

## 5.2.8 Pumps

Pumps are components that allow to increase the pressure level, like compressors, with the substantial difference that they only act on liquid streams. The most of the cases they operate on the water line (rSOC sections), but it is also present another one in the line of the solvent rich of carbon dioxide, removed in absorbent column (CCS).

According to the work of Wang C. [158], it is possible to empirically calculate the specific investment cost [€/MWh] of this component known the pressure variation [Pa] that the pump must guarantee, considering an efficiency ($\eta_{pump}$) equal to 80% and the volumetric flow rate ($V$) of the treated stream in [$m^3/s$]:

$$c_{pump} = \frac{\Delta p \ \dot{V}}{\eta_{pump} 10^{-6}} \tag{197}$$

By multiplying the specific cost by the nominal power of the component, it is possible to quantify the investment cost:

$$CAPEX = W_{pump} c_{pump} = \frac{W_{pump} \Delta p \ \dot{V}}{\eta_{pump} 10^{-6}} \tag{198}$$

According to Dr. Gary Rochelle, a chemical engineer working at Trimeric Corporation™, it is possible to use an alternative formulation that allows to estimate the investment cost:

$$CAPEX = C_{tri} \left( \frac{L}{L_{tri}} \right)^{S_L} \tag{199}$$

The equation derives from years of data collection in the industrial sector of the aforementioned company. Simply $C_{tri}$ indicates the cost of the component referred to the average values of the company, depending on the size. L represents the mass flow rate of the liquid, indicating the real value treated in the component under examination (L) and the value that refers to the company ($L_{tri}$). Finally, the exponent $S_L$ is the liquid flow scale factor, also determined according to tabulated values.

In the case presented in the thesis work, eq. (198) was considered for the calculation of the investment costs, while, due to the lack of data available in the literature, both the operation&maintenance costs and the replacement costs were considered with the same percentages as in the case of the compressor. This hypothesis was made in function of their similar behaviour because both are devices that consume electricity to produce a pressure increase.

### 5.2.9 Heat Exchangers

As in any economic analysis in which heat exchangers are involved, the area [m$^2$] is the parameter used to estimate the component costs. Using the inverse formula of the heat flow it can be easily obtained:

$$A = \frac{\phi}{U\,\Delta T_{ml}} \tag{200}$$

In addition to the heat flow [kW$_{th}$], acquired from the maximum values obtained during the realized annual simulation, its calculation also includes two other important variables:

- U [W/m$^2$K] is the global heat exchange coefficient, the thermodynamic parameter which allows to quantify the capacity of a material to exchange heat with the environment or with another surrounding material at different temperature, depending on its surface. This kind of coefficient is defined as global because it takes into account both the conduction and convection with the surrounding environment. The values used were calculated basing on the textbook [159];
- $\Delta T_{ml}$ is the reference temperature for heat exchangers calculated knowing inlet and outlet temperatures of flows which operate inside the component.

$$\Delta T_{ml} = \frac{\Delta T_1 - \Delta T_2}{\ln\left(\frac{\Delta T_1}{\Delta T_2}\right)} \tag{201}$$

$$\Delta T_1 = T_{hot,in} - T_{cold,out} \tag{202}$$

$$\Delta T_2 = T_{hot,out} - T_{cold,in} \tag{203}$$

Due to the absence of a pinch point analysis, the network of heat exchangers within the thesis plant has not been identified. For this reason, a simplification was adopted during the calculation of the logarithmic average differences of temperatures, namely its value was approximated to a normal temperature difference: $\Delta T = T_{end}-T_{start}$. Therefore, only one of the two fluids, whose temperatures should be known, was considered.

Once the area was determined, it was possible to calculate the CAPEX value using the Turton equations [131]. Among the various types of heat exchangers, those considered in the thesis were the double pipes. Therefore, regarding the procedure relating to the calculation of the CAPEX, reference is made to the absorber and stripper components in "5.3.2", with the sole exception that the value of the pressure factor $F_P$ calculated as expressed by eq. (196) in "5.3.7" for compressors. The following table 37 shows the values of the constants identified for the double pipe heat exchanger.

| $K_1$ | $K_2$ | $K_3$ | $F_p$ | Material | $F_m$ | $B_1$ | $B_2$ |
|---|---|---|---|---|---|---|---|
| 3,3444 | 0,2745 | -0,0472 | 1 | SS \| CS-SS | 2,75 \| 1,8 | 1,74 | 1,55 |

Table 38 - Heat Exchanger constants' values

As regards the estimate remaining costs, reference is made to [86], [161] and [162], from which a value equal to 2% of the CAPEX for operation and maintenance costs and a value of 100% of the CAPEX for replacement costs are deduced, with a useful life of the components equal to 20 years (only one replacement in the period considered).

### 5.2.10 CHP components

The last reported components are grouped within the Combine Heat Power (CHP) category, which includes the drum, the pre-reformer and the various flash units. They were considered together as all of them harness heat to produce the various processes they were designed for, from chemical reactions to phase separation.

The CAPEX were calculated basing on Turton [131]:

- The drum was considered as a demister equipment type, which uses as unit of measurement the [$m^2$], relative to its surface;
- The flash units were considered as evaporator equipment type, which uses as unit of measurement the [$m^2$], relative to its surface;
- The pre-reformer was considered as a furnaces equipment type, which uses the required power in [kW] as unit of measurement.

For all the components mentioned, the Turton equations [131] used are the same as those adopted for the heat exchangers in "5.2.9". Below, the values of the constants used are reported:

| COMPONENT | $K_1$ | $K_2$ | $K_3$ | $F_p$ | Material | $F_{BM}$ |
|---|---|---|---|---|---|---|
| **Drum** | 3,2353 | 0,4838 | 0,3434 | 1 | SS | 1 |
| **Flash Unit** | 5,0238 | 0,3475 | 0,0703 | 1 | SS | 1 |
| **Pre Reformer** | 3,068 | 0,6597 | 0,0194 | 1,07 | SS | 2,8 |

Table 39 - CHP constants' values

As regards the complementary costs, in the case of flash units, according to [163], the operation costs are related to the volume of flow to be managed, and the maintenance costs are negligible. This information is also approved by the company Sivalls Incorporated™, while the replacement cost is set at 100% of the CAPEX. The lifetime of these components has been obtained by using data from company Penn Separator Corporation™'s datasheet [164], which states that the lifetime of these components is not longer than 5 years, because the vessel walls tend to wear out due to corrosion phenomena. Furthermore, many problems of overpressure, overtemperature and vacuum condition arise in these components which tend to deteriorate further, shortening the life of the component. As for the drums, the data relating to OPEX, REPL and lifetime are set equal to those of the flash units due to the difficulty in finding information in contemporary literature.

Finally, as regards the reactors in which methane reforming reactions take place, the work of A. Calvo [86] is used as a reference. It provides specific values for these missing data, reporting them directly from manufacturers. A replacement cost is therefore considered equal to 100% of the CAPEX, an OPEX value equal to 0.009662 [€/kW] and a lifetime of 3 years.

Table 40 below summarizes the values adopted:

| COMPONENT | CAPEX [$/kW] | OPEX [$/kW] | REPL [$/kW] | LIFETIME [y] |
|---|---|---|---|---|
| **Drum** | Eq. (189) [131] | negl. [163] | 100%CAPEX [163] | 5 [164] |
| **Flash Unit** | Eq. (189) [131] | negl. [163] | 100%CAPEX [163] | 5 [164] |
| **Pre Reformer** | Eq. (189)[131] | 0,009662 [86] | 100%CAPEX [86] | 3 [86] |

*Table 40- CHP components economic information*

### 5.2.11 Auxiliary costs

The paragraph relating to the determination of the main economic variables of the components ends with a description of the auxiliary costs. This category includes the costs of all energy and material carriers necessary to ensure the operations of the plants and which in fact were consumed during the reference year 2018:

- The cost of biogas is the first operational cost considered. Its sales value in Italy has varied greatly in recent years, because of the incentives provided by the law that have drastically lowered its cost. Until 31 December 2012, the purchase price of biogas was about 0.28 [€/kWh] according to Legislative Decree 22/11/2007 n.222. Subsequently, with the entry into force of the FER decree 06/07/1012, the price dropped to 0.236 [€/kWh], while with the update of this decree, valid in the three-year period 2019-2021 (New FER Decree), the price stabilized at 0.2295 [€/Sm$^3$], inclusive of production and distribution costs. Reported in dollars, according to the conversion, its price is of 1.15 [€/$_{2018}$]. The total cost attributable to the biogas necessary for the operation of the CCS section is then determined by multiplying the specific cost by the annual volume required by the plant, which was calculated as equal to 479’632 Sm$^3$/y;

- The cost of the lean solvent refers to the MEA substance, necessary for the carbon dioxide removal processes, in the CCS section. The price of 0.925 [£/kg$_{CO2}$] derives from the work of Akinola T.E. [105], and it's reported in dollars considering the conversion [\$$_{2018}$/£] of 1.2747. The final value to be considered each year was calculated from the product between the specific cost and the total annual mass quantity of carbon dioxide removed of 272.76 tons/y;
- The cost of demineralized water must be taken into account in many sections of the plant. According to the work of Davis W. [165], confirmed by the study of Giglio E. [135], a cost of 1 [\$/ton$_{H2O}$] is attributed to this resource. According to T.E. Akinola [105], the reference text for the CCS removal system, a value of about 0.5 [\$/kg$_{CO2}$] can be attributed. The first price was adopted in the rSOC section, considering an annual flow rate of demineralized water, given by the sum of the water flows entering the SOEC (steam and co-electrolysis) section and the operations in SOFC, obtaining a total value of 5’145’400 [m$^3_{H2O}$] per year, to be brought back at standard conditions and finally in mass, considering a density of 1000 kg/Sm$^3$. The second price of demineralized water was implemented for the calculation of the substance in the section of CCS;
- The cost of natural gas withdrawn from the Italian distribution network was calculated by searching the web for the prices of local suppliers in the Sicilian region, for the town of Menfi (Ag). A series of prices was obtained, such as 0.18 [€/Sm$^3$] from the company ENI gas & luce ™, 0.24 [€/Sm$^3$] from NeN Special 48 Gas ™, 0.24 [€/Sm$^3$] from Iren Web Gas ™, 0.30 [€/Sm$^3$] from Sorgenia Next Energy Gas ™ and finally 0.26 [€/Sm$^3$] from ENEL E-Light gas™. The final value chosen was calculated as the average of the above values, obtaining a price of 0.244 [€/Sm$^3$] referred to the year 2021, and subsequently converted [\$$_{2018}$]. The specific cost of natural gas is multiplied by the volumetric flow rate under standard conditions of the only flow entering the SOFC, without considering the value of SNG produced in the methanation and CCS section;
- The cost of electricity required by the electrolysis processes (steam and co) is considered at the same price as that produced and hypothetically sold at the same price of the photovoltaic section, with a value of 9.13 [c\$/kWh], explained in detail in the following paragraph. This value will then be multiplied by the sum of the annual energy necessary for the operations in SOEC mode, without consider the PV electricity contribution (surplus energy);
- In the methanation section, the only extra cost to be considered is related to the replacement of the catalyst material. According to the reference text of this section, the work of Giglio E. [105], a cost can be considered equal to 440 [\$/ft$^3$], equivalent to 15538.468 [\$/Sm$^3$] considering the values taken by the agency NETL, regarding a study carried out on the use of the SNG;
- The last cost to be taken into consideration, only in the first year of life of the plant, is referred to the initial amount of hydrogen needed for storage. By consulting the

literature, a conservative price of 5 [$/kg] is adopted, obtained from a study conducted in UNSW Sydney by Yates J., [166].

This last paragraph concludes the description of the economic variables adopted for the economic analysis of the polygeneration plant and, in the next paragraph, the final results obtained will be described.

## 5.3 Analysis and Results: Levelized Cost Of Product

The final paragraph of the economic section is the final report of the thesis work. It aims to consider and quantify in economic terms the fruits of the sizing and operations carried out by the polygeneration plant. Using the costs obtained in the previous sub-paragraphs, it is possible to determine for each plant section the relative overall cost reported to the present (year 2018). The following equations, from (204) to (208), only indicate the components present in each NPC, the formula used instead will be like the one expressed by eq. (181) in "5.1":

$$NPC_{CCS} \rightarrow (CAPEX + OPEX + REPL)_{CCS} + OPEX_{biogas} \tag{204}$$

$$\begin{aligned} NPC_{rSOC} \rightarrow &(CAPEX + OPEX + REPL)_{rSOC} + (CAPEX + OPEX + REPL)_{H_2Storage} \\ &+ OPEX_{H_2} + OPEX_{W_{el}} + OPEX_{H_2O} + OPEX_{NG} \end{aligned} \tag{205}$$

$$NPC_{FC} \rightarrow (CAPEX + OPEX + REPL)_{SOFC} + OPEX_{NG} + OPEX_{H_2O,FC} \tag{206}$$

$$\begin{aligned} NPC_{METH} \rightarrow &(CAPEX + OPEX + REPL)_{METH} \\ &+ (CAPEX + OPEX + REPL)_{syngas,Storage} + OPEX_{catalyst} \end{aligned} \tag{207}$$

$$NPC_{PV} \rightarrow (CAPEX + OPEX + REPL)_{PV} \tag{208}$$

The final values shown in the following table 41 are finally obtained:

| Net Present Cost | Value [$2018] |
|---|---|
| NPCCCS | $19.110.596,13 |
| NPCrSOC | $53.462.882,05 |
| NPCfc | $44.103.742,19 |
| NPCMETH | $14.129.154,34 |
| NPCPV | $14.014.800,00 |

*Table 41 -Net Present Costs for each plant section*

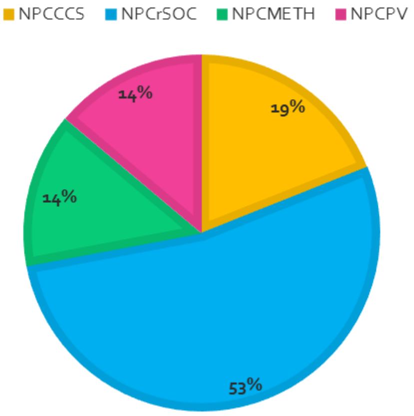

*Figure 50 - Graphical representation of table 41 in term of percentage*

As can be seen from the values obtained in table 41 and reported in percentage terms in the previously fig. 50, calculated for the 25 years of the polygeneration plant lifetime, the most expensive part equivalent to more than half of the whole cost is the section of the electrochemical device. This information was presumed a priori since, among the technologies adopted, it represents the youngest in terms of production and, despite the high size, costs continue to be high, at least for the present (industrial components decrease the cost as the size increases). Furthermore, as noted in eq. (205), its overall cost bears a series of costs other than the electrochemical device and its BOP. In fact, it takes into account the storage of hydrogen and all its costs of operation, maintenance and replacement, as well as the costs deriving from the streams of flows (in terms of mass and energy) inherent in this section, such as the initial hydrogen contained in the storage, the demineralized water used, the cost of natural gas taken from the grid for the electrochemical reactions of the SOFC and the electricity necessary for the operations in SOEC. Instead, eq. (206) expresses the costs associated exclusively to the SOFC section, as show in the fig. 35 of paragraph "4.4". It means that there is a difference between the term $(CAPEX+OPEX+REPL)_{SOFC}$ and $(CAPEX+OPEX+REPL)_{rSOC}$ due to BOP: the first consider all the auxiliary components for both modalities, while the second take into account the only one of SOFC section.

As regards the other plant sections, on the whole they have a very similar global cost, varying between 14 and 19 % of the total costs of the entire plant. The photovoltaic field amortizes part of its costs thanks to its high size, which allows to significantly reduce the costs of this now mature technology. The methanation section, in addition to counting the operating costs for the replacement of the catalyst material, takes into consideration the storage component of syngas. Finally, the CCS plant typically has a higher cost than the two previously described, for a reason very similar to that of the rSOC: the prices of its components are more expensive due to the technological youth of this section. Plants of this kind are starting to take hold in recent years but for this very reason, the price is falling sharply, and they are becoming increasingly widespread and used not only for new plants but also for the retrofitting of existing ones.

As stated in the introduction of paragraph "5.2", the value of the NPC calculated for the related plant section is only an initial variable from which it is possible to calculate others, in such a way as to provide even more accurate indications from the point of view of convenience of the plant. In the specific case of the thesis work, it was decided to exploit the global costs to derive the Levelized Cost Of Product, which are economic variables with that deduce a cost based on a quantity of energy or material produced by the same plant.

In order to best represent the polygeneration plant from an economic point of view, LCOPs have been drawn up based on the vectors leaving the system. The electricity produced by the photovoltaic field, the SNG produced in the methanation sections and CCS, the hydrogen produced by the SOEC were chosen. The first is the Levelized Cost Of Electricity ($LCOE_{PV}$), its value was derived from the ratio between the NPC referred to the photovoltaic field and the total electricity produced during the entire life of the plant (25 years):

$$LCOE_{PV} = \frac{NPC_{PV}}{\sum_{i=1}^{25} E_{PV,i}} = \frac{CAPEX_{PV} + \sum_{j=1}^{25}[\frac{OPEX_{PV,j}}{(1+d)^j} + \frac{REPL_{PV,j}}{(1+d)^j}]}{\sum_{i=1}^{25} E_{PV,i}} \tag{209}$$

The total electricity produced was obtained starting from the amount generated in the first year, equal to about 12 GWh (12053051 kWh) and scaled by 1% for each year to come, up to the twenty-fifth. The percentage reported indicates the loss of efficiency of the system according to which, after 20 years of operation, there is a drop in efficiency equal to 20% compared to the initial value.

The second economic parameter reported is the Levelized Cost Of Synthetic natural Gas (LCOS), calculated considering at the numerator both the present global cost of the methanation section and that of CCS, while the denominator shows the sum of the volumetric flow rates of SNG produced, referred to the standard conditions of 273.15 K and 1 bar produced during the entire life of the polygeneration plant, assuming also in this case an annual decrease in efficiency of about 1% (hypothesis of similarity with photovoltaics, also carried out in the plant section of the rSOC):

$$LCOS = \frac{NPC_{METH} + NPC_{CCS}}{\sum_{i=1}^{25}(\dot{V}_{METH,i} + \dot{V}_{CCS,i})_{SNG}} \tag{210}$$

In order to quantify the SNG produced in monetary terms, in addition to its cost per volume, another cost value can be considered as a function of the intrinsic thermal energy contained, so as to be able to compare it with the other variables, such as the LCOEPV, which are expressed by unit of energy. The following eq. (211) therefore reprints the cost at which 1 [kWh] produced by the SNG should be sold, considering its production both in the methanation and CCS section:

$$LCOE_{sng} = \frac{NPC_{METH} + NPC_{CCS}}{\sum_{i=1}^{25}(E_{METH,i} + E_{CCS,i})_{SNG}} \tag{211}$$

Finally, the last economic variable is presented, which aims to quantify the cost of the rSOC section, its BOP and other auxiliary components (equation (205) as a reference) using two different configurations. In the first case, the energy vectors produced in this section are separated, generating a Levelized Cost Of Hydrogen $LCOH_{rSOC}$ and a Levelize Cost Of Elecricity from fuel cell $LCOE_{fc}$. The following equations report the implemented formulas:

$$LCOE_{fc} = \frac{NPC_{fc}}{\sum_{i=1}^{25} E_{fc,i}} \tag{212}$$

$$LCOH_{rSOC} = \frac{NPC_{rSOC}}{\sum_{i=1}^{25} \dot{m}_{H_2,i}} \tag{213}$$

As can be seen from the numerator of the first eq. (212), a fictitious NPC is used, which takes into account only the system relating to the SOFC and its auxiliaries, referring to fig. 34 of paragraph "4.4". Furthermore, only the auxiliary costs of demineralized water and natural gas necessary for its electrochemical reactions are considered, excluding the remaining ones. The denominator, on the other hand, the total electricity produced during the 25 years of the plant's life is considered, with the same procedure implemented in the section of the photovoltaic field.

Instead, eq. (213) reports the monetary value at which one [kg] of hydrogen produced by the steam-electrolysis reactions should be sold, referring the cost to the entire plant of the electrochemical device, including all auxiliaries and hydrogen storage. Considering the hours of execution in which the SOEC operates in steam-electrolysis, approximately 435 global per year, the expected value is significantly higher than the average hydrogen sales values, [166]. Consequently, a further LCOP is formulated for this section, which considers as the denominator all the energy coming from the rSOC, adding the contribution of hydrogen and the power produced in SOFC mode. This economic parameter, which substantially takes into account the $LCOH_{rSOC}$ and the $LCOE_{fc}$, avoiding to consider the same components twice, takes the name of Levelized Cost Of Energy of rSOC ($LCOE_{rSOC}$) and is represented by the following equation:

$$LCOE_{rSOC} = \frac{NPC_{rSOC}}{\sum_{i=1}^{25} (E_{H_2,i} + E_{fc,i})} \tag{214}$$

The following table 42 shows the final values of the LCOPs described above, representing all the variables referring to the quantities of energy produced in cents of dollar referring to the year 2018, while the variables that express the cost as a function of the quantity of substance produced will be expressed in dollar of 2018:

| Levelized Cost Of Product | Value [$2018] | |
|---|---|---|
| $LCOE_{PV}$ | 9,1 | c$/kWh |
| $LCOE_{rSOC}$ | 14,0 | c$/kWh |
| $LCOE_{fc}$ | 11,9 | c$/kWh |
| $LCOE_{sng}$ | 55,1 | c$/kWh |
| LCOS | 4,1 | $/Sm3 |
| $LCOH_{rSOC}$ | 167,9 | $/kg$_{H_2}$ |

*Table 42 - Final economic results*

Referring to the Autorità di Regolazione per Energia Reti e Ambiente (ARERA[6]) of Italian government, an average price can be obtained, for the year 2018, referring only to expenditure on electricity equal to 10.175 [c€/kWh], which, converted into dollars, would be equivalent to about 12 [c$/kWh]. Therefore, the costs deriving from the transport and management of the meter are neglected, as well as the system charges and the various taxes foreseen, the sum of which expresses more than 50% of the final cost of electricity sold in Italy.

The ARERA provides interesting information, if used as a comparison parameter. For instance, considering the LCOE of the various products, the only one to have a value lower than that of the grid is the electricity produced by photovoltaics, indicating a strong convenience for this plant section and marking the positivity that the use of this technology would have, not only at an environmental level, but also at an economic level, reducing consumer costs.

Another very positive aspect considers the variable of the cost of energy attributed to the rSOC. It is evident that the costs do not differ much from the average value of the Italian network, especially the one relating to the SOFC alone which is practically of equal value. Obviously in the thesis work there were many simplistic assumptions which allowed to neglect some costs, such as the lower effective duration of the device operating hours, due to the instantaneous transients for the transition from fuel cell to electrolyser operations or vice versa, or the hypothesis of considering any heat produced by rSOC and BOP as recoverable, without having carried out any pinch analysis, thus using a large slice of energy that in reality would have been wasted due to the incongruity deriving from the coupling between fluids with incompatible temperatures. Moreover, the chose to buy energy at the PV price or to buy natural gas at the Italian grid price, further decrease the costs of the total OPEX considered in the rSOC section which are present each year of the plant lifetime. Nevertheless, especially for large sizes, an excellent future for this technology is foreseen, with the hope that it will be adopted as soon as possible, in order to start reversing the GHG production trend that is threatening the planet. The question changes when the cost referred to hydrogen amount is taken into consideration. Indeed, as previously announced, the disproportionate value obtained equal to 167 [$/kg$_{H2}$], practically equal to 33 times the maximum value considered for the purchase of this resource, [166], derives precisely from the fact that it is not possible for hydrogen to take charge of all the expenses related to the rSOC and auxiliary section (eq. (205) as a reference), as only 435 hours a year are dedicated to the production of this substance. In fact, it is noted that, referring the cost to all the energy produced by the device, therefore considering also the 7014 hours per year in which it operates as SOFC, the LCOE tends to drop drastically, becoming competitive (thanks to the hypothesis).

Finally, the cost at which a kWh produced by the SNG must be sold to cover the cost of the plants designated to produce it, equal to 55 cents of dollar in 2018, is practically double

---

[6] https://www.arera.it/it/dati/eep35.htm#

compared to the one from the network, considered in " 5.3.11", and worth 0,244 [$€_{2021}$/kWh]. This assumption, despite the high price, turns out to be optimistic because it considers two technologies that are not widely used today, especially that of carbon dioxide capture. In fact, considering a decrease in costs in the coming years, especially relating to this last section, it can therefore be said that technologies capable of replacing the extraction of new fossil fuels will soon be available, and the emission of associated pollutants will be avoided, in the case of use of these synthetic substances produced.

In conclusion, the high potential of these emerging technologies is confirmed, a prelude to their ever wider involvement and implementation deriving from the excellent technical and economic results achieved. Considering the methodology of the NPC, the economic analysis conducted did not take into consideration any sort of revenue and above all no incentives, which would be a huge source of income and which would make these technologies truly competitive on the global market, motivating and increasing production and hence the reduction of future costs.

# 6 Conclusion

The present thesis work is the result of an economic techno-analysis (modeling and simulation) of a polygeneration plant located in Menfi (AG) operating with the PtX model, for the production of three energy vectors: electricity, hydrogen and synthetic natural gas.

The primary purpose of the plant is to satisfy the electricity needs of a hypothetical urban network of 30 thousand people through a dedicated photovoltaic field, couple by the possibility to operate in fuel cell mode of a reversible solid oxide device (rSOC), thus compensating the fluctuation resulting from the nature of solar radiation. Thanks to the transparency of the company Terna - Rete Elettrica Nazionale™, it was possible to quantify an annual hourly trend in urban consumption to be met. On the basis of the maximum power required, equal to 5.65 MW, the sizes of the auxiliary plants were chosen, such as 9 MW for the photovoltaic field and 6 MW for the SOFC. In cascade a size of 30 MW was assumed for the alternative SOEC mode thanks to the assumptions obtained from the literature [110], which allowed to assume a power ratio of 5 due to the better thermal optimization between the two operating modes.

This last electrolyser mode was later induced to operate both in steam or co-electrolysis, producing pure hydrogen and syngas as output respectively. For both mass streams, two storages have been dimensioned for the accumulation of substances. The function of the 4-tons hydrogen storage is to store the pressurized gas, compressed to 250 bar at a temperature of 20 °C, supplying a refilling station weekly and transporting the substance between the two sites through the tube-trailers technology. Instead, the syngas storage with a capacity of 10 thousand $m^3$ at the conditions of 32.4 bar and 20 °C allows to operate continuously, in stationary conditions, in the methanation section from the beginning of July 2018 until the end of December of the same year.

The production of SNG takes place precisely thanks to the conversion of syngas inside the methanation reactors, according to the HICOM method, in which both the methanation reactions produced by monoxide and carbon dioxide are considered. This operating mode allowed a greater freedom, while providing a high quality SNG with a $97\%_{mol}$ of methane content at the outlet.

Finally, in the plant is included a carbon dioxide removal section, which purifies a biogas stream fed as input. In this way, it is possible to limit the environmental impact by capturing the GHG and at the same time exploiting it in the co-electrolysis processes for its conversion into a useful product (SNG at the end of the process).

After a first introductory chapter, dedicated to the problems of global pollution, the regulatory and operational responses of states around the world and an overview of Global and Italian energy consumption, the current conditions of the technologies mentioned above are described in the second chapter. Known the state of the art and therefore the starting point, a plant has been developed which operates in a circular way, in order to consider every aspect of the technologies used and to optimize the process overall. By connecting the various plants together, it was possible to obtain a system in which the waste of one became the input materials of another. Chapter three, in fact, was dedicated to modeling, primarily in order to create the electricity generation system by coupling the photovoltaic and SOFC. Secondly, a system was created including CCS, SOEC and methanation, in such a way as to avoid any waste that could happen in moments of energy surplus of the photovoltaic field, creating SNG alternated with the hydrogen generation system in which only the electrolyser system is used. Specifically, the operations were scanned in such a way as to operate in steam-electrolysis the first two days of the week in which the surplus occurred, and the remaining days in the co-electrolysis mode. Among the most important hypotheses considered in this chapter there is certainly the linear approximation of the electrochemical behaviour of the rSOC. In the process many loss phenomena have been neglected, which, in some extreme situations, would have drastically influenced and decreased the efficiency and production of the device. The second noteworthy approximation concerns the assumption of a zero-dimensional model for this device, which drastically simplified the physics of the process, bringing each equation back to the base case. The third assumption involved the recovery of all the thermal flows that the components were able to exchange. In this case, a pinch analysis could be adopted, in order to verify the coupling of these flows between the various heat exchangers of the same plant, providing more accurate values of plant efficiency. The fourth and final approximation actually concerns a set of conditions that were carried out in the following chapter (precisely in paragraph "4.1"), which allow to neglect loss phenomena that would affect the operations of all the plant sections, such as falls pressure, temperature and the adiabatic nature of the component casing. The main results of this modeling phase are the design of the electrochemical device consisting of 12 modules, each of which formed by 2420 cells and capable of delivering a power of 500 kW in SOFC mode and absorbing 2500 kW in the alternative mode. From the electrochemical point of view, on the other hand, the fundamental parameters have resulted in a value of 0.9161 V of OCV for both modes, while 1.211 V and 1.288 V for the thermoneutral voltage, respectively for co and steam-electrolysis. The modeling of the CCS and methanation plants was more based on the description and formulation of the kinetic aspects of the chemical reactions involved. Finally, the photovoltaic field was modelled by adopting an online software, PVGIS [74], which directly provided the simulation values of the 9 MW plant, consisting of monocrystalline silicon technology and module efficiency equal to 21 %.

After the description of the behaviour of each section, in the following fourth chapter the modeling results were implemented on the Aspen plus® software, in order to simulate its behaviour and obtain useful data to be analyzed at a later point. The plants were therefore reproduced on this program and, after inserting the various formulas necessary to describe their behaviour, it was possible to obtain a discrete mapping of the analyzed case in Excel format.

For an accurate representation, various cases related to each useful configuration expected (mainly dictated by the number of modules turned on in the rSOC) were simulated, obtaining a series of discrete maps, which were joined by linear interpolation, creating a continuous map for each configuration. Subsequently, using a tailor-made Matlab code, these final maps were filtered by attributing for each component, energy and associated flow, their descriptive values such as kW, temperature, pressure, mass or volumetric or molar composition etcetera, in each of the 8760 hours of the year 2018. The last paragraph of each plant section reported the performance parameters considered to fully describe their behaviour. Among the most important are certainly the annual average efficiencies of the rSOC: for the SOFC, the net combined efficiency value obtained was 87.06% and a net electrical efficiency of 47.19%, expressed in table 17 of paragraph "4.3.2"; while for SOEC (considering both cases of electrolysis), values equal to 87.18% and 96.01% were obtained respectively for the net combined and net electrical case, expressed in tab. 21 of paragraph "4.4.2". The values obtained for both SOFC and SOEC fully reflected the average efficiencies present in other articles of literature.

Finally, in the fifth and last chapter the economic analysis based on the Net Present Costs methodology was conducted. Only the costs for the construction of the plant were considered, excluding any sort of proceeds from sales and, above all, any sort of incentives that could have favored the study, the production and the use of these technologies. In the end, the costs of each plant section were calculated in 2018 dollars, obtaining an overall value characterized by more than 50% of the total costs of the rSOC plant and associated systems (BOP, hydrogen storage and material flows necessary for the operations). This result denotes the not technological maturity, but presages a decrease in costs in the years to come. As regards the other three plants (CCS, methanation and photovoltaic), the costs in percentage terms were very similar, ranging from 14 to 19 % of the total cost.

Once the costs of each section were determined, it was possible to set a Levelize Cost Of Products for each of the foreseen energy carriers, expressing the selling price of these substances both in energy terms [kWh] and in physical terms [kg], or [m$^3$] taking charge of their production plant. The values obtained and expressed in table 42 of paragraph "5.3" showed a very interesting trend for the coming years because, hypotheses aside, they have "ideal" values that tend to be in line with the real ones of conventional resources/plants.

# References

[1] Overview of High-Temperature Electrolysis for Hydrogen Production - Herring, J. S. ; O'Brien, J. E. ; Stoots, C. M. ; Hartvigsen, J. J. ; Petri, M. C. ; Carter, J. D. ; Bischoff, B. L. ; United States. Office Of The Assistant Secretary For Nuclear Energy

[2] Technology development and application of future hydrogen energy industry and Taiwan hydrogen industry; Chen-Chun Lin; Shyu, Joseph Z; PICMET 2010 TECHNOLOGY MANAGEMENT FOR GLOBAL ECONOMIC GROWTH, July 2010, pp.1-9

[3] *The Challenge of Climate Change: Which Way Now?* - Perlmutter, Daniel P., and Robert L. Rothstein - John Wiley & Sons, Incorporated, 2010

[4] The timing of climate change – Chris Huntingford, Lina Mercado, Eric Post – Nature 502, 174-175 (2013)

[5] World Meteorological Organization website: https://public.wmo.int/en

[6] UN environmental programme: https://www.unenvironment.org/explore-topics/sustainable-development-goals/about-sustainable-development-goals#ourwork

[7] The Intergovernmental Panel on Climate Change: https://www.ipcc.ch/

[8] United Nation Climate Change website: https://unfccc.int/about-us/about-the-secretariat

[9] https://www.unece.org/env/teia/cop.html

[10] Ex-post assessment of the Kyoto Protocol – quantification of CO2 mitigation impact in both Annex B and non-Annex B countries - Kuriyama, Akihisa; Abe, Naoya - Applied energy, 15 June 2018, Vol.220, pp.286-295

[11] Governo Italiano, Ministero degli Affari Esteri e della Cooperazione Internazionale: https://www.esteri.it/mae/it/politica_estera/temi_globali/ambiente/20090406_meccanismi kyoto.html

[12] Calls for Carbon Markets at COP21: a conference report – Lara Johannsdottir; Celine Mclnerney – Journal of Cleaner Production – Volume 124, 15 June 2016, pages 405-407

[13] Lima Paris Action Agenda: Focus on Private Finance – note from COP21 - Mcinerney, Celine; Johannsdottir, Lara - Journal of cleaner production, 10 July 2016, Vol.126, pp.707-710

[14] Achieving the Paris Climate Agreement Goals – Teske – Springer International Publishing, 2019

[15] Conference of the Parties Twenty-first session, Paris, 30 November to 11 December 2015 - Agenda item 4(b) - Durban Platform for Enhanced Action (decision 1/CP.17) -

Adoption of a protocol, another legal instrument, or an agreed outcome with legal force under the Convention applicable to all Parties

[16] Economic Growth, Electricity Consumption and Foreign Dependence in Italy Between 1963-2007 - Vecchione, G. - Energy Sources, Part B: Economics, Planning, and Policy, 23 June 2011, Vol.6(3), pp.304-313

[17] Electrify Italy - Bompard E., Botterud A., Corgnati S. P., Leone P., Mauro S., Montesano G., Papa C., Profumo F., Grosso D., Huang T., Delmastro C., Jafari M., Crespi G., Abbà I., Becchio C., Vergerio G., Viazzo S., Rosciarelli L., Battocchio T., Gaidano M., Fragno M. S., Armiento M., Napoli C., Di Rosa D. - Fondazione Centro Studi Enel ; 2020

[18] Sorgenia, yor next energy website: https://www.sorgenia.it/guida-energia/elettricita/consumo-di-energia-mondiale

[19] Eurostat, Statistics Explained: https://ec.europa.eu/eurostat/statistics-explained/index.php?title=Energy_production_and_imports#The_EU_and_its_Member_States_are_all_net_importers_of_energy

[20] REN21, Renewable now websit: https://www.ren21.net/gsr-2020/chapters/chapter_01/chapter_01/#sub_5

[21] https://en.wikipedia.org/wiki/World_energy_consumption

[22] International Energy Agency (IEA), “Energy and Air Pollution. World Energy Outlook Special Report”, IEA Publications, Paris, 2016

[23] World Health Organization (WHO), “Air Pollution: A Global Assessment of Exposure and Burden of Disease”, Geneva, 2016.

[24] IEA , Data and statistics: https://www.iea.org/data-and-statistics?country=ITALY&fuel=Energy%20consumption&indicator=Total%20final%20consumption%20(TFC)%20by%20source

[25] Autorità per L’energia Elettrica e il gas (AEEGSI). Relazioni Annuali Sullo Stato Dei Servizi e Sull’attività Svolta. Presidenza del Consiglio dei Ministri, Dipartimento per l’informazione e L’editoria. Available online: https://www.arera.it/allegati/relaz_ann/19/RA19_sintesi.pdf

[26] Key world energy statistics - *IEA. 2015. Retrieved 6 April 2017*

[27] Hydrogen - Bockris, John O'M - Materials (Basel, Switzerland), 30 November 2011, Vol.4(12), pp.2073-2091

[28] Hydrogen - Ngô, Christian ; Natowitz, Joseph B. - Hoboken, NJ: John Wiley & Sons, Inc ; 2016, Our Energy Future, Chapter 17, p.409-451

[29] Trends in design of distributed energy systems using hydrogen as energy vector: A systematic literature review - Fonseca, Juan D ; Camargo, Mauricio ; Commenge, Jean-Marc ; Falk, Laurent ; Gil, Iván D - International journal of hydrogen energy, 12 April 2019, Vol.44(19), pp.9486-9504

[30] Polygeneration and advanced energy systems, note of lectures – Massimo Santarelli, 2019/2020

[31] Gasification [Second Edition] (2008) - Christopher Higman and Maarten van der Burgt, Gulf Professional Publishing, ISBN: 978-0-7506-8528-3

[32] Performance assessment and evaluation of SOC stacks designed for application in a reversible operated 150 kW rSOC power plant - Benjamin Königshofer, Pavle Boškoski, Gjorgji Nusevb, Markus Koroschetz, Martin Hochfellner, Marcel Schwaiger, Đani Juričić, Christoph Hochenauer, Vanja Subotić, 2020

[33] High temperature and solid oxide fuel cells fundamentals, design and applications - Singhal S.C, K.K, Elsevier Science, 2003

[34] Recent advances in high temperature electrolysis using solid oxide fuel cells A review - J Power Sources, 2012, pp.4-16

[35] Transient reversible solid oxide cell reactor operation – Experimentally validated modeling and analysis - Srikanth S ; Heddrich, M.P ; Gupta, S ; Friedrich, K.A - Applied energy, 15 December 2018, Vol.232, pp.473-488

[36] Modeling and experimental performance of an intermediate temperature reversible solid oxide cell for high-efficiency, distributed-scale electrical energy storage - Wendel, Christopher H ; Gao, Zhan ; Barnett, Scott A ; Braun, Robert J - Journal of power sources, 01 June 2015, Vol.283, pp.329-342

[37] Current developments in reversible solid oxide fuel cells – S.Y. Gómez, Sergio Yesid ; Hotza, Dachamir - Renewable & sustainable energy reviews, August 2016, Vol.61, pp.155-174

[38] Energy storage – R.M. Dell, D.A.J. Rand - a key technology for global energy sustainability - J Power Sources, 100 (2001), pp. 2-17

[39] Intermediate temperature solid oxide fuel cells - D.J.L. Brett, A. Atkinson, N.P. Brandon, S.J. Skinner - Chem Soc Rev, 37 (8) (2008), pp. 1568-1578, 10.1039/b612060c

[40] A thermodynamic approach for selecting operating conditions in the design of reversible solid oxide cell energy systems - Wendel, Christopher H ; Kazempoor, Pejman ; Braun, Robert J - Journal of power sources, 01 January 2016, Vol.301, pp.93-104

[41] Advance Materials for Energy, note of lectures – M.Ferraris, F.Smeacetto – 2019/2020

[42] Gas-diffusion process in a tubular cathode substrate of an SOFC: I Theoretical analysis of gas-diffusion process under cylindrical coordinate system - Keqin Huang - Pennington, NJ: Electrochemical Society, Journal of the Electrochemical Society, 2004, Vol.151 (5), p.A716-A719

[43] Micro-tubular SOFCs to Measure the Effects of Cross Flow on Mass Transfer Rates Around the Perimeter of a Cylindrical Electrode - Vincent Lawlor, Dieter Meissner, Christoph Hochenauer, Stefan Griesser, Stefano Cordiner, Alessandro Mariani, Gerald Zauner, Abdul Olabi and Gerhard Buchinger - © 2009 ECS - The Electrochemical Society

[44] Electrolysis studies based on ceria-based composites - Zhu B, Albinsson I, Andersson C, Borsand K, Nilsson M, Mellander B|E - Electrochem Commun 2006; 8: 495–8

[45] High-temperature solid oxide fuel cells - Singhal SC, Kendall K. - fundamentals, design, and applicatons - New York: Elsevier Advanced Technology; 2003

[46] Comparative study of stand-alone and hybrid solar energy systems suitable for off-grid rural electrification - Akikur R.K., Saidur R., Ping H.W., Ullah K.R. – A review - RenewSustainEnergyRev2013;27:738–52

[47] Economic analysis of stand alone and grid connected hybrid energy systems - Türkay B.E., Telli A.Y - RenewEnergy2011;36:1931–43

[48] Advanced anodes for high-temperature fuel cells - Atkinson A., Barnett S., Gorte RJ., Irvine JTS., McEvoy AJ., Mogensen M., et al - Nat Mater 2004; 3 : 17–27

[49] Comparison of Y and La-substituted SrTiO3 as the anode materials for SOFCs – Ma Q., Tietz F. – Solid State Ion 2012; 225 : 108–12

[50] Highly efficient high temperature electrolysis – Hauch A., Ebbesen SD., Jensen SH., Mogensen M. – J Mater Chem 2008; 18 : 2331–40

[51] Silica segregation in the Ni/YSZ electrode – Hauch A., Jensen SH., Bilde-Sorensen JB., Mogensen M. – J Electrochem Soc 2007; 154 : A619–26

[52] Solid oxide electrolysis cells: Microstructure and degradation of the Ni/yttria-stabilized zirconia electrode - Hauch A., Ebbesen SD., Jensen SH., Mogensen M. – J Electrochem Soc 2008; 155 : B1184–93

[53] Solid oxide electrolysis cells: degradation at high current densities – Knibbe R., Traulsen ML., Hauch A., Ebbesen SD., Mogensen M. – J Electrochem Soc 2010; 157 : B1209–17

[54] Degradation phenomena in a solid oxide electrolysis cell after 9000 h of operation – Tietz F., Sebold D., Brisse A., Schefold J. – J Power Sources 2013; 223 : 129–35.

[55] Durable SOC stacks for production of hydrogen and synthesis gas by high temperature electrolysis - Sune Dalgaard Ebbesen, Jens Høgh, Karsten Agersted Nielsen, Jens Ulrik Nielsen, Mogens Mogensena

[56] Power-to-X green hydrogen for electrical energy and fuel, for production and products – Jochen Lehmann, Thomas Luschtinetz, and Johannes Gulden - Stralsund University of Applied Science, Institute of Renewable Energy Systems, 18435 Stralsund, Germany

[57] Power-to-X technology using renewable electricity and carbon dioxide from ambient air: SOLETAIR proof-of-concept and improved process concept – Francisco Vidal Vázquez, Joonas Koponen, Vesa Ruuskanen, Cyril Bajamundi, Antti Kosonen, Pekka Simell, Jero Ahola, Christian Frilunda, Jere Elfving, Matti Reinikainen, Niko Heikkinen, Juho Kauppinen, Paolo Piermartini.

[58] Methanation - Twigg, Martyn V (Editor)

[59] Review on methanation – From fundamentals to current projects - Stefan Rönscha, Jens Schneider, Steffi Matthischke, Michael Schlüter, Manuel Götz, Jonathan Lefebvre, Praseeth Prabhakaran, Siegfried Bajoh

[60] Methanation and methane synthesis - W. Boll, G. Hochgesand, W.-D. Müller - Ullmann's encyclopedia of industrial chemistry, Wiley-VCH Verlag GmbH & Co. KGaA, Weinheim (2006), p. 85

[61] Sabatier P, Senderens J-B. Comptes Rendus Des Séances De L'Académie Des Sciences, Section VI – Chimie. Paris: Imprimerie Gauthier-Villars; 1902.

[62] Product gas treatment - H. Hiller, R. Reimert, H.-M. Stönner - Ullmann's encyclopedia of industrial chemistry, Wiley-VCH Verlag GmbH & Co. KGaA, Weinheim (2006), p. 20

[63] Production of synthetic natural gas (SNG) from coal and dry biomass – a technology review from 1950 to 2009 - J. Kopyscinski, T.J. Schildhauer, S.M.A. Biollaz

[64] Reduction of carbon monoxide to methane in the presence of various metals - F. Fischer, H. Tropsch, P. Dilthey - Brennst-Chem, 6 (1925), pp. 265-271

[65] The catalytic synthesis of hydrocarbons from carbon monoxide and hydrogen - M.A. Vannice - Catal Rev, 14 (1976), pp. 153-191

[66] Heterogeneous catalyst deactivation and regeneration: a review - M.D. Argyle, C.H. Bartholomew - Catalysts, 5 (2015), pp. 145-269

[67] Separation of CO2 from Flue Gas A Review - Douglas Aaron & Costans Tsouris

[68] Process intensification for post-combustion CO2 capture with chemical absorption A critical review - Meihong Wang, Atuman S. Joel, Colin Ramshaw, Dag Eimer, Nuhu M. Musa

[69] Use of monoethanolamine (MEA) for CO2 capture in a global scenario Consequences and alternatives - Patricia Luis - Materials & Process Engineering (iMMC-IMAP), Université catholique de Louvain, Place Sainte Barbe 2, 1348

[70] Emerging CO2 capture systems - Abanades J.C ; Arias B ; Lyngfelt A ; Mattisson T ; Wiley D.E ; Li H ; Ho M.T ; Mangano E ; Brandani S - International journal of greenhouse gas control, 2015-09, Vol.40, p.126-166

[71] Physical Properties of MEA+Water+CO2Mixtures inPostcombustion CO2Capture A Review of Correlations andExperimental Studies - Sumudu S. Kaeunarathne, Dag A. Eimer and Lars E.

[72] https://www.terna.it/it/sistema-elettrico/dispacciamento/dati-esercizio

[73]
https://download.terna.it/terna/Annuario%20Statistico%202018_8d7595e944c2546.pdf

[74] https://re.jrc.ec.europa.eu/pvg_tools/it/#PVP

[75] Techno-economic feasibility analysis of hydrogen fuel cell and solar photovoltaic hybrid renewable energy system for academic research building - A. Singh, P. Baredar, and B. Gupta - *Energy Convers. Manag.*, vol. 145, pp. 398–414, 2017

[76] Energy management strategy based on short-term generation scheduling for a renewable microgrid using a hydrogen storage system - G. Cau, D. Cocco, M. Petrollese, S. Knudsen Kær, and C. Milan - *Energy Convers. Manag.*, vol. 87, pp. 820–831, 2014

[77] Dynamic modeling of a photovoltaic hydrogen fuel cell hybrid system - J. J. Hwang, L. K. Lai, W. Wu, and W. R. Chang - *Int. J. Hydrogen Energy*, vol. 34, no. 23, pp. 9531–9542, 2009

[78] *Fuel Cell Assisted PhotoVoltaic Power Systems* - S. G. Tesfahunegn, May. 2012

[79] A hybrid method for one-day ahead hourly forecasting of PV power output - C. M. T. Huang, Y. C. Huang, and K. Y. Huang - *Proc. 2014 9th IEEE Conf. Ind. Electron. Appl. ICIEA 2014*, pp. 526–531, 2014

[80] A Simplified Clear Sky Model for Direct and Diffuse Insolation on Horizontal Surfaces - R. E. Bird and R. L. Hulstrom - Golden, Colorado 80401, 1981.

[81] Prospects of solar photovoltaic-micro-wind based hybrid power systems in western Himalayan state of Himachal Pradesh in India - S. Sinha and S. S. Chandel - *Energy Convers. Manag.*, vol. 105, pp. 1340–1351, 2015

[82] Reversible solid oxide fuel cell for natural gas renewable hybrid powergeneration systems - Yu Luo, Yixiang Shi, Yi Zheng, Ningsheng Cai

[83] Thermodynamic, Economic and Environmental Evaluation of Solid-Oxide Fuel-Cell Hybrid Power-Generation Systems – Young Duk Lee - Berlin, 6 July 2015

[84] Analisi numerica di un innovativo sistema “Power-to-Gas” per l’accumulo energetico – A. Rendine, A. De Pascale, F. Catena

[85] Sistemi di accumulo di energia elettrica basati su celle a ossidi solidi reversibili (RSOC): dimensionamento e simulazioni preliminari – M. Scaltritti, S. Campanari, G. Guandalini

[86] Modeling of stand-alone $H_2$-based energy storage systems for electricity production and $H_2$ mobility – A. Calvo, A. Lanzini, M. Santarelli, P. Marocco

[87] Pressurized Operation of a Planar Solid Oxide Cell Stack – S. H. Jensen, X. Sun, S. D. Ebbesen, M. Chen – Departement of Energy Conversion and Storage, Technical University of Denmark, Raskilde, Denmark – 12 February 2016

[88] A study on a Polygeneration plant based on solar power and solid oxide cells – N. Cobos Ullvius, M. Rokni – Technical University of Denmark, Mechanical Department, Copehagen, Denmark

[89] Design, development and testing of SOEC-based Power-to-Gas Systems for conversion and storage of RES into synthetic methane – F. Domenico - 2016

[90] Modeling of High Temperature Electrolysis and Methanation processes for Syntheric Natural Gas Production – E. Giglio, M- Santarelli, A. Lanzini

[91] SOFC modelling considering hydrogen and carbon monoxide as electrochemical reactants – M. Anderson, J. Yuan, B. Sunden – Department of Energy Science, faculty of Engineering, Lund University, Sweden

[92] Syntheric natural gas via integrated high-temperature electrolysis and methanation: Part I-Energy performance – E. Giglio, A. Lanzini, M. Santarelli, P. Leone

[93] Performance analysis of a co-generation system using solar energy and SOFC technology – R. K. Akikur, R. Saidur, H. W. Ping, K. R. Ullah – UM Power Dedicated Advanced Centre (UMPEDAC) – University of Malaya, Department of Mechanical Engineering

[94] Performance comparison of Fick’s, dusty-gas and Stefan-Maxwell models to predict the concentration overpotential of a SOFC anode - Suwanwarangkul R, Croiset E, Fowler MW, Douglas PL, Entchev E, Douglas MA - J Power Sources 2003;122(1):9–18

[95] A mathematical model of a solid oxide fuell cell – N. F. Bessette, W. J. Wepfer, J. Winnick – Electrochemical Society 1995:142, 3792-3800

[96] Material Data Sheet no. 4046 (Crofer 22 APU) – ThyssenKrupp VDM – May 2010 Edition

[97] High-Temperature Electrochemical Process of CO2 Conversion with SOCs 1 Introduction and Fundamentals

[98] Modelling of One-Step Methanation Process Combining SOECs and Fischer-Tropsch-like Reactor – Bin Chen – 2016, Electrochemical Society

[99] Investigation of a novel multigeneration system driven by a SOFC for electricity and fresh water production – N. Chitgar, M. A. Emadi, A. Chitsaz, M. A. Rosen – School of Mechanical Engineering, Iran University of Science and Technology, Tehran 16844, Iran – Faculty of Mechanical Engineering, Urmia University, Urmia, Iran – Faculty of Engineering and Applied Science, University of Ontario Institute of Technology, 2000 Simcoe Street North, Oshawa, Ontario L1G 0C5, Canada

[100] Extensive analysis of SOFC fed by direct syngas at different anodic compositions by using two numerical approaches – O. Corigliano, P. Fragiacomo – Department of Mechanical, Energy and Management Engineering, University of Calabria, Arcavacata di Rende, 87036 Cosenza, Italy

[101] Model-based behaviour of a high temperature electrolyser system operated at various loads – F. Petipas, A. Brisse, C. Bouallou - European Institute For Energy Research (EIFER), Emmy Noether Strasse 11, 76131 Karlsruhe, Germany, MINES ParisTech, Centre for Energy efficiency of Systems (CES), 60 Boulevard Saint Michel, 75006 Paris, France

[102] Techno-economic modelling of a Power-to-Gas system based on SOEC electrolysis and CO2 methanation in a RES-based electric grid – F. Salomone; E. Giglio; D. Ferrero; M. Santarelli; R. Pirone; S. Bensaid - Elsevier B.V. ; 2019 - volume:377. - issue:120233. – number of pages:20. – CHEMICAL ENGINEERING JOURNAL. - ISSN: 1385-8947

[103] Selective absorption of hydrogen sulfide from gas streams - H.D. Frazier, A.L. Kohl - Industrial and Engineering Chemistry Research, 42 (1950), pp. 2288-2292

[104] Ionic liquid-amine blends and CO2 BOLs: Prospective solvents for natural gas sweetening and CO2 capture technology — A review Satish Kumar, Jae Hyun Cho, Il Moon – Department of Chemical and Biomolecular Engineering, Yonsei University, 50 Yonsei-ro, Seoul, Republic of Korea

[105] Study of CO2 removal in natural gas process using mixture of ionic liquid and MEA through process simulation - Toluleke Emmanuel Akinola, Eni Oko, Meihong Wang - Department of Chemical and Biological Engineering, University of Sheffield, United Kingdom

[106] The solubility of CO2 in a 30-mass-percent monoethanolamine solution - F.Y. Jou, A.E. Mather, F.D. Otto - Canadian Journal of Chemical Engineering, 1995

[107] Correlation and prediction of the solubility of carbon-dioxide in a mixed alkanolamine solution - Y.G. Li, A.E. Mather -Industrial and Engineering Chemistry Research, 1994

[108] Representing vapor-liquid equilibrium for an aqueous MEA-CO2 system using the electrolyte nonrandom-two-liquid model – Y.D. Liu, L.Z. Zhang, S. Watanasiri - Industrial and Engineering Chemistry Research, 1999

[109] A workhorse for gas sweetening - R.W. BucklinDGA - Oil and Gas Journal (1982), pp. 204-21

[110] Energy and environmental analysis of a flexible Power-to-X plant based on Reversible Solid Oxide Cells (rSOCs) for an urban district – G. Buffo, D. Ferrero, M. Santarelli, A. Lanzini – Dipartimento di Energia, Politecnico di Torino-C.so Duca degli Abruzzi 24, 10129, Torino, Italy

[111] Dynamic modelling and analysis of post-combustion $CO_2$ chemical absorption process for coal-fired power plants – A. Lawal, M. Wand, O. Stephenson, G. Koumpouras, H. Yeung - Process Systems Engineering Group, School of Engineering, Cranfield University, Bedfordshire MK43 0AL, UK; RWE npower, Windmill Park, Swindon SN5 6PB, UK; Process Systems Enterprise Ltd., Hammersmith W6 7HA, UK

[112] Anion influence on thermophysical properties of ionic liquids: 1-butylpyridinium tetrafluoroborate and 1-butylpyridinium triflate - Bandrés I, Royo FM, Gascón I, Castro M, Lafuente C. - J Phys Chem B, 2010

[113] Density and viscosity of pyridinium-based ionic liquids and their binary mixtures with water at several temperatures - Mokhtarani B, Sharifi A, Mortaheb HR, Mirzaei M, Mafi M, Sadeghian F. - J Chem Thermodynamic, 2009

[114] Densities and thermal conductivities of N-alkylpyridinium tetrafluoroborates at high pressure - Tomida D, Kenmochi S, Qiao K, Tsukada T, Yokoyama C. - Fluid Phase Equilibrium, 2013

[115] Effect of operating parameters on methanation reaction for the production of synthetic natural gas - Woo Ram Kang and Ki Bong Lee - Department of Chemical and Biological Engineering, Korea University, Seoul 136-713, Korea

[116] Evaluation of Fluidized-Bed Methanation Catalysts and Reactor Modeling - James T. Cobb Jr., Department of Chemical & Petroleum Engineering, University of Pittsburgh, Pittsburgh, Pennsylvania 15261 - Robert C. Streeter, Bituminous Coal Research, Inc., Monroeville, Pennsylvania 15146

[117] Aspen Plus: Chemical Engineering Applications - Al-Malah, Kamal I. M Newark: John Wiley & Sons, Incorporated ; 2016

[118] EVTC - Hydrogen Fueling Stations Infrastructure - N. Qin and P. Brooker - 2014.

[119] Hydrogen refueling station costs in Shanghai - J. X. Weinert, L. Shaojun, J. M. Ogden, and M. Jianxin, - *Int. J. Hydrogen Energy*, vol. 32, no. 16, pp. 4089–4100, 2007

[120] Thermal start-up behaviour and thermal management of SOFC's - H. Apfel, M. Rzepka, H. Tu, U.Stimming - Department of Physics E19, Technische Universität München, Interfaces and Energy Conversion, James-Franck-Str. 1, 85748 Garching, Germany; Bavarian Center for Applied Energy Research (ZAE), Walther-Meißner-Str. 6, 85748 Garching, Germany

[121] Thermodynamic Modeling and Assessment of Ionic Liquid-Based CO2 Capture Processes - Ying Huang, Xiangping Zhang, Xin Zhang, Haifeng Dong, and Suojiang Zhang - Beijing Key Laboratory of Ionic Liquids Clean Process, State Key Laboratory of Multiphase Complex Systems, Key Laboratory of Green Process and Engineering, Institute of Process Engineering, Chinese Academy of Sciences, Beijing 100190, China - School of Chemistry and Chemical Engineering, University of Chinese Academy of Sciences, Beijing 100049, China

[122] Predicting NRTL Binary Interaction Parameters from Molecular Simulations - Ashwin Ravichandran, Rajesh Khare, Chau-Chyun Chen - Department of Chemical Engineering, Texas Tech University, Box 43121 Lubbock, TX 79409

[123] CFD Study of Gas Flow Through Structured Separation Columns Packings Mellapak 250.X and Mellapak 250.Y – Martin Isoz

[124] Solubility of CO2 in 15, 30, 45 and 60 mass% MEA from 40 to 120 C and model representation using the extended - Aronu UE, Gondal S, Hessen ET, Haug-Warberg T, Hartono A, Hoff KA, et al - UNIQUAC framework. Chem Eng Sci 2011

[125] Comparison of Different Amine Solvents for the Absorption of CO2 - Peter Langa, Ferenc Denesb, Laszlo Hegelyaa - Department of Building Service and Process Engineering, Budapest University of Technology and Economics, H-1111,Budapest, Muegyetem rkp. 3. - Department of Energy Engineering, Budapest University of Technology and Economics, H-1111, Budapest, Muegyetemrkp. 3.

[126] Effect of residence time on selective H2S absorption on MDEA systems – Dara S., Berrouk A. S

[127] Investigation of the Fuel Utilization Factor in PEMFuel Cell Considering the Effect of Relative Humidity at the Cathode - Mojtaba Baghban Yousefkhani, Hossein Ghadamian, Keyvan Daneshvar, Nima Alizadeh and Brendy C. Rincon Troconis - Department of Energy, Materials and Energy Research Center (MERC), Tehran 4777-14155 - Department of Mechanical Engineering, University of Texas at San Antonio, San Antonio – Department of Natural Resources and Environment, Islamic Azad University, Science and ResearchBranch (SRBIAU), Tehran 775-14515

[128] Optimization of the Operating Condition of Production Hydrogen from Glycerol Autothermal Reforming for Fuel Cell – Giovanilton F da Silva, C. Jocélia, S. Mendes, A. Francisco, S. Mota, L. Andrea, O. Ferreira, A. Fabiano, N. Fernandes

[129] Selective CO methanation catalysts for fuel processing applications - Dagle RA, Wang Y, Xia G-G, Strohm JJ, Holladay J, Palo DR. - Appl Catal A 2007;326:213–8.

[130] Challenges and opportunity of H2 delivery via pipeline, Tube-trailer, liquid tanker – Chapter 35.5.1.2 – Tube-Trailer Delivery Pathway

[131] Analysis, Synthesis, and Design of Chemical Processes – Richard Turton/Richard C. Ballie/Wallace B. Whiting/Joseph A. Shaeiwitz

[132] A study of the techno-economic feasibility of H2-based energy storage systems in remote areas - Marocco P., Ferrero D., Gandiglio M., Ortiz M.M., Sundseth K., Lanzini A., and Santarelli M. - Energy Conversion and Management 211 (2020): 112768. Web.

[133] Technology Data Generation of Electricity and District heating – danush Energy Agency and Energinet

[134] State-of-the art CAPEX data for water electrolysers, and their impact on renewable hydrogen price settings – Proost, Joris - International Journal of Hydrogen Energy 44.9 (2019): 4406-413. Web

[135] Synthetic natural gas via integrated high-temperature electrolysis and methanation: Part II—Economic analysis - Emanuele Giglio, Andrea Lanzini, Massimo Santarelli, Pierluigi Leone - Department of Energy (DENERG), Politecnico di Torino, Corso Duca degli Abruzzi 24, 10129 Turin, Italy

[136] Advancing Europe's energy systems: Stationary fuel cells in distributed generation. A study for the Fuel Cells and Hydrogen Joint Undertaking – Roland Berger, Heiko Ammermann, Dr. Philipp Hoff, Mirela Atanasiu, Jo Aylor, Markus Kaufmann, Ovidiu Tisler

[137] Future cost and performance of water electrolysis: An expert elicitation study - O. Schmidt, A. Gambhir, I. Staffell, A. Hawkes, J. Nelson, S. Few

[138] Use of hydrogen in off-grid locations, a techno-economic assessment - L. Gracia, P. Casero, C. Bourasseau, and A. Chabert - Energies, vol. 11, no. 11, 2018

[139] An economic analysis of the production of hydrogen from wind-generated electricity for use in transport applications - P. Menanteau, M. M. Quéméré, A. Le Duigou, and S. Le Bastard - Energy Policy, vol. 39, no. 5, pp. 2957–2965, 2011

[140] Study on Early Business Cases for H2 in Energy Storage and More Broadly Power To H2 Applications - Tractebel and Hinicio - EU Comm., no. June, p. 228, 2017

[141] Techno-economic analysis of a stand-alone hybrid renewable energy system with hydrogen production and storage options - Y. Kalinci, A. Hepbasli, and I. Dincer, - Int.J. Hydrogen Energy, vol. 40

[142] Energy analysis of the Raggovidda integrated system - M. Santos and I. M. Tecnalia

[143] Manufacturing cost model for planar 5 kWel SOFC stacks at Forschungszentrum Julich - S. Harboe, A. Schreibe, N. Margaritis, L. Blum, O. Guillon, N.H. Menzler

[144] Cost and Energy Sensitivity Analysis of Absorber Design in CO2 Capture with MEA. - Razi, Neda, Svendsen, Hallvard F, and Bolland, Olav. - International Journal of Greenhouse Gas Control 19 (2013): 331-39. Web

[145] Decarbonizzazione e desolforazione del syngas proveniente dal processo di gassificazione per produrre idrogeno e tecnologie CTL – Bassano Claudia, Verdone Nicola, Deiana Paolo

[146] Estimate costs of distillation and absorption tower via correlations – Antonio Mulet, Armando B. Corripio, Lawrence B. Evans

[147] Cost and Performance Baseline for Fossil Energy Plants - Volume 2: Coal to Synthetic Natural Gas and Ammonia - Brasington Robert D., Haslback John L., Kuehn Norma J., Lewis Eric G., Pinkerton Lora L., Turner Marc J., Varghese Elsy, Woods Mark - National Energy Technology Laboratory (NETL), Pittsburgh, PA, Morgantown, WV, and Albany, OR (United States)

[148] Production costs for synthetic methane in 2030 and 2050 of an optimized Power-to-Gas plant with intermediate hydrogen storage - Jachin Gorre, Felix Ortloff, Charlotte van Leeuwen

[149] Hydrogen refueling station costs in Shanghai - J. X. Weinert, L. Shaojun, J. M. Ogden, and M. Jianxin - Int. J. Hydrogen Energy, vol. 32, no. 16, pp. 4089–4100, 2007

[150] Costs of Storing and Transporting Hydrogen – Wasw A. Amos – National Renewable Energy Laboratory, 1998

[151] Energy and cost analysis of small-size integrated coal gasification and syngas storage power plants – Giorgio Cau, Daniele Cocco, FabioSerra - Department of Mechanical Engineering, University of Cagliari

[152] Assessment of Energy and Economic Benefits Arising from Syngas Storage in IGCC Power Plants - Cocco, Daniele, Serra, Fabio, and Tola, Vittorio - Energy (Oxford) 58 (2013): 635-43. Web.

[153] Process Equipment Cost Estimation, Final Report. - Loh, H. P., Lyons, Jennifer, and White, Charles W. - United States: N. p., 2002. Web.

[154] 2019 Costs and Technical Parameter Review – Aurecon Australasia Pty Ltd – Consultation Report – Australian Energy Market Operator (AEMO)

[155] Economic Analysis and Policy Suggestions on Gas Power Generation Projects Considering Carbon Emission Reduction - Dong Jun, Zhang Xu, Jiang Xue, Xu Xiaolin, Tang Yuxi - School of Economics and Management North China Electric Power University Beijing, China

[156] Production of Fischer–Tropsch liquid fuels from high temperature solid oxide co-electrolysis units - W.L. Becker, R.J. Brown, M. Penev, M. Melaina - Energy 47 (2012) 99–115

[157] Techno-economic feasibility analysis of hydrogen fuel cell and solar photovoltaic hybrid renewable energy system for academic research building - A. Singh, P. Baredar, and B. Gupta - Energy Convers. Manag., vol. 145, pp. 398–414, 2017

[158] Packing characterization: Absorber economic analysis - Chao Wang , A. Frank Seibert, Gary T. Rochelle - Texas Carbon Management Program, McKetta Department of Chemical Engineering, The University of Texas at Austin, 200 East Dean Keeton Street,C0400, Austin, TX 78712-1589, United States;  eparations Research Program, Pickle Research Campus, The University of Texas at Austin, 10100 Burnet Road, Austin, TX 78758, United States

[159] Trasmissione del calore - Cesare Bonacina, Alberto Cavallini, Lino Mattarolo – 1989, Cleaup

[160] Gas turbines for electric power generation - S. Can Gülen - Cambridge University Press - 2019

[161] Techno-economical Evaluation of a Hydrogen Refuelling Station Powered by Wind-PV Hybrid Power System: A Case Study for İzmir-Çeşme. - Gökçek, Murat, and Kale, Cihangir - International Journal of Hydrogen Energy 43.23 (2018): 10615-0625. Web.

[162] Power-to-Gas Hydrogen: Techno-economic Assessment of Processes towards a Multi-purpose Energy Carrier. - D. Ferrero, M. Gamba, A. Lanzini, and M. Santarelli - Energy Procedia, vol. 101, no. September

[163] Optimize Glycol Circulation And Install Flash Tank Separators In Glycol Dehydrators – Environmental Protection Agency United States – Lessons Learned from Natural Gas STAR Partners

[164] Penn Flash Separator – Penn Separator Corp – P.O. 340 Brookville, PA 15624

[165] Optimal year-round operation for methane production from CO2 and water using wind and/or solar energy - W. Davis, M. Martìn - J. Clean. Prod. 80 (2014) 252–261

[166] Techno-economic Analysis of Hydrigen Electrolysis from Off-Grid Stad-Alone Photovoltaics Incorporating Uncertainty Analysis – Jonathon Yates, Rahman Daiyan, Robert Patterson, Renate Egan, Rose Amal, Anita Ho-Baille, Nathan L. Chang

# Ringraziamenti

Il ringraziamento più importante lo rivolgo alla mia famiglia, che mi ha sempre sostenuto sia economicamente ma soprattutto moralmente in tutta la mia carriera universitaria. In particolare, rivolgo un ringraziamento dal profondo del mio cuore a mia sorella Elena che mi ha sempre aiutato ogni volta che ne avevo bisogno senza mai chiedere nulla in cambio, proprio come farei io per lei. Un grazie enorme!

Ci tengo a ringraziare fortemente il professore Santarelli Massimo, senza il quale non avrei avuto l'opportunità di svolgere questo lavoro di tesi, il quale era proprio ciò che desideravo come argomento. Ringrazio tantissimo anche il mio correlatore Ferrero Domenico che ha sempre trovato del tempo da dedicarmi nonostante il periodo estremo di pandemia che stiamo vivendo, aiutandomi nello svolgimento del lavoro di tesi. Inoltre, vorrei ringraziare anche Buffo Giulio, con cui ho avuto l'opportunità di lavorare solamente all'inizio, ma che comunque mi ha dato preziosi consigli.

Desidero fare un caloroso ringraziamento ai miei amici di sempre, soprattutto ad Enrico, per la sua disponibilità e l'aiuto che mi ha fornito per Excel ed alla mia fantastica ragazza Francesca che mi è sempre stata vicino, supportandomi nei momenti di difficoltà e motivandomi ad impegnarmi costantemente fino a raggiungere i miei obiettivi.

Infine, un ringraziamento ai miei compagni dell'università, in special modo a Sabatino e Fabio con cui ho condiviso tutte le mie esperienze di vita universitaria rendendola molto più "leggera", aiutandoci a vicenda nello studio, condividendo appunti e soprattutto divertendoci.